

**Predictive second cancer risk models
based on peripheral neutron dosimetry
of patients undergoing radiotherapy**



Leticia Irazola Rosales

Sevilla 2016



FACULTAD DE MEDICINA
DEPARTAMENTO DE FISIOLÓGIA MÉDICA Y BIOFÍSICA
Grupo de Física Médica

**Predictive second cancer risk models based on
peripheral neutron dosimetry of patients
undergoing radiotherapy**

Leticia Irazola Rosales
16th September 2016

Francisco Sánchez Doblado. Catedrático del Departamento de Fisiología Médica y Biofísica, Facultad de Medicina de la Universidad de Sevilla

y

José Antonio Terrón León. Facultativo especialista de área del Hospital Universitario Virgen Macarena. Profesor Tutor Clínico de la Universidad de Sevilla.

Certifican:

Que Doña Leticia Irazola Rosales ha realizado bajo su dirección el trabajo de tesis “Predictive second cancer risk models based on peripheral neutron dosimetry of patients undergoing radiotherapy”, que presenta para optar al Grado de Doctor por la Universidad de Sevilla con Mención Internacional.

Sevilla, a 10 de Junio de 2016.

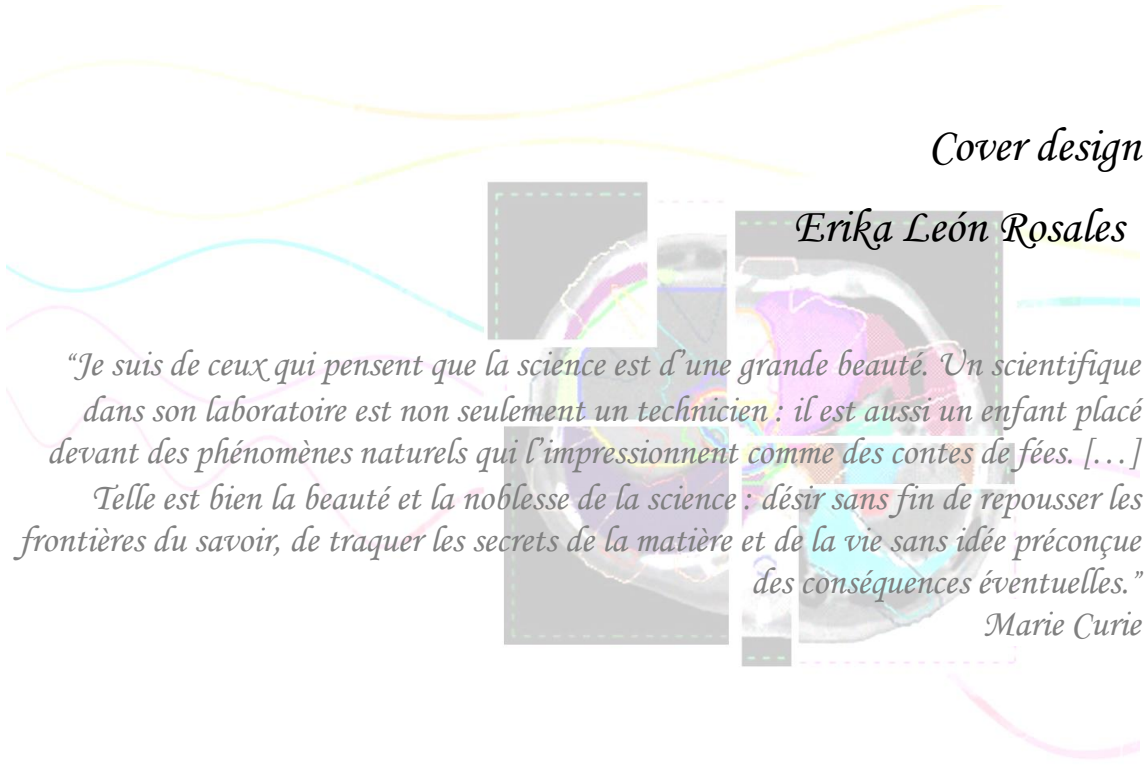
Fdo. Francisco Sánchez Doblado

Fdo. José Antonio Terrón León

A mis padres

*“Learn from yesterday, live for today, hope for tomorrow.
The important thing is not to stop questioning”
Albert Einstein*





Cover design

Erika León Rosales

“Je suis de ceux qui pensent que la science est d’une grande beauté. Un scientifique dans son laboratoire est non seulement un technicien : il est aussi un enfant placé devant des phénomènes naturels qui l’impressionnent comme des contes de fées. [...]”

Telle est bien la beauté et la noblesse de la science : désir sans fin de repousser les frontières du savoir, de traquer les secrets de la matière et de la vie sans idée préconçue des conséquences éventuelles.”

Marie Curie

Agradecimientos

El trabajo aquí presente no habría sido posible sin el esfuerzo del brillante grupo de científicos (y mejores personas si cabe) de las que me he rodeado durante esta etapa de mi vida. Por ello, mi agradecimiento a todos aquellos que se han cruzado en mi camino desde que comencé mi “aventura” en el mundo de la investigación, en lo cual tienen especial “culpa” mis compañeros del Centre Eugène Marquis, Rennes (gracias Jean Pierre y Caroline) y el Centro de Investigaciones BIomédicas de la Rioja (gracias Camilo). Me gustaría enfatizar mis agradecimientos a mis directores de tesis Paco y José Antonio, sin los cuales este sueño no hubiese sido posible.

Paco gracias por tu confianza en mí desde el minuto cero, por tu apoyo incondicional y por contagiarme la pasión por este mundo. Me siento afortunada de haber tenido la oportunidad de aprender de la mano de alguien como tú. No solo me has formado en la investigación, sino que me has hecho crecer como persona desde tu cariño. José Antonio, gracias por todas esas horas compartidas, por todos los conocimientos inculcados y sobre todo, por despertar en mí el amor por el mundo clínico. Gracias por ser mi familia en Sevilla.

No sería justa si no agradeciésemos a los principales colaboradores, sin los que este manuscrito nunca hubiese llegado a buen puerto... Beatriz, ha sido un honor trabajar a tu lado, gracias por tus brillantes ideas y maravillosas correcciones; Mónica gracias por aguantar nuestros “ataques” a tu persona y por las horas en el planificador; gracias Roberto por estar siempre dispuesto a ayudar e ilustrarme con tus inestimables aportaciones y Trini, gracias por tu incalculable disposición para echar siempre una mano.

Mi eterno agradecimiento a la gente del Departamento de Fisiología Médica y Biofísica. A Loli por su constante preocupación por mi persona y a Fernando por ayudarme a sobrevivir a la burocracia. En especial, al grupo física médica: Elisa, Rita, José Antonio y Ana, gracias por todos los buenos momentos compartidos que me han hecho querer seguir adelante con esta “locura”. Gracias Antonio por tus siempre alentadores comentarios. Y por supuesto, a toda la gente del departamento por las horas compartidas en la “biblioteca”.

No puedo olvidar de todo el personal del hospital con los que he compartido los a veces tediosos, pero satisfactorios momentos de medidas, por su aguante y ayuda: Rafa, gracias por tu colaboración y disposición para la realización de los experimentos, sin los cuales este trabajo no existiría. Álvaro gracias por las críticas, los buenos consejos y mejores ratos. María y Héctor, mi eterna gratitud por todos los buenos momentos compartidos dentro y fuera. Y, por supuesto, gracias a mis queridos técnicos (especialmente a Isa M, Mari, María P, Pili y Juani) con las que tantas horas he compartido.

Agradecer a todos y cada uno de los centros que han contribuido en los diversos trabajos: POLIMI gracias Michele por tu paciencia; CIEMAT, Juan Ignacio gracias por las brillantes lecciones y las horas de medidas; CNA gracias Javier, Begoña y Miguel por vuestra colaboración y vuestra paciencia durante los ratos pasados en el tándem; gracias Faustino (USC) por tus siempre audaces aportaciones; mi agradecimiento a la gente de la UAB Paco, Carles y Maite por las sabias aportaciones y por supuesto, a todos los centros que han colaborado en el último trabajo: ERESA en especial Joan, Trini y Luis; Duques del Infantado, especialmente a Santiago; Infanta Luisa en especial a Rafa; Ramón y Cajal, gracias Chano y M^a José . En fin, gracias a todo el personal que ha hecho posible estas colaboraciones.

Gracias Mikele por esa magia, por no dejarme caer nunca. Nerea, gracias por ser mi persona y estar ahí en las crisis. Gracias Blanca por mostrarme siempre el lado bueno de la vida. Sheila, por toda una vida de apoyo y Anjara por tu comprensión siempre. Luis...por esas ayudas 'técnicas' a cualquier hora, gracias David por estar siempre pendiente y Eduardo por tratar de hacerme sonreír en todo momento. Especial agradecimiento a mi amiga Zoey, por sus correcciones que han hecho de este manuscrito lo que es. Agradecer a todos mis amigos (los de Sevilla, Zaragoza, Rennes y Haro) por estar ahí, por su apoyo infinito en esta etapa de mi vida y en especial, a mi gente de Haro sin los que, a pesar de la distancia, nunca hubiese podido llegar hasta aquí. Por todo y a todos, muchas gracias.

Agradecer a toda mi familia por sus ánimos constantes, en especial a mi tía M^a Carmen y como no a mi hermana, uno de los pilares de mi vida que siempre me ha animado a seguir adelante.

Pero, en honor a la verdad, he de decir que este trabajo nunca hubiese sido posible sin ellos, las personas que han confiado en mí desde el principio, incluso en los momentos en que perdí la fe, mi todo en la vida, gracias papás. Mamá no hay palabras...tu amor incondicional, tu paciencia y tu apoyo infinitos. Papá tu juicio crítico que tanto me ha enseñado sobre la vida. Sois la causa y el motivo de que hoy esté donde estoy y sea quien soy, os quiero.

A todos aquellos en cuyos ojos me reflejo para ser mejor persona.



Contents

Abstract	i
List of publications as a consequence of the thesis	iii
I. Preface	1
1. Radiation-induced secondary cancer	1
2. Peripheral dose	6
2.1 Photon peripheral dose	10
2.2 Neutron peripheral dose	11
2.2.1 Evaluation of neutron dose: detectors.	13
2.2.2 Evaluation of neutron dose: calibration sources	16
2.3 Equivalent neutron doses and risk evaluation	18
2.4 Peripheral neutron dose models	21
2.4.1 SRAM detector	21
2.4.2 Monte Carlo simulations	23
2.4.3 Anthropomorphic phantom measurements.	
NORMA phantom	26
2.4.4 Neutron equivalent dose in organ and second cancer risk estimation	26
II. Hypothesis and objectives	31
III. Thesis core	33
1. Introduction	33
(A) Characterization of a new active thermal neutron detector.	33
(B) Limitations and solutions of <i>TNRD</i> detectors in	

radiotherapy environments	34
(C) Neutron peripheral dose model improvements	38
(D) Peripheral dose in clinical cases	40
2. Publications	43
(A) <i>“A new online detector for estimation of peripheral neutron equivalent dose in organ”</i>	43
(B.1) <i>“Using a Tandem Pelletron accelerator to produce a thermal neutron beam for detector testing purposes”</i>	59
(B.2) <i>“Improving the neutron-to-photon discrimination capability of detectors used for neutron dosimetry in high energy photon beam radiotherapy”</i>	75
(B.3) <i>“Neutron measurements in radiotherapy: a method to correct neutron sensitive devices for parasitic photon response”</i>	89
(C) <i>“Neutron model upgrade for peripheral neutron dose assessment evaluated in 510 radiotherapy patients”</i>	103
(D) <i>“SBRT, FFF and 10 MV irradiation techniques are associated to the lowest second cancer risk”</i>	133
IV. Conclusions	161
V. References	165
Glossary of abbreviations	177

Appendix A **179**

(A.1) *“Set-up of a new online digital detector for peripheral neutron equivalent dose estimation in radiotherapy patients”*. 179

(A.2) *“Evaluation of peripheral neutron equivalent dose and second cancer risk in radiotherapy patients”*.. . . . 183

(A.3) *“Online neutron fluence measurements in phantom for second cancer risk estimation in radiotherapy”*. 187

Appendix B **191**

(B.1) *“Effects of cable extension and photon irradiation on TNRD neutron detector in radiotherapy”*.. . . . 191

(B.2) *“Signal photon component of a new thermal neutron detector TNRD in radiotherapy environments”* 199

(B.3) *“Photon energy response of TNRD neutron detector in a ⁶⁰Co irradiator and a 6 MV clinic”* 203

(B.4) *“TNRD neutron detector signals for different gantry angles in 6 and 15 MV “* 207

Appendix C

(C.1) *“Peripheral neutron dose estimation: comparison between experimental measurements and TPS estimation”*. 211

(C.2) *“Peripheral neutron dose model verification for real IMRT cases “* 219

*“Comparison of peripheral doses associated to SBRT, VMAT, IMRT, FFF and
3D-CRT plans for lung cancer”* 223

Abstract

The study of Secondary Malignant Neoplasms (SMNs) after radiotherapy is becoming a topic of interest nowadays, as a consequence of the higher healing rates and life expectancy accomplished with current diagnose procedures and radiotherapy treatments. In the case of modern techniques, there is a tendency to prefer low (i.e. 6 MV) energies to high ones (e.g. 15 or 18 MV), sometimes to the detriment of treatment conformity, as the latter are known to increase equivalent dose to patients due to neutron production.

The Medical Physics Group of the University of Seville, pioneered the development of a simple and universal methodology for the estimation of peripheral neutron doses, based on the correlation between readings of a SRAM-based detector (in a reference location, far from the patient) and those of passive detectors, located inside an adult anthropomorphic phantom. This correspondence model directly links detector readings (referring to thermal neutron fluence in the room) to equivalent neutron doses at specific organs in the patient. One of the main problems of this methodology was the need of using the specific SRAM-based digital detector for the characterization of every facility. In addition, the passive behavior of plastic and thermoluminescent devices used for 'in-phantom' measurements, together with their limitations in these environments, restricted the repetition and reliability of some critical points.

The acquisition of a new prototype of a miniaturized active thermal neutron detector, initially designed for nuclear purposes, opened the possibility of improving the existing peripheral neutron dose estimation methodology in high-energy radiotherapy. The goal of this work was the use of these devices for the validation, improvement and generalization of the existing models, in order to make the real time estimation of peripheral neutron doses directly available in any facility. The online disposal of thermal neutron fluence estimations from the new TNRD detectors (Thermal Neutron Rate Detector), allowed the simplification and generalization of this procedure. Thus, making it feasible with any thermal neutron detector following a simple characterization procedure. Additionally, their active and miniaturized behavior permitted their use in both locations 'in-phantom' and external (for patient measurements).

In order to enhance the existing models, further and more precise measurements of real radiotherapy treatments were performed with TNRD detectors, ensuring that the two existing model locations (i.e. H&N and abdomen) are general enough to cover any specific treatment. We thought that at this stage, patient age and anatomy was an

important aspect that should be taken into account for second cancer risk estimations, being of special importance for children, whose life expectancy and radiosensitivity are greater. For that, measurements with the new miniaturized active devices were performed for three different phantom sizes (child, teen and adult). Once these results were implemented, this new methodology was applied to 510 patients, starting the generation of an improved database that would allow a more patient specific analysis of second cancer risk, as a consequence of neutron contamination.

Besides, the analytical peripheral photon model simultaneously developed by our group, has allowed the generation of a piece of software for the estimation of both peripheral doses. This has enabled a quick assessment of photon and neutron peripheral doses in clinical routine, from readily available parameters. Estimations of these doses were finally evaluated for some of the most common tumor locations, comparing conventional techniques and fractionations (3D-CRT, IMRT, VMAT) to newer ones (SBRT, FFF), regarding the three main linac manufacturers and energies (6, 10, and 15 MV). As a general pattern, hypofractionated modality, 10 MV photon energy and FFF irradiation mode have shown as the best alternatives in terms of peripheral dose reduction. Thus, a combined use of these options would imply a decrease of second cancer probability.

Second cancer risk estimations could be easily performed from the here presented procedures by the direct use of the existing risk models, established by the international organisms (i.e. ICRP or BEIR). The universal methodology presented aims to provide an objective additional criterion (Second Cancer Probability, SCP), to be used in combination with the previously existing radiobiological parameters as Tumor Control Probability (TCP) and Normal Tissue Complication Probability (NTCP), for the choice of the best radiotherapy strategy, thanks to its easy implementation in Treatment Planning Systems.

List of publications as a consequence of the thesis

Full papers as first author

Irazola L, Lorenzoli M, Bedogni R, Pola A, Terrón JA, Sánchez-Nieto B, Expósito MR, Lagares JI, Sansaloni F and Sánchez-Doblado F. *A new online detector for estimation of peripheral neutron equivalent dose in organ*. Med Phys 2014;41:112105.

Irazola L, Praena J, Fernandez B, Macias M, Terrón JA, Bedogni R, Sánchez-Nieto B and Sánchez-Doblado F. *Monitoring the stability of a thermal neutron detector using a moderated neutron beam from a Tandem Peletron*. Appl Radiat Isot 2016;107:330-334.

Irazola L, Terrón JA, Bedogni R, Pola A, Lorenzoli M, Sánchez-Nieto B, Gómez F and Sánchez-Doblado F. *Improving the neutron-to-photon discrimination capability of detectors used for neutron dosimetry in high energy photon beam radiotherapy*. Appl Radiat Isot, in press.

Irazola L, Terrón JA, Bedogni R, Jiménez-Ortega E, Barbeiro AR, Sánchez-Nieto B and Sánchez-Doblado F. *Neutron measurements in radiotherapy: a method to correct neutron sensitive devices for parasitic photon response*. Sent to Appl Radiat Isot.

Irazola L, Terrón JA, Sánchez-Nieto B, Bedogni R and Sánchez-Doblado F. *Neutron model upgrade for peripheral neutron dose assessment evaluated in 510 radiotherapy patients*. Sent to Phys Med Biol.

Irazola L, García-Hernández MT, Terrón JA, Ortiz-Seidel M, Velázquez S, Linares R, Sánchez-Nieto B, and Sánchez-Doblado F. *SBRT, FFF and 10 MV irradiation techniques are associated to the lowest second cancer risk*. To be sent to Radiat Oncol J.

CMA National Instruments. Best application, 1st national prize

Irazola L, Lorenzoli M, Bedogni R, Pola A, Gentile A, Terrón JA, and Sánchez-Doblado F. *Helping to reduce patient risk of second cancer*. CMA 2014, National Instruments (<http://sine.ni.com/cs/app/doc/p/id/cs-15867>).

Full papers as collaborator

Sánchez-Nieto B, El-far R, Irazola L, Expósito MR, Lagares JI, Mateo JC, Terrón JA and Sánchez-Doblado F. *Analytical model for photon peripheral dose estimation in radiotherapy treatments*. Biomed Phys Eng Express 2015;1:045205.

Romero-Expósito M, Sánchez-Nieto B, Irazola L and Sánchez-Doblado F. *In regard to "Neutron contamination in radiotherapy: estimation of second cancers based on measurements in 1377 patients"*. Sent to Radiother Oncol.

Sánchez-Nieto B, Romero-Expósito M, Terrón JA, Paiusco M, Cagni E, Ghetti C, Filice S, Irazola L, Gómez F, Domingo C and Sánchez-Doblado F. *Risk assessment of second cancer incidence after intensity-modulated radiation therapy and volumetric modulated arc therapy versus conventional conformal techniques*. Sent to Br J Radiol.

Short publications as first author

Irazola L, Sanchez-Doblado F, Sánchez-Nieto B, Expósito MR, Mazzotti G, Morelli M, Lorenzoli M, Bedogni R, Pola A and Terrón JA. *Evaluation of peripheral neutron equivalent dose and second cancer risk in radiotherapy patients*. Radiother Oncol 2014;111:708-709.

Irazola L, Lorenzoli M, Terrón JA, Bedogni R, Pola A, Sánchez-Nieto B, Romero-Expósito M and Sánchez-Doblado F. *Neutron model upgrade for radiotherapy patients monitoring using a new online detector*. Med Phys 2014;41:280.

Irazola L, Terrón JA, Bedogni R, Lorenzoli M, Pola A, Sánchez-Nieto B and Sánchez-Doblado F. *Signal photon component of a new thermal neutron detector TNRD in radiotherapy environments*. Radiother Oncol 2015;115(1):S870(EP-1589).

Irazola L, Terrón JA, Bedogni R, Lorenzoli M, Pola A, Sánchez-Nieto B and Sánchez-Doblado F. *TNRD neutron detector signals for different gantry angles in 6 and 15 MV*. Radiother Oncol 2015;115(1):S761 (EP-1410).

Irazola L, Terrón JA, Sánchez-Nieto B, Bedogni R, Gómez F and Sánchez-Doblado F. *Effects of cable extension and photon irradiation on TNRD neutron detector in radiotherapy*. IFMBE Proceedings 2015;51:645-648.

Irazola L, Ortiz-Seidel M, García-Hernández MT, Terrón JA, Sánchez-Nieto B and Sánchez-Doblado F. *Peripheral neutron dose estimation: comparison between experimental measurements and TPS estimation*. IFMBE Proceedings 2015;51:397-400.

Irazola L, Terrón JA, Sánchez-Nieto B, Ortiz-Seidel M and Sánchez-Doblado F. *Photon and Neutron Peripheral Dose Ratio for Low (6 MV) and High (15 MV) Energy for Treatment Selection*. Med Phys 2015;42(6):3476.

Irazola L, Domingo C, Romero-Expósito M, García-Fuste M, Terrón JA, Sánchez-Nieto B, Bedogni R and Sánchez-Doblado F. *Estimation of Neutron Ambient Dose Equivalents for Radioprotection Exposed Workers in Radiotherapy Facilities Based On Characterization Patient Risk Estimation*. Med Phys 2015;42(6):3417.

Irazola L, Brualla L, Roselló J, Terrón JA, Sánchez-Nieto B, Bedogni R and Sánchez-Doblado F. *Commissioning the neutron production of a Varian TrueBeam linac*. Med Phys 2015;42(6):3376.

Irazola L, Ortiz-Seidel M, Velázquez S, García-Hernández MT, Terrón JA, Sánchez-Nieto B, Romero-Expósito M, Roselló J and Sánchez-Doblado F. *Comparison of peripheral doses associated to SBRT, VMAT, IMRT, FFF and 3D-CRT plans for lung cancer*. ePoster at 35th ESTRO Congress 2016; EP-1613. https://www.postersessiononline.eu/pr/aula_poster.asp

Irazola L. *A new online detector for estimation of peripheral neutron equivalent dose in organ*. Rev Fis Med 2015;16(3):60.

Irazola L, Terrón JA, Sánchez-Nieto b, Romero-Expósito M and Sánchez-Doblado F. *Peripheral neutron dose model verification for real IMRT cases*. Poster at the 1st European Congress of Medical Physics (ECMP) 2016.

Short publications as collaborator

Terrón JA, Irazola L, Lorenzoli M, Bedogni R, Pola A, Introini MV, Bortot D, Gentile A, Esposito A, Sánchez-Nieto B, Expósito MR and Sánchez-Doblado F. *Set-up of a new online digital detector for peripheral neutron equivalent dose estimation in radiotherapy patients*. Radiother Oncol 2014;111:564.

Sánchez-Doblado F, Irazola L, Lorenzoli M, Pola A, Bedogni R, Gentile A, Lagares, JI Muñiz JL, Sansaloni F, Introini MV, Bortot D, Sánchez-Nieto B, Expósito MR, and JA Terrón. *Online neutron fluence measurements in phantom for second cancer risk estimation in radiotherapy*. Radiother Oncol 2014;111:709-710.

Sánchez-Nieto, El far R, Romero-Expósito M, Lagares J, Mateo JC, Terrón JA, Irazola L and Sánchez-Doblado F. *Analytical model for Photon Peripheral Dose in Radiotherapy Treatments*. Med Phys 2014;41:231.

Sánchez-Nieto B, El-far R, Expósito MR, Lagares JI, Mateo JC, Terrón JA, Zeladas G, Irazola L and Sánchez-Doblado F. *Peripheral dose assessment after IMRT and VMAT vs CFRT*. Phys Medica: EJMP 2014;30:e33.

Praena J, Irazola L, Fernández B, Terrón JA, Bedogni R, Lorenzoli M, Pola A, Sánchez-Nieto and Sánchez-Doblado F. *Proposal of thermal neutron detector stability for peripheral dose estimation in clinic at a novel neutron facility*. Radiother Oncol 2015;115(1):S735.

Terrón JA, Irazola L, Morilla Y, Muñiz G, Bedogni R, Lorenzoli M, Pola A, Sánchez-Nieto B and Sánchez-Doblado F. *Photon energy response of TNRD neutron detector in a ⁶⁰Co irradiator and a 6 MV clinac*. Radiother Oncol 2015;115(1):S757-S758.

García Hernández MT, Ortiz M, Irazola L, Terrón JA, Romero-Expósito MR, Sánchez-Nieto B and Sánchez-Doblado F. *Neutron peripheral dose estimation: treatment planning system implementation*. Radiother Oncol 2015;115(1):S442.

Sánchez-Nieto B, El-far R, Castrillón M, Irazola L, Terrón JA and Sánchez-Doblado F. *Validation of a photon peripheral dose model for IMRT treatments*. Radiother Oncol 2015;115(1):S541.

Sánchez-Nieto B, Irazola L, Romero-Expósito M, Terrón JA and Sánchez-Doblado F. *Validation of a peripheral photon dose model for clinical use: a prostate IMRT irradiation of the Alderson phantom*. 35th ESTRO Congress 2016; PO-808. https://www.postersessiononline.eu/pr/aula_poster.asp

Oral presentations

Irazola L, Terrón JA, Bedogni R, Lorenzoli M, Sánchez-Nieto B and Sánchez-Doblado F. *Gantry angle influence in the neutron commissioning of a linac*. Oral Presentation at Congreso conjunto SEFM-SEPR 2015; Valencia.

Sánchez-Doblado F, Terrón JA, Irazola L, Sánchez-Nieto B. *Peripheral Neutron and Photon Doses*. Oral presentation at IUPESM 2015; Toronto, Canada.

Sánchez Nieto B, El Far R, Irazola L, Terrón JA, Sánchez-Doblado F. *Peripheral photon dose in organs*. Oral presentation at IUPESM 2015; Toronto, Canada.

I. Preface

1. Radiation-induced secondary cancer

Cancer represents one of the most important public health problems in developed societies. It has been estimated that about one in two men and women born today will be diagnosed with some type of cancer in their lifetimes (Newhauser et al.,2016; SEER website), being the leading cause of death among adults (23% of total deaths in 2012, Siegel et al.,2016). Close to 14 million of new cases were diagnosed in the world in 2012, and it is predicted that by 2030, this value will rise by 75% reaching nearly 24.6 million cases (Ferlay et al.,2015). The technological revolution that has taken place in the medical imaging field and diagnosis procedures, have allowed a better and earlier detection of cancer pathologies. In addition, the great improvements achieved in treatment techniques have led to an increased number of long-term survival patients (Coleman et al.,2011), as shown in Figure 1. For instance, the 5 year survival rate of cancer in the USA has grown to almost 68% and 83% in adults and children, respectively (Newhauser et al.,2016).

Nowadays, there are three main weapons used to fight cancer disease, namely surgery, chemotherapy and radiotherapy. Although these treatment modalities are generally used in combination, almost two-thirds of cancer patients receive some form of radiation therapy during their treatment (Delaney et al.,2005; Jameson et al.,2013). In particular, considering the 10 most frequent cancer pathologies (prostate, female breast, lung, colorectal, bladder, non-Hodgkin lymphoma, skin melanoma, kidney, ovarian, and uterine), it is estimated that at least 50.3% of them are treated with radiotherapy as a part or the totality of the treatment (either X-ray based or with charged particles, Siegel et al.,2016; Delaney et al.,2005).

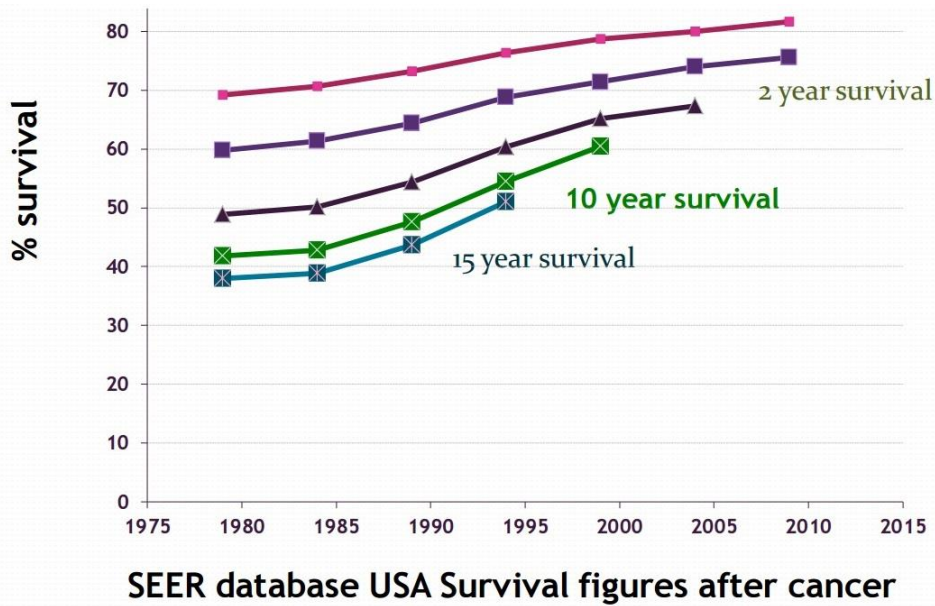


Figure 1. SEER (Surveillance, Epidemiology and End Results program) database USA survival figures after cancer. Figure extracted from AAPM Congress 2015, Anaheim (<http://amos3.aapm.org/abstracts/pdf/99-27178-365478-110196.pdf>).

Radiotherapy treatments are based on the use of ionizing radiation beams to destroy cancerous cells, obstructing their reproduction capability. The goal of this treatment modality is to deliver a high dose to the tumor (defined as Planned Target Volume, PTV) while surrounding organs (named Organs At Risk, OAR) and healthy tissues remain under certain established dose levels. One of the most common radiotherapy techniques, named external radiotherapy (cited hereafter as RT), consists in the use of an external radiation source, located outside the patient. This modality remains as the most used one, with an estimated number of 7 million cases for which radiotherapy was indicated in 2012 and a prediction of 12 million in 2030 (Atun et al.,2015). However this dual goal in an ideal scenario, where the PTV receives the 100% of the prescribed dose while the rest of the tissues remain at zero, is not feasible. This is mainly due to the unavoidable dose deposition at the beam entrance, lateral scattering and production of secondary uncharged particles (coming

from the interaction of the primary beam with different materials along its path).

The great benefits achieved with new RT techniques have been translated into higher healing rates, implying an extension of patient survival. This fact has led to a growing concern regarding second cancer incidence among long-term survivors, as they are at increased risk to develop treatment-induced side effects (Murray et al.,2015a;b; Hall et al.,2003; Xu et al.,2008; Berdnarz et al.,2010; Milecki et al.,2009; Trott et al.,2009a; Dörr et al.,2002a;b; Ruben et al.,2008; Brenner et al.,2000;2006; Tubiana et al.,2009;Murray et al.,2014; Hall et al.,2004; Chargari et al.,2013). These kind of radio-nduced malignancies have nothing to do with methastatic ones, coming from primary tumours. In general, Second Malignant Neoplasms (SMNs), account for around 17-19% of all cancers (Newhauser et al.,2016). As cancer patients have become younger, having thus a longer life expectancy after RT treatments, radiation effects are now more evident than in the past (Smith et al.,2010; Travis et al.,2003; Chao et al.,2016; Hung et al.,2016; Sharma et al.,2008). This increased risk of SMNs in healthy tissues as a consequence of RT, may appear usually after a period greater than a decade and, in around 10-20% of cases, 30 years after treatment (Tubiana et al.,2009; Newhauser et al.,2011; Kumar et al.,2012). This long-term side effect, although unusual, is a feared later complication of this “double-edged sword” that RT represents. Second cancer risks seem to be higher for tissues receiving low doses (≤ 6 Gy) and highly dependent on the dose deposited outside the PTV (Diallo et al.,2009; Dörr et al.,2002b).

Treatment selection is usually based on several factors (i.e. life expectancy, clinical stage and associated toxicities; Robles et al.,2012; Bentzen et al.,2010; Shuryak et al.,2009), whereas these non-desired doses aren't frequently considered in detriment of a benefit-risk ratio. Although second cancer risks attributable to radiotherapy are small ($\approx 8\%$), bearing in mind the large number

of population treated annually and the overall survival rate, we think that their consideration should be mandatory at this step (Kry et al.,2005a; Brenner et al.,2003; Nguyen et al.,2015; Berrington et al.,2011; Schenider et al.,2011; Grantzau et al.,2015). Particularly, major concern should be taken for pediatric and young patients, for which a very large variation in radiation sensitivity can be found (around 10 times more for middle-aged than adults in some tissues; UNSCEAR 2013; Hall et al.,2002; Lee et al.,2016).

Even though the International Commission on Radiological Protection (ICRP) explicitly considers patient radiological protection in [Publication-103](#): *“...in radiation therapy it requires delivery of the required dose to the volume to be treated, avoiding unnecessary exposure of healthy tissues”*, far out-of-field doses are hardly ever considered in clinical routine. Additionally, despite the technological improvements accomplished in modern RT techniques, such as Intensity Modulated Radiation Therapy (IMRT), Image Guided Radiation Therapy (IGRT), Volumetric Modulated Radiation Therapy (VMAT) or Stereotactic Body Radiation Therapy (SBRT); there are some trade-offs related to peripheral doses. Even if they allow higher conformation levels to target volumes and better OAR sparing, usually this is at the expense of an increased number of Monitor Units (MU) and consequent beam on time (except for hypofractionated techniques), compared to conformal radiotherapy (CRT). Thus, modern techniques may require linac energized for longer (even a factor 3-4) than conventional modalities, involving an increase in overall patient exposition to unwanted doses to healthy tissues, outside the treatment field. These out-of-field doses are due to activation, scattered and leakage photons as well as contaminating neutrons (the latter for energies ≥ 10 MV; Xu et al.,2008). A question should be pointed out here, considering if the achieved improvement in local tumor control worths the compromise of patient protection against radioinduced

effects (Timlin et al.,2015; Hall et al.,2006; D'Agostino et al.,2013; Slaz et al.,2012; La Tessa et al.,2012; Schneider et al.,2006).

In addition, actual dose-response relationships for cancer risk predictions are mainly obtained from retrospective cohort studies regarding Japan atomic bomb incident (risks studied in the range between 0.1 and 2.5 Gy, BEIR VII; Gudowska et al.,2014; UNSCEAR 2006; Thomas et al.,2011; Schneider et al.,2015). However, as current RT radiation deliverance mode highly differs from this case, long-term epidemiological studies of SMNs incidence in treated patients would be highly desirable (Kohandel et al.,2015). This would allow a better assessment for the selection of the best treatment strategy, concerning patient protection (Claude et al.,2015; Antoni et al.,2015; Eaton et al.,2015; Olch et al.,2015; Malick et al.,2015; Murray et al.,2015a; Tubiana et al., 2006; Vaño et al.,2011; Trott et al.,2009b).

Conservative approaches note that around 6-13% of RT patients may develop a second malignancy as a consequence of the treatment (Van Leeuwen et al.,2004; Hall et al.,2007; Clarke et al.,2005; Berrington de González et al.,2013; Kamran et al.,2016), from which at least 5000 cases/year would be due to neutron contamination (Hall et al.,1995). Although these values may increase considering current cancer predictions previously mentioned (Frankish et al.,2003), they are usually not considered due to the long latency periods of these malignancies (≥ 5 years) and the small percentages. Nevertheless, several studies have pointed out their concern for those young patients whose free-cancer survival evolution is expected to be greater than these periods (Lee et al.,2016; Chargari et al.,2016), as the age at exposure remains as an important factor in risk modeling.

2. Peripheral dose

Concerning individual radiological protection in RT, patient anatomy can be divided into three regions: target area (PTV), OAR (adjacent to the tumor) and the rest of the body (Figure 2). Out-of-field doses, affecting mainly the latter region are unnecessarily received by the patient as a consequence of scatter and leakage photons and contaminating neutrons ($E \geq 10$ MV), are usually referred to as peripheral doses (PD). There is also a contribution due to activation of material present in radiotherapy rooms that may be of relevance for staff, being less than 1% of that received by the patient due to PD (Sánchez Doblado et al.,1989; Vega-Carrillo et al.,2016). Commercial Treatment Planning Systems (TPS) used in clinical routine, are conventionally designed to correctly estimate doses up to 1% isodose, leading to a distance of approximately ≤ 10 cm from the field edge, with no consideration of photon PD or neutron contamination.

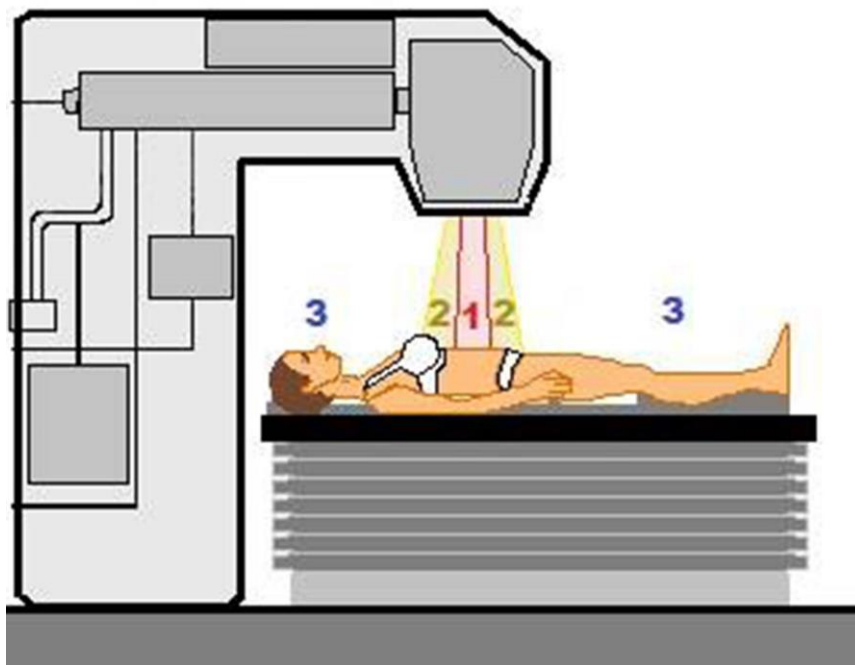


Figure 2. Patient's anatomy division regarding radiological protection in RT: (1) target area (PTV), (2) OAR (adjacent to the tumor) and (3) rest of the body (receiving PD).

Figures for these undesired doses become significant if we consider the increase in life expectancy and survival rates of radiotherapy patients and compare them to occupational and general dose limits per year (Figure 3). Although they can result quite small when compared to in-field doses, PD may cause relevant damages if delivered to particularly radiosensitive organs (specifically in the case of neutrons), causing around 50% of second cancers (Diallo et al.,2009; Sánchez-Nieto et al.,2016).

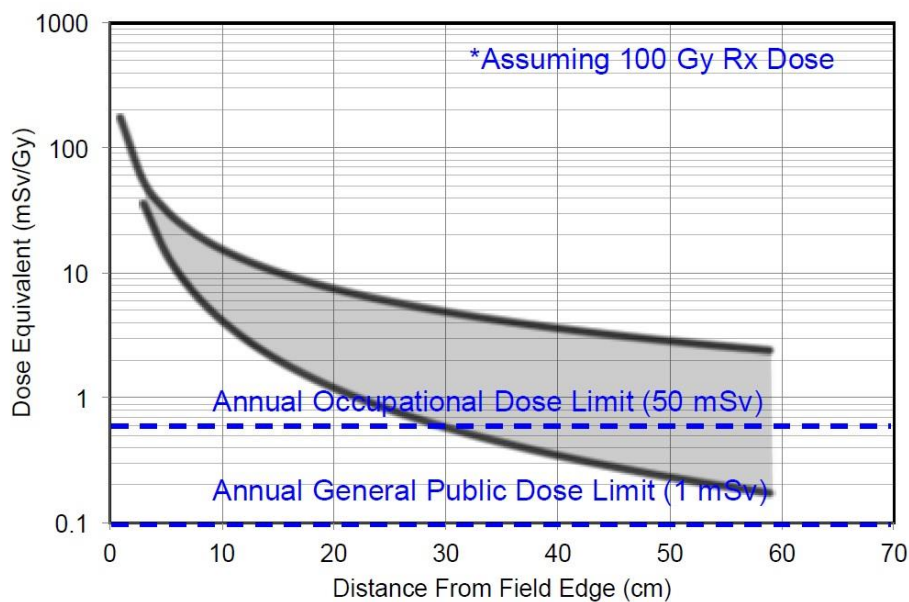


Figure 3. Dose estimations received by non-target regions for generic RT treatments, compared to annual limits for occupational and general public. Extracted from: *Calculation Techniques for Determining Non Target Photon, Electron and Neutron Doses*, AAPM Annual Meeting 2015, Anaheim, CA 16/07/2015, Bryan Bednarz (<https://www.aapm.org/education/VL/vl.asp?id=4832>).

Risks associated to a specific radiation dose can be divided in two classes: genetic (revealed in the progeny of an exposed individual) and somatic (manifested in the exposed individual). The criteria followed for a neoplasm to be classified as radiation-induced (second cancer) was originally defined by Cahan et al.,1948, and can be summarized into the following points:

- (a) SMNs are found in regions irradiated by primary or secondary RT beams.
- (b) SMNs display a different histology, being easily differentiable from metastasis.
- (c) Long-term latency period (5-10 years).
- (d) No presence evidence at the time of RT.
- (e) No cancer-prone syndrome.

The previously mentioned increased in beam on time for new RT techniques could lead to an increase in total body irradiation of around 2-3 times, since larger volumes of normal tissues can be exposed to lower doses as a consequence of the tight dose conformations and severe dose gradients required ([Schneider et al.,2011](#); [Followill et al.,1997](#)).

Although several calculation techniques for out-of-field doses (TPS, empirical and Monte Carlo) have been developed ([Harrison et al.,2013](#); [Voyant et al.,2014](#); [Bordy et al.,2013](#); [Zhang et al.,2015](#); [Kry et al.,2005b](#); [Kaderka et al.,2012](#)), to our knowledge, none of them has yet established a general model for PD estimations in RT treatments. This is due not only to the variability between different techniques but also to the difficulty of these peripheral measurements, particularly regarding the neutron component. Generally speaking commercial TPS (where only photon contribution is considered), use deterministic algorithms that provide good dose accuracy in-field and nearby regions, while noticeable underestimation for isodoses smaller than 5% can be found. These estimations are shown to dramatically deteriorate with increasing distance and may lead to errors in the order of 20-80% ([Huang et al.,2013](#); [Howell et al.,2015](#); [Newhauser et al.,2016](#)). On the other hand, Monte Carlo (MC) simulations need of a high level of fidelity for linac modeling, especially when considering doses for peripheral zones. In addition, in-field and out-of-field simulations should be benchmarked to experimental measurements ([Xu et al.,2008](#); [Berdnarz et](#)

al.,2010). It is known that these experimental measurements of PD in the clinic may be overestimated from real values when made following accuracy recommendations (Howell et al.,2015). Thus, the knowledge of the magnitude of this inaccuracy might be of important relevance for some specific groups of patients, such as pregnant women and children, to avoid compromising treatment quality (Lefebvre et al.,2014).

Commercial dosimeters usually employed for both neutron and photon PD measurements present several limitations, mainly regarding three features (additional problems may be found concerning neutrons, Nath et al., 1986; NCRP-79):

- Radiation field: average photon beam energy spectrum is much lower in these peripheral regions. Neutron fluence rates are also difficult to evaluate, as a consequence of the large photon to neutron ratio present in these environments.
- Pulse pile-up problems in detectors employing electronic pulse measurements.
- Detector response: correction factors are usually needed for these photon low energies to avoid detector over-estimation. Response of neutron detectors depends on incident neutron energy and fluence-to-dose conversion factors strongly vary with spectra.
- Special attention is required concerning tissue equivalences.

Additional problems may be found for superficial locations (i.e. skin), due to the presence of stray electrons and higher photon and fast neutron contributions.

Usually peripheral photon, electron and neutron doses from RT (either X-ray or proton beams; energy ranging from 4-250 MeV) are in the range of 5 cGy for low-dose levels and 5-50 Gy for the intermediate ones (primary target receiving ≤ 100 Gy). When compared to other treatment modalities, these dose values may

result 5 times those of brachytherapy (regarding peripheral organs), around 100 times those of conventional radiodiagnosis images and on the order of radioimmunotherapy ones (concerning gamma doses; [Xu et al.,2008](#)).

2.1 Photon peripheral dose

Photon doses delivered outside geometrical field limits and surrounding tissues are referred to as Peripheral Photon Doses (PPD). In clinical photon beams, these doses are produced by photons originated from: (i) linac head leakage, (ii) linac head scatter and (iii) scatter radiation inside the patient ([Chofor et al.,2012](#)).

Although this component is the most studied one, as a consequence of the well-established photon dosimetry procedures, its estimation in peripheral organs is complex. Despite the fact that there are some algorithms and software available for the calculation of photon absorbed doses ([Taddei et al.,2013](#); [Jagetic et al.,2013](#); [Van der Giessen et al.,2001](#); [Hauri et al.,2016](#)), to our knowledge there was no general model that could be readily applied to any RT treatment. The mentioned methods seem to be too narrowly focused, either in terms of available energies or treatment field configurations. What is more, although there are other studies containing baseline data for specific treatment techniques, they seem to be not generalizable to other circumstances.

As an appropriate study of PD and second cancer risks may consider both contributions, our group was also highly interested in the evaluation of these PPD. Thus, along the duration of this work, close collaborations have been carried out with Dr. Beatriz Sánchez-Nieto for the generation of a clinically useful simple PPD model, applicable to any isocentric treatment and usable beyond 10 cm far from the field edge ([Sánchez-Nieto et al.,2015a;b](#)). This model accounts for linac head leakage, patient and linac head scatter, as well as activation, if any.

2.2 Neutron peripheral dose

The use of high photon energies is generally preferred to improve treatment effectiveness and decrease skin dose in deeply settled tumors. For this purpose, linacs up to 25 MeV (primary electron beams) were originally manufactured. However, as these photon beams are obtained by means of electron bremsstrahlung in a metallic target with a high atomic number (e.g., tungsten, gold) there is an unavoidable neutron production. These primary neutrons are approximately isotropic and can penetrate the shielding (usually tungsten or lead) in all directions. Additionally, secondary neutrons can be produced in photonuclear reactions with the high Z materials that compose linac head for photon shielding and collimation purposes (Figure 4). Electronuclear ($e, e'n$) and photonuclear (γ, n) reactions can also take place as a consequence of the interaction of high-energy photons (greater than photonuclear reaction threshold of the present materials) with Fe and Cu (NCRP-79).

The minimum energy required to remove one neutron from a nucleus lies between 6-16 MeV (6-13 MeV for most stable nuclei, those heavier than carbon), for the majority of constituents of RT bunkers. As a consequence, a wide variety of short-life radionuclides are generated via photon and neutron activations. In order to minimize this contribution, generally materials present in RT facilities are chosen to have a negligible neutron production for megavoltage photon modalities below 10 MV (Uselmann et al., 2015). Although neutrons can be also produced by other reactions as ($\gamma, 2n$) and (γ, pn), they have smaller cross sections and are thus considered to be less relevant (Sánchez-Doblado et al., 1989).

Different works have challenged the estimation of Peripheral Neutron Doses (PND) from a clinical point of view. Although their initial conclusion showed a minimal importance for exposed professionals and patients, later publications

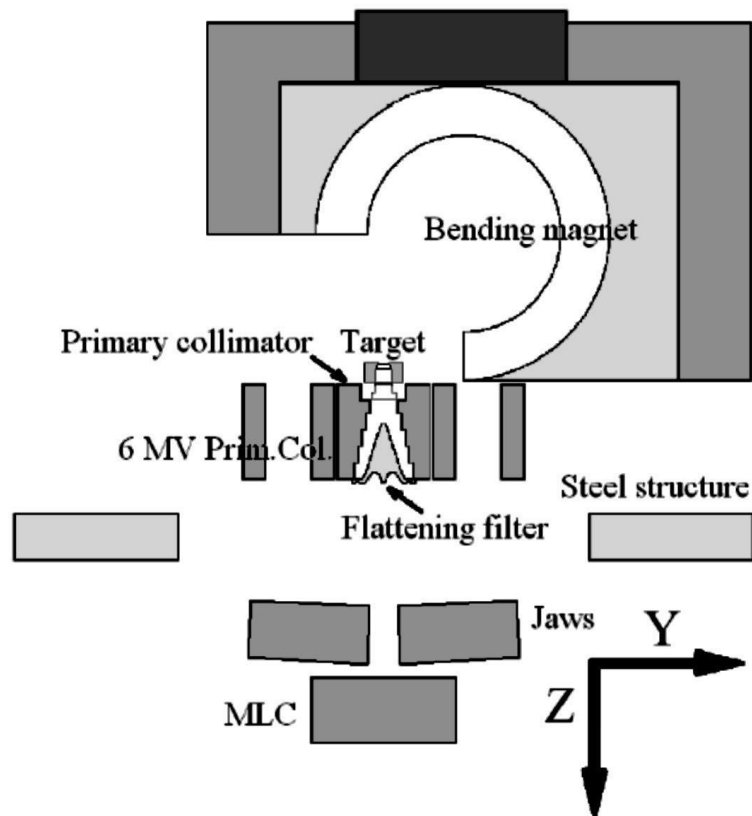


Figure 4. Sketch of head components of a Siemens Primus linac geometry. The different components responsible for photo-neutron production in high energy (>10 MV) are plotted: lead (black), tungsten (grey) and steel (light grey). Figure extracted from (Pena et al.,2005).

presented a more precise scenario of neutron energy and fluence distribution in treatment rooms, related to linac manufacturer, energy and bunker size (Kry et al.,2009; Howell et al.,2005;2009; Followill et al.,2003).

However, as previously mentioned, this is hardly ever considered in clinical routine, as there is no commercial TPS that includes information regarding neutron contribution. This fact can be justified by the high photon doses delivered at the studied locations, compared to the peripheral neutron ones. However, PND may become equally important than PPD for some peripheral tissues, due to the higher neutron Relative Biological Effectiveness (RBE, Ottolenghi et al.,2015). As a consequence, modern RT is mainly oriented to low energy

treatments, sometimes to the detriment of conformity and using longer beam-on times. This is justified by the pretext of avoiding damage to biological tissues and preventing from latter complications due to neutrons.

2.2.1 Evaluation of neutron dose: detectors

Neutron dose measurement inside radiotherapy rooms is a mandatory task that has to be performed accomplishing some requirements (Thomas et al.,1973):

- (i) Measurement of neutron fluence ($\text{n}\cdot\text{cm}^{-2}$)
- (ii) Measurement/simulation of neutron spectrum as a function of energy inside the treatment room ($\text{n}\cdot\text{cm}^{-2}\cdot\text{MeV}^{-1}\cdot\text{s}^{-1}$)
- (iii) Measurement of total dose equivalent
- (iv) Study of neutron detector response to other radiations that may be present in RT mixed fields

Neutron energy spectra present in RT environments can be divided into three regions: thermal (< 0.4 eV), epithermal (0.4 eV $< E < 0.1$ MeV) and fast (> 0.1 MeV). However neutron dosimetry is a very complex task and there is no single detector commercially available that can perform all the above detailed measurements. Consequently, detector choice must be done regarding the specific purpose of the experiment. As neutrons are uncharged particles, these devices are based in the detection of particles resulting from their interaction with atomic nuclei. The most commonly used neutron devices can be divided in two main groups, some of the most typical ones are shown in [Figure 5](#) as an example (NCRP-79).

(a) Passive detectors

These kinds of detectors are the most used ones due to their good response to the pulsed nature of RT radiation. However their complex and delayed reading procedures make their use non-ideal for research or clinical purposes, where measurement repetitivity and online behavior is an important aspect.

- *Activation detectors.* These devices are based on the use of specific materials that become radioactive when exposed to neutrons (Figure 5a). This behavior may result from capture reactions as inelastic scattering; (n,p) (n,α) or $(n,2n)$ reactions; nuclear reactions or spallation reactions. Activation samples are typically used to characterize energy spectrum and neutron field intensity.

- *Etched Track Detectors.* These types of detectors are composed of a particular kind of solids that present microscopic radiation damage tracks when irradiated with heavy particles. These tracks can be made visible under a microscope in a variety of dielectric materials (Figure 5b).

(b) Active detectors

These detectors present an online behavior, highly desirable for research purposes. Nevertheless, several problems related to saturation, response dependencies and detector size can be found in the existing devices.

- *Ionization Detectors.* Ionization chambers, and proportional and Geiger-Müller counters, are included here (Figure 5c). They provide large electronic signals and good discrimination against a relatively small photon background, being usually employed for ambient measurements due to their large size.

- *Diodes.* Neutron-induced nuclear reactions can produce measureable changes in the electrical properties of various semiconductors (Figure 5d). The most common radiation damage is the displacement of lattice atoms, as in the case of diode detectors.

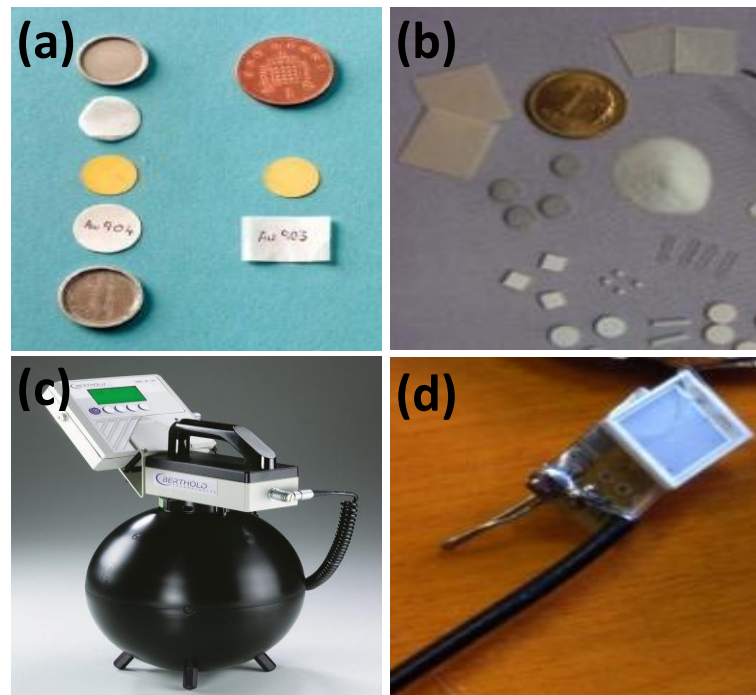


Figure 5. *Passive: (a) Activation foils, (b) track-edge and Active: (c) proportional counters and (d) diode detectors.*

Passive detectors require considerable processing and analyzing times while active counters show signal saturation and pile-up due to the pulsed nature of linac radiation. Therefore, methods traditionally used for neutron evaluation have been the first ones, as recommended by the American Association of Physicists in Medicine (AAPM) and the National Council on Radiation Protection & measurements (NCRP, [Nath et al.,1986](#)). However, our group succeeded in the introduction of a new active detector in RT environments for peripheral neutron dose estimation purposes ([Gómez et al.,2010a](#); further details can be found on section [2.4.2](#)).

2.2.2 Evaluation of neutron dose: calibration sources

As for any other detectors, neutron devices have to be calibrated (and tested in terms of stability) against reference neutron sources to ensure appropriate estimations. A wide variety can be employed for this purpose (NCRP-38;151):

- *Natural radioactive neutron sources type (α,n) or (γ,n).* In the first case, the alpha emitter is mixed with the target material, being the most common ones ^{210}Po , ^{239}Pt and ^{241}Am , usually combined with Be. The latter are generally surrounded by the material in which neutron reaction takes place.

- *Spontaneous fission neutron sources.* They present small mass and a fission-like spectrum with relative low gamma-ray yield. Special caution must be taken when manipulating, as many alpha rays are produced per neutron. A nuclide of special interest is ^{252}Cf .

- *Constant voltage accelerators.* Used to produce high voltage proton beams by mechanical transportation of charge using a belt (Van der Graaff accelerator) or other alternative systems that imping into a specific target to produce neutrons. Large number of neutrons ($>10^{22} \text{ s}^{-1}$) can be achieved depending on incident beam and target nature. In some cases, like PTB laboratory (Physikalisch-Technische Bundesanstalt), monoenergetic beams can be achieved in the range of 24 KeV-19 MeV.

- *High-frequency positive ion accelerators (including cyclotron, synchrocyclotron, proton synchrotron and heavy ion linear accelerators).* These pulsed beams can produce a neutron spectra spread over a wide range of energies.

- *High-frequency electron accelerators (including circular betatron and synchrotron and linear accelerators).* Although primary radiation are X-rays, these accelerators can produce large numbers of neutrons depending on target nature, by terms of (γ,n) reactions.

- *Nuclear reactors.* Here neutron production occurs as a result of the fission process, achieved by a definite arrangement of fuel (uranium or plutonium), moderator (light or heavy water, beryllium or graphite) and neutron absorbers. Neutron energies range from thermal to over 15 MeV, with many gamma rays present.

Some studies have already pointed out the importance of primary and secondary reference neutron fields for calibration of these instruments as necessary for advances in research methodologies ([Newhauser et al.,2016](#)). An additional problem concerning the use of neutron detectors in radiotherapy environments is the great change of the neutron spectra with increasing depth in tissue. This can generate misleading in readings of some detectors when used for different locations for 'in-phantom' measurements. Thus, the ideal choice for neutron measurements in clinical environments would be a combined use of different devices. Besides, the variable attenuation and scattering that neutrons undergo when trespassing human body implies the need of MC simulations to fully determine neutron fluences at any point. MCNPX code is typically used to simulate neutron spectra inside RT rooms and patients. Calculation of this neutron spectrum may need information related to bunker and phantom geometries as well as linac composition, in order to obtain the most realistic photoneutron spectrum possible. Moreover, neutron photoproduction strongly depends on nominal energy of initial electrons, and a whole commissioning process, with accurate information about linac head composition is also desirable ([González-Soto et al.,2011](#)). Thus, in order to provide adequate PND estimations, data should be based on a combination of both experimental measurements and simulations in air and phantom locations.

2.3 Equivalent neutron doses and risk evaluation

As previously stated, the RBE factor highly depends on radiation type (e.g., photons, neutrons, electrons) as well as particle energy, dose and biological endpoint. Peripheral dose estimations previously detailed represent a former step for the evaluation of Second Cancer Probability (SCP) related to radiotherapy treatments. Photoneutron spectrum varies along the patient, presenting thermal, epithermal and fast neutron fluence components; the latter especially important for superficial points and decreasing for deeper positions, due to neutron thermalization. In consequence, for an adequate organ neutron dose estimation, experimental measurements and MC simulations should be performed for different locations and depths in anthropomorphic phantoms. However, as previously explained, there is no single detector able to measure total neutron fluences and they are usually estimated in terms of the thermal component, which is the simplest one to measure.

For PND estimations in radiotherapy environments, *dose equivalent at a point* and *organ-equivalent dose* are the most significant magnitudes (Romero-Expósito et al.,2016). The first one can be defined as follows:

$$H_T = D \cdot Q = \int_m \int_{LET} Q(LET) \cdot D_L \cdot dL \cdot \frac{dm}{m} \quad (\text{eq. 1})$$

where D_L represents absorbed dose, Q is the quality factor for the specific radiation and integrals range over unrestricted Linear Energy Transfer (LET) and mass of the studied organ (m). Although Q factor is difficult to evaluate due to its dependence on particle energy, recent publications (Romero-Expósito et al.,2016) demonstrated that dose equivalents calculated using Q and the much simpler radiation weighting factor w_R (introduced by ICRP-103) are compatible. Thus eq. 1 can be rewritten as:

$$H_T = \sum_T w_R \cdot D_{T,R} \quad (\text{eq. 2})$$

According to ICRP definition, *Equivalent Dose* (H [Sv]) is a protection quantity calculated as the averaged *absorbed dose* (D [Gy]) in an organ or tissue T multiplied by radiation weighting factor w_R (ICRP-103). For low-dose levels, this factor is used as a conservative and simplified measure of RBE (Figure 6), taking into account different particle nature, concerning radiobiological effect ($w_R(\text{photons/e})=1$, $w_R(\text{neutrons})=2.5-20$ depending on their energy). On the other hand, *Effective Dose* (E [Sv]) corresponds to the mean dose in organs or tissues of the whole human body, weighted by their radiosensitivity. This quantity is usually employed to indicate whole-body stochastic risk.

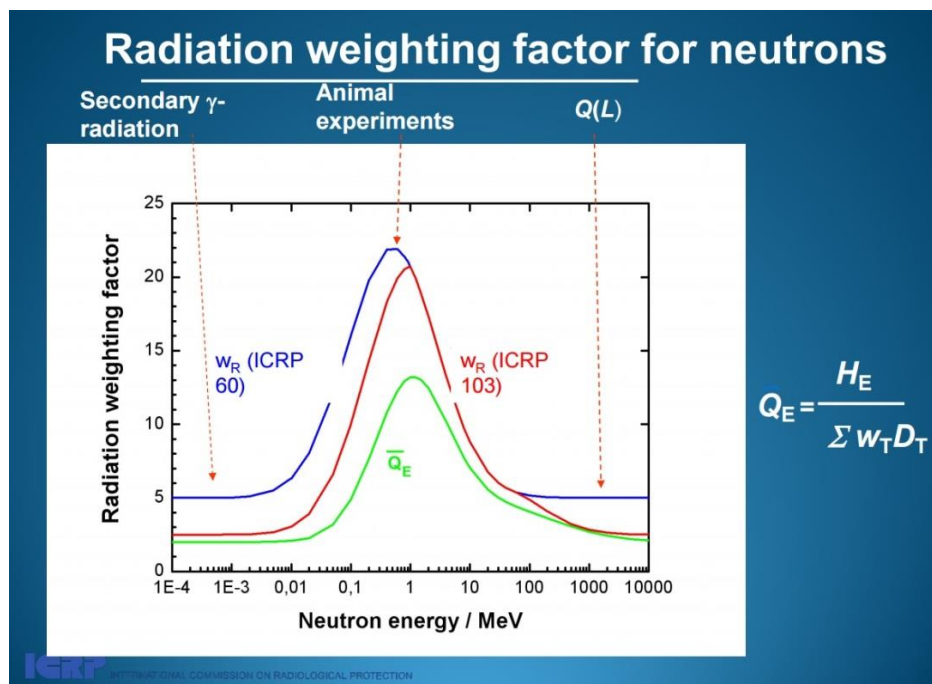


Figure 6. Different radiation weighting factors and dependence with neutron energy.

Extracted from:

http://www.eurados.org/~media/Files/Eurados/events/7thwinterschool/4_Menzel%20Hans_Current%20Approach%20to%20Radiation%20Quality%20Specification%20in%20Radiation%20Protection.pdf?la=en.

As previously mentioned, the main knowledge regarding ionizing radiation effects on humans comes from atomic-bomb survivors, who suffered acute radiation exposures over a very short period of time. However, this exposure implied different biological damage mechanisms than those generated by radiotherapy, concerning low doses delivered in non-prolonged exposures separated in fractionated intervals. In consequence, there is still great debate on how this relationship can be extrapolated to radioinduced SMNs. SCP due to peripheral neutron and photon doses can be calculated using [eq. 3](#), taking special attention to the Dose and Dose-Rate Effectiveness Factor (DDREF) for neutron contribution ([Expósito et al.,2013](#)):

$$SCP = \lambda \cdot w_R \cdot D \quad (\text{eq. 3})$$

where *Equivalent doses* ($w_R \cdot D$) are multiplied by λ risk factors, established by [ICRP-103](#) or [BEIR IV](#) (Biological Effects of Ionizing Radiation) models. This second cancer risk estimation factors are derived from the Lifetime Attributable Risk (LAR), representing the probability of an individual to develop (or die) from a disease associated to the irradiation. LAR values are obtained from the ERR (Excess Relative Risk: rate of an effect in an exposed population divided by the rate of the effect in an unexposed population minus 1) or EAR (Excess Absolute Risk, rate of an effect in an exposed population minus that of the effect in an unexposed population) over the expected lifetime.

Currently existing epidemiological data have shown that an exposure above 50-100 mSv can produce an increase on SCR among two of the most common cancer sites within 30 years after the RT treatment ([Travis et al.,2003](#); [Hung et al.,2016](#)).

2.4 Peripheral neutron dose models

The project lead by the Medical Physics Group of the University of Sevilla was based on the estimation of neutron equivalent dose in organs of patients undergoing high energy (≥ 10 MV) RT, by terms of a correlation model. This methodology associates readings from a neutron digital detector (located in the room, far from the patient) to equivalent doses at different locations inside an anthropomorphic phantom.

One of the main problems was finding appropriate coefficients that correlated measured neutron fluences with equivalent doses at any point. Although [ICRU Report 57](#) provides factors for the estimation of *ambient dose equivalent* $H^*(10)$, *personal dose equivalent* in a slab phantom (for several incidence angles) and *effective dose* E (for complete body external irradiation at some specific geometries), these conditions are far from that of RT treatments. However the group succeeded in the implementation of a methodology for the systematic evaluation of these equivalent doses (eq.2) by the convolution of normalized Monte Carlo neutron spectra with the kerma factor (k , [Siebert et al.,1995](#)), radiation weighting factor (w_R , [ICRP-103](#)) and measured thermal neutron fluences (Φ_{th}) at every phantom point (see [2.4.3](#)). Neutron equivalent doses were then correlated to readings from a SRAM-based online digital detector ([Gómez et al.,2010b](#); [Domingo et al.,2010a](#); [Sánchez-Doblado et al.,2012](#)) used to estimate thermal neutron presence in the room. Before generating this methodology, several topics here summarized had to be addressed:

2.4.1 *SRAM detector*

Introduced by our group, this device is based on the neutron-induced Single-Event Upset (SEU) phenomenon that takes place in Static Random Access Memories (SRAM) when radiation LET overcomes their threshold ([Vázquez-](#)

Luque et al.,2013; NCRP-151). In addition to the active behavior, its high photon rejection makes this device especially useful in RT facilities.

This detector (Figure 7) was present during all the experiments performed to generate the neutron equivalent dose models, located inside the treatment room in an external position considered as the reference, as detailed in Figure 8 (Romero-Expósito et al.,2015). A previous exhaustive study was performed in order to identify the most suitable location for this device inside the treatment room in order not to disturb the patient and obtain a uniform thermal neutron dose response, for all the possible bunker configurations (Jiménez-Ortega et al.,2011).

This allows the later correlation of different phantom measurements to detector readings at the reference location, performed during patient treatments. The goal was the direct estimation of organ doses by terms of a single measurement with the active detector located inside the room, during at least one of the RT sessions.

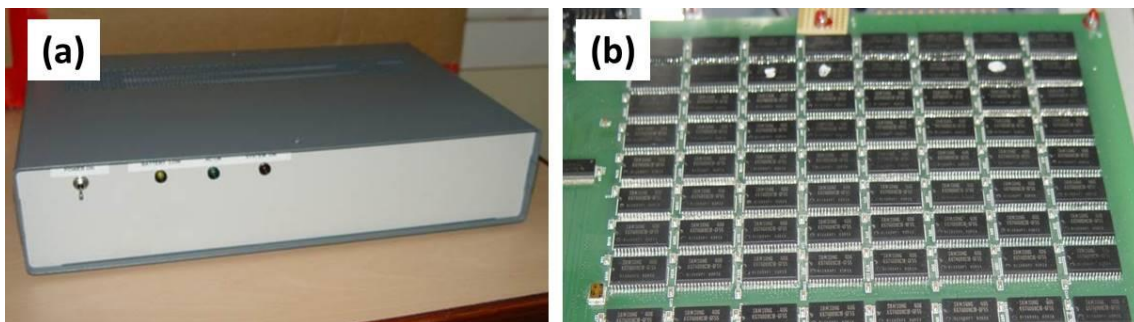


Figure 7. SRAM based detector (a) exterior and (b) interior (128 SRAM memories).

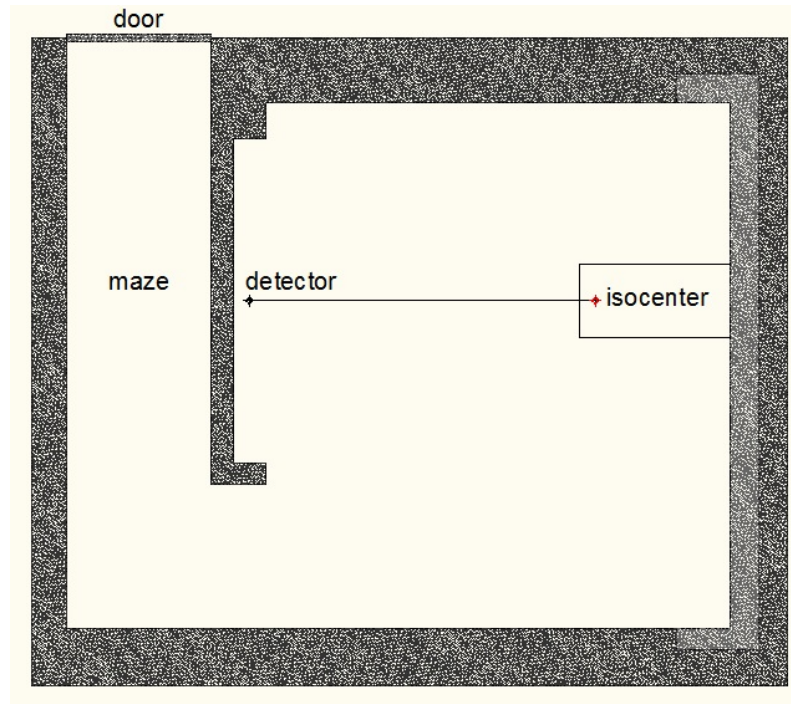


Figure 8. Detector reference location in an example of the usual RT bunkers geometry.

2.4.2 Monte Carlo simulations

To characterize neutron spectra at measuring points, a detailed study of photoneutron field in the radiotherapy treatment room and inside each phantom point was performed by terms of Bonner Sphere Spectrometers (Domingo et al.,2009;2010b) and MC simulations (González-Soto et al.,2012a;b). A combination of both data was used to obtain the normalized neutron spectra at each calculation point. Full Monte Carlo simulations were carried out for a Siemens Primus linac (Hospital Universitario Virgen Macarena, Sevilla) (Figure 9).

Although the thermal component of total neutron fluence resulted almost uniform in the treatment room, fast component demonstrated to be inversely proportional to the square of the distance to the source. Dependences of these

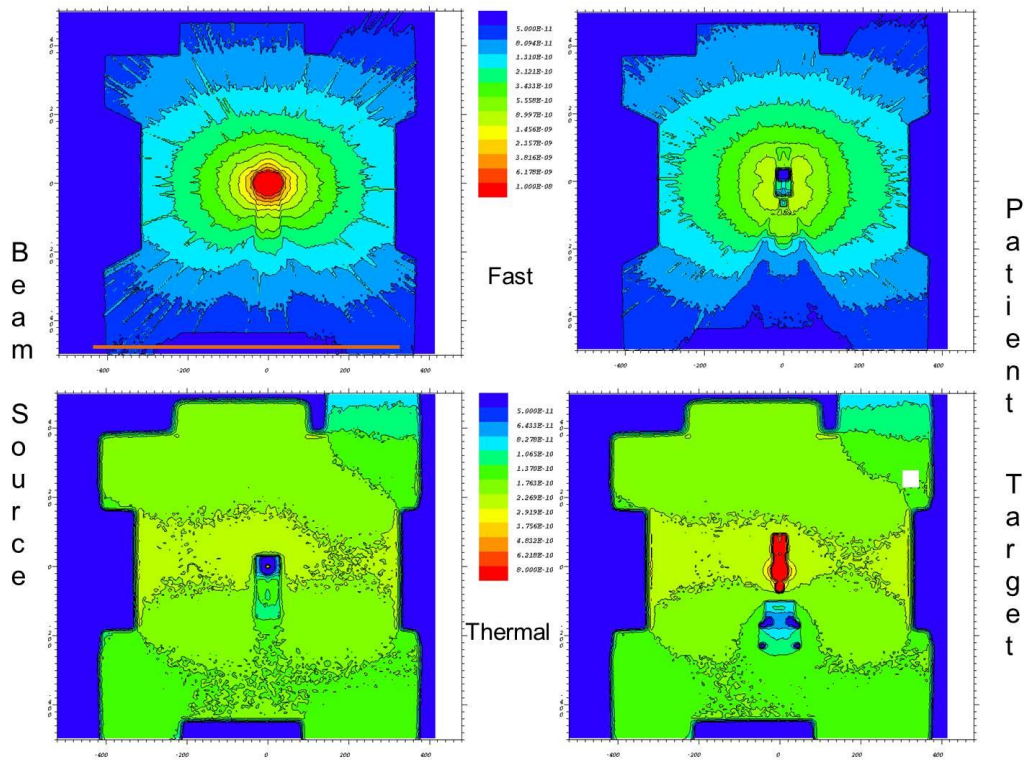


Figure 9. MCNPX simulation of fast (up) and thermal (down) neutron fluence distributions inside the reference bunker at beam source (left) and patient (right) plain levels. Extracted from [González-Soto et al. 2012a](#).

spectra with several parameters, such as field size, linac energy and manufacturer, were evaluated and compared to experimental measurements ([Sánchez-Doblado et al.,2012](#)).

Simulations and experimental measurements sagreed in different neutron production for each manufacturer, with small dependences on neutron spectrum regarding linac energy (affecting only the total number of neutrons generated). Neutron spectra demonstrated to be independent of the field size (ranging from 2x2 cm² to 20x20 cm²) and gantry angle incidence for midline points. Differences found for other positions were considered as negligible, bearing in mind the circular geometry of usual RT treatments around the isocenter. Finally, a variation in neutron spectra was found for the studied points when considering different treatment locations.

Taking into account these results, two generic models¹ were performed for Head and Neck (H&N) and abdomen locations, grouping the majority of high-energy pathology locations. Normalized neutron spectrum inside the phantom $\{\varphi_{i,j}(E)\}$, are shown for some calculation points in [Figure 10](#) for both treatment locations, being valid regardless of nominal energy, machine manufacturer, field size and gantry angle.

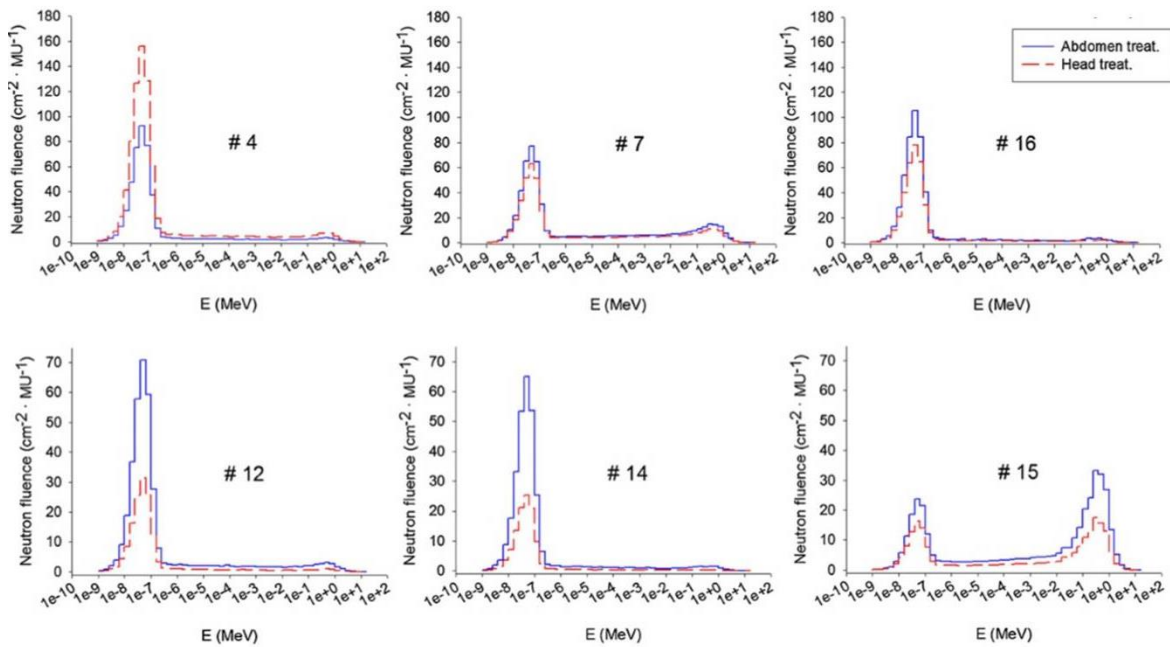


Figure 10. Neutron fluence spectra simulated inside NORMA phantom using a Siemens Primus linac in 15 MV for H&N (red) and abdomen (blue) conformal treatments¹ for six representative points. Plot extracted from [Sánchez-Doblado et al.2012](#).

In order to model the dependence of neutron fluences with room size, MC simulations were also performed for different bunker geometries, obtaining a fitting function where one of the bunkers of Hospital Universitario Virgen Macarena was used as the reference ([Sánchez-Doblado et al.,2012](#)).

¹Conformal treatments consisting on 8 equispaced irradiations (every 45°) of 125 MU in 10x10 cm² fields with source to axis distance of 100 cm (SSD= 93 and 91 cm respectively for H&N and abdomen locations). Isocenter location is represented as *H* and *A* in [Figure 7](#).

2.4.3 Anthropomorphic phantom measurements. NORMA phantom

An anthropomorphical adult phantom was designed to mimic neutron interaction with human body. In order to correctly simulate this behavior of human tissue, several materials were previously studied (Domingo et al.,2011). Finally, polyethylene was chosen as a surrogate of human tissue and low-density wood was used to simulate lungs (Figure 11). For organ dose estimation, sixteen accommodations for passive detectors (plastic and thermoluminescent, TLD) were chosen as representative for organ location in the human body (Sánchez-Doblado et al.,2012). Correspondence among the 16 NORMA measuring points and patient organs for is shown in the Table of Figure 11. These correspondences were done by comparing NORMA anthropomorphic phantom to the reference mathematical one, named *Cristy*.

2.4.4 Neutron equivalent dose in organ and second cancer risk estimation

Neutron equivalent doses for each point in NORMA phantom were evaluated, from eq.2, considering kerma approximation² and using previously mentioned convolution procedure, described in the following equation:

$$H_T = \Phi_{th} \int_E k(E) \cdot \varphi(E) \cdot w_R(E) dE \quad (\text{eq. 4})$$

²Absorbed dose can be approximated by factor kerma as follows: $D=k \cdot \Phi$. Equivalent dose can be then calculated by: $H_T=w_R \cdot D$ introducing neutron radiation weighting factor (w_R ; ICRP-103). Differences between dose equivalent and equivalent doses are much smaller than neutron measurement uncertainties making this approximation as acceptable for this purpose (Romero et al.,2016)

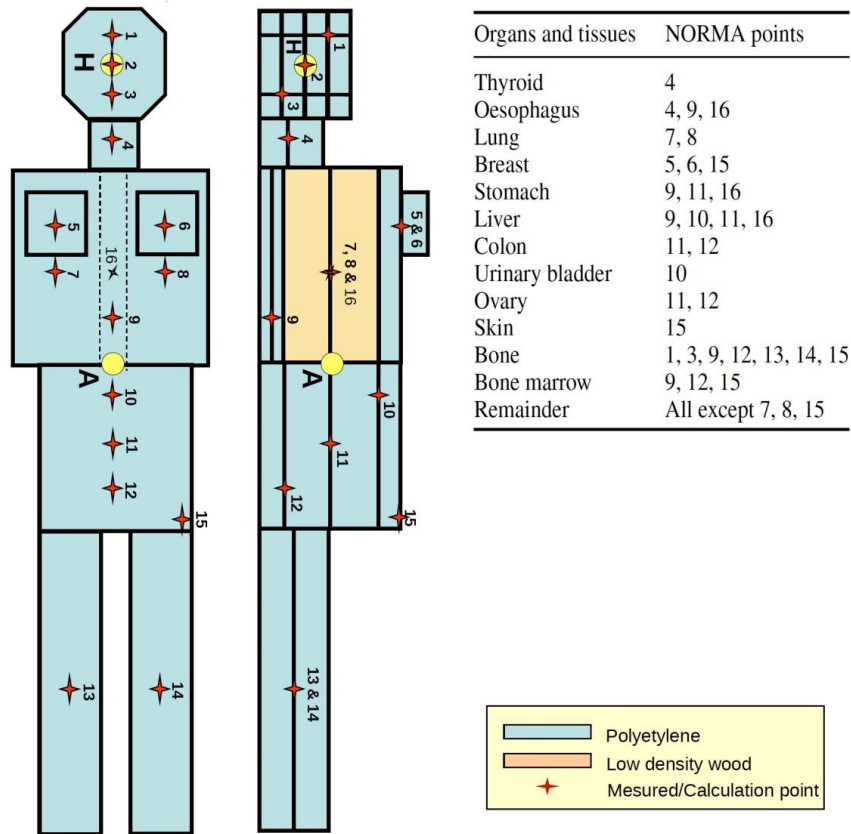


Figure 11. Scheme of the NORMA phantom composition and point location. Table in the right correlates these points with evaluated patient organs. Figure modified from [Sánchez-Doblado et al.2012](#); [Expósito et al.,2013](#).

where:

- Φ_{th} : thermal neutron fluences measured by the passive detectors located inside the phantom
- $k(E)$: kerma factor for ICRU tissue ([Siebert et al.,1995](#))
- $\varphi(E)$: MC neutron fluence energy spectra, normalized to the thermal contribution
- w_R : energy-dependent radiation weighting factor from [ICRP-103](#)

Two types of passive detectors (PADC and TLD) were used for the measurement of neutron fluences at the 16 i -points inside NORMA for the two j -studied treatments (Sánchez-Doblado et al.,2012). Due to their different sensitivity to thermal, epithermal and fast components, a combination of both readings was used to correctly rescale total neutron fluence Φ from MC simulations, depending on treatment location and specific point.

The methodology established by this group for peripheral neutron dose calculation, was designed to directly estimate SCP to 13 organs from the total number of high-energy MU received by the patient during the whole treatment, differentiating between two different treatment locations (Sánchez-Doblado et al.,2012; Expósito et al.,2013). A linear relation depending only on facility characterization, in terms of neutron production, was obtained. Thus, a simple commissioning for every facility is needed. This procedure consists in 3 single measurements at the reference location with a SRAM-based detector (Romero et al.,2015). Thus SCP, in cases per 1000, for an organ $-k$ using model $-j$, can be calculated as follows (Sánchez-Doblado et al.,2012):

$$[SCP]_{k,j} \left(\frac{\text{cases}}{1000} \right) = c \left(\frac{\text{events}^*}{1000} \right) \cdot N(MU) \cdot s \cdot \left[\frac{[g]_{k,j} \left(\frac{\mu Sv}{\text{event}} \right) \cdot [\lambda]_{p,k} (\% \text{ per Sv})}{10} \right] \text{ (eq. 5)}$$

where:

- c represents the characterization factor, obtained for each facility by following the procedure detailed in Romero-Expósito et al.,2015. This factor has two dependencies: one in terms of detector used, which has to be referred to events of the reference device (F_C) and the other related to bunker surface (F_A), taking into account the effect of room size on thermal neutrons distribution.
- N is the total number of high energy MU delivered in one session of the treatment.

- s is the total number of sessions that contain high energy along the whole treatment.
- $g^{k,j}$ are the factors that correlate neutron equivalent dose in organ $-k$ (μSv) to events of the digital reference detector for each treatment $-j$ (Table I).
- $\lambda_{p,k}$ risk factors for organ $-k$ tabulated by $-p$ protocol (BEIR VII or ICRP-103), that correlate neutron doses to second cancer risk probabilities.
- factor 10 was introduced to express the result in cases per 1000.

According to this expression, the previously mentioned locations were considered to encompass the most common RT treatments. Then, $g^{k,j}$ factors were estimated from the combination of MCNPX simulations and passive detectors readings, giving values presented in Table I.

Table I. Neutron equivalent dose in organ (μSv) per event at the SRAM-based detector, corrected by the area factor at digital device ($g^{k,j}$), for the two general treatments. Sex is considered when selecting affected organs. Extracted from (Sánchez-Doblado et al.2012; Expósito et al.,2013).

Organ	Head Treatment	Abdomen treatment
Thyroid	0.71 ± 0.21	0.37 ± 0.11
Esophagus	0.45 ± 0.13	0.65 ± 0.19
Lung	1.32 ± 0.40	2.22 ± 0.67
Breast	0.66 ± 0.20	1.62 ± 0.49
Stomach	0.22 ± 0.07	0.55 ± 0.16
Liver	0.23 ± 0.07	0.69 ± 0.21
Colon	0.05 ± 0.01	0.21 ± 0.06
Urinary bladder	0.27 ± 0.08	1.11 ± 0.33
Ovary	0.05 ± 0.01	0.21 ± 0.06
Skin	2.64 ± 0.79	2.64 ± 0.79
Bone surface	0.50 ± 0.15	0.96 ± 0.29
Red marrow	0.57 ± 0.17	1.90 ± 0.57
Remainder	0.38 ± 0.11	0.41 ± 0.12

These models allow the estimation of SCP (cases per 1000) for 13 organs for two different treatment locations. However, the appearance of new online active

miniaturized thermal neutron detectors, open the door to further investigations in order to improve and generalize these models. The advantage of the new detectors chosen, named *TNRD* (*Thermal Neutron Rate Detector*), was the possibility of performing online measurements at external and 'in-phantom' locations, directly in terms of thermal neutron fluences with the same device (Bedogni et al.,2014). This would allow the generalization of the established methodology to be expressed in terms of thermal neutron fluence, without the need of referring data to the reference detector (in terms of SEU, Gómez et al.,2010b; Domingo et al.,2010a; Sánchez-Doblado et al.,2012). In addition, the active and miniaturized behavior would allow the verification and optimization of these models, as well as the introduction of patient anatomy and treatment technique influences (different locations and available techniques).

II. Hypothesis and objectives

The acquired new miniaturized active thermal neutron detectors (*TNRD*), initially designed for nuclear purposes, can be used for patient dosimetry in radiotherapy. The use of these devices for peripheral neutron dose estimations would be useful not only for online patient measurements following the previously established methodology, but also for 'in-phantom' measurements. This would allow the improvement of the previously existing models, consisting on Head & Neck and abdomen locations for adult phantom, to more patient specific ones, including patient size. This methodology can be also generalized to be expressed in terms of thermal neutron fluences, thanks to its dual use. This would represent a previous step to model implementation in Treatment Planning Systems for risk evaluation in clinical routine. Peripheral neutron and photon doses could be then considered as an objective decision tool for treatment selection strategy.

Thus, the main objectives of this work are:

1. Validation and characterization of the new *TNRD* thermal neutron detectors with the previously existing ones for their use in radiotherapy environments for both patient and 'in-phantom' measurements.
2. Guarantee the validity of the existing models by terms of the new existing detectors.
3. Adapting detectors setup to clinical environments considering electronics capability, as well as improving photon rejection for radiotherapy backgrounds.
4. Enhancement of the existing models ensuring the reproducibility of 'in-phantom' measurements.

II. Hypothesis and objectives

5. Generalization of the currently existing models for peripheral neutron dose estimations, to express them directly in terms of thermal neutron fluence. Introduce patient dimensions by measuring different phantom sizes, performing patient measurements and comparing estimations for specific real cases.
6. Clinical implication: evaluation of peripheral doses (neutron and photon) for different treatment locations, techniques, energies and linacs. Establishing a model that can be applied in the clinic for peripheral dose assessment and second cancer risk estimations.

III. Thesis core

This section describes the body of this work, firstly introducing the necessity and purpose of each experiment. Then, a brief description of the methodology and measurements carried out will be presented. Finally, a selection of the main related publications concerning each topic will be added to illustrate accomplished results and conclusions. A total of six full papers have been added within the body of the text (framed and highlighted in light beige) in this chapter, being published, accepted or sent to journals in the first tercil. In addition, seven short publications containing partial results, also published in indexed journals and two in the World Congress on Medical Physics & Biomedical Engineering as full paper, have been included in the Appendix.

1. Introduction

(A) Characterization of a new active thermal neutron detector

The newly acquired Thermal Neutron Rate Detector (*TNRD*) is a miniaturized active thermal neutron detector initially designed for nuclear purposes. Therefore former to its introduction for peripheral dose measurements, the acquired prototypes had to be tested and adapted for clinical routine. For that:

- (i) Detectors were irradiated under several conditions in order to verify their adequate response in RT environments. *TNRD* readings were correlated to those of the SRAM-based reference detector, in order to establish a calibration factor. In addition, as pulsed neutron signals have to be measured under an intense photon background, linear response and reproducibility were studied under these specific conditions ([Terrón, Irazola et al.,2014](#), **Appendix A.1**).

- (ii) *TNRD* ‘external’ thermal neutron measurements, were compared to those of the reference detector by using the established methodology for the online assessment of second cancer risk in radiotherapy patients ([Irazola et al.,2014a](#), **Appendix A.2**).
- (iii) In order to use these devices for the enhancement of the existing models, consisting in the correlation among readings of a reference detector (located in the room) and neutron dose estimations in several phantom points ([Sánchez-Doblado et al.,2012](#); [Expósito et al.,2013](#)), ‘in-phantom’ measurements had to be performed with *TNRD* devices. Preliminary results were compared to those of TLD devices, previously used for this purpose ([Sánchez-Doblado F, Irazola L et al.,2014](#), **Appendix A.3**).

(iv) Thermal neutron fluences were evaluated with TLD and *TNRD* detectors in all the phantom points for the two general treatments (H&N and abdomen), as well as a real IMRT one. Once both ‘external’ and ‘in-phantom’ uses of *TNRD* detectors were validated against reference detectors, we were able to ensure the use of these new devices for the final purpose of improving the existing peripheral neutron dose models. These global results, regarding *TNRD* use in radiotherapy environments, were published in Medical Physics journal ([Irazola et al.,2014b](#), **Section III.2.A**).

(B) Limitations and solutions of *TNRD* detectors in radiotherapy environments

The prolonged use of *TNRD* devices for ‘external’ and ‘in-phantom’ measurements in clinical routine, showed several incongruences in detector response over time:

- (i) A different loss in sensitivity to thermal neutron fluences was noticed for each one of the six available TNRD detectors after 9 months of continuous use. Meaning a possible different detector ageing in time, we decided to recalibrate them in a new thermal neutron source available at INFN, Frascati (Bedogni et al.,2016). In addition, we thought that having the option of periodically verify their stability under an external neutron source would be highly desirable. The neutron beam available at Centro Nacional de Aceleradores (CNA, Sevilla), seemed to be a good option, considering the proximity of this facility and its relation to the University of Seville. Several measurement tests and MCNPX simulations were performed in order to achieve an appropriate thermal neutron beam and detector setup. The goal was to obtain a stable beam that provided thermal neutron fluences in the order of those from calibration conditions at detector location, avoiding photon presence as much as possible. Preliminary results were published as a short work in Radiother Oncol (Praena et al.,2015). Final configuration concerning not only the validation of this source for the study of TNRD stability verification, but also bringing to light the possibilities available at the Pelletron Tandem accelerator of CNA, was published as a full article in Applied Radiation and Isotopes (Irazola et al.,2016a, **Section III.2.B.1**).

- (ii) Uncertainties introduced by the possible loss of signal, as a consequence of the necessary cable extension and/or cable irradiation throughout 'in-phantom' measurements may also represent a minor problem. Initial TNRD cable length showed problems when trying to reach different NORMA phantom points at the same time. Thus, we decided to elongate them and improve device electronic to make it

more compact and robust for clinical purposes. However this increase in cable length could lead to a decrease on TNRD signal, due to the small value of neutron fluences that are being measured. We first built an adaptor to test devices with both, original and extended lengths under the same irradiation conditions. The other problem that we noticed was the inevitability of cable irradiation when measuring at different locations inside the phantom at the same time. To quantify how this fact can affect TNRD response, we decided to perform the same measurements with and without cable irradiation. Setup was chosen to irradiate either none of the cable or the maximum possible length. Main results obtained for the exhaustive study performed, regarding influence of these two parameters, were published on the World Congress on Medical Physics & Biomedical Engineering as a full paper ([Irazola et al.,2015a](#), **Appendix B.1**).

- (iii) The odd behavior found in TNRD signal when performing measurements under 'critical' conditions (in terms of photon background), made us think that detector readings were not completely reliable in clinical environments. TNRD detectors are mainly based on the combination of two solid state devices, one of which is sensitized to thermal neutrons. Neutron component is thus obtained from the subtraction of both readings. Theoretically differences in terms of photon sensitivity among the devices had already been reduced in the manufacturing process to maximize photon rejection. However, due to the uncertainty related to real photon rejection of the detectors, we were not able to quantify and thus, correct the over- or under-estimation in their readings. This fact is of particular interest for our purpose, since we're measuring small neutron signals under an intense photon background. Additionally, the broad range of circumstances that can

take place in clinical environments (facility, detector location, energy, etc.), make photon rejection uncertainties of TNRD readings unpredictable. As a first step we decided to evaluate its photon rejection capability under different photon fields and irradiation/detector conditions to verify dependencies. For that, measurements in a pure photon source as ^{60}Co were firstly performed to ensure that their sensitivity to photons was a real problem. In addition, to quantify its contribution in clinical environments and dependence in energy, several tests were performed in 6 MV for clinical linacs (where a negligible neutron contribution is expected). Finally, directional dependence on detector response to photons, concerning gantry incidences, was also evaluated. These preliminary results were published as short works in Radiotherapy and Oncology (Irazola et al.,2015b; Terrón, Irazola et al.,2015; Irazola et al.,2015c, **Appendix B.2-4**).

(iv) Theoretical approaches, considering detector composition together with the observed irregular inconsistencies found, made us think that noticed TNRD photon rejection problems under critical conditions in clinical environments could be minimized. As devices are based on the subtraction of the signal of the non-chemically treated solid state device to that of treated one, the idea was quantifying photon final contribution to detector readings (representing differences in terms of photon sensitivity of the devices), in order to later correct the values. For that, a simple procedure leading to an improvement of neutron-to-photon discrimination capability of TNRD detectors in radiotherapy environments was proposed, consisting of the use of a neutron absorber material based on a borated rubber. Paper was sent to Applied Radiation and Isotopes (Irazola et al., 2016b, **Section III.2.B.2**).

(v) However, as this procedure implies not only the acquisition of the mentioned material but several modifications in detector setup (e.g. phantom accommodations for detector location), we thought of an easier and more universal method, consisting on the use of low-energy (i.e. 6 MV) measurements to evaluate this photon contribution. Paper was sent to Radiation Measurements ([Irazola et al.,2016c](#), **Section III.2.B.3**).

(C) Neutron peripheral dose model improvements

Once the detector was validated and its implementation in clinical routine demonstrated as reliable, with the previously mentioned problems solved, we were able to use *TNRD* for their final purpose of enhancing peripheral neutron dose models in high-energy radiotherapy treatments. One of the main advantages of these devices is its small size, which allows their use for both 'external' and 'in-phantom' measurements. This, together with their online behavior, permits not only the verification and improvement of the existing models (Head & Neck and abdomen), but also the generation of new ones regarding different phantom sizes (apart from adult ones).

- (i) As a first step, previous existing models (Head & Neck and abdomen) were validated with *TNRD* detectors, evaluating which points are the most troublesome ones ([Irazola et al.,2014c](#)). In addition, considering the goal of this work consisting of the implementation of a simple tool for patient risk estimation in commercial TPS, we evaluated the implemented script, containing the old version for peripheral neutron dose assessment, by comparing theoretical estimations to those obtained with *TNRD* ([García Hernández et al.,2015](#)). Results seemed to be in concordance, allowing the direct implementation of future enhanced models in TPS ([Irazola et al.,2015d](#), **Appendix C.1**).

(ii) Then in order to validate the general behavior of these models, real treatments were measured with *TNRD* detectors inside the anthropomorphic phantom and compared to estimations obtained with the two generic models ([Irazola et al.,2016d](#), **Appendix C.2**).

(iii) Once the generality of these models has been proved and as it involves a global methodology (previously validated for all the existing linac, [Sánchez-Doblado et al.,2012](#)), we were in the position of improving the existing models. As a first step, the generalization of the methodology, in order to make it usable for any thermal neutron detector (the previous one was expressed in terms of SEU events of SRAM detectors) was a mandatory task. This was feasible thanks to the direct thermal neutron fluence estimations provided by *TNRD* devices for both locations (external and 'in-phantom'), being able thus to directly correlate 'external' reference thermal neutron fluence measurements to peripheral doses at patient organs. Then conflictive points were evaluated, improving some of the previously established correlation factors. Finally, in order to take into account patient anatomy, which represents an important aspect concerning specific cohorts of patients (e.g. children or pregnant women), *TNRD* measurements were performed for the three available phantom sizes (child, teen and adult). Thus an enhanced global model that takes into account patient anatomy was established. This methodology is now available for any facility and thermal neutron detector. These improved models were employed for the evaluation of 510 measured patients, comparing the obtained results to those of the simple old models. Paper was sent to Physics in Medicine and Biology ([Irazola et al., 2016e](#), **Section III.2.C**).

(D) Peripheral dose in clinical cases

As a final step, we wanted to clinically validate the use of these improved models for the assessment of peripheral neutron doses. However in order to perform suitable cancer risk estimations, the consideration of both photon and neutron contributions to peripheral doses, is advisable (Sánchez-Nieto et al.,2016). Thus, our group has been working in parallel on an analytic peripheral photon dose model, valid for any isocentric technique and usable beyond 10 cm from the field edge (Sánchez-Nieto et al.,2015a). This allowed the global estimation of peripheral photon and neutron doses in order to have additional objective comparison parameters between different RT techniques.

- (i) An initial study, based in prostate pathology was performed to compare photon and neutron peripheral doses for inverse and forward IMRT and 3D-CRT in low (6 MV) and high (15 MV) energies, at 7 relevant organs (Irazola et al.,2015e), using former versions of both methodologies. Obtained results together with the recent interest in hypofractionated techniques, such as SBRT (Stereotactic Body Radiation Therapy), made us reflect on the necessity of deeper studies, containing these modalities as well as those avoiding the use of flattening filter (FFF). A preliminary study was performed for a lung case, comparing conventional techniques and fractionation (3D-CRT) to modern (IMRT and VMAT) and hypofractionated ones (SBRT), with and without the use of flattening filter (FF) for three different linac manufacturers (Siemens, Varian and Elekta) and energies (6, 10 and 15 MV) (Irazola et al.,2016f, **Appendix D**).

(ii) Due to the scientific interest on this topic and the growing amount of publications related to hypofractionated techniques, we decided to perform a more exhaustive study. For that, we extend it to other pathologies, selecting the ten most common SBRT treatment types. The same CT contours and planning parameters were considered. Due to the general aspect and easy implementation of both models, thanks to the ready availability of input parameters, both peripheral doses (neutrons and photons) were directly calculated in a homemade Matlab script, which would be ideally transferred into a commercial TPS in the close future. The use of these data, either in terms of peripheral doses or second cancer risk probability would provide an objective parameter for the selection of the best treatment strategy, regarding patient anatomy and treatment characteristics (in terms of energy used and type of fractionation). Paper will be sent to Radiation Oncology ([Irazola et al.,2016g](#), **Section III.2.D**).

2. Publications

(A)

A new online detector for estimation of peripheral neutron equivalent dose in organ

Irazola et al., Med Phys 2014;41:112105

Abstract

Purpose: Peripheral dose in radiotherapy treatments represents a potential source of secondary neoplastic processes. As in the last few years, there has been a fast-growing concern on neutron collateral effects, this work focuses on this component. A previous established methodology to estimate peripheral neutron equivalent doses relied on passive (TLD, CR39) neutron detectors exposed in-phantom, in parallel to an active [static random access memory (SRAMnd)] thermal neutron detector exposed ex-phantom. A newly miniaturized, quick, and reliable active thermal neutron detector (TNRD , Thermal Neutron Rate Detector) was validated for both procedures. This first miniaturized active system eliminates the long postprocessing, required for passive detectors, giving thermal neutron fluences in real time.

Methods: To validate TNRD for the established methodology, intrinsic characteristics, characterization of 4 facilities [to correlate monitor value (MU) with risk], and a cohort of 200 real patients (for second cancer risk estimates) were evaluated and compared with the well-established SRAMnd device.

Finally, *TNRD* was compared to TLD pairs for 3 generic radiotherapy treatments through 16 strategic points inside an anthropomorphic phantom.

Results: The performed tests indicate similar linear dependence with dose for both detectors, *TNRD* and *SRAMnd*, while a slightly better reproducibility has been obtained for *TNRD* (1.7% vs 2.2%). Risk estimates when delivering 1000 MU are in good agreement between both detectors (mean deviation of *TNRD* measurements with respect to the ones of *SRAMnd* is 0.07 cases per 1000, with differences always smaller than 0.08 cases per 1000). As far as the in-phantom measurements are concerned, a mean deviation smaller than 1.7% was obtained.

Conclusions: The results obtained indicate that direct evaluation of equivalent dose estimation in organs, both in phantom and patients, is perfectly feasible with this new detector. This will open the door to an easy implementation of specific peripheral neutron dose models for any type of treatment and facility.

1. Introduction

It is widely known the paradoxical fact that ionizing radiations, while being an effective therapeutic mean to fight cancer, also represent a potential source of new neoplastic processes. The study of risks associated to certain dose distributions is usually limited to the areas surrounding the tumor. However the rest of the body is similarly affected by the radio-induced toxicity with dose values that, although initially were considered insignificant, can be of the order of the ones that may affect any exposed professional. Although they have rarely been considered in the clinical routine of the institutions around the world, in the last few years, there has been a fast-growing concern about the peripheral radiation dose, outside the treatment volume, that patients receive additionally and unnecessarily.

Although in the case of photons (the main radiation contribution to the peripheral dose), there are well-known dosimetric mechanisms, there is not any comparable system to measure the neutron contribution (Xu et al., 2008). We have focused our studies on the latter, as it was the least analyzed because of its great complexity.

During the last few years, some neutron detectors were developed and numerous experimental tests were done with medical linacs. The first results obtained with an active neutron detector, based on Static Random Access Memory (*SRAMnd*), indicated that the estimation of neutron dose in patients could be feasible (Gómez et al., 2010; Sánchez-Doblado et al., 2012). A first study on risk estimation for 1377 patients in 50 international facilities has been carried out for the 14 most frequent pathologies and 15 linac models (which virtually represent the totality of the existing machines; Expósito et al., 2012).

The methodology presented in Sánchez-Doblado et al., 2012, is not restricted to a specific detector but applicable to any other. For example, to the new digital diode-based detector introduced by Guardiola et al., 2013. The aim of the present work is the validation of a novel miniaturized active digital detector named *TNRD* (*Thermal Neutron Rate Detector*), developed by Bedogni et al., 2014, for its use in a clinical environment. The great advantage of this device is its dual use, both as online detector in clinical routine and for in-phantom measurements, due to its reduced size.

2. Material and Method

2.A. Digital detector *TNRD*

The new thermal neutron detector, developed by the NESCOFI@BTF project (Scientific Commission V, INFN-LNF, Italy) is based on a commercial solid-state device sensitized to thermal neutrons through a customized physical-

chemical treatment. Details on design and composition of the detector can be found in [Bedogni et al.,2014](#). With an active area of 1 cm² and overall dimensions of approximately 1.5 x 1 x 0.4 cm³, it linearly responds in terms of thermal neutron fluence rate from 10 up to 10⁶ cm⁻²·s⁻¹. The *TNRD* signal is amplified in a low-voltage electronics module and sent to a PC-controlled programmable ADC. The control software was developed in LabView© (2010 National Instruments), by the Politecnico di Milano. Compared to the *SRAMnd* detector ([Gómez et al.,2010](#)), the *TNRD* can correctly measure lower intensity fields. The *TNRD* output is a DC voltage directly proportional to the thermal neutron fluence rate ([Bedogni et al.,2014](#)). The calibration factor is obtained for every *TNRD* by exposing it in a reference thermal field at INFN-Frascati. The detector-to-detector response variability is in the order of ±5% (1SD). An additional uncertainty contribution is needed to account for the dependence of the *TNRD* response from the energy and direction distribution of the incident field, so that a 10% overall uncertainty for the *TNRD* response was estimated.

2.B. Li thermoluminescence dosimeters

Standard ⁶LiF/⁷LiF pairs of TLD-600/TLD-700 (3 × 3 × 0.9 mm³ chips) dosimeters were used as an independent system to validate the thermal neutron fluences, obtained with *TNRD* detectors in different points inside a NORMA phantom ([Sánchez-Doblado et al.,2012](#)). Conventional neutron calibration was performed at Physikalisch-Technische Bundesanstalt in scattered neutron reference radiation fields, produced by a bare ²⁵²Cf and a D₂O-moderated ²⁵²Cf neutron source and for gamma, using a ¹³⁷Cs calibration source at a secondary standard dosimetry laboratory in CIEMAT (*Centro de Investigaciones Energéticas Medioambientales y Tecnológicas*).

On the basis of the results of glow curve analysis, thermal neutron fluences were obtained using the differences between TLD-600 and TLD-700 readings for each measured point in NORMA and the calibration factors as follows:

$$\phi_{i,j}^{TLD} = f_{600/700}^n [R_{600}^{i,j} - kR_{700}^{i,j}] \quad k = f_{600}^Y / f_{700}^Y \quad (\text{eq. 1})$$

Where the calibration factors used are $f_{600/700}^n = 465n \cdot cm^{-2}$ (12%, $k=2$) for neutrons and $f_{600}^Y = 1.86 \times 10^{-4} mGy \cdot au^{-1}$ (8%, $k=2$) and $f_{700}^Y = 1.99 \times 10^{-4} mGy \cdot au^{-1}$ (10%, $k=2$) for gammas. The global uncertainty for these procedures has been estimated at 15%.

In order to validate *TNRD* for its use in the methodology established by [Sánchez-Doblado et al.,2012](#), it was compared to both: the active *SRAMnd* detector, used for ex-phantom measurements in clinical routine and passive ones (here TLD), which are used for in-phantom measurements, to generate risk models.

2.C. TNRD validation for clinical use

First, the “reference factor”, defined as the quotient between the *SRAMnd* and the *TNRD* readings (unit: $V^{-1} \cdot s^{-1}$), was studied by exposing the devices under the reference irradiation conditions in a linac: 10×10 cm² field, 0° gantry angle and 1000 Monitor Units (MU), and detectors located in front of the gantry axis, close to the wall ([Figure 1](#)) as recommended in [Jíménez-Ortega et al.,2011](#) (reference position for patient measurements). Thus, once this factor is obtained [with a better accuracy than in ([Terrón et al., 2014](#)) by increasing the number of measurements], measurements can be performed in any facility by applying the methodology established in [Sánchez-Doblado et al.2012](#), to estimate patient neutron equivalent dose in organ.

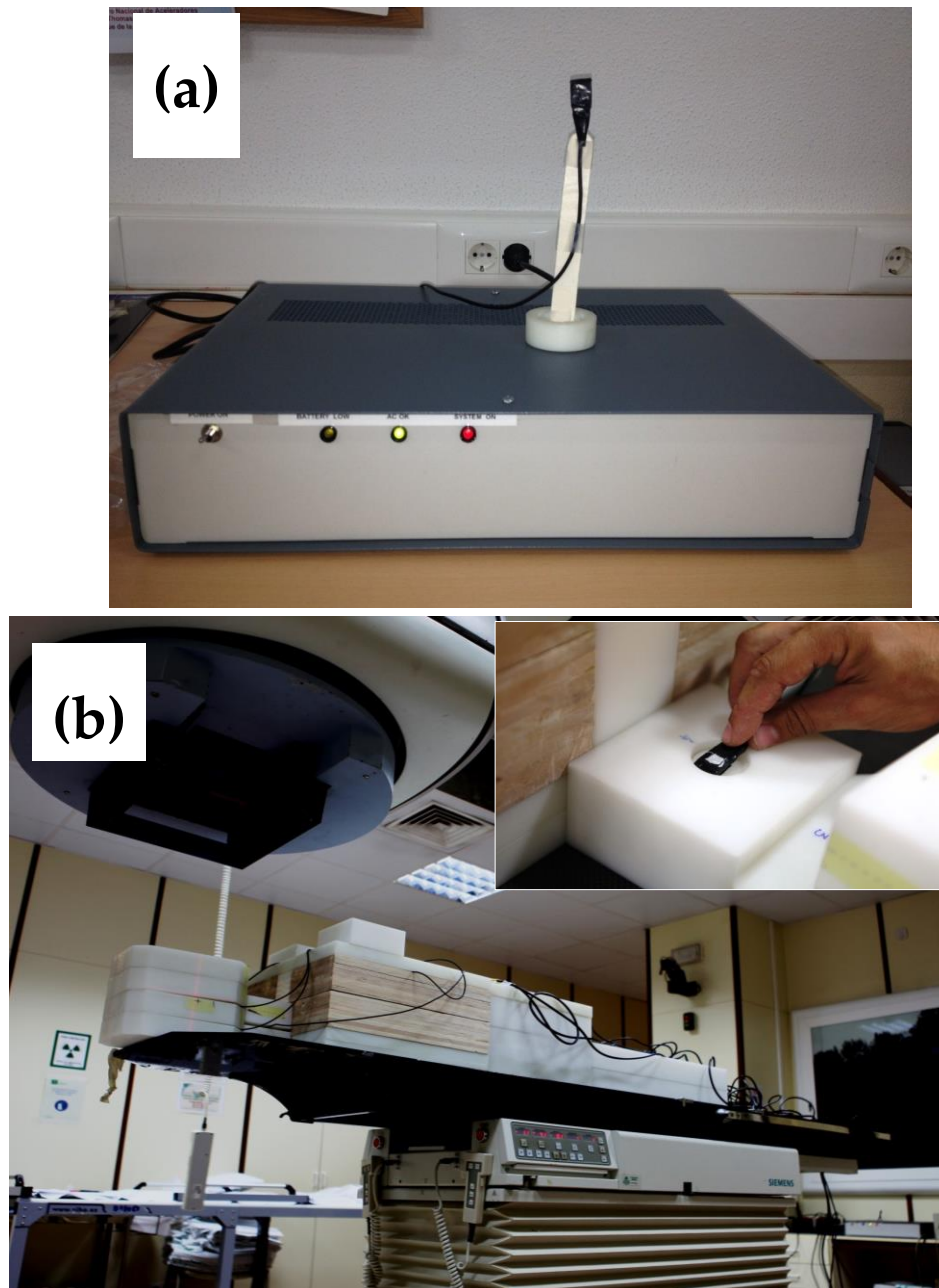


Figure 1. (a) SRAMnd and TNRD detectors (the metallic box is the detector based on SRAM, while the black one is the new detector TNRD presented in this paper) and (b) Location of the detectors in the treatment room when NORMA phantom is used (Sánchez-Doblado et al.2012). The insert shows how TNRD detector is placed inside the phantom.

As previously mentioned (section 2.A), intrinsic characteristics of *TNRD* detector had already been studied under a pure neutron beam by the manufacturer. However this device is also sensitive to the photon component, which is highly present in radiotherapy environments, thus its validation under clinical conditions becomes essential. Reproducibility and linearity were studied in this environment and compared to the previously used *SRAMnd* device. A series of 18 measurements were performed with *TNRD* and *SRAMnd* detectors, under the above-mentioned reference irradiation conditions during six days (3 each day). Readings were corrected for linac stability by means of an ionization chamber placed inside the photon beam (this was not considered in previous measurements; Terrón et al., 2014). Linearity was studied for two of the detectors, in an extended range of typical monitor units (MU) of radiotherapy treatments (25 to 4000 MU) measured under the defined reference conditions. This study allows the knowledge of the minimum reliable measurable fluence.

The next step was to compare their capabilities for facility characterization and patient measurements, for which this new detector would be useful from a clinical point of view.

Characterization procedure (Expósito et al., 2013), was done for *TNRD* and *SRAMnd* in four different linacs (Terrón et al., 2014) (nominal energies ranging from 15 to 18 MV) in Hospital Universitario Virgen Macarena (*HUVM*) in Sevilla and Santa Maria delle Croci Hospital (*SMCH*) in Ravenna.

By applying the reference factor to the readings of the *TNRD*, located in the reference position, neutron equivalent dose in organs was assessed as proposed in (Sánchez-Doblado et al., 2012). A cohort of 200 real patients from the 4 facilities, were evaluated in terms of second cancer risk with both detectors. Estimates were done by two alternative methods. The first one uses the models

obtained during the characterization of each facility, as a function of the delivered MU for each patient treatment. The second one makes the estimations by applying the methodology established in [Sánchez-Doblado et al.,2012](#) to the direct readings from the detectors, placed in the treatment room during patient irradiation.

2.D. TNRD validation for in-phantom measurements

The added new possibility of in-phantom measurements with an active detector for the first time has to be validated with the well-established methodology of classical passive detectors, sensitive to thermal neutrons [here TLDs; [Sánchez-Doblado et al.2012](#)]. Measurements were performed in a Siemens Primus linac at HUVM with detectors located inside the NORMA phantom [[Sánchez-Doblado et al.2012 \(Figure 1b\)](#)], to confirm their viability. Three treatments were considered:

- (i) Head and neck, eight beam incidences (at 0° , 45° , 90° , 135° , 180° , 225° , 270° , 315°), 10×10 cm² field size, 1000 MU, isocenter in the middle of the head.
- (ii) Abdomen, same beam incidences, same field size and number of MU as in *i*, isocenter in the middle of abdomen, just in the border of the lower lungs.
- (iii) Prostate IMRT, seven beam incidences (at 0° , 52° , 95° , 156° , 204° , 265° , 308°), 420 MU, isocenter at the prostate level.

3. Results and discussion

3.A. TNRD validation for clinical use

A mean reference factor of 53.55 ± 1.54 events/V·s (1SD) has been obtained for the TNRD detector with respect to the SRAMnd, used as a reference.

The uncertainty in reproducibility of neutron fluence measurements, normalized to the mean value along the days, is lower than 1.7% (1SD) for *TNRD*, which is slightly better than the 2.2%(1SD) obtained for the *SRAMnd* detector.

A well-fitting linear regression model ($R^2=0.9999$) was obtained without saturation effects observed, for both detectors. Figure 2 shows the mean standard deviation (error bars for variations among both detectors used) for two of the six available *TNRD* detectors, as a function of thermal neutron fluence (logarithmic representation) in the typical radiotherapy treatment range. We can estimate that, considering an uncertainty over 5%, the minimum reliable thermal neutron fluence is about $0.19 \times 10^5/\text{cm}^2$, corresponding to approximately 5 MU in this reference conditions.

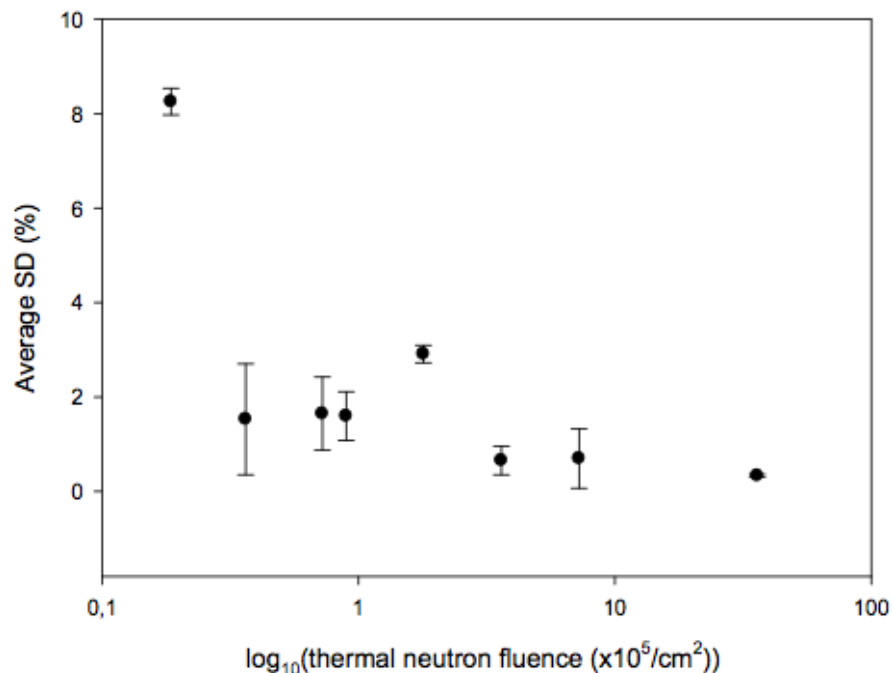


Figure 2. Average Standard Deviation (%SD) with the variation between two of the six *TNRD* detectors represented as error bars, as a function of thermal neutron fluence ($\times 10^5/\text{cm}^2$) in logarithmic representation.

The risk specific models for the four studied cases (sex and treatment site combinations) were generated for each facility. Using average values for risk estimates when delivering 1000 MU, in the four possible situations for the 4 studied facilities, obtained mean deviation of *TNRD* measurements with respect to the ones of *SRAMnd* is 0.07 cases per 1000. Differences were always smaller than 0.08 cases per 1000. In consequence, *TNRD* represents a good alternative to the previous detector.

Figure 3a and 3b show the *Total Risk of acquiring a second cancer (cases per 1000)* estimated from the characterization of one of the 4 studied facilities (lines) and for the *TNRD* [3a] and *SRAMnd* [3b] direct measurements (symbols). The good agreement between these two alternatives (*TNRD* vs. *SRAMnd*) can be observed in this example.

3.B. *TNRD* validation for in-phantom measurements

Figures 4a-c show the good results for in-phantom measurements with TLD and *TNRD*. Note that, for each treatment type, there are some missing points, which were inside the photon treatment field and, therefore, were not considered (they are not reliable as they are performed under an intense photon field; however, this does not represent a problem as interest is focused on peripheral dose).

4. Conclusions

A new miniaturized active online thermal neutron detector named *TNRD*, has proven itself as a good alternate to previously necessary active and passive detectors for patient-related neutron dosimetry (*SRAMnd*), and second cancer risk assessment in radiotherapy (TLD, CR-39). This device has been validated and set-up. We can conclude that it is equally acceptable for patient measurements, being not only slightly more reproducible and sensitive than the

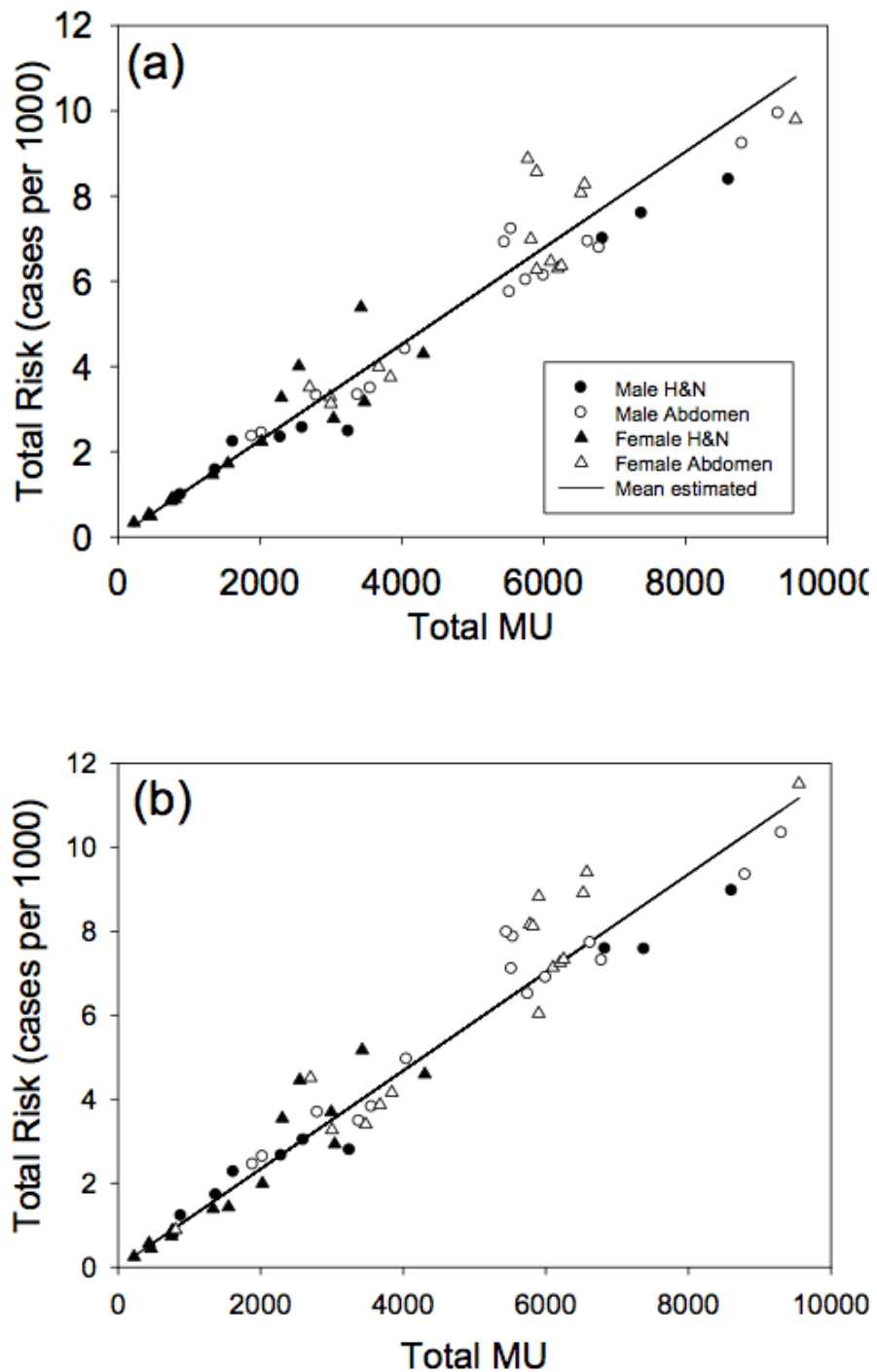


Figure.3. Comparison of experimental (symbols) and estimated (line) Total Risk, cases per 1000, for radiotherapy patients in one of the four studied facilities, obtained by (a) TNRD and (b) SRAMnd procedures.

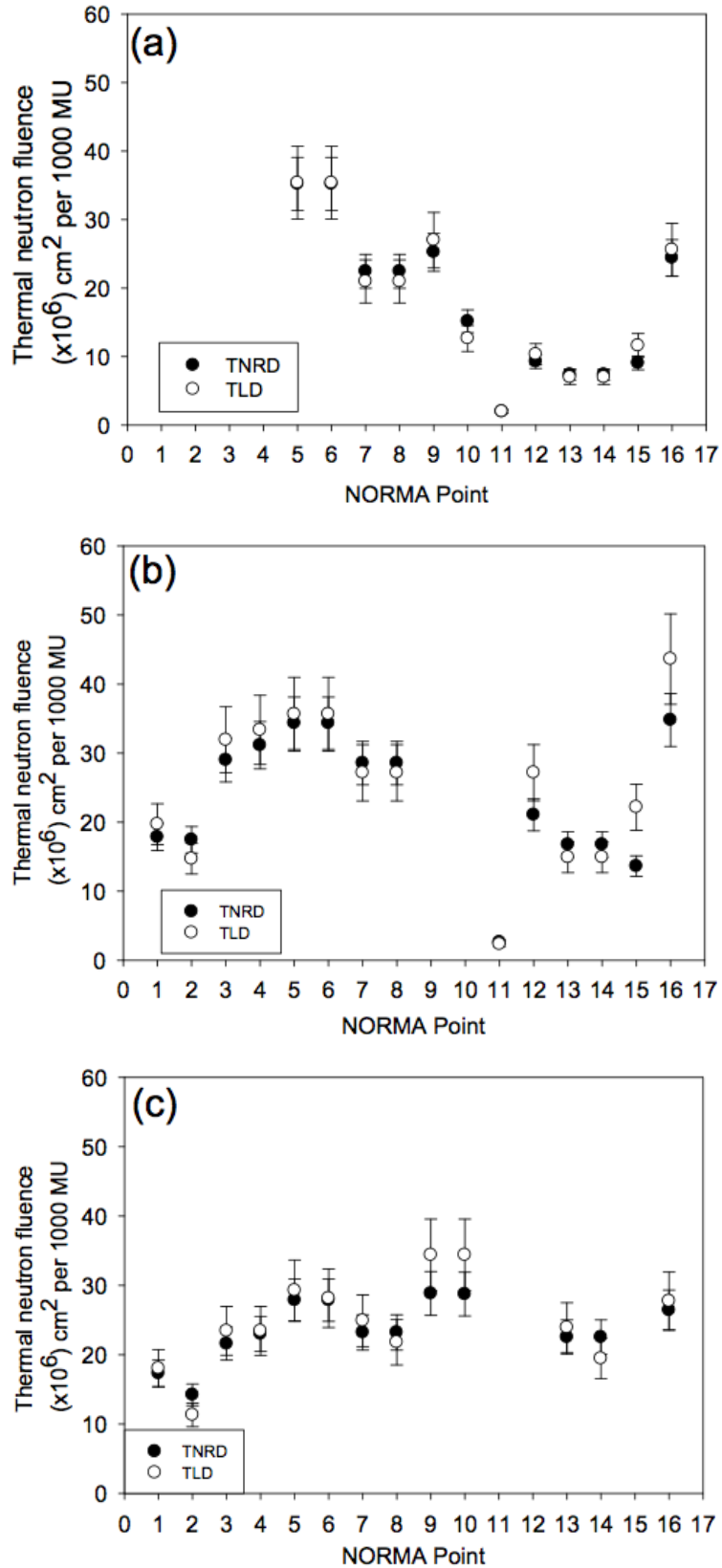


Figure.4. Thermal neutron fluence ($\times 10^6 \text{ cm}^2$) obtained by the new digital detector TNRD compared to TLD readings, in the 16 NORMA phantom points, for the three treatments.

well-established SRAM-based digital device, but also because it can be used for in-phantom measurements, which was not possible for the previous device. *TNRD* will allow the expression of reference measurements in terms of physical magnitude (neutron fluence) instead of events, as used in the previous methodology. Moreover, the new device is built with low cost commercially available materials, using modest electronics. In addition, *TNRD* could offer the possibility of measuring, at the same time, photon component of peripheral dose, although further investigation is needed for these two functionalities.

TNRDs, can be used in the reference ex-phantom position to estimate equivalent dose in organs. Additionally, given its reduced volume, the *TNRD* can be used in-phantom, in conjunction with location-specific neutron spectral information, for the direct estimation of neutron peripheral doses. This will allow to:

- improve the existing general risk models (developed so far for head & neck and abdomen, in the case of adult size)
- produce new specific models, for different pathologies and treatment techniques.

This opens the door to the implementation of these models for peripheral neutron dose in the context of treatment planning systems.

5. Acknowledgments

This work would not be possible without the use of hospital resources which were kindly provided by the management of the *Department of Radiotherapy and Oncology of the University Hospital Virgen Macarena* in Seville and M. C. Presello from *Ospedale San Camilo* in Rome. The authors would also like to thank M. V. Intriolini and D. Bortot of the *Departimento di Ingegneria Nuclear* from *Politecnico di Milano*, L. Lembo from the *Nuclear Service di Lembo Cristina S.a.s.*, and G. Mazzoti and M. Morelli from *Servizio di Fisica Sanitaria, S. Maria de lle Croci*

Hospital, Ravenna. They also wish to express their gratitude to J. L. Muñiz and M. Gómez-Ros from *Centro de Investigaciones Energéticas y Medioambientales y Tecnológicas (CIEMAT)* in Madrid for their support in TLD measurements and Monte Carlo simulations and, especially, to the Spanish Nuclear Safety Council (CSN) for its support through a specific agreement with the University of Seville. A. Esposito and A. Gentile from *Istituto Nazionale di Fisica Nucleare of Laboratori Nazionali di Frascati (INFN)* provided helpful information and technical support. The authors would like to acknowledge the technical help provided by R. Chamorro and L. Hidalgo from the *Electromedecine Department of HUVM*. They would also like to thank H. Galán-Dorado and Zoey Krulick for her revision of grammar and style. This work was partially supported by INFN Commissione Scientifica V through the NESCOFI@BTF and NEURAPID projects.

6. References

- Bedogni R, Bortot D, Introini MV, Gentile A, Esposito, A., Gómez-Ros, J.M., Palomba, M., Gross, A., 2014. *A new active thermal neutron detector*. *Radiat Prot Dosim* 2014;16(1-4):241-244.
- Expósito MR, Sánchez-Nieto B, Grishchuk D, Kuznetsova E, Chervyakov A, Bochkareva T, Fomintseva M, Ponezha T, Baranov E, Sandín C, Moral-Sánchez S, Bragado-Álvarez L, Guisasaola-Berasategui A, JA Terrón and Sánchez-Doblado F, *Experimental estimation of the second cancer risk due to neutron contamination in radiotherapy treatments*. *Radiother Oncol* 2012;103(1):S516-S517.
- Expósito MR, Terrón JA, Barquero R, Domingo C, García-Fusté MJ, Gómez F, Núñez L, Sánchez-Nieto B and Sánchez-Doblado F. *Neutron contamination in radiotherapy: estimation of second cancers based on measurements in 1377 patients*. *Radiother Oncol* 2013;107:234–241.
- Gómez F, Iglesias A and Sánchez-Doblado F. *A new active method for in-room neutron measurements in radiotherapy*. *Phys Med Biol* 2010;55:1025-1039.
- Guardiola C, Gómez F, Fleta C, Rodríguez J, Quirion D, Pellegrini G, Lousa A, Martínez-de-Olcoz L, Pombar M and Lozano M. *Neutron measurements with ultra-thin 3D silicon sensors in a radiotherapy treatment room using a Siemens PRIMUS linac*. *Phys Med Biol* 2013;58:3227–3242.
- Jiménez-Ortega E, Expósito MR, González-Soto X, Terrón JA, Gómez F and Sánchez-Doblado F. *Characterization of the neutron induced single event upset in SRAM around high megavoltage clinical accelerators*. *IEEE, RADECS 2011 Proceedings*. 2011;978-1-4577-0587-9:922-925.

- Sánchez-Doblado F, Domingo C, Gómez F, Sánchez-Nieto B, Múñiz JL, García-Fusté MJ, Expósito MR, Barquero R, Hartmann GH, Terrón JA *et al.* *Estimation of neutron equivalent dose in organs of patients undergoing radiotherapy by the use of a novel online digital detector.* *Phys Med Biol* 2012;57:6167–6191.
- Terrón JA, Irazola L, Lorenzoli M, Bedogni R, Pola A, Introini MV, Bortot D, Gentile A, Esposito A, Sánchez-Nieto B, Expósito MR and Sánchez-Doblado F. *Set-up of a new online digital detector for peripheral neutron equivalent dose estimation in radiotherapy patients.* *Radiother Oncol* 2014;111:564.
- Xu X-G, Bednarz B and Paganetti H. *A review of dosimetry studies on external-beam radiation treatment with respect to second cancer induction.* *Phys Med Biol* 2008;53:193-241.

III. Thesis core

2. Publications: **(A)** *A new online detector for estimation of peripheral neutron equivalent dose in organ*

(B.1)

Using a Tandem Pelletron accelerator to produce a thermal neutron beam for detector testing purposes

Irazola et al., Appl Radiat Isot 2016;107:330-334

Abstract

Active thermal neutron detectors are used in a wide range of measuring devices in medicine, industry and research. For many applications, the long-term stability of these devices is crucial, so that very well controlled neutron fields are needed to perform calibrations and repeatability tests. A way to achieve such reference neutron fields, relying on a 3 MV Tandem Pelletron accelerator available at the CNA (Seville, Spain), is reported here. This paper shows thermal neutron field production and reproducibility characteristics over few days.

1. Introduction

Achieving stable thermal neutron beams for calibrating and testing thermal neutron detectors is an important challenge in a number of fields where ionizing radiations are employed. Traditionally, metrology-grade thermal neutron fields are obtained by moderating radionuclide sources of ^{252}Cf or $^{241}\text{Am}\text{-Be}$, with large polyethylene or graphite blocks. An example is the SIGMA facility of IRSN France (Muller et al.,2003; Lacoste et al.,2007). However, most of the existing facilities were decommissioned because their internal

sources were too old to guarantee a safe operation. In addition, achieving large radionuclide sources for new facilities has become unfeasible for both economical and safety reasons. As a consequence, the scientific community is searching for alternative sources of thermal neutron fields. Exploiting the ${}^7\text{Li}(p,n)$ reaction at near-threshold proton energies is a good option because established nuclear data are available and very low-energy neutrons can be achieved, thus requiring very reduced amount of additional thermalizing material.

The 3 MV Tandem Pelletron accelerator¹ (Praena et al.,2013) at CNA (Centro Nacional de Aceleradores, Sevilla, Spain) was used for this purpose. Some sheets of lead were added to reduce the photon field and a few cm of thick polyethylene moderator was adopted as moderator.

The field was monitored, over three days of operation, using (a) a proton current integrator connected to the target backing, and (b) the active thermal neutron detector called *TNRD* (Thermal Neutron Rate Detector) (Bedogni et al.,2014), used in medical physics (Irazola et al.,2014; 2015b) to estimate neutron equivalent doses to peripheral organs for oncological patients treated with medical accelerators (Expósito et al.,2013), using the methodology established by Sánchez-Doblado et al.,2012, Gómez et al.,2010 and Romero-Expósito et al.,2015.

2. Material and method

2.1 *TNRD* neutron detector

Figure 1 shows the *TNRD* detector, developed by INFN-LNF, Italy (Bedogni et al., 2014). This detector is based on a low-cost commercial solid-state device sensitized to thermal neutrons through a customized physical–chemical

¹ <http://www.pelletron.com/negion.htm>



Figure 1. One of the TNRD detectors (marked with a white box) and associated six electronics channels.

treatment. Its active area is 1 cm^2 and the overall dimensions are approximately $1.5 \times 1 \times 0.4 \text{ cm}^3$. It linearly responds in terms of thermal neutron fluence rate from 10^2 up to $10^6 \text{ cm}^{-2} \text{ s}^{-1}$. TNRD signal is amplified in a low-voltage electronics module and sent to a PC-controlled programmable ADC. Control software was developed in LabView© (2010 National Instruments). TNRD output is a DC voltage directly proportional to the thermal neutron fluence rate. Every TNRD is individually calibrated. The accuracy of the detector is within 75%, or better, for the fluence rate interval from 500 up to $10^6 \text{ cm}^{-2} \text{ s}^{-1}$ (Bedogni et al.,2014). Additional uncertainty terms should be added, in practical measurements, if the neutron field has unknown direction distribution and is superposed to an intense gamma component. The parasitic response of TNRD to photons has been additionally evaluated (Terrón et al.,2015; Irazola et al.,2015a,c). The

reproducibility of *TNRD*, previously assessed using a constant thermal field from a moderated ^{241}Am –Be source, is $\pm 1.2\%$ over a time interval of days.

2.2 Neutron spectrum determination

The $^7\text{Li}(p,n)^7\text{Be}$ reaction has been studied in terms of total neutron yield, energy and angle distribution of the secondary neutrons as a function of the target thickness and projectile energy (Yu et al.,1998; Lederer et al.,2012). A FORTRAN code was written to generate the angle – and energy – distribution of neutrons based on analytical description of experimental data (Lee et al.,1999). MCNPX (v2.5) (Pelowitz et al.,2005) was used for their transport. ENDF/B-VII.0 and ENDF/ B-VI were used for particle-production and transport data and photoatomic data, respectively. The neutron spectra generated by $^7\text{Li}(p,n)^7\text{Be}$ at 1912 keV, which is used in the present experiment, was successfully modeled previously by Praena et al.,2013. The method of modelization, FORTRAN code for generation and MCNPX for transport, was also checked with neutron spectra emitted at different angles by the $^7\text{Li}(p,n)^7\text{Be}$ reaction near-threshold, Praena et al.,2014. MCNPX was also used to determine the optimal thickness of lead needed to reduce the parasitic photon field, due to the 477 keV photons from $^7\text{Li}(p,n)^7\text{Be}$ reaction. This value was fixed to 2.55 cm (17 lead sheets of 1.5 mm each), located 0.4 cm after the target. To thermalize the field, an optimized 2.2 cm thick polyethylene sheet was added immediately after the lead. Lateral size of both pieces was 20x20 cm². *TNRD* detector was then placed in an aluminum support 3.5 cm after the polyethylene block (Praena et al.,2015). This is the conventional point of test. The complete setup is shown in Figure 2.

Figure 3a shows simulated angle-integrated primary neutron spectrum at source position while Figure 3b displays the simulated neutron spectrum at detector position. It can be noticed that only neutrons of energy below 1 eV

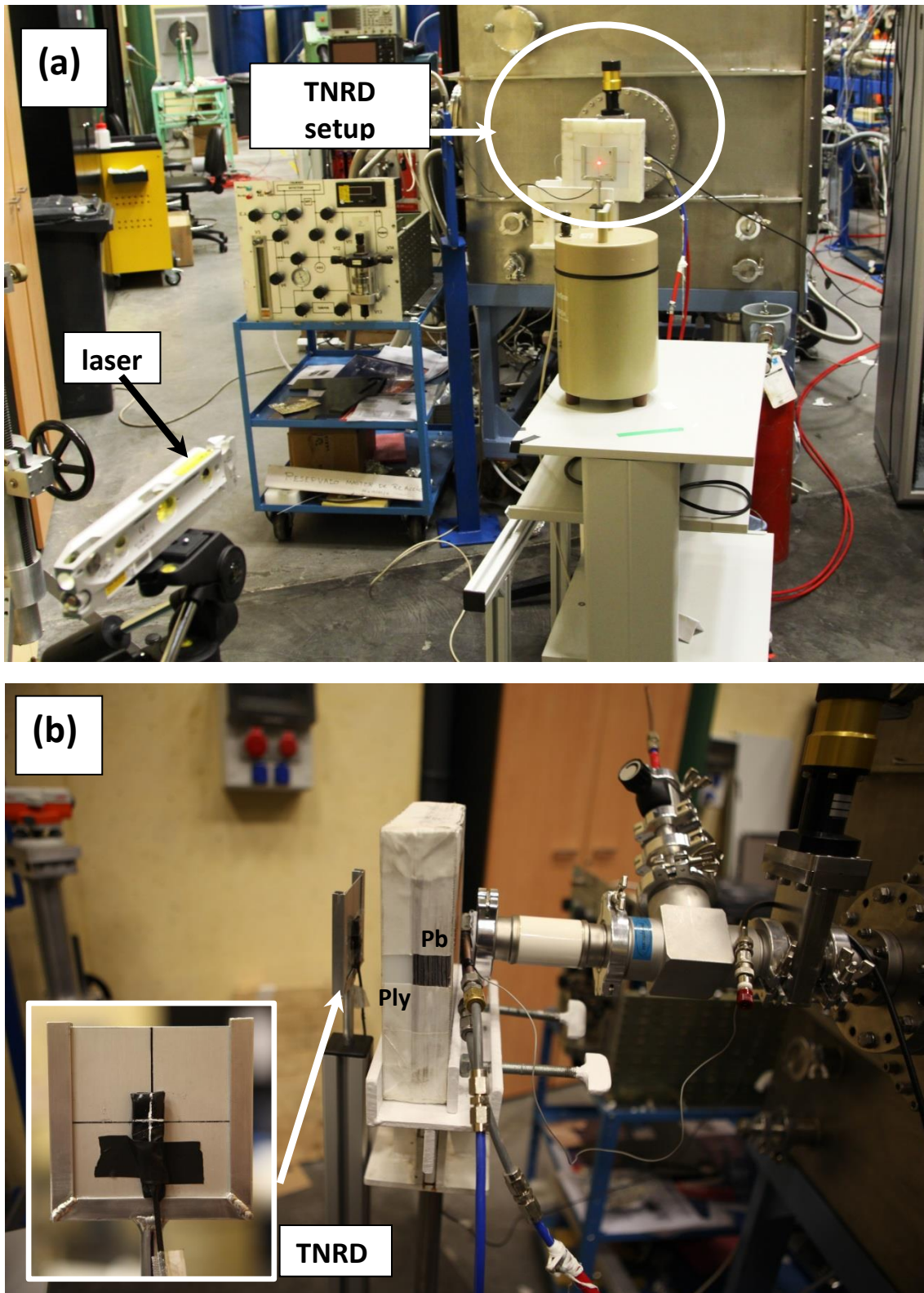


Figure 2. (a) Experimental setup aligned following the lithium target by using a fixed laser. (b) Detail of TNRD setup consisting on: a 2.55 cm lead layer and a 2.2 cm polyethylene (Ply) layer (both of 20x20 cm²) located between the lithium target and the detector (distance of approximately 8.9 cm). Inset shows TNRD location in the aluminum support.

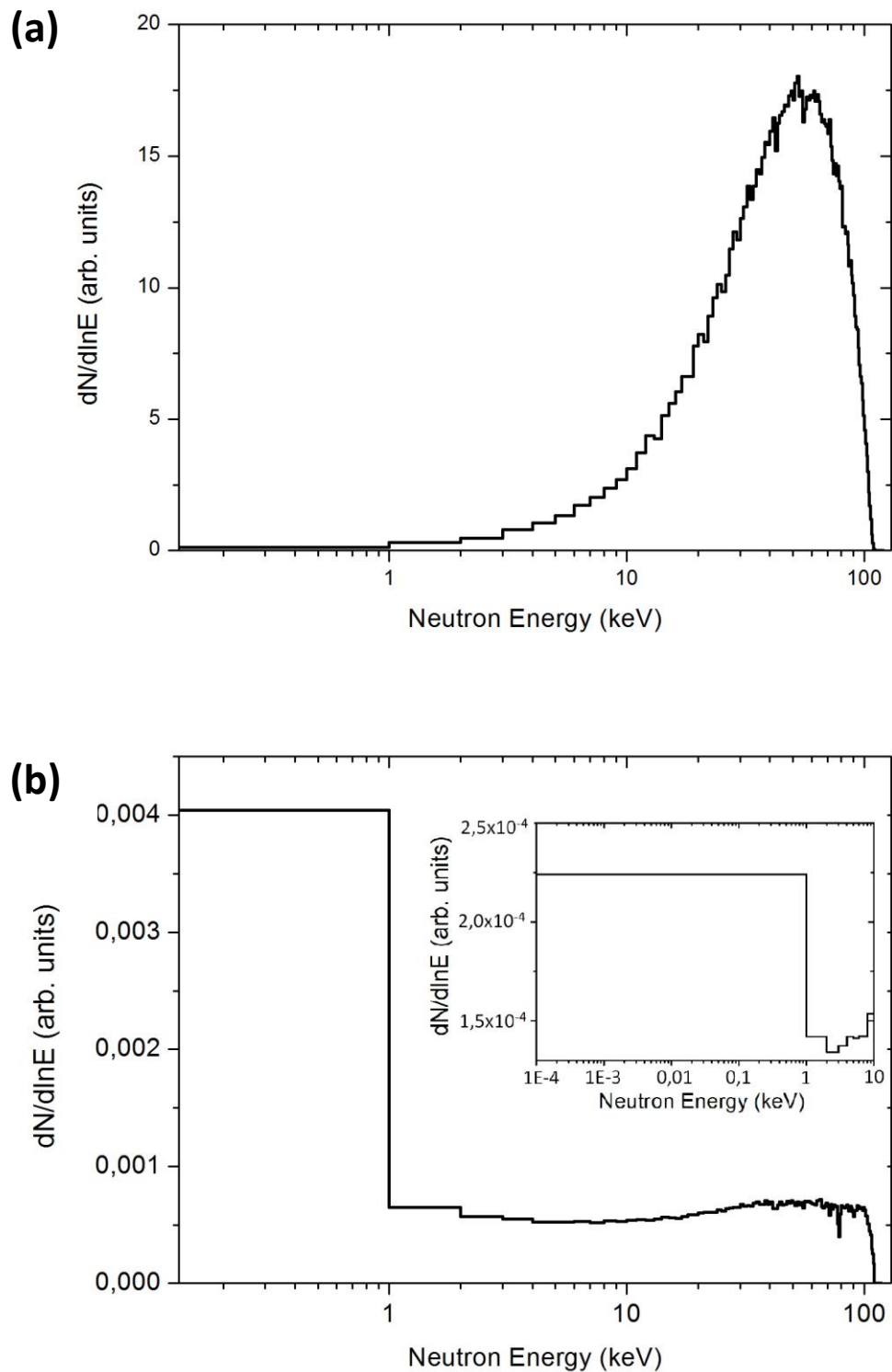


Figure 3. (a) Simulated neutron unitary spectrum: (a) at source position with ${}^7\text{Li}(p,n)$ reaction at $E_p=1912$ keV and (b) at TNRD position using 2.2 cm polyethylene and 2.55 cm lead filters. Inset shows how the majority of neutrons below 1 keV have an energy lower than 1 eV.

reach *TNRD*. Neutron spectra were obtained with a MCNP tally 4 which calculates de flux (n/cm^2) averaged over the lithium target (a) *TNRD* detector (b) normalized to total number of neutrons generated in the simulation.

2.3 Proton accelerator and target

The neutron beam was obtained from the CNA 3 MV Tandem Pelletron accelerator at 917 kV nominal voltage. [Figure 4a](#) shows the final part of the Basic Nuclear Physics (FNB) Tandem accelerator line, used in this experiment. It consists on a vacuum pipe housing a copper backing as cooling system. This backing holds a 50 μm thickness aluminum foil and the lithium target layer. The dimensions of this piece are $3 \times 3 \times 0.8$ cm^3 with a centered cylinder hole of 1 cm of diameter and 0.75 cm height, used to place the lithium layer (380 μm thickness). To prevent target melting, the copper support contains an internal cooling water circuit. Proton current on the lithium target was measured by connecting the copper backing to an Ortec Digital Current Integrator (Model 439). The nominal reproducibility of the electrometer is $\pm 0.01\%$. Proton current could be varied up to about 2 μA , corresponding to a thermal neutron fluence of about 2500 $cm^{-2} s^{-1}$ at the point of test.

To prevent non-target contributions to the measured proton current, a double collimator system consisting of two rings, one in copper and the other in Teflon® (connected through two ceramic screws, as shown in [Figure 4b](#)), was used. Collimators and target holder have external diameter of 3 cm. Internal diameter is 1.1 cm for copper ring and 1 cm for Lithium target and Teflon® ring.

Beam focusing ([Figure 4c](#)) was checked using a ViewPort² (DN 40 CF) device coupled with a luminescent quartz screen.

² <https://www.pfeiffer-vacuum.com/productPdfs/420GSG040.en.pdf>

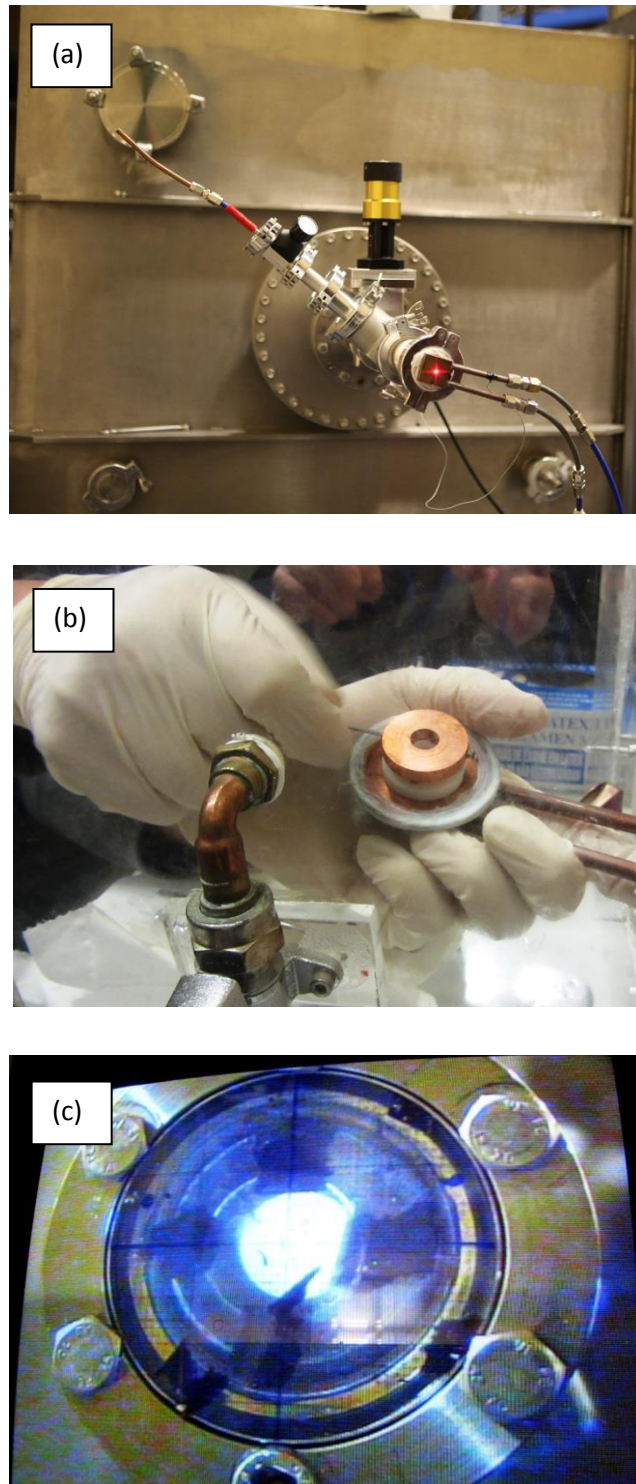


Figure 4. (a) Experimental setup at the 3 MV Tandem Pelletron accelerator at CNA (Seville), (b) copper-Teflon® disc used to estimate the current directly reaching the lithium target (blurred of the image is due to the fact that target has to be manipulated inside an Argon chamber to avoid lithium oxidation) and (c) monitor screen detail of the neutron beam collimated in the ViewPort.

3. Measurement results

Measurements were performed during 3 different days. Every day, the accelerator setup (focalization, energy and proton current values) was fixed. In this phase, *TNRD* reading was observed as a function of the nominal proton energy, allowing to identify the reaction threshold (1880 keV) and to verify the energy calibration of the accelerator. Energy was then increased to the project value of 1912 keV. The proton current was tuned to achieve values of thermal neutron fluence in the order of $2 \times 10^3 \text{ cm}^{-2}\text{s}^{-1}$. The three series of 15 min measurements performed in this condition are shown in [Figure 5](#). For every measurement, the 15 min-time-integrated reading of the *TNRD* (termed *TNRD*) and of the proton current monitor (termed *Q*) were collected. The ratio between these two quantities, termed *TNRD_n*, is the normalized *TNRD* reading. These quantities are reported in [Table I](#) for all measurements. The column *s%* reports the standard deviation of the measurements collected during each day. As expected, *s%* values for *Q* are slightly lower than for *TNRD*, meaning that the proportionality between proton current and thermal neutron fluence rate at the point is slightly perturbed by other beam-related sources of influence (positioning, focus, energy constancy). The impact of these sources of influence on the beam reproducibility may be estimated from the values of *s%* for *TNRD_n*. These values, $\pm 3.5\%$, $\pm 2.2\%$ and $\pm 1.7\%$, have been corrected by subtracting in quadrature the *TNRD* reproducibility ($\pm 1.2\%$), obtaining $\pm 3.3\%$, $\pm 1.9\%$ and $\pm 1.2\%$. Every measurement day is characterized by a different average value of *TNRD_n* (± 1.24 , ± 1.31 and ± 1.21), indicating that each time the accelerator is turned on and regulated, a slightly different point of work is achieved. Thus, the global inter-day uncertainty obtained for the thermal neutron beam is $\pm 4.0\%$, taking into account *TNRD* reproducibility. The availability of a reliable thermal neutron monitor, in parallel to the proton current measuring device, will be a mandatory condition to achieve reproducible irradiation conditions on

Table I. *TNRD readings, accumulated charge (Q) and TNRDn values along the three measurement days.*

Day	Measurement	Q (mC)	S _n (%)	TNRD (V·s)	TNRDn (V·s/mC)
1	1	15.3		19.8	1.29
	2	13.6	9.7%	16.7	1.22
	3	12.7		15.3	1.21
2	1	15.9		21.4	1.35
	2	13.9		18.5	1.33
	3	13.3	7.9%	17.2	1.29
	4	13.6		17.4	1.28
	5	13.2		17.1	1.30
3	1	14.9		18.3	1.23
	2	14.2	2.5%	16.9	1.19
	3	14.8		17.8	1.20

this thermal neutron field. When irradiating generic devices in routine condition, the thermal neutron detector could be permanently positioned at a given angle from the target (different from 0°), or embedded in the moderating block, in order not to perturb the device under test. This would allow providing the exact value of thermal fluence delivered to a sample during a given exposure, with uncertainties comparable with the *TNRD* reproducibility.

Rough estimation of the thermal field homogeneity was performed with additional acquisitions by shifting the *TNRD*, 3 mm vertically and, successively, 3 mm laterally, from the conventional point of test. This shift was much larger than the positioning uncertainty guaranteed by the laser-based alignment

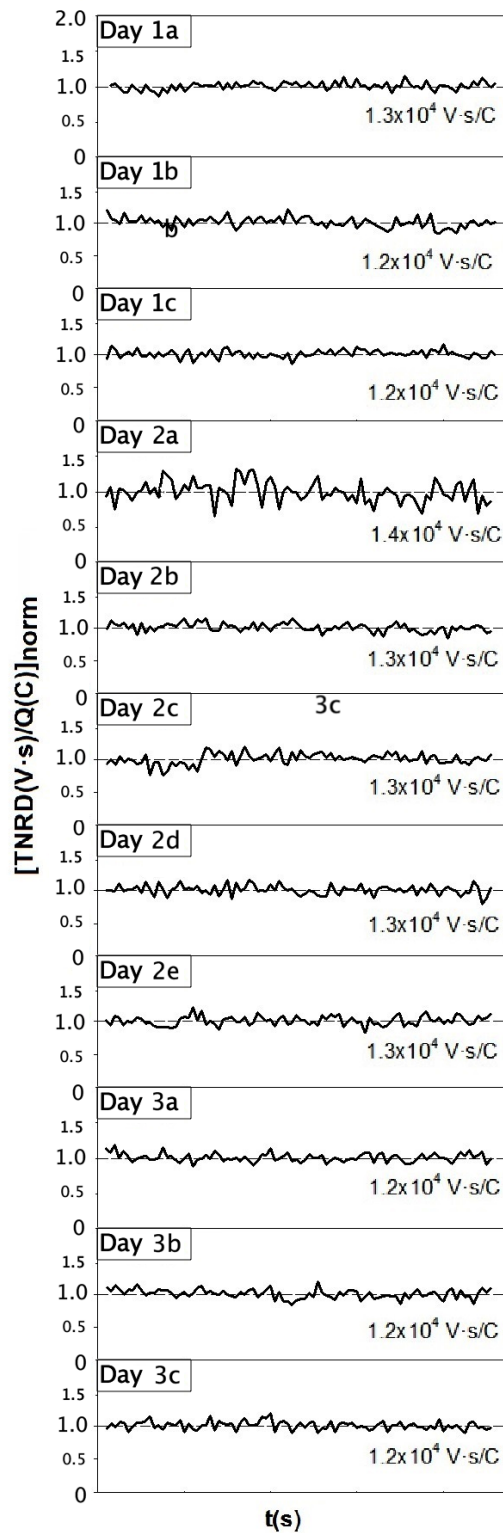


Figure 5. On-line monitoring of the normalized ratio: (signal in V·s per accumulated charge in C) due to the thermal neutron fluence for each measurement. The number in the right part of each graph represents the global ratio among the whole measurement.

system (<1 mm). The corresponding $TNRD_n$ values differed by less than 1% from the value at the point of test.

An additional test was performed by rotating the $TNRD$ of about $\pm 20^\circ$. The observed decrease in the $TNRD_n$ value was about 7%, fully coherent with a cosine correction with angle 20° . This indicates that the angular distribution of the emitted thermal neutrons is nearly monodirectional. It is therefore clear that a good detector orthogonality is crucial for reproducible irradiation condition.

4. Conclusions

A thermal neutron test facility was achieved at the 3 MV Tandem Pelletron accelerator at CNA. A specific combination on proton energy, target thickness, lead shield and polyethylene moderator was studied to achieve an almost pure, photon-free, thermal field at the conventional point of test. Values of thermal neutron fluence rate up to $2 \times 10^3 \text{ cm}^{-2}\text{s}^{-1}$ can be easily achieved. The reproducibility of the thermal neutron beam was estimated in $\pm 4\%$, over three days of operation, using a proton current integrator fixed on the target backing, and a $TNRD$ -type miniaturized thermal neutron detector placed at the point of test. As expected, the proportionality between the proton current and the thermal neutron fluence rate, is perturbed by a complex set of beam-dependent factors of influence. These factors limit to about $\pm 3\%$ the reproducibility of the thermal field at the point of test. However, this facility can still be used to deliver accurate values of thermal neutron fluence, if a thermal neutron detector is permanently adopted in parallel to the proton current monitor. Embedding this detector in the moderator, in a peripheral position with respect to the 0° direction, would constitute a convenient option. Additional experiments are planned to (a) estimate the overall accuracy of the delivered thermal neutron fluence with a couple of $TNRDs$, one embedded in the moderator (monitor) and another at the point of test, (b) evaluate the spatial homogeneity of the thermal

field over the whole area of the moderating plate, (c) measure the associated photon field with a reference instrument calibrated in air-kerma, and (d) establish metrologic traceability to a primary metrology Institute, for the value of thermal neutron fluence rate. After completing these actions, the studied field could be used in practice as thermal neutron calibration facility. Main advantages of this facility are:

- The spectral purity, meaning that the field is not contaminated by fast neutrons;
- Absence of radioactive sources, with considerably less safety problems with respect to radionuclide-based thermal fields.
- The installation of a continuous beam monitor will allow to use the facility with both rate-meter type or integration-type detectors.

5. Acknowledgments

This work would not be possible without the financial support of the CSN (Consejo de Seguridad Nuclear), Junta de Andalucía (FQM-8229), Mineco (FPA2013-47327-C2-1-R) and CEI-Biotic Granada (P-BS-64). The authors thank Juan Manuel Macarro for his inestimable technical help in the construction of the collimator and the assembly of the setup. They also wish to express their gratitude to the CNA staff, in special to Juan Angel Labrador and Angel Jesús Romero, for the high quality of the provided proton beam and their help during the experiments. They would also like to acknowledge the help provided by R. Chamorro and L. Hidalgo from the Electromedicine department of HUMV. TNRD detector was manufactured within the INFN projects NESCOFI@BTF and NEURAPID (Commissione Scientifica 5, INFN Italy).

6. References

- Bedogni R, Bortot D, Introini MV, Gentile A, Esposito A, Gómez-Ros JM, Palomba M, Gross A. *A new active thermal neutron detector*. Radiat Prot Dosim 2014;161(1–4):241–244.
- Expósito MR, Sánchez-Nieto B, Terrón JA, Domingo C, Gómez F, Sánchez-Doblado F. *Neutron contamination in radiotherapy: estimation of second cancers based on measurement in 1377 patients*. Radiother Oncol 2013;107:234–241.
- Gómez F, Iglesias A, Sánchez-Doblado F. *A new active method for the measurement of slow-neutron fluence in modern radiotherapy treatment rooms*. Phys Med Biol 2010;55:1025–1039.
- Irazola L, Lorenzoli M, Bedogni R, Pola A, Terrón JA, Sánchez-Nieto B, Expósito MR, Lagares JI, Sansaloni F, Sánchez-Doblado F. *A new online detector for estimation of peripheral neutron equivalent dose in organ*. Med Phys 2014;41:112105.
- Irazola L, Terrón JA, Bedogni R, Lorenzoli M, Pola A, Sánchez-Nieto B, Sánchez-Doblado F. *Signal photon component of a new thermal neutron detector TNRD in radiotherapy environments*. Radiother Oncol 2015a;115(1):S870 (EP-1589).
- Irazola L, Terrón JA, Bedogni R, Lorenzoli M, Pola A, Sánchez-Nieto B, Sánchez-Doblado F. *TNRD neutron detector signals for different gantry angles in 6 and 15 MV*. Radiother Oncol 2015b;115(1):S761 (EP-1410).
- Irazola L, Terrón JA, Sánchez-Nieto B, Bedogni R, Gómez F, Sánchez-Doblado F. *Effects of cable extension and photon irradiation on TNRD neutron detector in radiotherapy*. WC 2015, IFMBE Proceedings 51/IV, Berlin, Springer, 2015c;645–649.
- Lacoste V. *Design of a new IRSN thermal neutron field facility using MonteCarlo simulations*. Radiat Prot Dosim 2007;126(1–4):58–63.
- Lederer C, Käppeler F, Mosconi M, Nolte R, Heil M, Reifarh R, Schmidt S, Dillmann I, Giesen U, Mengoni A, Wallner A. *Definition of a standard neutron field with the ${}^7\text{Li}(p,n){}^7\text{Be}$ reaction*. Phys Rev C 2012;85:055809.
- Lee CL, Zhou X-L. *Thick target neutron yields for the ${}^7\text{Li}(p,n){}^7\text{Be}$ reaction near threshold*. Nucl Instrum Methods Phys Res SectB 1999 ;152:1–11.
- Muller H, Gressier V, Lacoste V, Lebreton L, Pochat J-L. *Characterization of the Thermal Neutron Field Produced by the IRSN Sigma Facility*. Abstract book Neudos, Delft, The Netherlands 9;2003.
- Pelowitz DB. *MCNPX Users Manual Version 2.5.0-LA-CP05-0369*. Los Alamos National Laboratory LACP, USA. 2005.
- Praena J, Mastinu PF, Pignatari M, Quesada JM, García-López J, Lozano M, Dzysiuk N, Capote R, Martín-Hernández G. *Measurement of the MACS of ${}^{181}\text{Ta}(n,\gamma)$ at $kT^{1/4}30\text{ keV}$ as a test of a method for Maxwellian neutron spectra generation*. Nucl Instrum Methods Phys Res 2013;727:1–6.
- Praena J, Mastinu PF, Pignatari M, Quesada JM, Capote R, Morilla Y. *Measurement of the MACS of ${}^{159}\text{Tb}(n,\gamma)$ at $kT^{1/4}30\text{ keV}$ by activation*. Nucl Data Sheets 2014;120:205–207.
- Praena J, Irazola L, Fernández B, Terrón JA, Bedogni R, Lorenzoli M, Pola A, Sánchez-Nieto B, Sánchez-Doblado F. *Proposal of thermal neutron detector stability for peripheral dose estimation in clinic at a novel neutron facility*. Radiother Oncol 2015;115(1):S735 (EP-1365).
- Romero-Expósito MR, Sánchez-Nieto B, Terrón JA, Lopez MC, Ferreira BC, Grishchuk D, Sandíns C, Moral-Sánchez S, Bragado-Álvarez L, Melchor M, Domingo C, Gómez

- F, Sánchez-Doblado F. *Commissioning the neutron production of a linac: development of a clinical planning tool for second cancer risk estimation*. Med Phys 2015;42:276–281.
- Sánchez-Doblado F, Domingo C, Gómez F, Sánchez-Nieto B, Muñoz JL, GarcíaFusté MJ, Expósito MR, Barquero R, Hartmann G, Terrón JA, et al. *Estimation of neutron equivalent dose in organs of patients undergoing radiotherapy by the use of a novel online digital detector*. Phys Med Biol 2012;57:6167–6191.
- Terrón JA, Irazola L, Morilla Y, Muñoz G, Bedogni R, Lorenzoli M, Pola A, Sánchez-Nieto B, Sánchez-Doblado F. *Photon energy response of TNRD neutron detector in a ^{60}Co irradiator and a 6 MV clinic*. Radiother Oncol 2015;115(1):S757–S758 (EP-1404).
- Yu W, Yue G, Han X, Chen J, Tian B. *Measurements of the neutron yields from $^7\text{Li}(p,n)^7\text{Be}$ reaction (thick target) with incident energies from 1.885 to 2.0 MeV*. Med Phys 1998;25(7 Pt 1):1222–1224.

III. Thesis core

2. Publications: **(B.1)** *Using a Tandem Pelletron accelerator to produce a thermal neutron beam for detector testing purposes*

(B.2)**Improving the neutron-to-photon discrimination capability of detectors used for neutron dosimetry in high energy photon beam radiotherapy**

Irazola et al., Appl Radiat and Isot, in press

Abstract

The increasing interest of the medical community to radioinduced second malignancies due to photoneutrons in patients undergoing high-energy radiotherapy, has stimulated in recent years the study of peripheral doses, including the development of some dedicated active detectors. Although these devices are designed to respond to neutrons only, their parasitic photon response is usually not identically zero and anisotropic. The impact of these facts on measurement accuracy can be important, especially in points close to the photon field-edge.

A simple method to estimate the photon contribution to detector readings is to cover it with a thermal neutron absorber with reduced secondary photon emission, such as a borated rubber. This technique was applied to the TNRD (Thermal Neutron Rate Detector), recently validated for thermal neutron measurements in high-energy photon radiotherapy. The positive results, together with the accessibility of the method, encourage its application to other detectors and different clinical scenarios.

1. Introduction

New radiotherapy techniques, such as those with intensity modulation of the beam fluence, reduce the amount of healthy tissue exposed to high radiation doses. However, these techniques are usually associated to a greater demand in terms of Monitor Units (MU), which implies an increase of the out-of-field doses (also called peripheral doses; [Xu et al.,2008](#)). The latter, together with increment of the low-dose volumes and the larger survival after radiotherapy treatments, have made the incidence of late effects, such as second malignant neoplasms more relevant. Therefore, an important number of dosimetry studies have been conducted to determine peripheral doses more accurately. These doses have two main components: leakage/scattered photons and neutron contamination. Since dosimetric methods for photon doses are well-known ([Sánchez-Nieto et al., 2015](#); [Taddei et al.,2013](#)), our group has focused on the neutron component, and established a methodology to estimate neutron peripheral doses ([Sánchez-Doblado et al., 2012](#); [Expósito et al., 2013](#), [Romero-Expósito et al.,2015](#); [Vázquez-Luque et al.,2013](#)). This procedure was developed for a particular thermal neutron detector ([Gómez et al., 2010](#)) but applicable to any other ([Guardiola et al., 2013](#); [Bedogni et al., 2014](#)).

Specifically, the methodology by [Sánchez-Doblado et al., 2012](#) was applied to a *TNRD* (*Thermal Neutron Rate Detector*) detector, designed and developed by [Bedogni et al., 2014](#) and thus characterized for neutron peripheral dose measurements in radiotherapy environments. The *TNRD* showed satisfactory performances in terms of user friendliness and high sensitivity ([Irazola et al.,2014](#)). Nevertheless, recent experiments with the detector located ‘in-phantom’ close to the border of the field, indicated the need for further investigations in relation to unexpected behaviors. A comprehensive analysis on the electronic, cable length and detector ageing, as possible causes for the rear events, was carried out. However, it turned out to be related with photon

rejection issues and detector anisotropy under some critical conditions (Irazola et al., 2015a;b;c; Praena et al., 2015; Irazola et al., 2016). These parasitic effects were indeed directly observed during exposures with ^{60}Co and 6 MV Linac (Terrón et al., 2015), where no neutrons are present. However, a methodology for the neutron-to-photon discrimination in TNRD readings during high-energy photon radiotherapy has yet to be found.

This paper proposes a simple method to estimate photon contribution to TNRD readings by covering the detector with a thermal neutron absorber (with reduced secondary photon emission), such as a borated rubber. For the present work a commercial material, called Flex-Boron[®] (http://www.deqtech.com/Shieldwerx/Data_Sheets/SWX-238.pdf), was used. This material (Gómez et al., 2010; D'Mellow et al., 2007) is expected to reduce incident thermal neutron field to less than 1%. Thus, the pure thermal neutron reading of a detector can be obtained by subtracting the reading of the rubber-covered detector to the uncovered one.

2. Material and method

2.1 TNRD detector

TNRD detector, developed by Bedogni et al., 2014 in the framework of the NESCOFI@BTF project (2011-2013, Scientific Commission V, INFN-LNF, Italy), is based on a low-cost commercial solid-state device made sensitive to thermal neutrons through a customized physical–chemical treatment (mainly consisting on a ^6Li deposition layer). Its active area is 1 cm^2 and its overall dimensions are $1.5\text{ cm} \times 1\text{ cm} \times 0.4\text{ cm}$ (Figure 1). Its output is a DC voltage, which is proportional to the thermal neutron fluence rate (for this reason the device is called "rate detector"). This signal is amplified in a low-voltage electronics module especially developed by the project team. The amplified output is sent to a programmable ADC (NI USB-6218 BNC, 16 bit, up to 250 kilo samples per

second) controlled by a PC through a LabView application. TNRD has a linear response to thermal neutron fluence rates exposures from 10^2 up to 10^6 $\text{cm}^{-2}\cdot\text{s}^{-1}$. Every single TNRD (Figure 1) is individually calibrated by exposing it to a suitable reference thermal field (Bedogni et al.,2016). Detector-to-detector response variability is of the order of $\pm 5\%$ (1 SD).

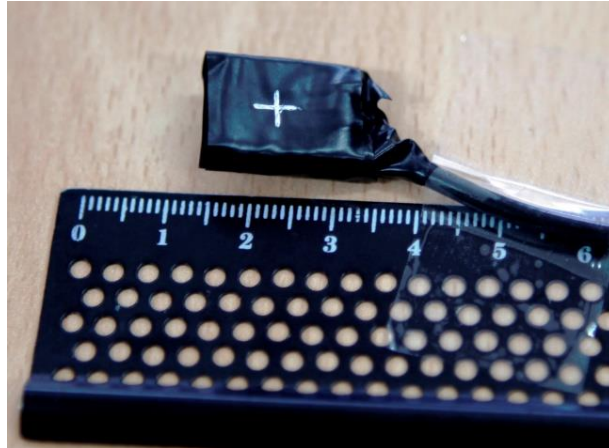


Figure 1. TNRD (Thermal Neutron Rate Detector).

2.2 The borated rubber

Firstly, the photon absorption of borated rubber was characterized in relation to equivalent water material (a common surrogate of human tissue). Results showed that 0.32 cm ($\rho=1.64$ g/cm^3) of rubber presented the same photon attenuation as 0.5 cm of polystyrene ($\rho=1.05$ g/cm^3) usually employed. This equivalence is independent of the primary photon field energy, since the out-of-axis photon spectrum is mainly composed by photons below 0.5 MeV (D'Mellow et al.,2007; Chofor et al.,2012). In addition, due to the high neutron capture cross section of ^{10}B , the borated rubber acts as an efficient neutron absorber (Guardiola et al.,2013; <http://www.johncaunt.com/shielding/neutron-shielding/jc238/>), with a nominal thermal neutron transmission factor of 3.8×10^{-3} . Two layers of Flex-boron® (5 cm x 20 cm) were used to cover above and below the set of five detectors used here.

2.3 Irradiation tests

Exposures were performed in a Siemens Primus Linac (6 and 15 MV) at Hospital Universitario Virgen Macarena, Seville (Spain) for a 40x10 cm² field and 300 MU (1 MU delivers 1 cGy under reference conditions, e.g. 10x10 cm², gantry 0°, source-axis distance 100 cm, depth of maximum for each energy in water). The following test were performed:

(a) Free-in-air measurements

During the irradiation of the patients, thermal neutron measurements are performed with bare detectors located in front of the couch, at about 3 m distance ([Expósito et al.,2013](#); [Figure 2](#)). Neutron peripheral dose estimations are done from detector readings following the methodology established in [Sánchez-Doblado et al., 2012](#). Under this conditions, it is expected a minimal photon contribution to the detector reading and a low directionality dependence for the detector. This assumption was tested under an adverse clinical scenario representative of a breast treatment. It consisted of four beams of high (15 MV) and low (6 MV) energy, applied alternatively using 122° and 300° incidence angles for each energy. 8 MU and 168 MU for the high and low energy beams were used, respectively.

(b) In-phantom measurements at different distances

Out-of-field photon doses were determined with a PTW Farmer® ion chamber 30013 (operated at -250 V) and a PTW Unidos electrometer. Measurements were carried out at a set of positions from 0.1 to 2 m from the border of the field, with 0° gantry incidence (perpendicular to the treatment couch). Ion chamber and/or five TNRD detectors were inserted in a set of plastic layers (30x30 cm²) simulating 'in-phantom' attenuation; patient scatter was mimicked with additional plastic material ([Figure 3](#)).

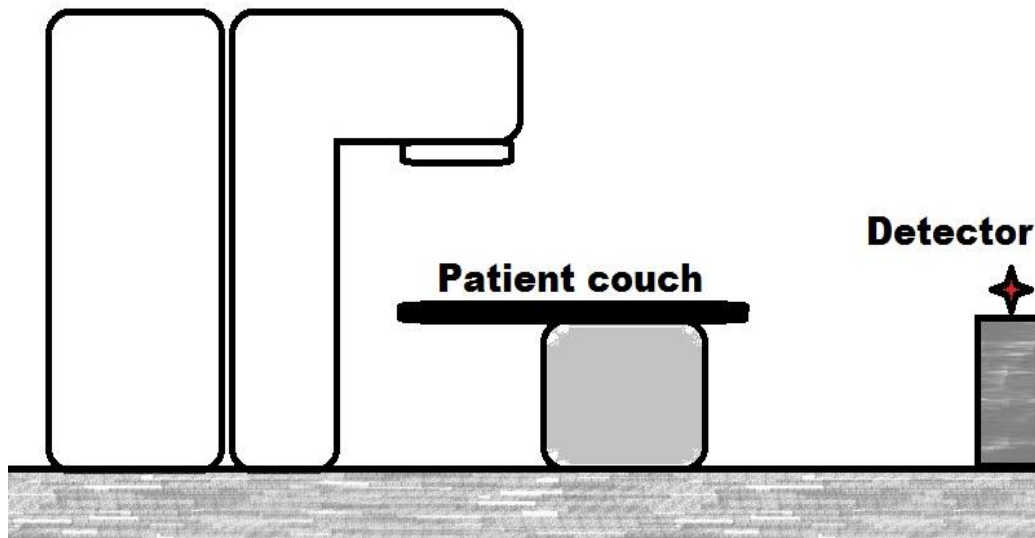


Figure 2. TNRD location for patient measurements (*free-in-air*).

Two different settings inside the (8 cm thick) phantom were used: one where the ion chamber and the TNRD detectors were placed together at mid depth of the plastic phantom (insert *i* in Figure 3) and the other one where the TNRD detectors were placed (insert *ii* in Figure 3) between borated rubber layers (Flex-boron®) with the equivalent replaced plastic thickness (see section 2.2).

“Plastic” and “borated” measurements were carried out at low energy (6 MV), where neutron presence is negligible and at high energy (15 MV).

(c) *In-phantom measurements at different beam incidence angles*

In order to evaluate TNRD anisotropic response, two specific field-edge distances (0.15 and 0.35 m) were measured for 14 different beam angle incidences, covering 360°.

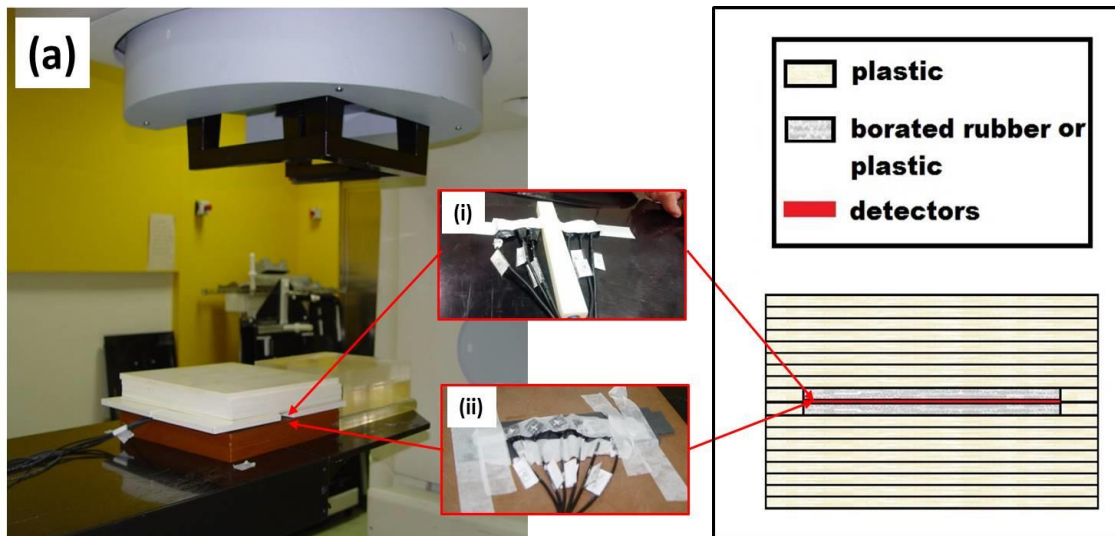


Figure 3. (a) Set up for the photon sensitivity study for measurements outside the treatment field (0.1 to 2 m from the field edge) for five of the devices. Additional plastic material has been used to simulate patient scatter. TNRD detectors were placed as shown in insert (i) with Flex-boron material above and below and (ii) with an ionization chamber location for photon dose estimations when plastic is used. Figure (b) represents a schema of detector location in the slab phantom.

3. Results and discussion

3.1 Free-in-air measurements

Figure 4a shows the time-dependent TNRD reading for the selected clinical scenario. Detector "baseline" is represented by the red dashed line. The α and β peaks correspond to the neutron signal from the 15 MV beam. Inserts show a zoom of TNRD readings when: (4b) no beam is present and (4c) only the 6 MV beam is on (negligible neutron presence). The behavior of TNRD readings showed in insert (4c), indicates that photons induce baseline oscillations but, as expected, their average is null in practice.

It should be noted that, due to the anisotropic response of the detector, the point where a photon-induced secondary electron is generated would affect the

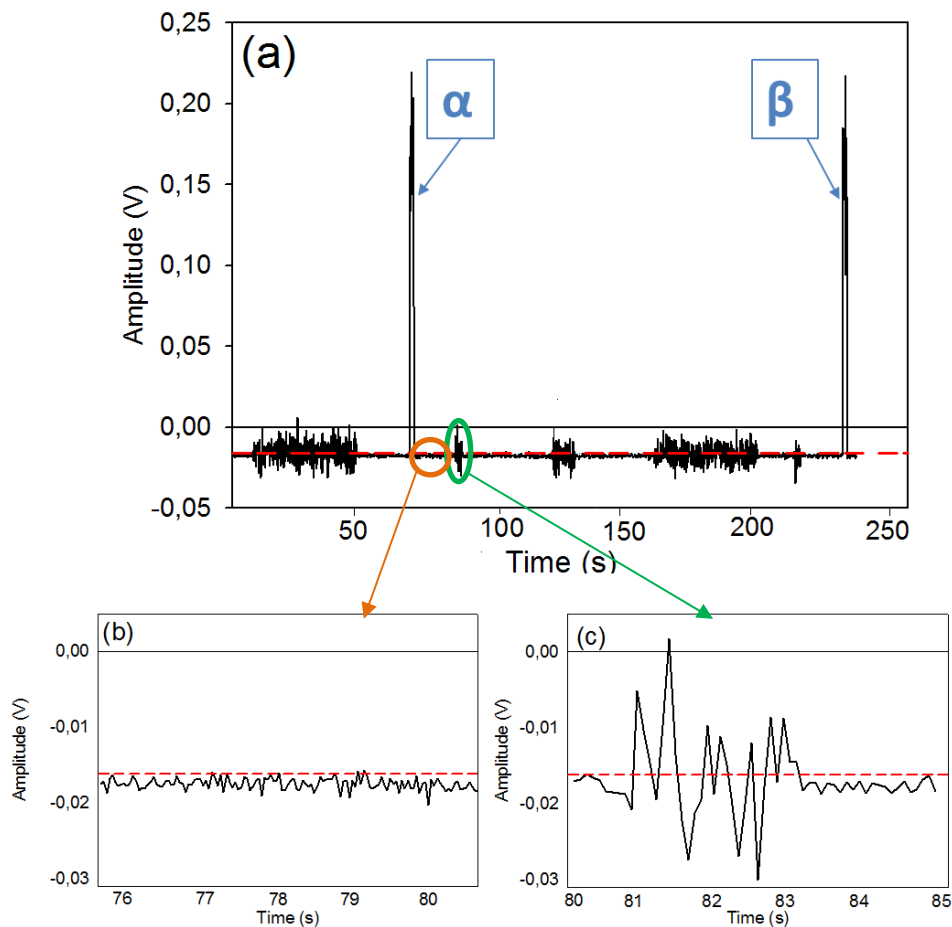


Figure 4. (a) TNRD signal during the free-in-air measurement for a real breast treatment case, combining 6&15 MV. Baseline is represented by the red dashed line. Insert (b) and (c) show a zoom of TNRD signal for no beam and 6 MV beam, respectively.

charge collection event, which may result in a positive or negative pulse. The internal structure of the detector was designed so that the convolution of these signals yields a zero-average voltage level in photon fields. By contrast, in neutron fields, the average level is a positive value proportional to the fluence rate. This TNRD behavior makes it valid during patient irradiation (free-in-air measurements) where photon contribution is slight compared with neutron one. However, problems in photon rejection can become more important when photon background increases as during “in-phantom” measurements (see later on).

3.2 In-phantom measurements at different distances

Figure 5 reports TNRD readings for "plastic" and "borated" measurements with 6 MV. Photon doses at each measurement point were known as detectors were exposed together with the ion chamber (see 2.3a). As expected, in absence of neutrons, both readings coincide within uncertainties. That is, borated rubber does not introduce perturbation to photon attenuation.

Similarly, Figure 6 shows "plastic" and "borated" measurements in 15 MV. The line represents neutron signal (obtained as the following subtraction: "plastic" - "borated"). As expected, the parasitic photon signal gains relevance at short distances (≤ 0.3 m from the field-edge). Percentage of photon to total signal it ranges from 3.7% at 2 m up to 26% at 0.15 m.

3.3 In-phantom measurements at different beam incidence angles

Figure 7a shows TNRD "borated" readings for fourteen different beam incidences (Figure 7b) at two border of the field to detector distances. As expected from previous experiences (Irazola et al.,2015c), photon component compensates for complementary angles. Thus, its influence is almost negligible if "balanced" incidence angles (uniformly covering 360°) are used. This is a usual approximation used in conventional radiotherapy treatments that was also used in Irazola et al.,2014. There is an important angular photon dependence of TNRD devices, being clearly different for beam incidences comprised in the range (280° - 75°) or (250° - 105°). This problem would be solved with the use of the proposed methodology. However, when bare detectors are used for these measurements in "balanced" treatments, due to the almost complementary TNRD response, the parasitic averaged photon contribution found was -4.4% at 0.15 m and +1.5% at 0.35 m, being lower for further points.

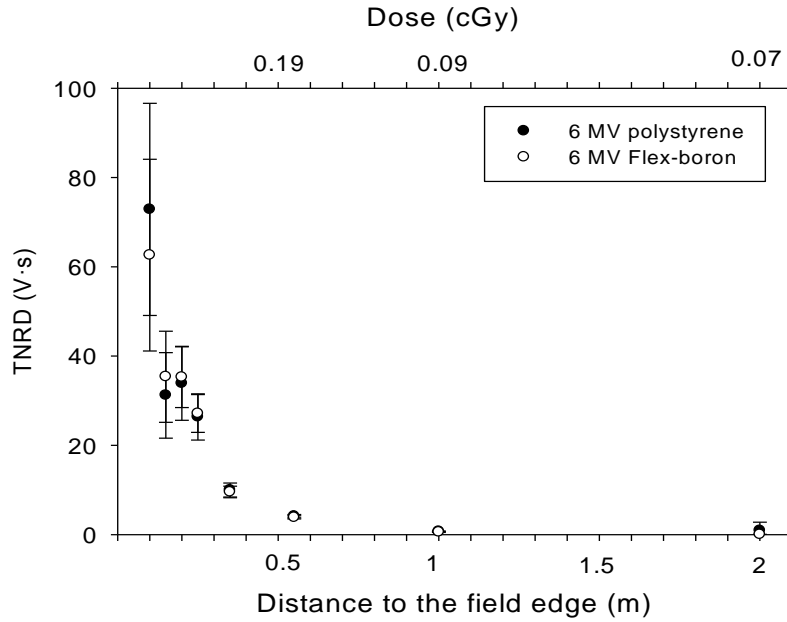


Figure 5. "Plastic" and "borated" measurements in a 6 MV field, with field-edge distances from 0.1 to 2 m. Photon doses were determined with a Farmer ionization chamber.

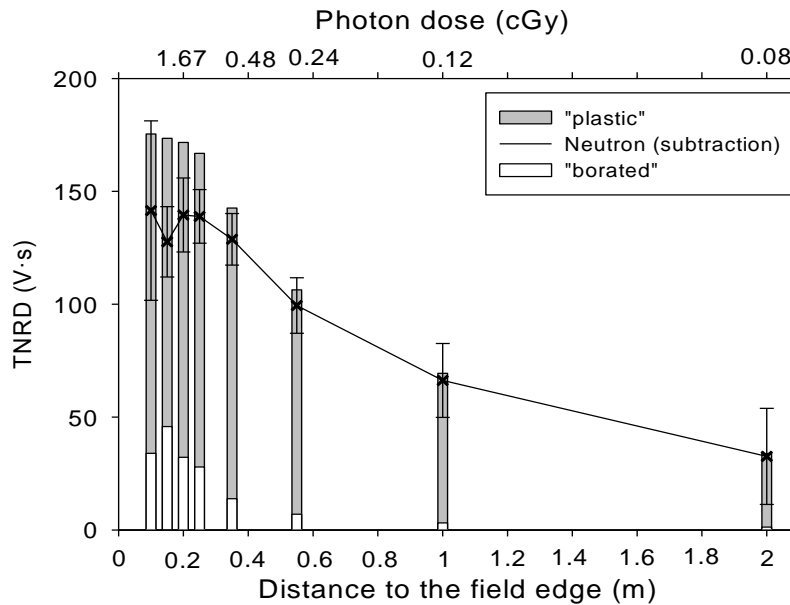


Figure 6. Neutron contribution (lines) to TNRD readings for 15 MV. Grey + white bars correspond to "plastic" readings for different field edge to detector distances (lower axis) and corresponding photon doses estimated with the Farmer ionization chamber (upper axis). Photon estimates (white areas) have been obtained by terms of 15 MV readings when the detector is covered with borated rubber material. Error bars have been estimated considering both uncertainties.

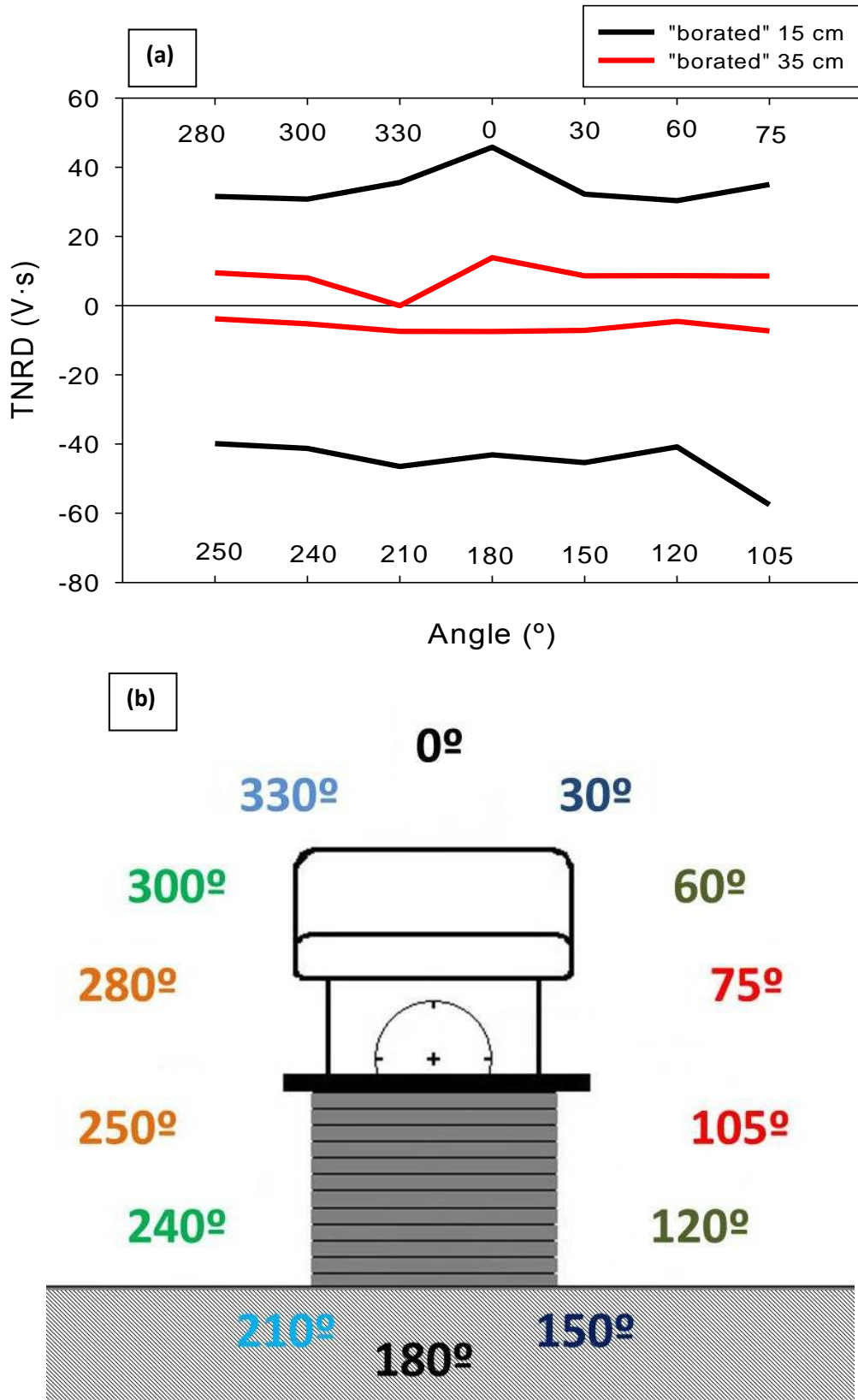


Figure 7. (a) Photon contribution to TNRD readings, estimated by measuring with Flex-boron material (in 15 MV) for different gantry incidences, at two different field edge-detector distances ($d=35$ cm red and $d=15$ cm black). (b) Gantry angle schema for the studied incidences. Complementary angles are represented with the same color.

4. Conclusions

This work showed a simple methodology to improve the photon rejection in thermal neutron detectors used in medical physics for the measurement of neutron equivalent doses in peripheral organs, during high-energy radiotherapy treatments. The importance of such measurements increased in recent years, in correspondence with the introduction of modern radiotherapy techniques, implying a higher demand of MU with respect to conventional ones.

The use of TNRD detectors in peripheral neutron dose estimations showed some problems related with photon rejection. Thus, a methodology to improve neutron-to-photon discrimination capability of TNRD detector has been established, applicable to any other thermal neutron detector. It consists in the use of two borated rubber layers covering the detector with an equivalent thickness in terms of photon absorption. The "borated" measurement directly gives the photon contribution of the detector reading, whilst the thermal neutron contribution is given by the difference: "plastic" - "borated".

Tests with TNRD detector showed that this methodology is not needed when detector is located far from the field-edge (such as the here mentioned free-air patient measurements) while its importance is clear for closer distances (≤ 0.3 m). This parasitic signal decreases from 26% at 0.15 m up to 3.7% at 2 m, where 100% is the "bare" reading.

Angular incidence is also an important fact due to the anisotropic response of the detector, solved with the use of borated rubber. Nevertheless, when a treatment is carried out with "balanced" incidence angles (uniformly covering 360° in terms of delivered MU), the overall effect is reduced to $\leq 1.5\%$ further than 0.35 m.

A further activity, especially intended to generalize this technique and to extend it to other groups, could be the development of equivalent plastic and borated bags exactly containing the detector. This would completely shield the detector and, at the same time, reduce to the minimum extent the photon field perturbation.

5. Acknowledgments

This work would not be possible without the use of hospital resources which were kindly provided by the management of the Department of Radiotherapy and Oncology of the University Hospital Virgen Macarena in Seville. The authors would like to acknowledge the technical help provided by R. Chamorro and L. Hidalgo from the Electromedicine Department of HUVM. We would also like to thank Z. Krulick for her revision of grammar and style.

6. References

- Bedogni R, Bortot D, Pola A, Introini MV, Gentile A, Esposito A, Gómez-Ros JM, Palomba M, Grossi A. *A new active thermal neutron detector*. Radiation Protection Dosimetry. Radiat Prot Dosim 2014;161(1–4):241–244.
- Bedogni R, Sacco D, Gómez-Ros JM, Lorenzoli M, Gentile A, Buonomo B, Pola A, Introini MV, Bortot D and Domingo C. *ETHERNES: A new design of radionuclide source-based thermal neutron facility with large homogeneity area*. Appl Radiat and Iso 107 (2016) 171–176.
- Chofor N, Harder D, Willborn K C and Poppe B. *Internal scatter, the unavoidable major component of the peripheral dose in photon-beam radiotherapy*. Phys Med Biol 2012;57: 1733–1743.
- D’Mellow B, Thomas D J, Joyce M J, Kolkowski P, Roberts N J, Monk S D. *The replacement of cadmium as a thermal neutron filter*. Nucl Instr Meth Phys Res A 2007; 577(3):690 – 695.
- Expósito MR, Sánchez-Nieto B, Terrón JA, Domingo C, Gómez F and Sánchez-Doblado F. *Neutron contamination in radiotherapy: Estimation of second cancers based on measurement in 1377 patients*. Radiother and Oncol 2013;107:234-241.
- Gómez F, Iglesias A and Sánchez-Doblado F. *A new active method for the measurement of slow-neutron fluence in modern radiotherapy treatment rooms*. Phys Med Biol 2010;55:1025-1039.
- Guardiola C, Gómez F, Fleta C, Rodríguez J, Quirion D, Pellegrini G, Lousa A, Martínez-de-Olcoz L, Pombar Mand Lozano M. *Neutron measurements with ultra-thin 3D silicon sensors in a radiotherapy treatment room using a Siemens PRIMUS linac*. Phys Med Biol 2013;58 :3227–3242.

- Irazola L, Lorenzoli M, Bedogni R, Pola A, Terrón J A, Sanchez-Nieto B, Expósito M R, Lagares J I, Sansaloni F and Sanchez-Doblado F. *A new online detector for estimation of neutron equivalent dose in organ*. Med Phys 2014;41(11):112105:1-5.
- Irazola L, Terron J A, Sanchez-Nieto B, Bedogni R, Gomez F and Sanchez-Doblado F. *Effects of cable extension and irradiation on TNRD neutron detector in radiotherapy*. IFMBE Proceedings 2015a;51:645-648.
- Irazola L, Terron J A, Bedogni R, Lorenzoli M, Pola A, Sanchez-Nieto B and Sanchez Doblado F. *Signal photon component of a new thermal neutron detector TNRD in radiotherapy environments*. Radiother Oncol 2015b;115(1):S870.
- Irazola L, Terron J A, Lorenzoli M, Pola A, Sanchez-Nieto B and Sanchez-Doblado F. *TNRD neutron detector signals for different gantry angles in 6 and 15 MV*. Radiother Oncol 2015c;115(1):S761.
- Irazola L, Praena J, Fernandez B, Macias M, Terron JA, Bedogni R, Sanchez-Nieto B and Sanchez-Doblado F. *Monitoring the stability of a thermal neutron detector using a moderated neutron beam from a Tandem Peletron*. Appl Radiat Isot 2016;107:330-334.
- Praena J, Irazola L, Fernández B, Terrón J A, Bedogni R, Lorenzoli M, Pola A, Sánchez-Nieto B and Sánchez-Doblado F. *Proposal of thermal neutron detector stability for peripheral dose estimation in clinic at a novel neutron facility*. Radiother and Oncol 2015;115(1):S735.
- Romero-Expósito M, Sánchez-Nieto B, Terrón JA, Lopez MC, Ferreira BC, Grishchuk D, Sandíns C, Moral-Sánchez S, Bragado-Álvarez L, Melchor M, Domingo C, Gómez F and Sánchez-Doblado F. *Cominsioning the neutron production of a linac: development of a clinical planning tool for second cancer risk estimation*. Med Phys 2015;42:276-281.
- Sánchez-Doblado, F, Domingo, C, Gómez, F, Sánchez-Nieto B, Múñiz J L, García-Fusté M J, Expósito M R, Barquero R, Hartmann G H, Terrón J A, et al. *Estimation of neutron equivalent dose in organs of patients undergoing radiotherapy by the use of a novel online digital detector*. Phys Med Biol 2012;57:6167-6191.
- Sánchez-Nieto B, El-far R, Irazola L, Expósito MR, Lagares JI, Mateo JC, Terrón JA and Sánchez-Doblado F. *Analytical model for photon peripheral dose estimation in radiotherapy treatments*. Biomed Phys Eng Express 2015;1:045205.
- Taddei JP, Wassim J, Howell RM et al. *Analytical model for out-of-field dose in photon craniospinal irradiations*. Phys Med Biol 2013;58, 7463-7479.
- Terron J A, Irazola L, Morilla Y, Muñiz G, Bedogni R, Lorenzoli M, Pola A, Sanchez-Nieto B and Sanchez-Doblado F. *Photon energy response of TNRD neutron detector in a ⁶⁰Co irradiator and a 6 MV clinic*. Radiother Oncol 2015;115(1):S757-758.
- Vazquez-Luque A, Marin J, Terrón J A, Pombar M, Bedogni R, Sánchez-Doblado F and Gomez F. *Neutron Induced Single Event Upset Dependence on Bias Voltage for CMOS SRAM With BPSG*. IEEE TRANSACTIONS ON NUCLEAR SCIENCE, 2013;60(6):4 692-4696.
- Xu X-G, Bednarz B, Paganetti H. *A review of dosimetry studies on external-beam radiation treatment with respect to second cancer induction*. Phys Med Biol 2008;53:R193-R241.

(B.3)

Neutron measurements in radiotherapy: a method to correct neutron sensitive devices for parasitic photon response

Irazola et al., Sent to Applied Radiat Isot

Abstract

One of the major causes of secondary malignancies after radiotherapy treatments are peripheral doses, known to increase for some newer techniques (such as IMRT or VMAT). For accelerators operating above 10 MV, neutrons can represent important contribution to peripheral doses. This neutron contamination can be measured using different passive or active techniques, available in the literature. As far as active (or direct-reading) procedures are concerned, a major issue is represented by their parasitic photon sensitivity, which can significantly affect the measurement when the point of test is located near to the field-edge. This work proposes a simple method to estimate the unwanted photon contribution to these neutrons. As a relevant case study, the use of a recently neutron sensor for “in-phantom” measurements in high-energy machines was considered. The method, called “Double Energy Photon Subtraction” (DEPS), requires pairs of measurements performed for the same treatment, in low-energy (6 MV) and high energy (e.g. 15 MV) fields. It assumes that the peripheral photon dose (PPD) at a fixed point in a phantom, normalized to the unit photon dose at the isocenter, does not depend on the

treatment energy. Measurements with ionization chamber and Monte Carlo simulations were used to evaluate the validity of this hypothesis. DEPS method was compared to already published correction methods, such as the use of neutron absorber materials. In addition to its simplicity, an advantage of DEPs procedure is that it can be applied to any radiotherapy machine.

1. Introduction

New radiotherapy (RT) techniques, such as those based on beam fluence intensity modulation, are known to provide higher healing rates and larger survival after treatments. However, this increase in life expectancy has brought to light some late effects such as second malignant neoplasms. Although these techniques provide a greater degree of conformity, they are also known to increase peripheral doses (PD) due to their higher demand of Monitor Units (MU) and to dose escalation strategies, usually associated to these modern techniques (Xu et al.,2002). PD are mainly composed of two different contributions: leakage/scattered photons and neutrons. While photon peripheral doses have been widely investigated (Van der Giessen et al.,2001; Sánchez-Nieto et al., 2015; Jagetic et al.,2015), neutron contamination has been largely undervalued.

In previous works, this group established a method to infer peripheral neutron doses, estimated from in-phantom thermal neutron measurements. (Gómez et al.,2012; Sánchez-Doblado et al.,2012; Expósito et al.,2013; Romero-Expósito et al.,2015). These neutron doses have been used to assess secondary cancer risks. On this basis, different treatment strategies can be compared and precious contribution can be given to the process of choosing the best treatment for a given clinical case.

A recently developed thermal neutron detector named *TNRD* (*Thermal Neutron Rate Detector*, [Bedogni et al.,2014](#)), was successfully used for these in-phantom thermal neutron measurements ([Irazola et al.,2014](#)). The detector is based on solid-state devices which thermal neutron response is enhanced using ${}^6\text{Li}$ radiators. Although the detector was designed to minimize the response to photons, this effect cannot be neglected when the measurement point is located near the field-edge, i.e. under intense photon background ([Terrón et al.,2015](#); [Irazola et al.,2015c](#)). Overestimating thermal neutron fluence in peripheral organs could lead to systematic errors in calculating secondary cancer risks, with potential impact on the clinical decisions.

Thus, a thorough study was performed to better understand these effects on the *TNRD* reading ([Irazola et al., 2015a](#); [Praena et al., 2015](#); [Irazola et al., 2016](#); [Irazola et al., 2015b](#); [Terrón et al., 2015](#); [Irazola et al., 2015c](#)).

The method proposed in this work, called “Double Energy Photon Subtraction” (DEPS), derives from the hypothesis that photon doses to peripheral points are energy independent in the megavoltage range ([Mazonakis et al.,2008](#)). Under this assumption, the pure photon contribution to the *TNRD* reading could be estimated from measurements at a treatment energy where no (or very little) neutrons are produced, such as 6 MV. The same treatment delivered at higher energy will thus produce an over-reading in the detector, due to neutron contribution. Clearly, the machine calibration must be the same for both energies.

2. Material and method

2.1 TNRD detector

TNRD detector ([Bedogni et al., 2014](#)) is based on a low-cost commercial solid-state device made sensitive to thermal neutrons through a customized physical-chemical treatment. Its active area is 1 cm^2 and its overall dimensions are 1.5 cm

$\times 1 \text{ cm} \times 0.4 \text{ cm}$. *TNRD* output is a DC voltage, which is proportional to the thermal neutron fluence rate (for this reason the device is called "rate detector"). This signal is amplified in a specifically developed low-voltage electronic board. The amplified output is sent to a programmable ADC (NI USB-6218 BNC, 16 bit, sampling rate up to 2.5×10^5 samples per second) controlled by a PC through a LabView application developed by the Politecnico di Milano. *TNRD* linearly responds to thermal neutron fluence rates from 10^2 up to $10^6 \text{ cm}^{-2}\cdot\text{s}^{-1}$. Every detector is calibrated in terms of thermal neutron fluence in a reference thermal field (Bedogni et al., 2016). Detector-to-detector response variability is in the order of $\pm 5\%$ (1 SD). An additional uncertainty term of about 10%, applicable in clinical conditions, was estimated by Irazola et al., 2014.

2.2 DEPS Method

The DEPS method is based on the hypothesis that photon doses to peripheral points are energy-independent in the megavoltage range (Mazonakis et al., 2008). Under this assumption, the pure photon contribution to the *TNRD* reading could be estimated from measurements at a treatment energy where no (or very little) neutrons are produced, such as 6 MV (hereafter called "low-energy" beam). The same treatment delivered at higher energy (15 MV in this work) will thus produce an over-reading in the detector, due to neutron contribution. Clearly, the machine calibration must be the same for both energies. This energy-independence of PPD was tested by Monte Carlo simulations and measurements, as described below.

2.2.1 Monte Carlo simulations

Monte Carlo simulations have been used to compute mean energy of the photon spectra for both nominal energies, from the isocenter to 55 cm. EGSnrc Monte Carlo user code BEAMnrc (Kawrakow et al., 2011; Rogers et al., 2011) was used to simulate 6 and 15 MV photon beams from a Siemens Primus linac.

The following BEAMnrc/EGSnrc transport parameters were employed: NIST for bremsstrahlung cross sections; EXACT as boundary crossing algorithm and PRESTA-II as electron-step algorithm. For bremsstrahlung angular sampling, the leading term of Koch-Motz distributions was chosen; electron and photon cutoff energies were 0.512 MeV (0.001 MeV kinetic energy) and 0.001 MeV, respectively. Electron range rejection, with an energy cutoff of 2.0 MeV, was implemented. Bremsstrahlung splitting was activated to obtain the first Phase Space Data (PSD) file for the 6 MV case. The PSD files corresponding to each aperture were obtained below the MLC for a 10x10 cm² field in a plane located 10 cm depth (SSD=100 cm) in a water block (60x60x30 cm³). The number of primary histories launched from the source in the PSD was 5 and 50 million for the 6 and 15 MV cases respectively, chosen to satisfy a spatial density of 10⁵ particles/cm² and trying to avoid latent uncertainty in order to obtain an adequate level of statistical accuracy. For out-of-field energy distribution comparison, the fact that simulations were performed with the information provided by the manufacturer (incomplete in terms of external shielding) could result in a minor overestimation that is not expected to distort our results. As the out-of-field statistics are lacking, several simulations with different initial seeds were performed. The mean photon energy was regarded as a relevant quality index for the photon spectra in peripheral points.

Simulated mean energies at different distances from the field-edge can be used to identify the proper calibration factor for ionization chambers (IC).

2.2.2 Farmer ionization chamber measurements

An IC based dosimetry system (PTW 30013 IC operating at -250 V and a PTW UNIDOS® electrometer) was used. Measurements for low- and high-energy beams were taken by varying the field-edge distance from 0.1 to 2 m. The IC was allocated in a plastic insert, sandwiched between 8 cm of polystyrene and

with additional blocks of plastic mimicking patient scatter. Irradiations were performed in a Siemens Primus linac for a 40x10 cm² field (in order to fully cover the 6 available *TNRD* devices, accounting for scattering), delivering 300 MU (dose rate of 300 MU·min⁻¹) with gantry angle at 0°.

2.2.3 Irradiations with *TNRD*

TNRD measurements at low- and high-energy, were performed under the same setup and irradiation conditions as those previously described for the IC (section 2.2.2). The photon contribution to *TNRD* readings at a peripheral point was measured using the 6 MV beam. Then, neutron contribution to *TNRD* readings, *TNRD*-n, was calculated by subtracting the low-energy reading from the high-energy one.

To validate the DEPS method, *TNRD*-n values were directly compared with those obtained with a different method adopting a Flex-boron® filter to remove the thermal neutron component (Irazola et al.,2016).

3. Results and discussion

3.1 Monte Carlo simulations: results

Figure1 depicts mean photon energy computed by Monte Carlo simulations. At the isocenter the mean energy is 1.4 and 3.2 MeV for the 6 and 15 MV fields, respectively. At peripheral points (≥ 10 cm to the field edge), the mean photon energy is 280 keV with $\pm 10\%$ maximum variation when the beam is changed from 6 MV to 15 MV. The corresponding variability in the mass energy absorption coefficient (μ_{en}/ρ) for Silicon is smaller than $\pm 1.1\%$, implying no effect on the *TNRD* photon response (Terrón et al., 2015).

The energy response of the IC is also flat in this energy range (Shani, 2000; Aird et al.,1972; Andreo et al.,2006).

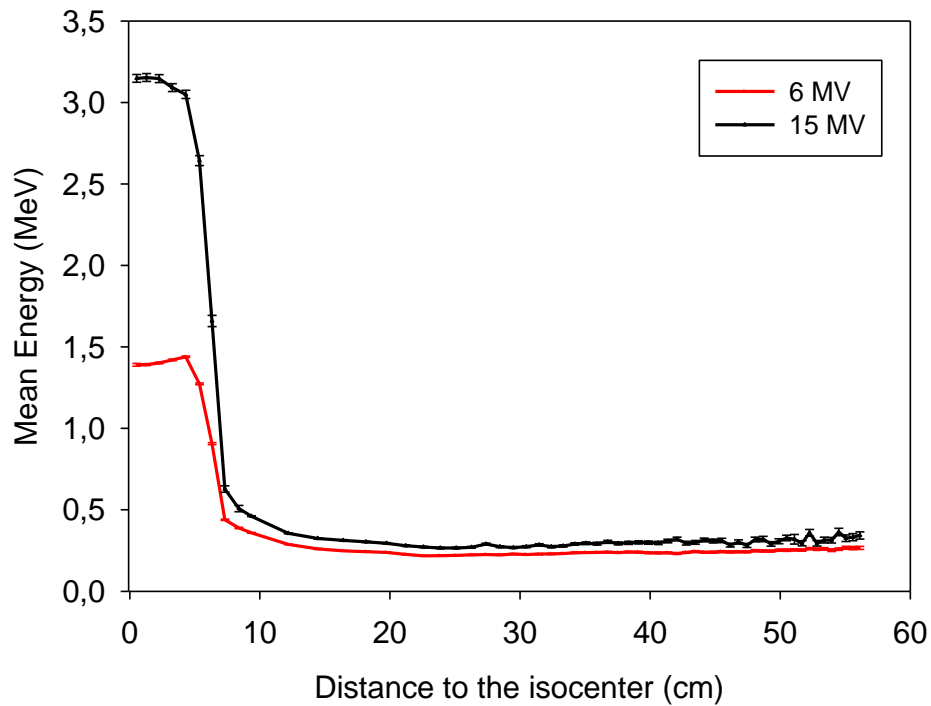


Figure 1. Photon mean energy of the spectra, in water, computed by Monte Carlo for distances ranging from 0 to 55 cm far from the isocenter in a Siemens Primus linac in 6 and 15 MV.

3.2 Results from Farmer IC measurements

Figure 2 shows the readings of the IC at 6 and 15 MV as the field-edge distance varies from 0.1 to 2 m. Readings have been normalized to the 15 MV case at 0.1 m. The corresponding absorbed dose for 300 MU ranges from 0.07 cGy (at 2 m) to 4.00 cGy (at 0.1 m).

The plot experimentally demonstrates that PPD does not depend on beam energy.

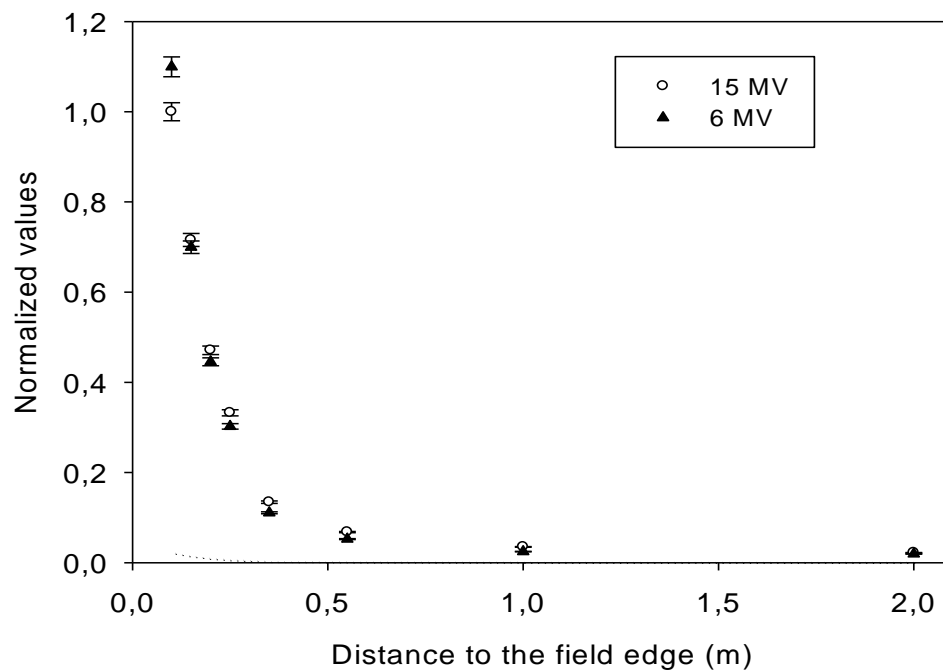


Figure 2. Normalized Farmer ionization readings obtained for the studied field edge-detector distances (0.1 to 2 m) in 6 and 15 MV.

3.3 TNRD results

Figure 3 shows TNRD signals at 6 and 15 MV for the studied field-edge distances. For the high-energy case, both photons and neutrons contribute to the reading of the detector (solid dots) whereas for the low-energy beam TNRD only sees photons (hollow triangles).

TNRD readings in 6 MV can be subtracted from those of the 15 MV case (containing photon and neutron signals), in order to obtain the neutron contribution (TNRD-n).

Figure 4 compares the TNRD-n values with those obtained with a different method, adopting a Flex-boron[®] filter to remove the thermal neutron

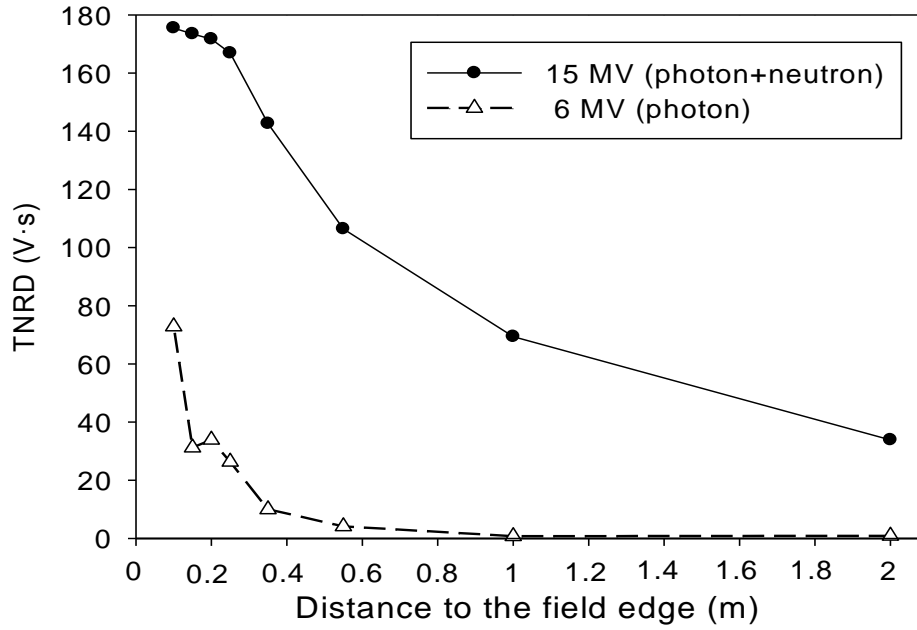


Figure 3. Global TNRD measurement in high (photon+neutron represented as solid dots) and low (photon, hollow triangles) energies for the studied distances. All measurements refer to 300 MU. TNRD axis readings correspond to thermal neutron fluences up to around $18 \times 10^6 \text{ n}\cdot\text{cm}^2$, depending on detector calibration factor.

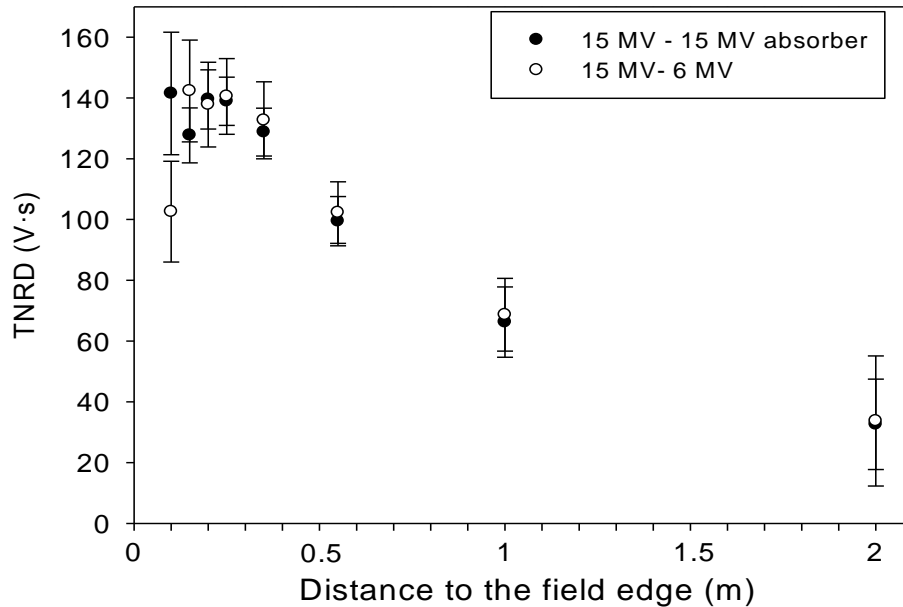


Figure 4. Neutron contribution to TNRD reading at 15 MV obtained by Flex-Boron (black) or DEPS method (white). All measurements refer to 300 MU. TNRD axis readings correspond to thermal neutron fluences up to around $16 \times 10^6 \text{ n}\cdot\text{cm}^2$, depending on detector calibration factor.

component (Irazola et al.,2016). In the latter case, a pair of exposures at 15 MV are performed for every field-edge distance: one with the *TNRD* covered with Flex-boron®, the other uncovered. Again, the neutron contribution is obtained by subtraction.

Differences are smaller than uncertainties of the estimations, proving that the two methods are equivalent.

4. Conclusions

This work proposes a simple method to correctly estimate the thermal neutron reading of active thermal neutron detectors used ‘in-phantom’ for peripheral neutron dose experiments in high-energy RT. Despite these detectors are designed to reject photons, their photon response cannot be neglected when the measurement point is near to the field-edge.

The method is called “Double Energy Photon Subtraction” (DEPS) and relies on the hypothesis that photon doses to peripheral points are energy independent in the megavoltage range. Under this assumption, the pure photon contribution to the detector reading is estimated from measurements at a treatment energy where no (or very little) neutrons are produced, such as 6 MV. Measurements at low (6 MV) and high (15 MV) energies are performed under the same setup. The neutron contribution to detector reading is obtained by subtracting the low energy reading from the high energy one.

Monte Carlo simulations, as well as ion chamber measurements were used to validate the basic assumptions of DEPS method. This was applied to the recently developed thermal neutron detector *TNRD*. Experiments were performed by varying the field-edge distance from 0.1 to 2 m. The results were successfully compared with those obtained by another method, based on Flex-Boron filters.

The DEPS approach represents a simple and universal correction method, usable at any high energy facility equipped with low energy (i.e. 6 MV). It offers an operative procedure without the need of any extra specific material, setup modifications for 'in-phantom' accommodation of the detectors and avoiding the necessary dismantling and re-assembling of this setup for each pair series of measurements.

5. References

- Aird EG and Farmer FT. *The design of a Thimble Chamber for the Farmer Dosimeter*. Phys Med Biol 1972;17(2):169-174.
- Andreo P, Burns DT, Hohlfeld K, Saiful Huq M, Kanai T, Laitano F, Smth V and Vynckier S. IAEA TRS-398. *Absorbed Dose Determination in External Beam Radiotherapy: An International Code of Practice for Dosimetry based on Standards of Absorbed Dose to Water*. IAEA 2006.
- Bedogni R, Bortot D, Pola A, Introini MV, Gentile A, Esposito A, Gómez-Ros JM, Palomba M, and Grossi A. *A new active thermal neutron detector*. Radiat Prot Dosim 2014;161(1-4):241-244.
- Bedogni R, Sacco D, Gómez-Ros JM, Lorenzoli M, Gentile A, Buonomo B, Pola A, Introini MV, Bortot D and Domingo C. *ETHERNES: A new design of radionuclide source-based thermal neutron facility with large homogeneity area*. Appl Radiat and Iso 2016;107:171-176.
- Chofor N, Harder D and Poppe B. *Non-reference condition correction factor k_{NR} of typical radiation detectors applied for the dosimetry of high-energy photon fields in radiotherapy*. Z Med Phys 2012;22:181-196.
- Expósito MR, Sánchez-Nieto B, Terrón JA, Domingo C, Gómez F and Sánchez-Doblado F. *Neutron contamination in radiotherapy: Estimation of second cancers based on measurement in 1377 patients*. Radiother and Oncol 2013;107:234-241.
- Gómez F, Iglesias A and Sánchez-Doblado F. *A new active method for the measurement of slow-neutron fluence in modern radiotherapy treatment rooms*. Phys Med Bio. 2010;55:1025-1039.
- Irazola L, Lorenzoli M, Bedogni R, Pola A, Terrón JA, Sánchez-Nieto B, Expósito MR, Lagares JI, Sansaloni F and Sánchez-Doblado F. *A new online detector for estimation of peripheral neutron equivalent dose in organ*. Med Phys 2014;41:112105.

- Irazola L, Terrón J A, Sánchez-Nieto B, Bedogni R, Gómez F and Sánchez-Doblado F. *Effects of cable extension and irradiation on TNRD neutron detector in radiotherapy*. IUPESM 2015 Abstract book, 615, PS05.043 (2015a).
- Irazola L, Terrón J A, Bedogni R, Lorenzoli M, Pola A, Sánchez-Nieto B and Sánchez Doblado F. *Signal photon component of a new thermal neutron detector TNRD in radiotherapy environments*. *Radiother and Oncol* 2015b;115(1):S870.
- Irazola L, Terrón J A, Lorenzoli M, Pola A, Sánchez-Nieto B and Sánchez-Doblado F. *TNRD neutron detector signals for different gantry angles in 6 and 15 MV*. *Radiothera and Oncol* 2015c;115(1):S761.
- Irazola L, Terrón JA, Bedogni R, Lorenzoli M, Pola A, Sánchez-Nieto B and Sánchez-Doblado F. *Signal photon component of a new thermal neutron detector TNRD in radiotherapy environments*, *Radiother. and Oncol* 2015;115(1).
- Irazola L, Terrón JA, Bedogni R, Pola A, Lorenzoli M, Sánchez-Nieto B, Gómez F and Sánchez-Doblado F. *Improving the neutron-to-photon discrimination capability of detectors used for neutron dosimetry in high energy photon beam radiotherapy*. *Appl Radiat Isot*, in press (2016a).
- Jagetic LJ and Newhauser WD. *A simple and physics-based analytical method to calculate therapeutic and stray doses from external beam, megavoltage x-ray therapy*. *Phys Med Biol* 2015;60:4753-4775.
- Kawrakow I et al., *The EGSnrc Code System: Monte Carlo Simulation of Electron and Photon Transport* NRCC Report 2011;PIRS-701 (National Research Council of Canada, Ottawa).
- Mazonakis et al. *Peripheral dose measurements 6 and 18 MV photon beams on a linear accelerator with Multi Leaf Collimator*. *Med Pys* 2008;35: 4396-403.
- Praena J, Irazola L, Fernández B, Terrón J A, Bedogni R, Lorenzoli M, Pola A, Sánchez-Nieto B and Sánchez-Doblado F. *Proposal of thermal neutron detector stability for peripheral dose estimation in clinic at a novel neutron facility*. *Radiother and Oncol* 2015;115(1):S735.
- Rogers D W O, Walters B and Kawrakow I, *BEAMnrc Users Manual*, NRCC Report 2011; PIRS 509 rev L (National Research Council of Canada, Ottawa).
- Romero-Expósito M, Sánchez-Nieto B, Terrón JA, Lopez MC, Ferreira BC, Grishchuk D, Sandíns C, Moral-Sánchez S, Bragado-Álvarez L, Melchor M, Domingo C, Gómez F and Sánchez-Doblado F. *Commissioning the neutron production of a linac: development of a clinical planning tool for second cancer risk estimation*. *Med Phys* 2015;42:276-281.
- Sánchez-Doblado F, Domingo C, Gómez F, Sánchez-Nieto B, Muñoz JL, García-Fusté MJ, Expósito MR, Barquero R, Terrón JA, et al. *Estimation of neutron*

- equivalent dose in organs of patients undergoing radiotherapy by the use of a novel online digital detector.* Phys Med Biol 2012;57:6167–6191.
- Sánchez-Nieto B, El-far R, Irazola L, Expósito MR, Lagares JI, Mateo JC, Terrón JA and Sánchez-Doblado F. *Analytical model for photon peripheral dose estimation in radiotherapy treatments.* Biomed Phys Eng Express 2015;1:045205.
- Shani G. *Radiation Dosimetry. Instrumentation and Methods.* CRC Press, 2nd edition 2000.
- Terrón JA, Irazola L, Morilla Y, Muñiz G, Bedogni R, Lorenzoli M, Pola A, Sánchez-Nieto B and Sánchez-Doblado F. *Photon energy response of TNRD neutron detector in a ⁶⁰Co irradiator and a 6 MV linac.* Radiother and Oncol 2015;115(1):S757-S758.
- Van der Giessen PH. *Peridose, a software program to calculate the dose outside the primary beam in radiation therapy.* Radiother and Oncol 2001;58:209-213.
- Xu GX, Bednarz B and Paganetti H. *A review of dosimetry studies on external-beam radiation treatment with respect to second cancer induction.* Phys Med Biol 2008;53:193-241.

III. Thesis core

2. Publications: **(B.3)** *Neutron measurements in radiotherapy: a method to correct neutron sensitive devices for parasitic photon response*

(C)

Neutron model upgrade for peripheral neutron dose assessment evaluated in
510 radiotherapy patients

Irazola L, et al. Sent to Phys Med Biol

Abstract

Purpose: Neutron peripheral contamination in high-energy radiation therapy implies an increase on secondary radiation-induced cancer risk. Although Peripheral Neutron Dose (PND) has been studied in organs, few studies have been done regarding patient size. This work aims to improve an existing methodology for adult patient PND estimations in several aspects, mainly to generalize it to teen and child.

Methods: As a first step we proposed the generalization of the existing methodology to be expressed in terms of thermal neutron fluence in the room, being thus measurable with any thermal neutron detector. Then, dose-to-point measurements were performed with active miniaturized thermal neutron detectors and compared to those of the previous used passive (TLD) devices for three phantom sizes (adult, teen and child) and two common treatment locations (H&N and abdomen). The objective was to improve these models by introducing patient anatomy with the consideration of individual weight and height. Finally comparison between estimations and measurements, as well as validation against the old model, was carried out for 510 measured patients.

Results: Good agreement was obtained between *TNRD* and TLD measurements for the studied phantom points. A parameterized extended model, accounting for patient anatomy and usable with any thermal neutron detector has been

achieved. Concordance found between experimental and theoretical estimations makes us confident for later implementation in treatment planning systems. Comparison among old and new models shows no significant differences for adult case, although important underestimation (34.1% in average) of the old model can be observed regarding child case.

Conclusions: An improved generalization of an existing model for PND, considering patient anatomy has been validated and used in real patients. The methodology results easily implementable in clinical routine, thanks to the ready availability of input parameters (patient height and weight, number of high-energy MU and characterization of the facility in terms of neutron production).

1. Introduction

Modern radiotherapy techniques such as Intensity Modulated Radiotherapy (IMRT) and Volumetric Modulated Arc Therapy (VMAT), although minimizing acute and late side effects of radiation exposure, are known to increase peripheral doses when compared to conventional treatments as conformal radiotherapy (3D-CRT) (Hall et al.,2003; Kry et al.,2005; Howell et al.,2006; Ruben et al.,2008). Besides as additional neutron contamination is produced when using energies greater than 8 MV (NCRP-79, Nath et al., 1986), several discussions have been conducted concerning if these techniques should be administered in high energies (Followill et al., 2007). The increase of out-of-field radiation doses and corresponding growth of radio induced secondary malignancies has been widely studied recently (Diallo et al.,2009; Newhauser et al.,2011; Harrison et al.,2013). Many groups have conducted their investigations in the modeling of peripheral photon and neutron doses (Jagetic et al.,2015; Sánchez-Nieto et al.,2015). However, the majority of these studies are focused

on peripheral photon doses, with less works reporting neutron component in high-energy photon radiotherapy.

As the main source of photoneutrons is found in linac head (Pena et al.,2005), patient lying on the couch below the machine, receives an almost total-body neutron dose. This fact, together with the great complexity of neutron measurements in radiotherapy environments (where a high photon background is present) make that the study of neutron spectrum variations with depth in tissue, where sensitive organs are located, has to be usually done with Monte Carlo simulations (Xu et al.,2008). Thus, additional data would be necessary to study patient-specific scenarios. Despite the lower neutron-absorbed dose values compared to photon ones (Kry et al.,2005), neutron radiation weighting factor can make this component to be similar, in terms of tissue damage, for some specific locations (Berdnarz et al.,2009). In addition, despite the controversy related to carcinogenic risk of secondary neutrons, these doses are hardly ever considered in current clinical routine, as they are not contemplated in conventional radiotherapy treatment planning systems (TPS) and no general models are widely available. These doses become of major importance for specific group of patients such as child (Diallo et al.,2009) or pregnant women (Stovall et al.,1995). For instance, in child survivors, morbidity and mortality risks remain high beyond the fourth decade of their life (Armstrong et al.,2013), causing even more deaths than primary malignancies in some pediatric cancers (Tubiana et al.,2009). Although some studies suggest that secondary cancers remain rare in adult patients (representing around 8% of solid cancers in adult patients overcoming at least one year after RT), it has been shown that cancer recurrence is the main cause of death in child patients, representing around 67% of all deaths, from which 21.3% can be attributed to treatment related causes, a 12.7% due to including secondary malignancies (Chargari et al.,2016). In addition, the knowledge of properly generated dosimetric data is essential to

establish a reasonable assessment of low dose risk estimates in radiotherapy (Diallo et al.,2009).

The methodology proposed by our group (Gómez et al.,2010; Sánchez-Doblado et al.,2012; Expósito et al.,2013) provides a systematic estimation of neutron organ-equivalent doses at 12 organs for patients undergoing high energy external photon beam radiotherapy. However, despite the simplicity of this method, it requires the characterization of the facility in terms of neutron production by a specific SRAM-based detector, or the use of general values tabulated for each linac model (Sánchez-Doblado et al.,2012). In consequence, a more universal methodology would be desirable for this procedure. This model enables the consideration of patient sex and treatment location, namely head and neck (H&N) or abdomen. Once methodology was clinically validated (Expósito et al.,2013), we thought that a more general procedure being also more patient-specific would be highly desirable for clinical routine. Second Cancer Probability (SCP) estimation represents a step further in peripheral dose studies and some uncertainties remain regarding these magnitudes based on data from the Japanese atomic bomb survivors and the RBE of neutrons (Newhauser et al., 2016). However, recent studies have established the pass from neutron dose to risk by the direct use of tabulated values (Expósito et al.,2013), we have focused this study in the enhancement of neutron dose assessment, which would allow a direct estimation of SCP by only applying these factors, choosing the more convenient protocol. Former to the improvement of the existing models, we wanted to ensure that these two model locations were general enough to cover real treatment ones. For that, the goodness of these models was previously evaluated in real treatments, giving good concordance with *TNRD* estimations (Irazola et al.,2016).

The goal of this work is the improvement of the previously existing methodology for PND estimation to organ, in order to make it more global and customized. We aimed to generate further patient-specific (regarding anatomy) neutron organ dose models that can be used in any facility, by terms of a simple characterization of linac neutron production, which can be easily performed with any thermal neutron detector. These new models will be used to compare calculated and measured peripheral neutron organ-equivalent doses for 510 patients, evaluated against results obtained with the old methodology.

2. Material and method

A thermal neutrons-sensitive detector called *TNRD* (Thermal Neutron Rate Detector) was used. This neutron detector was initially designed by INFN-LNF (Italy; [Bedogni et al.,2014](#)) for nuclear purposes. The device is based on a low-cost commercial solid-state device sensitized to thermal neutrons through a customized physical-chemical treatment, with overall dimensions of approximately $1.5 \times 1 \times 0.4 \text{ cm}^3$ (active area of 1 cm^2). Further details on its composition can be found in ([Bedogni et al.,2014](#)). Those detectors respond linearly to any thermal neutron fluence rate in the range of 10 up to $10^6 \text{ cm}^{-2} \cdot \text{s}^{-1}$ neutrons and show detector-to-detector response variability of the order of $\pm 5\%$ (1SD). However, for clinical environments an additional source of uncertainty, coming from beam angular entry and energy dependences had to be considered. Therefore, a global uncertainty of 11% was estimated by [Irazola et al.,2014](#) for these devices in radiotherapy environments. Encompassing this value with procedure own incertitude, a global uncertainty of around 15% was establish for model generation methodology.

One advantage of the *TNRD* detectors is their online-features, which greatly ease the processes of model improvement for which repeated measurements have to be usually made. Additionally, the reduced size of these active

detectors allows not only 'external' (as used during the development of the neutron equivalent dose estimation model in [Sánchez-Doblado et al.,2012](#)) but also and 'in-phantom' measurements. *TNRD* thermal neutron fluence estimations are obtained in compliance with [ISO 8529-1](#).

2.1 Facility neutron fluence characterization

The original methodology ([Sánchez-Doblado et al.,2012](#)) relied on the correlation between neutron production (expressed as single events upset (SEU) of a SRAM-based neutron detector) and the neutron equivalent dose to peripheral organs. The latter required the neutron detector to be present during patient irradiation.

[Romero-Expósito et al.,2015](#) proposed a generalization of that methodology by characterizing the facility, in terms of photoneutron production, so that the presence of the detector was not required posteriorly during patient irradiations. For this, the previous determination, under certain reference conditions, of a characterization parameter (in units of events per MU, termed c) was required. The former parameter, escalated by the MU used during specific irradiations, correlated with neutron equivalent dose to organs. This neutron characterization should be done just once (e.g., during linac commissioning).

A further step in the generalization of the neutron dose estimation methodology involves the characterization of the facility in terms of thermal neutron fluence. Therefore, the implementation of the neutron dosimetry methodology in any facility could be carried out by characterizing it by means of any thermal neutron detector.

This involves the estimation of the characterization parameter (c^*) in units of neutrons per cm^2 and MU using [eq.1](#) with the neutron detector outside the

beam (in front of the gantry and close to the bunker wall) under reference conditions (i.e., gantry angle at 0°, field size of 10×10 cm²) as proposed in (Romero-Expósito et al.,2015).

$$c^* = \frac{\Phi_{th} \cdot F_B}{MU} \quad (\text{eq.1})$$

where:

- Φ_{th} represents the accumulated thermal neutron fluence in the reference location and irradiation conditions;
- MU is the total number of high energy MU delivered (usually 1000 MU)
- F_B is a factor accounting for the ratio from the bunker volume, with a floor area of A (m²), to a reference one with a floor area of 64.6 m². This factor was modeled as $F_B = 1/(0.46 + 34.13/A)$ calculated from that described in in (Sánchez-Doblado et al.,2012)

In the present work, the TNRD detectors will be used for the implementation of this upgraded methodology together with the incorporation of patient's size.

2.2 In-phantom measurements

Three anthropomorphic NORMA phantom models (Figure 1) were available to cover several patient ages (child teen and adult). Phantoms were manufactured in polyethylene whereas low-density wood was used for simulating the lung tissue. 16 customized detector holes were distributed along each phantom, at different depths, representing relevant cancer-at-risk organ locations for the estimation of equivalent dose in organs. Table I lists the point(s) used for organ dose investigation, extended from that of Sánchez-Doblado et al.,2012.

Firstly, a validation of the use of the model by Sánchez-Doblado et al.,2012, with TNRD was carried out for the adult phantom. Afterwards, the

generalization of the existing model to account for different patient sizes was carried out.

The same irradiation conditions as those of the original model (Sánchez-Doblado et al.,2012) were used:

- (i) Abdomen treatment: eight beam incidences (at 0°, 45°, 90°, 135°, 180°, 225°, 270°, 315°), 10x10 cm² field sizes, 15 MV, isocentre at point A (Figure 1)
- (ii) Head and neck treatment: the same beam incidences, field sizes and energy than in (i), isocentre at point H (Figure 1)

Irradiations were set to 1000 monitor units (MU) with a dose rate of 300 MU·min⁻¹ and were carried out with a Siemens Primus linac.

2.2.1 Model generalization for its use with thermal neutron detectors

In order to use of *TNRDs* detectors in the methodology established by Sánchez-Doblado et al.,2012 a comparison between thermal neutron fluences measured with passive detectors (TLDs and PACD, Poly Allyl Diglycol Carbonate) during model development and those of *TNRDs* was carried out for the adult phantom. Previous to this comparison, passive detector fluence values were corrected to account for the differences in the cut-off energies used during the calibration procedures for both types of detectors (Irazola et al.,2014).

Model in Sánchez-Doblado et al.,2012, encompassed average values for a wide range of available combinations of linacs and energies; thus, model estimations were associated to an uncertainty of around 30%. It will be assumed that agreement, within uncertainties, of both sets of fluence measurements will imply that the generalized model (in terms of thermal neutron fluence) is also applicable to any linac.

The agreement between these results and those of the previous models, together with the previously generalized characterization procedure to be performed in terms of thermal neutron fluence (eq.1), allows the use of this methodology with any thermal neutron detector, instead of being expressed in terms of events (Sánchez-Doblado et al.,2012).

Table I. NORMA's optimized detector locations specific to 14 radiosensitive internal organs. Modified from Sánchez-Doblado et al.,2012, adding two extra organs*.

k	Organ	NORMA Points
1	Thyroid	4
2	Oesophagus	4,9,16
3	Lung	7,8
4	Breast	5,6,15
5	Stomach	9,11,16
5	Liver	9,10,11,16
6	Colon	11,12
7	Urinary Bladder	10
8	Ovary	11,12
9	Skin	15
10	Bone surface	1,3,9,12,13,14,15
11	Marrow	9,12,15
12	Remainder	All except 7,8,15
13	Prostate*	11,12
14	Uterus*	11,12

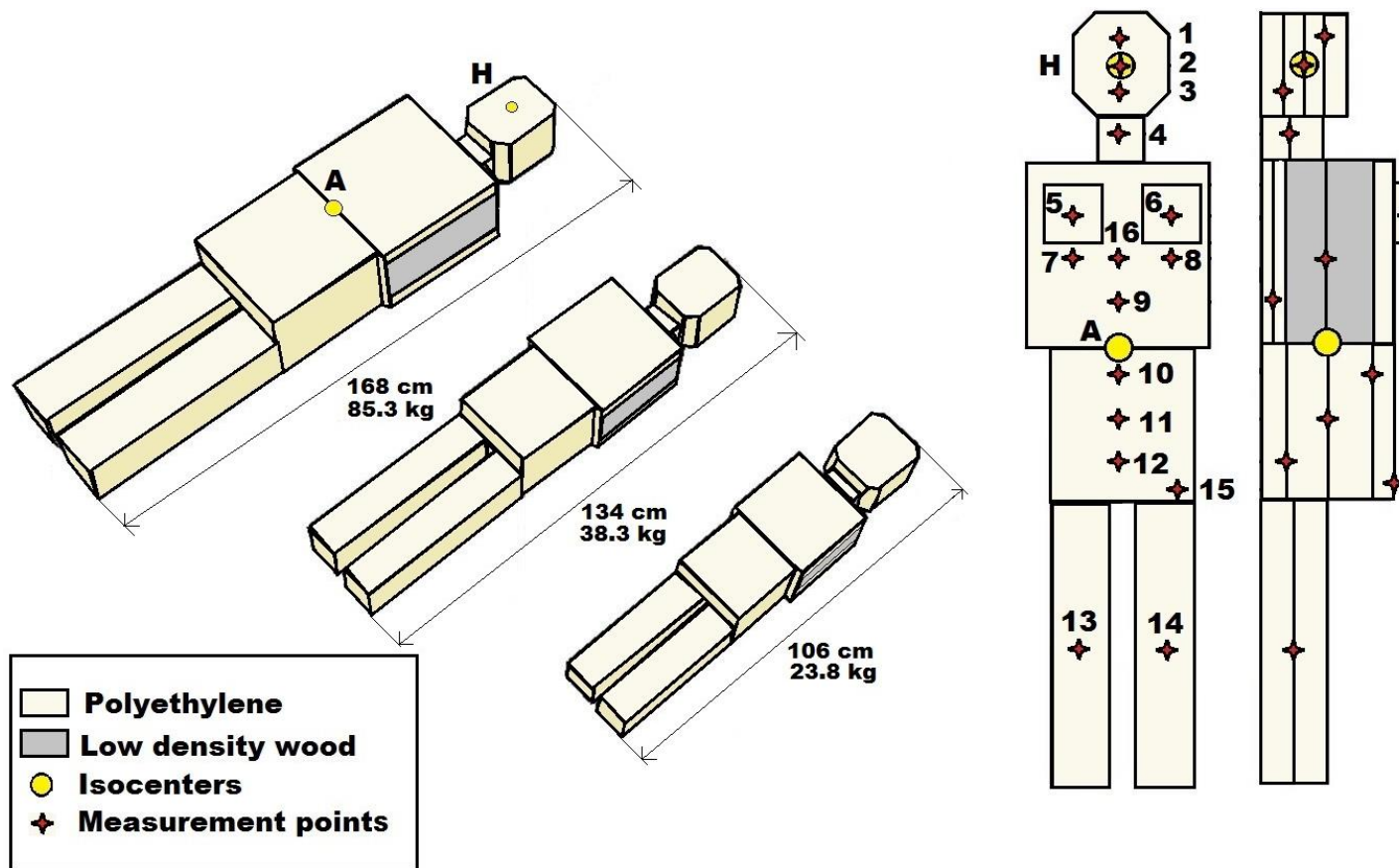


Figure 1. NORMA Phantom models to cover adult, teen and child sizes and points locations specific to 14 cancer-at-risk organs (Table I). Figure modified from Sánchez-Doblado et al.,2012; González-Soto et al.,2012.

2.2.2 Model generalization to account for patient size

(a) Thermal neutron fluence measurements for the three phantom sizes

The already available Thermal neutron fluences ([Sansaloni et al.,2011](#)), measured with TLDs, were to be confirmed with the new TNRD devices for the three phantoms and irradiation sets above described (for abdomen and H&N locations) in the 16 points. Both uncertainties were estimated at 15%, as measurements were carried out using the same linac.

(b) Organ-equivalent neutron dose model

The previously mentioned methodology ([Sánchez-Doblado et al.,2012](#)) is based on the convolution at the 16 points of the normalized Monte Carlo neutron fluence energy spectra with the kerma factor for ICRU tissue (k) ([Siebert et al.,1995](#)) and energy-dependent radiation weighting factor from [ICRP-103](#) (w_R).

The same convolution approach to estimate the neutron-equivalent dose in an organ k , estimated from average of measured points i of a patient undergoing a treatment j ([Sánchez-Doblado et al.,2012](#); [Romero-Expósito et al.,2016](#)), but using directly the thermal neutron fluence (Φ_{th}), is now proposed as follows:

$$H_{i,j} = \Phi_{i,j}^{th} \cdot F_{i,j} \quad (\text{eq.2})$$

where:

- $\Phi_{i,j}^{th}$ is the accumulated thermal neutron fluence ($\text{n}\cdot\text{cm}^{-2}$), corrected by bunker size parameter (F_B , firstly introduced in [eq.1](#)), at any point (i) for any treatment (j)
- $F_{i,j}$ are the neutron-equivalent dose transformation factors, for each NORMA point i and for type of treatment j , considering total neutron

spectra $\varphi_{i,j}(E)$, radiation weighting factors $w_R(E)$ and kerma factor ($k(E)$).

Therefore, eq.2 can be used to estimate the neutron-equivalent dose in an organ k (from the averaged values of measured i -points) of a patient undergoing a j -treatment from the thermal neutron fluence at that point (provided, in this case, by the *TNRDs* detector).

In order to introduce the facility characterization (section 2.1) in the expression, the $\{\Phi_{i,j}^{th}\}$ matrix data were correlated to thermal neutron fluences measured with the *TNRD* detector located at reference position in the bunker, R (Sánchez-Doblado et al.,2012). If $M_{i,j}$ represent those correlation coefficients, eq.3 can be then rewritten as follows:

$$H_{i,j}(\mu Sv) = R \cdot M_{i,j} \quad (\text{eq.3})$$

where:

- R ($\times 10^6$ $n \cdot \text{cm}^{-2}$) is the accumulated thermal neutron fluence at the reference location inside the bunker during a treatment. In practice, R value can be estimated using either:

- the characterization approach ($R_{cal} = c^* \cdot MU$) which makes use of the specific MU used for the irradiation,
- or directly measuring thermal neutron fluence at the reference location during the irradiation (R_{meas}) and correcting it by bunker surface factor (F_B).

- $M_{i,j}$ ($\mu Sv \cdot 10^{-6}$ $n^{-1} \cdot \text{cm}^2$) represent the corresponding $H_{i,j}$ values from eq.3 per thermal fluence of the reference detector (establishing a correlation among dose equivalent at every i -point and reference thermal neutron measurement in the treatment room). It allows the direct estimation of neutron dose equivalent at

the studied i -points for the desired j -treatment location by the only knowledge of thermal neutron contamination in the reference location for the studied treatment.

In order to evaluate organ-equivalent neutron doses to the 12 k -organs detailed in Table I, we used the same point to organ aggrupation than those established in Sánchez-Doblado et al.,2012 to go from the $M_{i,j}$ dose-to-point factors to the $M_{k,j}$ organ-to-dose factors that govern the model (correlating organ-equivalent dose to reference thermal neutron fluence in the room, R).

(c) Organ-equivalent neutron dose model considering patient dimensions

Finally, in order to consider different patient anatomy (height and weight), the Body Surface Area (BSA) concept, introduced by Du Bois et al.,1916, was considered. Accordingly, the height and weight of a patient were combined in a single BSA parameter (termed HW from now onwards) as follows:

$$HW (m^2) = 0.007184 \cdot h^{0.725} \cdot w^{0.425} \quad (\text{eq.4})$$

where h and w stand for patient height (cm) and weight (kg) respectively. Then, the HW parameter was used as a surrogate for mapping for each patient distances form the organ to the source as well as the depth of the i -points, corresponding to each k -organ. The later mainly affects to the neutron spectra at the point.

Thus, the neutron equivalent dose to the k -organ during the j -treatment can be calculated from the following equation:

$$[H]_T^{k,j} (\mu Sv) = R \cdot [E(HW)]_{k,j} \quad (\text{eq.5})$$

where:

- R can be either estimated *a priori* (using facility characterization approach) or directly measured (eq.4)
- $E(HW)_{kj}$ is the corresponding equation for organ- k in j -treatment regarding patient size (obtained from fitting corresponding $M_{k,j}$ parameters with HW values). Thus expressed in terms of ($\mu\text{Sv}\cdot 10^{-6} \text{ n}^{-1}\cdot\text{cm}^2$).

2.3 Clinical application: neutron equivalent dose estimations in 510 patients

Organ-equivalent doses for a cohort of 510 patients were computed by applying the generalized methodology and using the new *TNRD* detector in the reference position. For a 240-patients subgroup, patient-specific results (regarding weight and height) were compared to the doses estimated with the original methodology, as all of them are adult patients. Comparison for the whole group between the experimental measurements (R_{meas}) and theoretical estimations (R_{est}) were also carried out. Patients were divided in four groups attending the location of the pathology (see Table II).

Table II. Group distribution of the 510 patients according to location of the tumour (Pelvic: bladder, cervix, colon, endometrium, ovary, prostate, rectum, uterus, vesicle and vagina; H&N: brain, pharynx, larynx, oesophagus, head, neck; Thorax: lung, lymphoma, gastric)

Pathology	Patients
Pelvic	203
Breast	199
Head & Neck	55
Thorax	53

As retrospective studies do not always count with specific patient size data, the direct use of the $M_{k,j}$ coefficients (available for three size options) should represent an improvement with respect to the original model.

Finally, the case of an abdominal tumor in a child was simulated (900 MU of 15 MV, as part of a treatment combined with 6 MV). Neutron equivalent dose to organs were estimated with the original (adult) and generalized (introducing corresponding child dimensions) models.

3. Results and discussion

3.1 In-phantom measurements

3.1.1 *Model validation*

Figure 2 depicts thermal neutron fluences measured with *TNRDs* inside NORMA and those obtained with passive detectors (extracted from [Sánchez-Doblado et al.,2012](#)) for the head and neck model. Error bars are displayed according to the estimated uncertainties.

Results show agreement within uncertainties, except for skin (#15) and mediastinum (#16) point. At the first one, the fast and epithermal components of the spectrum are higher and passive detectors such as plastics PACD and TLDs, used to generate the original model, may be sensitive. This is not the case of *TNRD* detectors, which are essentially sensitive to the thermal neutron component. The case of point #16 (mediastinum) seems to be related to an incorrect estimation of the fluence (there is a low density material to both sides of the point) with the passive detectors, since this behavior was not found in later results.

3.1.2 Model generalization to account for patient size

(a) Thermal neutron fluences for the three phantom sizes

Figure 3 depicts the thermal neutron fluences measured with the *TNRDs* and the available *TLDs* measurements (from Sansaloni et al.,2011) for the three phantom sizes and both treatment types studied.

In 83% of the measurements points, both sets agreed within uncertainties. Points close to the field-edge (i.e., $\leq 5\text{cm}$) systematically showed the greatest differences (i.e., point #11 for the adult and teen phantoms as well as points #7 and #8 for the child phantom, all during abdominal irradiation). This is due to the very intense photon field which might induce greater uncertainties both in *TLDs* and *TNRDs* (Irazola et al.,2015; Irazola et al.,2016). For those points, thermal neutron fluence was assumed to be the average from both types of detectors. For the case of points inside the treatment field (#1, #2 and #3 for the H&N case and #9 and #10 for the abdomen one), for which none of the two types of detectors offer a proper performance, thermal neutron fluence from previous MC simulations (Pena et al.,2005) were considered. Finally, in the case of symmetric points such as breast, lungs and legs, the odd values (Table I) have been chosen for both (average deviation of 1.7%).

After all these considerations, $M_{i,j}$ factors were established.

(b) Organ-equivalent neutron dose model

$M_{k,j}$ were obtained by averaging the $M_{i,j}$ values according to the locations specific, to each of the 14 radiosensitive internal organs, which are listed in Table I. Results are presented in Table III.

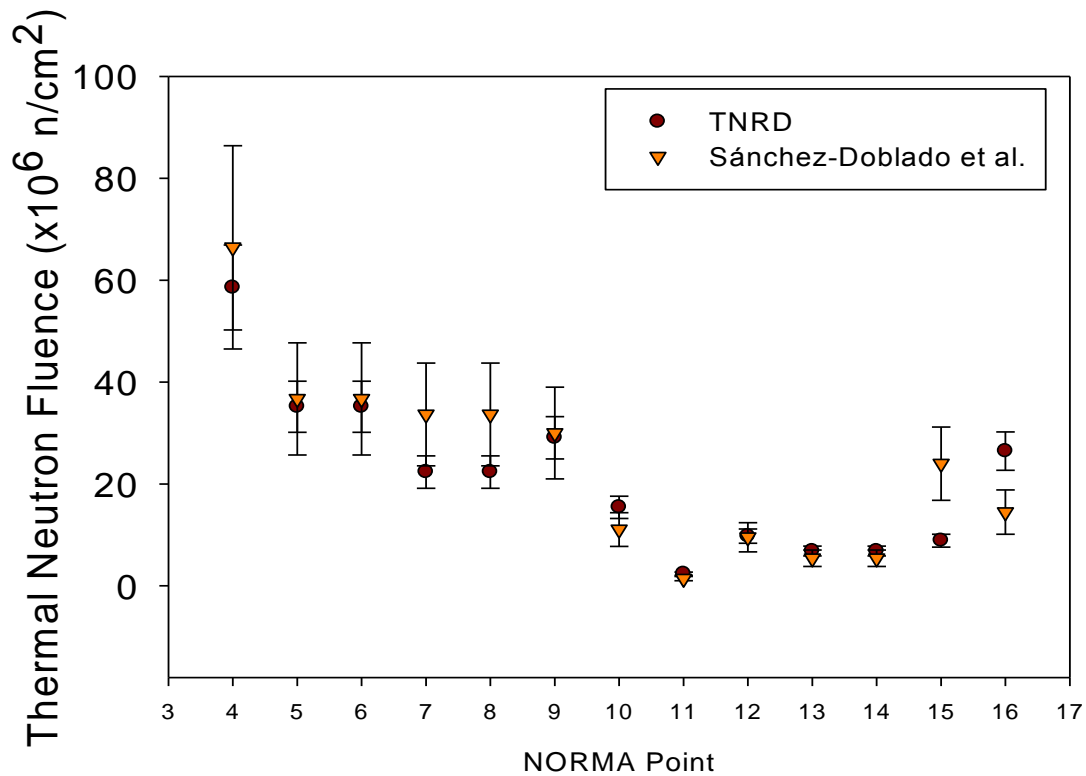


Figure 2. Thermal neutron fluences for H&N. Circles correspond to measurements with TNRD detectors inside NORMA. Triangles represent passive detector measurements from [Sánchez-Doblado et al., 2012](#), corrected by differences in cut-off energies.

By using [eq.3](#), the $M_{k,j}$ factors allow the estimation of the organ-equivalent (k) neutron doses from the only knowledge of factor R , which can be either estimated from the characterization procedure or directly measured. For the former case, the number of high energy MU of the specific treatment is also required.

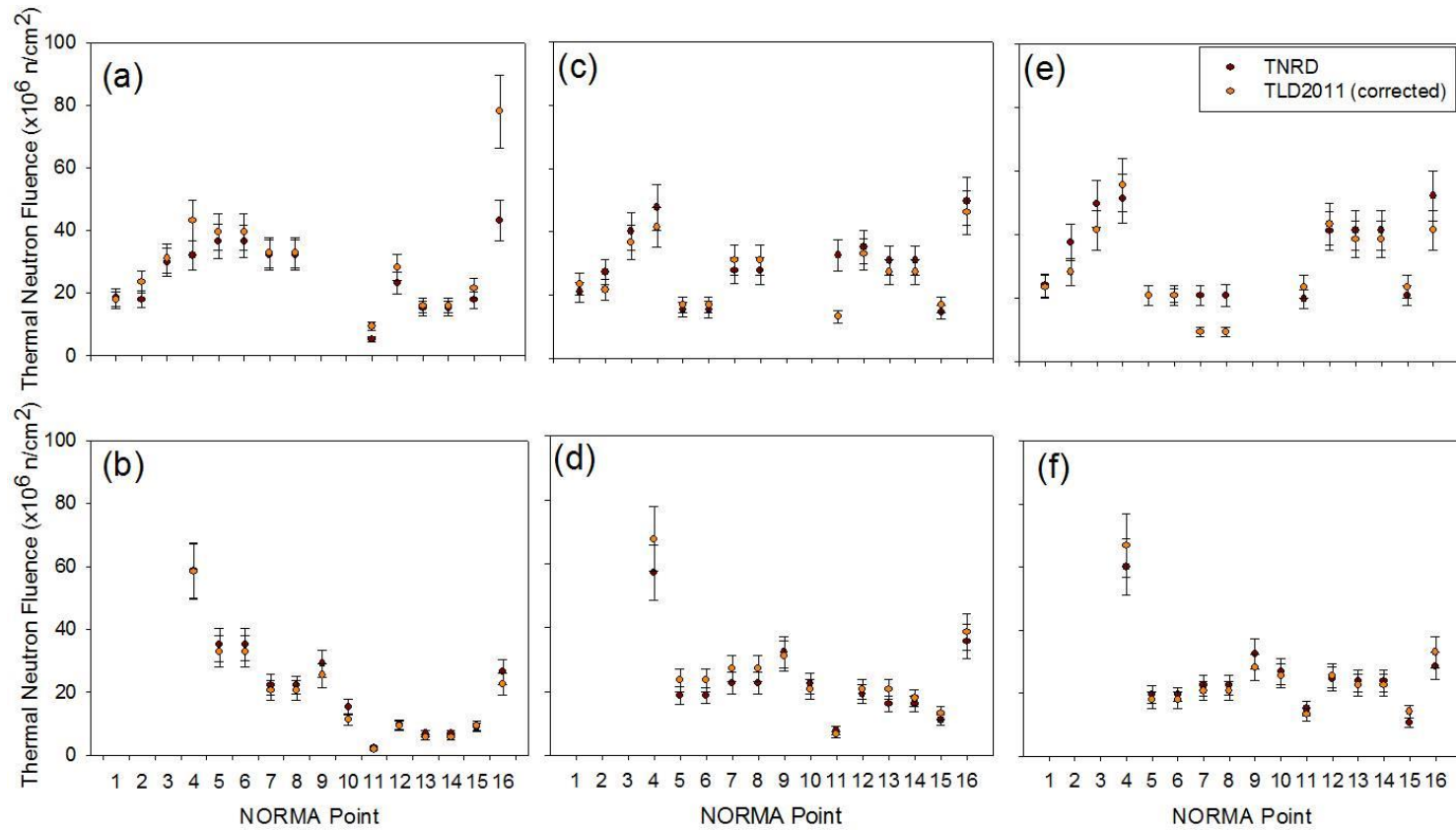


Figure 3. Comparison of thermal neutron fluences measured with TNRD for the 3 NORMA phantoms and 2 generic type of treatments (Abdomen and H&N) with previous data from TLD thermal neutron fluences (Sansaloni et al.,2011): (a) Adult abdomen, (b) Adult H&N, (c) Teen abdomen, (d) Teen H&N, (e) Child abdomen and (d) Child H&N. Corrected by differences in cut-off energies.

Table III. $M_{k,j}$ ($\mu\text{Sv}\cdot 10^{-6}\text{n}^{-1}\cdot\text{cm}^2$) represent relationship between reference thermal neutron fluence in the treatment room (R) and organ neutron dose equivalent ($H_T^{k,j} = M_{k,j} \cdot R$). Factor 10^{-3} was included for a better visualization of significative figures.

Organ	$M_{k,j}(\times 10^{-3}) [\mu\text{Sv}\cdot 10^{-6}\text{n}^{-1}\cdot\text{cm}^2]$					
	Adult		Teen		Child	
	Abdomen	H&N	Abdomen	H&N	Abdomen	H&N
Thyroid	145.20	358.10	314.63	472.91	388.15	500.19
Oesoph	311.28	253.39	492.42	398.28	679.35	484.16
Lung	735.23	460.13	884.57	710.30	606.20	873.52
Breast	956.20	426.05	1318.66	964.40	2116.95	1419.93
Stomach	271.75	136.04	414.22	247.64	574.98	332.93
Liver	320.16	136.23	455.61	256.62	591.39	336.87
Colon	76.64	21.10	178.39	73.01	246.45	136.17
Bladder	465.38	136.80	579.76	283.58	640.61	348.68
Ovary	76.64	21.10	178.39	73.01	246.45	136.17
Skin	2503.98	919.14	2229.71	823.54	3410.45	1500.56
Bone	517.27	278.671	591.50	350.04	870.02	517.43
Marrow	1074.91	419.27	1107.66	480.74	1640.29	803.09
Remainder	181.85	168.32	388.72	383.99	571.06	488.11
Prostate	76.64	21.10	178.39	73.01	246.45	136.17
Uterus	76.64	21.10	178.39	73.011	246.45	136.17

(c) Organ-equivalent neutron dose model considering patient dimensions

The HW parameter for each phantom size was calculated so that the functions $E(HW)_{k,j}$ describing the $M_{k,j}$ values as a function of the HW parameter were estimated for the abdomen and H&N as follows:

$$[E]_{k,abd} = 10^{-3} \cdot \begin{bmatrix} (-214.1HW + 563.9)_{thyroid} \\ (-309.2HW + 900.7)_{oesophagus} \\ (-834.9HW^2 + 2420HW - 808)_{lung} \\ (1496HW^2 - 5153.8HW + 5314)_{breast} \\ (-253.4HW + 753.3)_{stomach} \\ (-228.3HW + 755.7)_{liver} \\ (-146.3HW + 359.4)_{colon} \\ (-152.9HW + 762.8)_{bladder} \\ (-146.3HW + 360)_{ovary} \\ (3133.5HW^2 - 9453.6HW + 9019.1)_{skin} \\ (581.4HW^2 - 1916.1HW + 2042.2)_{bone} \\ (1235HW^2 - 3911.1HW + 4000.1)_{marrow} \\ (-330HW + 814.2)_{remainder} \\ (-146.3HW + 360)_{prostate} \\ (-146.3HW + 360)_{uterus} \end{bmatrix} \quad \text{and}$$

$$[E]_{k,H\&N} = 10^{-3} \cdot \begin{bmatrix} (-128.3HW + 618.4)_{thyroid} \\ (-200.1HW + 641.6)_{oesophagus} \\ (-356.6HW + 1149.9)_{lung} \\ (-844.8HW + 2046.9)_{breast} \\ (-168.4HW + 460.1)_{stomach} \\ (-172.9HW + 470.4)_{liver} \\ (-95.7HW + 202.6)_{colon} \\ (-186.5HW + 501.4)_{bladder} \\ (-95.73HW + 202.6)_{ovary} \\ (1726.7HW^2 - 5281.3HW + 4649.6)_{skin} \\ (319.06HW^2 - 1091.1HW + 1192.8)_{bone} \\ (700.71HW^2 - 2272.9HW + 2186.3)_{marrow} \\ (-280.3HW + 715.1)_{remainder} \\ (-95.73HW + 202.6)_{prostate} \\ (-95.73HW + 202.6)_{uterus} \end{bmatrix}$$

Those expressions are to be used in [eq.5](#) for organ-equivalent dose estimation.

Figure 4 depicts a selection of the qualitative behavior found for the fitting functions.

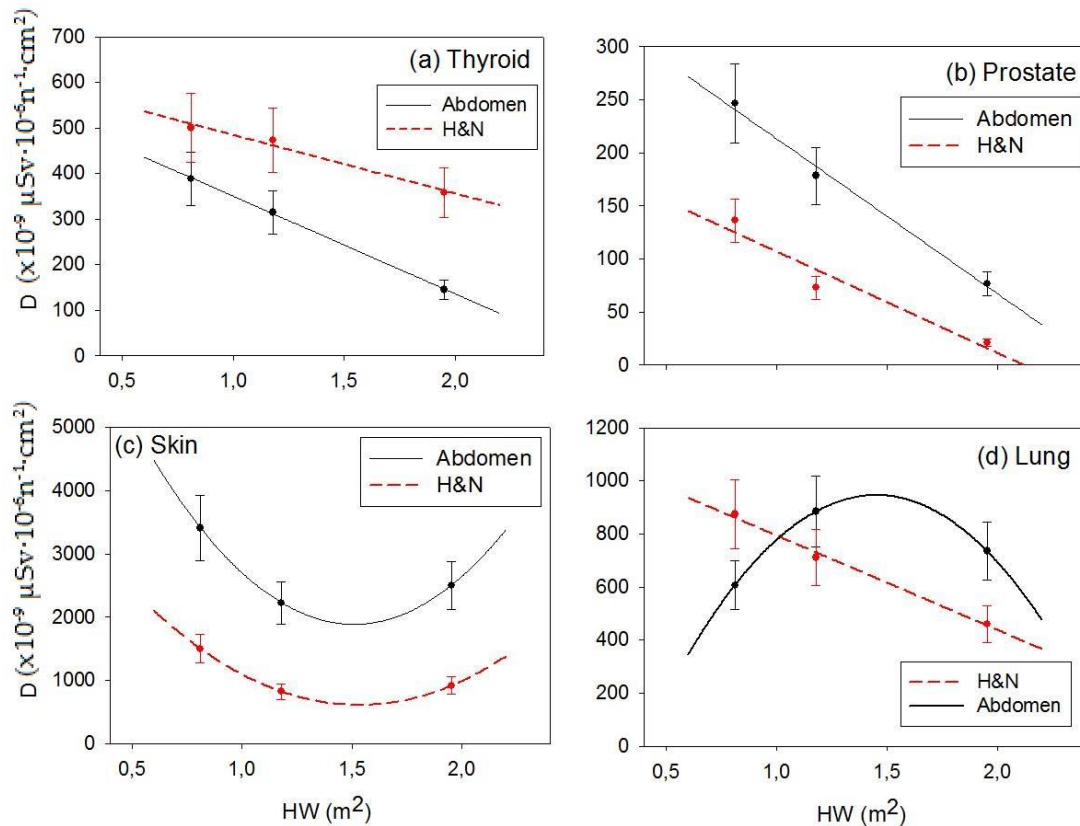


Figure 4. Selection of some representative fitting curves for Abdomen and H&N cases considering the patient size parameter (HW) for: (a) Thyroid and (b) Prostate (similar to the fitting behavior obtained for oesophagus, stomach, liver, colon, bladder, ovary, remainder and uterus); (c) Skin (similar to breast, bone and marrow) and special case of (d) Lung.

As expected, for the majority of the organs, the equivalent dose decreases when patient size increases, either due to a higher height (implying further distance from the source) or to a greater weight (entailing higher neutron thermalization and decrease in the neutron fluence).

However skin (or organs containing this point for calculation as breast, bone and marrow) showed a different pattern. That behavior can be explained through the two confounding factors. In small patients (i.e., $\text{HW} < 1.5 \text{ m}^2$), the

higher dose is mainly due to the greater fast-neutrons component which decreases with the inverse square law of the distance to the source. In patients with $HW > 1.5 \text{ m}^2$ the fast neutron component should be lower but seems to be compensated by the higher surface exposed to neutron radiation.

Equivalent dose to lungs during abdominal irradiation also shows a particular dependence with patient size. During this irradiation part of the lungs lays inside the treatment field (isocenter in point A, [Figure 1](#)), which has been shown to be representative of treatments in the abdominal area ([Irazola et al.,2016a](#)). The measured *TNRD* thermal neutron fluences showed [Figures 3a, 3b a,d 3c](#) are in agreement with MC simulations ([Figure 5](#)). The final behavior of the fitting curve can be understood as a result of the balance of the thermal and fast neutron component.

Thus, starting from different behavior of the neutron fluence components: thermal (increasing with) and fast (decreasing with phantom size).

This option is especially useful for retrospective studies for which not all the patient information (height or weight) is available, using as a first approximation patient age to choose the most adequate phantom size. This would improve peripheral neutron dose estimation, especially in the case of child patients.

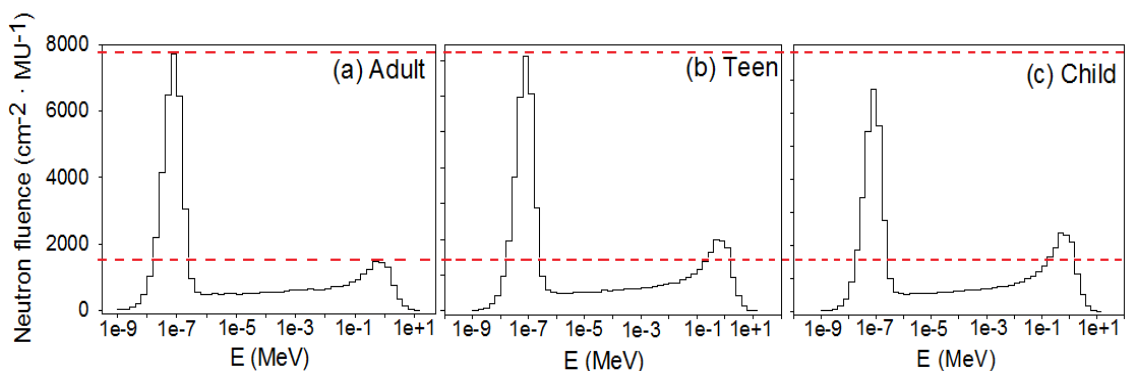


Figure 5. Monte Carlo simulation of neutron spectra for abdomen treatment location for the three phantom sizes ([González-Soto et al.,2012](#)), lethargy representation.

3.2 Patient estimations

Figure 6 depicts average organ-equivalent neutron doses estimated with the original and the generalized (eq.5) models for 240 patients in three organs. Those organs (thyroid, liver and marrow) were just selected for illustrative purposes. Differences among these values represent improvements in thermal neutron estimations at some points thanks to *TNRD* capabilities and the added modification of including patient size (*HW*). As a general behavior previous values seemed to overestimate the dose (in agreement with results from Figure 2).

In order to evaluate the goodness of the $M_{k,j}$ values for retrospective studies (or other cases where there is no information about patient size), measurements and theoretical estimations for organ-equivalent neutron doses for the 510 studied patients were compared. As all the patients are adult-aged, $M_{k,j}$ adult values (abdomen and H&N models) were chosen for this purpose. Results are plotted in Figure 7. As expected, as all patients included in the study were adult, no high deviations were found between methodologies. Nevertheless, greater deviations should be expected for young patients due to the higher differences in height and weight from the adult NORMA phantom. For the chosen example (Figure 8), the old model underestimated in average the organ-equivalent doses by 34.1% (assuming that the new model provides the correct patient-size estimation).

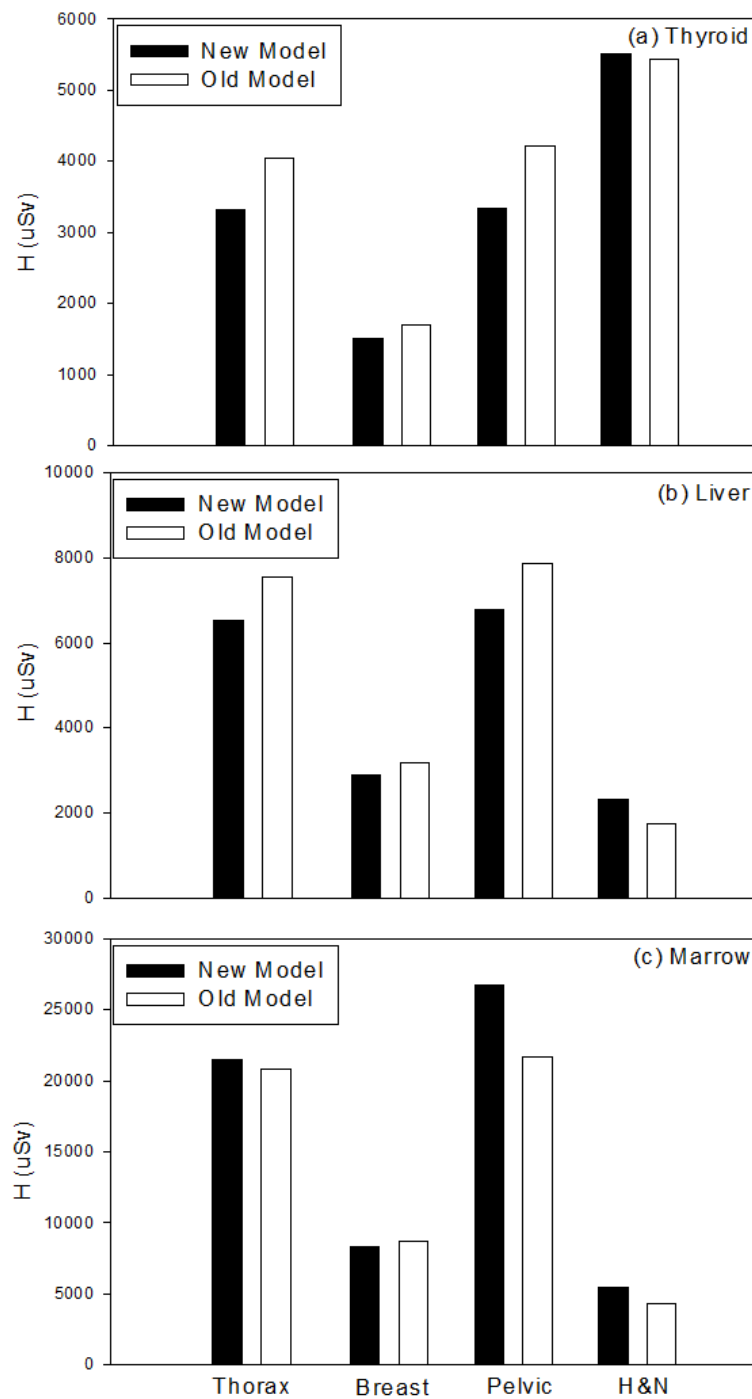


Figure 6. Comparison between organ-equivalent neutron doses estimated with the old (white) and the new (black) models for 240 patients in three organs: (a) Thyroid, (b) liver and (c) marrow for the four studied pathologies.

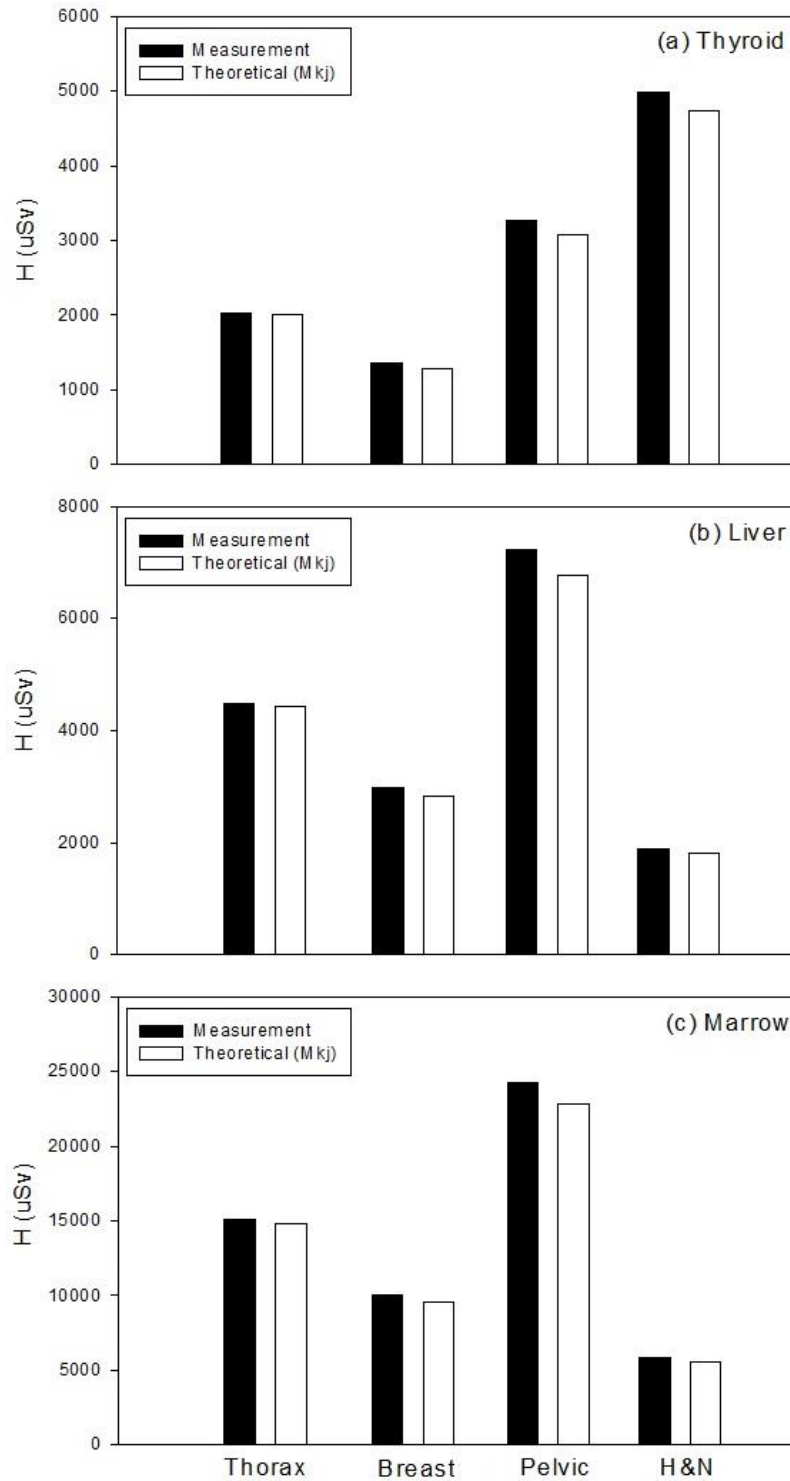


Figure 7. Comparison of measurement and theoretical estimations (Mkj factors for adult) for organ-equivalent doses for the 510 studied patients.

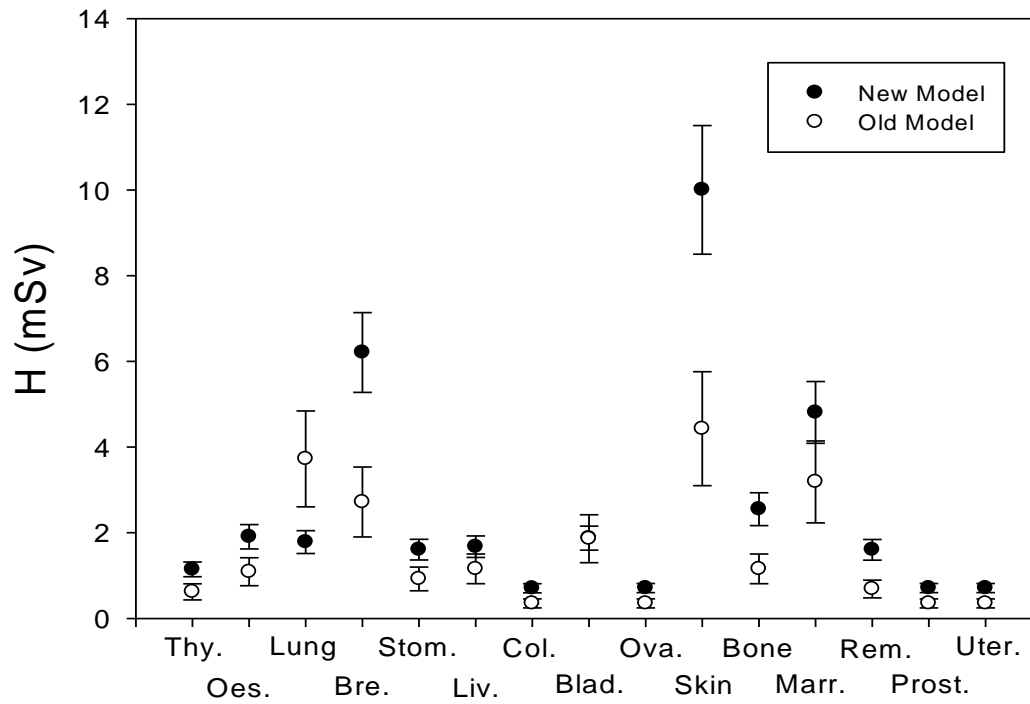


Figure 8. Comparison of peripheral doses for an abdomen location child treatment case calculated with the old model and the new one (considering patient size).

Concerning SCP, as we are working in low-dose range (e.g. <2.5 Gy), linear models could be used for this purpose (Schneider et al.,2005). Thus, eq.5 can be employed for SCP estimates by using tabulated coefficients from ICRP-103 or BEIR-VII (sex- and age-at-exposure- specific) protocols:

$$SCR = H_{k,j} \cdot \lambda_k \quad (\text{eq.6})$$

where $H_{k,j}$ are peripheral neutron doses for organ $-k$ in the specific model $-j$ and λ_k are the organ risk factors from ICRP-103 or BEIR-VII protocols.

4. Conclusions

The use of the new online thermal neutron miniaturized active *TNRD* detectors, for peripheral neutron dose assessment, has allowed the improvement of existing models for organ-equivalent neutron dose estimation in any facility.

Several aspects have been enhanced:

- Characterization of the facility has been established in terms of thermal neutron fluence instead of the events of the previously used SRAM-based detector, generalizing the methodology to any thermal neutron detector.
- The online behavior of *TNRD* detector, has simplified the procedures followed for model enhancements.
- Models have been modified to be more patient-specific, introducing weight and height to better evaluate organ-equivalent neutron doses, which results especially relevant for children cases.

A universal methodology for peripheral neutron organ-equivalent doses estimation has been established. It only requires the characterization of the facility in terms of thermal neutron fluence, the total number of high energy MU delivered and patient size (height and weight). Finally these models have been validated by the comparison of estimations from the existing models to a cohort of 510 patients. This would be useful for future second cancer risk evaluation and its implementation in TPS.

5. References

- Armstrong GT, Kawashima T, Leisenring W, Stratton K, Stovall M, Hudson MM, et al. Aging and risk of severe, disabling, life-threatening, and fatal events in the childhood cancer survivor study. *J Clin Oncol* 2014;32:1218-27.
- Bedogni R, Bortot D, Pola A, Introini MV, Gentile A, Esposito A, Gómez-Ros JM, Palomba M, Grossi A. *A new active thermal neutron detector*. *Radiation Protection Dosimetry. Radiat Prot Dosim* 2014;161(1-4)241-244.

- Bedogni R, Sacco D, Gómez-Ros JM, Lorenzoli M, Gentile A, Buonomo B, Pola A, Introini MV, Bortot D and Domingo C. *ETHERNES: A new design of radionuclide source-based thermal neutron facility with large homogeneity area*. Appl Radiat and Iso 107 (2016) 171–176.
- BEIR Phase 2, NRC National Research Council. *Health risks from exposure to low levels of ionizing radiation.*, 2006.
- Berdnarz B, Hancox C and Xu XG. *Calculated organ doses from selected prostate treatment plans using Monte Carlo simulations and an anatomically realistic computational phantom*. Phys Med Biol 2009;54:5271-86.
- Chargari C, Goodman KA, Diallo I, Guy JB, Rancoule C, Cosset JM, Deutsch E and Magne N. Risk of second cancers in the era of modern radiation therapy: does the risk/benefit analysis overcome theoretical models? Cancer Metastasis Rev 2016;1-13.
- Diallo I, Haddy N, Adidj E, Samand A, Quiniou E, Chavaudra J, Alziar I, Perret N, Guérin S, Lefkopoulos D and de Vathaire F. *Frequency distribution of second cancer locations in relation to the irradiated volume among 115 patients treated for childhood cancer*. Int J Rad Oncol Biol Phys 2009;74 (3):876-883.
- Dubois D, Dubois EF. *A formula to estimate the approximate surface area if height and weight be known*. Arch Intern Med 1916; 17:863-871.
- Expósito MR, Sánchez-Nieto B, Terrón JA, Domingo C, Gómez F and Sánchez-Doblado F. *Neutron contamination in radiotherapy: Estimation of second cancers based on measurement in 1377 patients*. Radiother and Oncol 2013;107:234-241.
- Followill D, Nüsslin F and Orton CG. *IMRT should not be administered at photon energies greater than 10 MV*. Med Phys 2007;34(6):1877-1879.
- Gómez F, Sánchez-Doblado F, Iglesias A and Domingo C. *Active on-line detector for in-room radiotherapy neutron measurements*. Radiat Meas 2010;45:1532-1535.
- González-Soto X, Expósito M., Sánchez-Nieto B, Amgarou K, Lagares JL, Gómez F, Domingo C and Sánchez-Doblado F. *Neutron spectra inside an adult and children anthropomorphic phantoms in high energy radiotherapy*. In: Long M, editors WC 2012, IFMBE Proceedings 39, Berlin:Springer. 2012:1145-1148.
- Hall EJ and Wu CS. *Radiation-induced second cancers: The impact of 3D-CRT and IMRT*. Int J Radiation Oncology Biol Phys 2003;56(1):83-88.
- Harrison RM. *Introduction to dosimetry and risk estimation of second cancer induction following radiotherapy*. Radiat Meas 2013;57:1-8.
- Howell RM, Hertel NE, Wang Z, Hutchinson J, Fullerton GD. *Calculation of effective dose from measurements of secondary neutron spectra and scattered photon dose from dynamic MLC IMRT for 6 MV, 15 MV and 18 MV beam energies*. Med Phys 2006;33:360-8.
- ICRP International Commission on Radiological Protection. *The 2007 Recommendations of the International Commission on Radiological Protection*. ICRP Publication 103, 2007.
- Irazola L, Lorenzoli M, Bedogni R, Pola A, Terrón JA, Sanchez-Nieto B, Exposito MR, Lagares JL, Sansaloni F and Sanchez-Doblado F. *A new online detector for estimation of peripheral neutron equivalent dose in organ*. Med Phys 2014;41:112105.
- Irazola L, Terrón JA, Bedogni R, Lorenzoli M, Pola A, Sánchez-Nieto B and Sánchez-Doblado F. *Signal photon component of a new thermal neutron detector TNRD in radiotherapy environments*. Radiother and Oncol 2015;115(1):S870.

- Irazola L, Terrón JA, Sánchez-Nieto B, Romero-Expósito M and Sánchez-Doblado F. *Peripheral neutron dose model verification for real IMRT cases*. Poster at the 1st European Congress of Medical Physics (ECMP) 2016, Athens; Greece (2016a)
- Irazola L, Terron JA, Bedogni R, Pola A, Lorenzoli M, Sanchez-Nieto B, Gomez F and Sanchez-Doblado F. *Limitations and solutions of TNRD neutron detector in high energy photon beam radiotherapy*. Sent to Appl Radiat Isot (2016b)
- ISO Standard, TC 85 Nuclear energy, nuclear technologies, and radiological protection SC 2. *Reference neutron radiations – Part 1: Characteristics and methods of production*. ISO 8529-1;2001.
- Jagetic L and Newhauser WD. *A simple and fast physics-based analytical method to calculate therapeutic and stray doses from external beam, megavoltage x-ray therapy*. Phys Med Biol 2015;60:4753-4475.
- Kry SF, Slehpour M, Followill DS, Stovall M, Kuban DA, White RA and Rosen II. *Out-of-field photon and neutron dose equivalents from step-and-shoot intensity-modulated radiation therapy*. J Radiation Oncology Biol Phys 22005;62:1204-16.
- Nath R, Boyer A, LaRiviere PD, McCall RC and Price KW. *Neutron measurements around high energy X-ray radiotherapy machines*. A Report of Task Group 27, Radiation Therapy Committee, American Association of Physicists in Medicine. AAPM Report No.19. Medical Physics Publishing, NY, 1986.
- Newhauser WD and Durante M. *Assessing the risk of second malignancies after modern radiotherapy*. Nat Rev Cancer 2011;11(6):439-448.
- Newhauser WD, Berrington de Gonzalez A, Schulte R and Lee C. *A Review of Radiotherapy-Induced Late Effects Research after Advanced Technology Treatments*. Front Oncol 2016;6:13.
- NCRP-79, National Council on Radiation Protection and Measurements. *Neutron contamination from medical electron accelerators*. Reperot No. 79. National Council on Radiation Protection and Measurements, Bethesda, MD, 1984.
- Pena J, Franco L, Gómez F, A Iglesias, J Pardo, and M Pombar. *Monte Carlo study of siemens PRIMUS photoneutron production*. Physics in Medicine and Biology, 50:5921–5933, 2005.
- Romero-Expósito M, Sánchez-Nieto B, Terrón JA, Lopez MC, Ferreira BC, Grishchuk D, Sandíns C, Moral-Sánchez S, Bragado-Álvarez L, Melchor M, Domingo C, Gómez F and Sánchez-Doblado F. *Commisioning the neutron production of a linac: development of a clinical planning tool for second cancer risk estimation*. Med Phys 2015;42:276-281.
- Romero-Expósito M, Domingo C, Sánchez-Doblado F, Ortega-Gelabert O and Gallego S. *Experimental evaluation of neutron dose in radiotherapy patients: which dose?* Med Phys 2016;43:360.
- Romero-Expósito M, Sánchez-Nieto B, Irazola L and Sánchez-Doblado F. *In regard to “Neutron contamination in radiotherapy: Estimation of second cancers based on measurements in 1377 patients.”* Letter to the Editor. Sent to Radiother and Oncol
- Ruben JD, Davis S, Evans C, Jones P, Gallgiardi F, Haynes M and Hunter A. *The effect of intensity-modulated radiotherapy on radiation-induced second malignancies*. J Radiation Oncology Biol Phys 2008;70(5):1530-1536.
- Sánchez-Doblado F, Domingo C, Gómez F, Sánchez-Nieto B, Muñoz JL, García-Fusté MJ, Expósito MR, Barquero Terrón JA, et al. *Estimation of neutron equivalent dose in*

- organs of patients undergoing radiotherapy by the use of a novel online digital detector.* Phys Med Biol 2012;57:6167–6191.
- Sánchez-Nieto B, El-far R, Irazola L, Expósito MR, Lagares JI, Mateo JC, Terrón JA and Sánchez-Doblado F. *Analytical model for photon peripheral dose estimation in radiotherapy treatments.* Biomed. Phys. Eng. Express 2015;1:045205.
- Sánchez-Nieto B, Romero-Expósito M, Terrón J A, Irazola L, Paiusco M, Cagni E, Ghetti C, Filice S, Gómez F, Domingo C and Sánchez-Doblado F. *Risk assessment of second cancer incidence after intensity-modulated radiation therapy and volumetric modulated arc therapy versus conventional techniques at high energy.* Sent to J Appl Clin Med Phys
- Sansaloni F, Lagares JI, Muñoz J, Expósito MR, Terrón JA, Núñez L, Barquero R and Sanchez-Doblado F. *Peripheral gamma dose and thermal neutron fluencies evaluation for IMRT on adult, teen and child.* Radiother Oncol 2011;99:S558.
- Schneider U, Zwahlen D, Ross D, Kaser-Hotz B. *Estimation of radiation-induced cancer from three-dimensional dose distributions: concept of organ equivalent dose.* Int J Radiat Oncol Biol Phys 2005;61(5):1510-1515.
- Siebert BRL and Schuhmacher H. *Quality factors, ambient and personal dose equivalent for neutrons, based on the new ICRU stopping power data for protons and alpha particles.* Radiat Prot Dosim 1995; 58:177–83.
- Tubiana M. *Can we reduce the incidence of second primary malignancies occurring after radiotherapy? A critical review.* Radiother Oncol 2009;91(1):4-15.
- Xu X-G, Bednarz B, Paganetti H. *A review of dosimetry studies on external-beam radiation treatment with respect to second cancer induction.* Phys Med Biol 2008;53:R193-R241.
- Stovall M, Blackwell CR, Cundiff J, Novack DH, Palta JR, Wagner LK, Webster EW and Shalek RJ. *Fetal dose from radiotherapy with photon beams: Report of AAPM Radiation Therapy Committee Task Group No.36.* Med Phys 1995;22:63-82.

(D)

SBRT, FFF and 10 MV irradiation techniques are associated to the lowest second cancer risk

Irazola et al., To be sent to Radiat Oncol J

Abstract

Purpose: Recently there has been a growing interest in Stereotactic Body Radiation Therapy (SBRT) and Flattening Filter Free (FFF) irradiation techniques. The high local control rates achieved and the “low-dose” radiation delivered to the near out-of-field regions, together with the hypofractionation, are expected to reduce doses beyond the target. The aim of this work is to determine the impact of SBRT modality in peripheral doses, when compared to other ones, such as 3D-CRT, IMRT and VMAT.

Methods: Photon and neutron peripheral doses at large distances from the field-edge (beyond 5% isodose) have been estimated using two analytic models, operating from readily available parameters. Ten real treatments, including the most common pathologies treated with SBRT have been evaluated. Different techniques (3D-CRT, IMRT, VMAT and SBRT) and energies (6, 10 and 15 MV) for Varian (including FF and FFF modalities), Siemens and Elekta linacs have been considered, leading to 144 treatment plans, whose peripheral doses have been compared.

Results: Comparison between modalities showed an important decrease of peripheral doses for SBRT respect to more conventional fractionations, being more evident when tumor size is highly diminished respect to the other

techniques. In addition, the use of FFF irradiation mode implies an extra reduction, especially when used at 10 MV.

Conclusions: The obtained results for peripheral doses suggest that hypofractionated modality in 10 MV using FFF mode, could represent the best compromise between dose delivery efficiency and peripheral doses reduction. The implementation of second cancer risk estimations to TPS, based in the here presented methodology, could mean the addition of an important parameter for best treatment plan selection.

1. Introduction

In recent times there has been a growing concern on peripheral dose (PD) estimation in external radiotherapy. This issue is attributable to the larger cancer incidence as well as to the higher survival rates. These unwanted outlying doses are associated to an increased risk of Second Malignant Neoplasms (SMNs) in cancer survivors (Xu et al.,2008). Additionally, an accurate knowledge of out-of-field doses is of major importance for a specific range of population such as children, pregnant patients and those with implantable electronic devices, which are becoming more and more usual (Cardenas et al.,2015). PD in radiotherapy treatments are due to scatter, leaf transmission, radiation head leakage and neutron contamination.

An escalation of these PD, as a consequence of beam-on-time increase, has been noticed in newer techniques such as Intensity Modulated RadioTherapy (IMRT) and Volumetric Modulated ArcTherapy (VMAT) (Kry et al.,2005a). Compared to conformal radiotherapy (3D-CRT), modern modulated modalities use a greater number of treatment fields and monitor units (MU) to accomplish highly conformal dose distributions around the target volume. This generally leads to an increase of the portion of normal tissue exposed to “low-doses”. At distances close to the field-edge (e.g. <10 cm), PD is mainly due to photon patient scatter, while when getting further, photon scatter from linac head

becomes more important. Finally, photon leakage component dominates at distances ≥ 30 cm approximately (Benadjaoud et al.,2012; Joosten et al.,2011). In addition, when high photon energies are used (≥ 10 MV), neutron contamination should be also considered for second cancer risk estimations (Kry et al.,2005b).

Latterly there has been an emergent interest on Stereotactic Body Radiation Therapy (SBRT) as an alternative method to conventional fractionation for a wide range of primary and metastatic lesions. Clinical studies have pointed it out as an effective technique, which allows the deliverance of ablative radiation doses in few fractions with excellent local control (up to 88-92% in lung cases) for patients suffering from pathologies unfit for surgery or conventional techniques (Ong et al.,2010; Demaria et al.,2012). Thus, this technique is expected to show potential therapeutic advantage, regarding “low-doses” delivered to tissues outside the target. However, although there are several clinical results demonstrating the great local control achieved with minor toxicities (Rubio et al.,2013; Martin et al.,2010; Kirkpatrick et al.,2014; Timmerman et al.,2007), longer follow-ups are needed to evaluate latter implications.

In addition, the combination of this hypofractionated modality with medical accelerators operating in flattening filter free mode (FFF) is becoming more frequent. The interest behind this combination is the incorporation of the reduction in out-of-field doses (obtained with FFF mode) to SBRT modality, given that the latter guarantees a high local control rate (Huang et al.,2015; Prendergast et al.,2013). The time reduction achieved in treatments using this linac operation mode is of special interest for SBRT modality, where respiration control while delivering is of great importance due to the highly fractionation employed (Prendergast et al.,2013; Fu et al.,2004; Stathakis et al.,2009). According to several studies (Irazola et al.,2015; Cashmore et al.,2008; Kragl et al.,2011; Kry et al., 2007) a lower neutron contamination and less Multi Leaf

Collimator (MLC) leakage is expected for this operation mode. Furthermore, some research suggests that the use of FFF mode could lead to lower incidence of SMNs ([Cashmore et al.,2011](#)).

Although PD coming from conventional radiotherapy have been widely study, there are a limited number of works concerning SBRT and FFF modalities ([Kragl et al.,2011](#), [Prendergast et al.,2013](#); [Fu et al.,2004](#); [Stathakis et al.,2009](#); [Xu et al 2008](#); [Xie et al.,2014](#)). There are several comparisons between newer techniques and conventional ones (3D-CRT, IMRT or VMAT) in terms of dose conformity and delivery times ([Benadjaoud et al.,2012](#); [Huang et al., 2015](#); [Ong et al.,2010](#)). However, to our knowledge, there are no comparative studies ([Irazola et al.,2016](#)) in terms of photon and neutron peripheral doses, including SBRT ([Kragl et al.,2011](#); [Murray et al.,2015](#); [Schneider et al.,2010](#)). The purpose of this work is the estimation and comparison, in terms of PD, of SBRT with conventional fractionation techniques as 3D-CRT, IMRT and VMAT, in normal and FFF modes. The main pathologies treated in SBRT modality have been selected for this peripheral dose study ([Scorsetti et al.,2015](#)). We did not consider the impact of Image-Guided Radiotherapy (IGRT) on PD estimations, as this will vary with the technique employed.

2. Material and method

2.1 Patient selection

Ten patients previously diagnosed with primary or metastatic lesions, treated following currently existing SBRT protocols, were selected for this study. The choice was done for different tumor sizes and locations, in order to encompass all the pathologies sensitive to be treated with SBRT ([Scorsetti et al.,2015](#); [Irazola et al.,2016](#)). Thus, the most common cases treated in this technique such as lung, prostate, paravertebral, brain, oligo-metastasis, breast, adrenal, hepatic or breast; multiple and single lesions have been evaluated.

2.2 Target and OAR delineation

Delineation has been done by expertise radiation oncologists by contouring all the phases from 4D-CT images for lung cases and from 4D-PET for the hepatic ones. MRI has been used for brain lesions, while combined CT and PET images were used for the oligo-nodules case. The rest of the treatments were delineated using conventional CT images. All patients were treated in supine position using either vacuum bags, immobilization masks or a custom-model cradle system (ExaCradle©). The Gross Tumor Volume (GTV) has been chosen accounting for tumor motion. Then Internal Target Volume (ITV) was created for SBRT plans by combining GTV phases. In the case of conventional treatments, Planning Target Volume (PTV) was conservatively designed by adding different margin expansions from the Clinical Target Volume (CTV) for each case, in order to account for positioning uncertainties and potential tumor shifting.

Organs At Risk (OAR) contouring and dose prescriptions and limits, have been performed by the same expertise following AAPM TG-101 ([Benedict et al.,2010](#)) guidelines for SBRT modality and QUANTEC ([RTOG., 2010](#)) protocols for normal fractionations.

2.3 Treatment plans

All clinical cases were planned using several techniques and energies, according to the clinically viable options (3D-CRT, IMRT, VMAT and SBRT modalities in 6, 10 and 15 MV) for the three main linac manufacturers (Elekta, Siemens and Varian). Additionally, FFF mode for 6 and 10 MV was used when available. For SBRT modality most clinically acceptable option has been chosen among the available techniques (between 3D-CRT, IMRT or VMAT). [Table I](#) summarizes characteristics of all the studied plans. The same dosimetric constraints (in percentage) were considered in all the facilities for OAR sparing

and PTV coverage. As an example, OAR and PTV dosimetric results for the single-lesion hepatic case (treated in 10 MV) is shown in [Figure 1](#) comparing 10 MV 3D-CRT and SBRT plans in terms of Dose Volume Histogram (DVH) for one of the facilities (Varian TrueBeam) to ensure a virtually identical PTV coverage and OAR sparing.

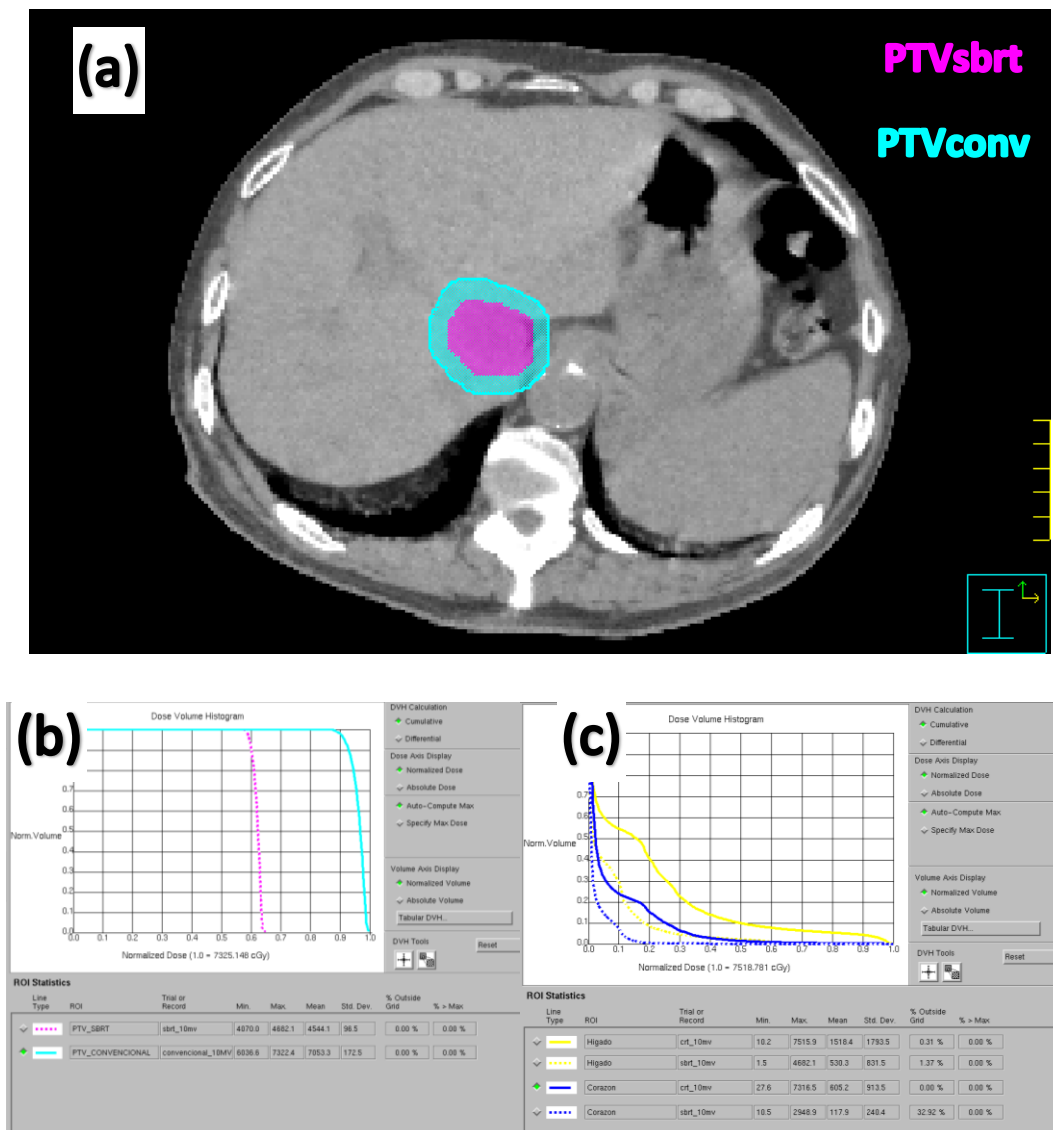


Figure 1. (a) Comparison, for a single-lesion hepatic case, of PTV dimensions for an SBRT modality (pink) and a conventional fractionation scheme (blue). Comparison of DVH obtained in SBRT (dashed) and conventional (solid) fractionations (10 MV) for (b) target volumes and (c) liver (yellow) and heart (blue) OAR.

Table I. Summary of treatment plans, modalities and energies used, dose prescription and target volume size studied*.

Case	Pathology	Technique	Energy	Dose per fraction (Gy)	N fractions	ITV (cm ³)	PTV (cm ³)
1	Lung simple (primary)	3D-CRT	6, 6 FFF	2	33	16.92	76.35
		VMAT		20	3		
2	Lung 2 lesions (metastatic)	SBRT	6, 6 FFF	10	5	5.32**	10.26**
3	Multiple brain metastasis	3D-CRT	6, 6 FFF	4	5	0.11**	1408
		SBRT		6	5		
4	Prostate (primary)	3D-CRT	6, 6 FFF, 10, 10 FFF, 15	1.8	42	138.46	191.73
		IMRT		2.6	29		
		VMAT		7.25	5		
		SBRT					
5	Hepatic 3 lesions (metastatic)	SBRT	6&15, 10, 10 FFF	20	3	7.09**	26.51**
6	Oligo-nodules (primary)	3D-CRT	6, 6 FFF, 10, 10 FFF, 15	PTV1: 2	33	294.3	421.13
		IMRT		PTV2: 2	25		
		VMAT		PTV1: 7.5 PTV2: 5	6		
		SBRT					
7	Breast (primary)	3D-CRT/IMRT/VMAT	6, 6 FFF	2	25	16.92	76.35
		SBRT (partial)		3.85	10		
8	Hepatic (primary)	3D-CRT/IMRT/VMAT	6&15, 10, 10 FFF	2	35	8.15	19.13
		SBRT		15	3		
9	Kidney (metastatic)	SBRT	6, 6 FFF, 10, 10 FFF, 15	10	4	4.28	14.65
10	Paravertebral (metastatic)	CRT (reirrad)	6, 6 FFF, 10, 10 FFF, 15	8	3	16.92	76.35
		SBRT		9	3		

*FFF modes were not used for 3D-CRT modality as we consider as not a realistic case. The rest of the treatment plans were calculated for all the mentioned energies for each technique.

** Averaged values considering all the lesions.

Plans were calculated in Pinnacle -v.9.10- (Monaco -v.2.03- was used in the case of Elekta Axesse) Treatment Planning Systems (TPS) and delivered using a Simens Oncor (except VMAT technique), Elekta Synergy/Axesse and Varian TrueBeam linacs. FFF photon mode was only available for the later (Varian Medical Systems, Inc, Palo Alto, CA), equipped with a millennium multileaf collimator.

In order to illustrate the advantage of the FFF operating mode for each modality, a comparison of averaged irradiation times ratios of FF to FFF irradiation modes are shown in [Table II](#), for prostate, oligo-nodules, breast and lung cases. Our results are in agreement with previous reports ([Prendergast et al.,2013](#)) that suggested the higher efficiency for SBRT treatments using FFF mode when compared to conventional fractionations. FFF for conformal technique was not considered as it lacks from clinical sense. As previously mentioned, the main advantage of the reduction IN delivery time would be the lower intra-fraction motion ([Prendergast et al.,2013](#)). The greatest time reduction is obtained for the 10 MV FFF modality. Note that reduction in time (from 6 to 10 MV) is not proportional to the dose rate increase (1400 to 2400 MU/min) due to limitations in the leaf motion velocity.

2.4 Peripheral dose calculation

In the present work, two models for the estimation of photon and neutron peripheral equivalent doses for some of the most relevant cancer-at-risk organs have been used. They provide doses outside beyond the region where the accuracy of commercial TPS is questioned and where no CT data is usually available (typically outside the 5% isodose, representing around 10 cm from the field-edge; [Howell et al.,2010](#); [Sánchez-Nieto et al.2015a](#)). The knowledge of these PD would allow the assessment of second cancer risk in the studied techniques.

Table II. Average irradiation times ratios and MU achieved in FF and FFF modes of the Varian linac for the prostate, oligo-nodules, breast and lung cases.

Treatment modality	Energies (MV)	Time factor
SBRT	10 / 10 FFF	2.2
	6 / 6 FFF	1.8
VMAT	10 / 10FFF	1.2
	6 / 6 FFF	1.2
IMRT	10 / 10FFF	1.3
	6 / 6 FFF	1.2

2.4.1 Photon Equivalent Dose

The analytical model described in [Sánchez-Nieto et al.2015a](#) has been employed for the evaluation of Photon Peripheral Doses (PPD), accounting for leakage and scatter contributions. In this model, the first component is considered as a constant value while the latter is obtained from a simulated virtual isotropic source that decreases with an inverse-square law and an exponential attenuation, based on the proportion of air and tissue traversed. Thus, photon dose to points can be estimated by terms of the following expression:

$$PPD(x, z, f, \epsilon) = A + \frac{B}{x^2} \epsilon F(f) e^{-r_{eff}} \quad (\text{eq.1})$$

Where:

- A represents the constant leakage component, which has been obtained from each manufacturer for the studied linacs and energies.
- The second term accounts for scatter radiation in linac head. B is a constant value, fixed by the model and x represents distance from the calculation point to the treatment isocenter. Exponential term accounts for the weighted average of linear attenuation coefficients for distance

traversed by the radiation (in air and tissue). Additional correction factors account for treatment efficiency ϵ (in terms of MU) and field size F .

Equivalent dose to organs is then evaluated as the integration of point PPD, calculated along organ length. Further details of this model can be found in (Sánchez-Nieto et al.,2014;2015a;b; 2016a; 2016b).

For field size estimation, tumor size (x and y) for PTV and ITV volumes at isocenter location were used. In the case of multiple lesions, the average volume values were considered as representative of a single tumor size positioned at the depth of the *center of mass* of all lesions.

2.4.2 Neutron Equivalent Dose

Peripheral Neutron Dose (PND) model used in this work is also based in dose to point estimations (Sánchez-Doblado et al.,2012). Organ doses are calculated from point averaged values, calculated from clinically relevant points estimated inside an anthropomorphic phantom. Dose equivalent have been obtained regarding Monte Carlo simulations, ICRP-103 radiation weighting factors and thermal neutron detector measurements at 16 selected points for two different models, namely Head & Neck and Abdomen (Sánchez-Doblado et al.,2012; Expósito et al.,2013; Irazola et al.,2014b; Irazola et al.,2016b). These neutron doses are correlated to thermal neutron readings of a digital detector (located in the room, far from the patient). Thus, this methodology allows direct estimation of peripheral neutron doses for any facility by the only knowledge of the number of high energy MU (≥ 10 MV) of the specific treatment (Irazola et al.,2016a). For that, it only requires the commissioning of the facility in terms of neutron production by a simple characterization procedure (Romero-Expósito et al.,2015; Irazola et al.,2014a; Irazola et al.,2014b; Irazola et al.,2016b). PND can be estimated as follows:

$$PND_{k,j} = c^* \cdot MU \cdot M_{k,j} \quad (\text{eq.2})$$

Where:

- c^* is the facility characterization factor in terms of neutron production. This factor can be either estimated from tabulated values for all the available linacs (Sánchez-Doblado et al.,2012) or by direct measurement (Romero-Expósito et al.,2015; Irazola et al.,2016c).
- MU is the total number of high energy MU of the specific treatment.
- $M_{k,j}$ are the organ (k) and treatment (j) dependent correlation coefficients extracted from Irazola et al.,2016b (updated from g_j^k factors calculated in Sánchez-Doblado et al.,2012).

A modified version of Periphocal software (Sánchez-Nieto et al.,2015;2016) has been used for PD calculation. Photon leakage parameters used were provided by the manufacturer. Regarding neutron dose calculations, a previous commissioning (Romero-Expósito et al.,2015), in terms of neutron production, was performed at each of the installations involved in this study. Uncertainties of these estimations, using the here described methodologies, are around $\pm 25\%$ and $\pm 30\%$ in the case of photons and neutrons, respectively. As previously explained, these models are used for calculations beyond 5% isodose where TPS estimates (in the case of photons, as neutrons are never considered in conventional radiotherapy TPS) are not reliable.

The estimation of these peripheral doses opens the door to second cancer probability (SCP) estimations. This additional parameter should be used in combination with TCP and NTCP parameters for the best treatment strategy selection. As total PD obtained remained below 4 Gy, the linear no-threshold (LNT) models can be applied for this purpose (Schneider et al.,2015; Chargari et

al.,2016) as an acceptable qualitative approach (Schneider et al.,2010). For illustrative purposes, only SCP calculations for the prostate case were included.

3. Results and discussion

Firstly, we aimed to compare PDs among the 4 studied techniques (3D-CRT, IMRT, VMAT and SBRT) at low and high energies. As an example, doses (mSv) for the 14 representative organs chosen are shown in Figure 2 for lung (6 MV), paravertebral (10 MV) and prostate (15 MV) cases for Varian TrueBeam linac. Organs without dose information were either because laid within the 10 cm margins or had been excluded regarding patient sex.

All clinical cases studied led to the lowest PD for the SBRT modality with respect to conventional fractionation techniques. As suggested in previous publications (Irazola et al.,2016a), this could be due not only the lower doses used for SBRT modality but to differences found in target volumes (Table I). For some of the calculated scenarios, 3D-CRT (standard fractionated modality) led to lower PDs than IMRT and VMAT, which showed similar values.

Next step was the evaluation of differences between low and high energies. To illustrate the obtained results, paravertebral and adrenal cases for 6, 10 and 15 MV in SBRT modality for the Varian linac were chosen. Figure 3 depicts PDs obtained at the same previously mentioned selected organs.

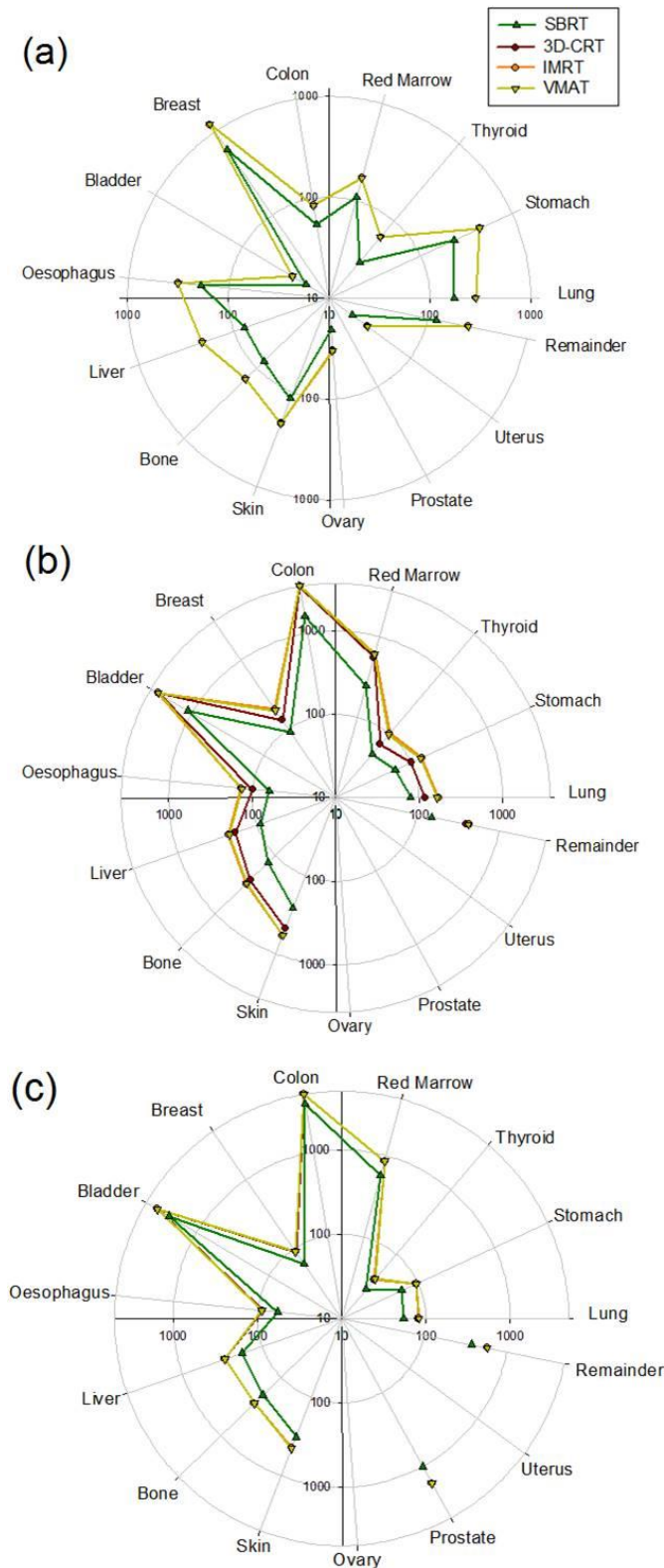


Figure 2. Comparison of PD for 14 representative out-of-field organs in: (a) lung 6 MV, (b) oligo-nodules 10 MV and (c) prostate 15 MV cases using the 4 possible treatment modalities. Polar axis is displayed in logarithmic scale, representing doses ranging between 17 mSv-1.3x10³ mSv, 0.3 mSv-5x10³ mSv and 3 mSv-3.7x10³ mSv, respectively. Curves overlapping do not permit see all the options in some graphs.

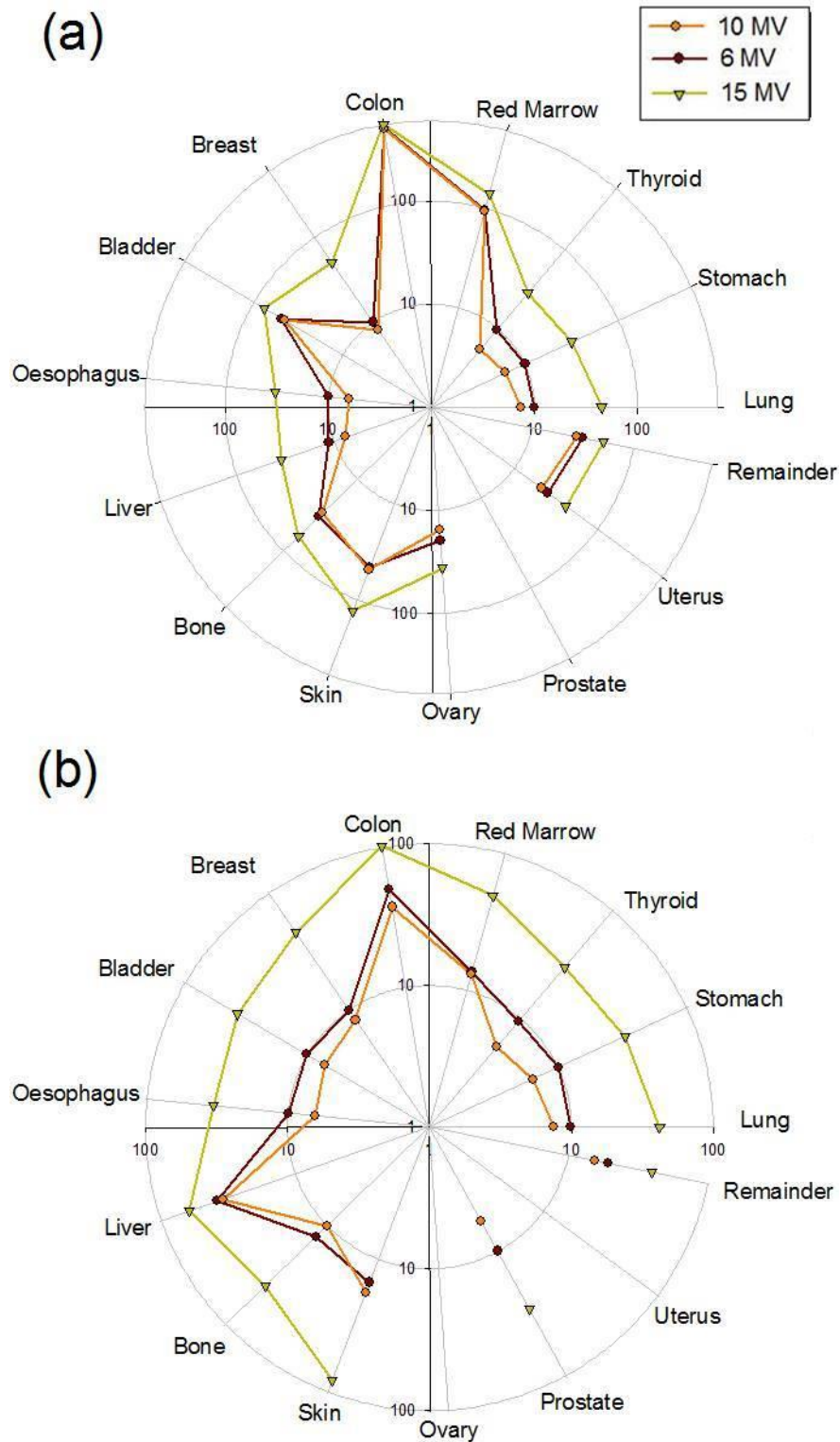


Figure 3. Comparison of PD for 14 representative out-of-field organs in SBRT modality for (a) paravertebral and (b) adrenal cases in 6, 10 and 15 MV in SBRT modality for Varian linac. Polar axis is displayed in logarithmic scale, representing doses ranging between 5 mSv-600 mSv and 2.5 mSv- 1.4×10^3 mSv respectively.

As a general behavior, 10 MV has shown as the best option in terms of PD, followed by 6 and 15 MV respectively. However, the impact on PD of photon leakage (which is different for each vendor) could invert this result in some cases, as larger leakage can compensate the usually lower number of MU of the 15 MV plans. Figure 4 depicts PDs for the SBRT prostate for the Siemens linac. In this case, leakage parameters are similar for 6 and 15 MV for this machine; which is not the case for the Varian one (that seems to be highly optimized to reduce leakage for low energy modalities).

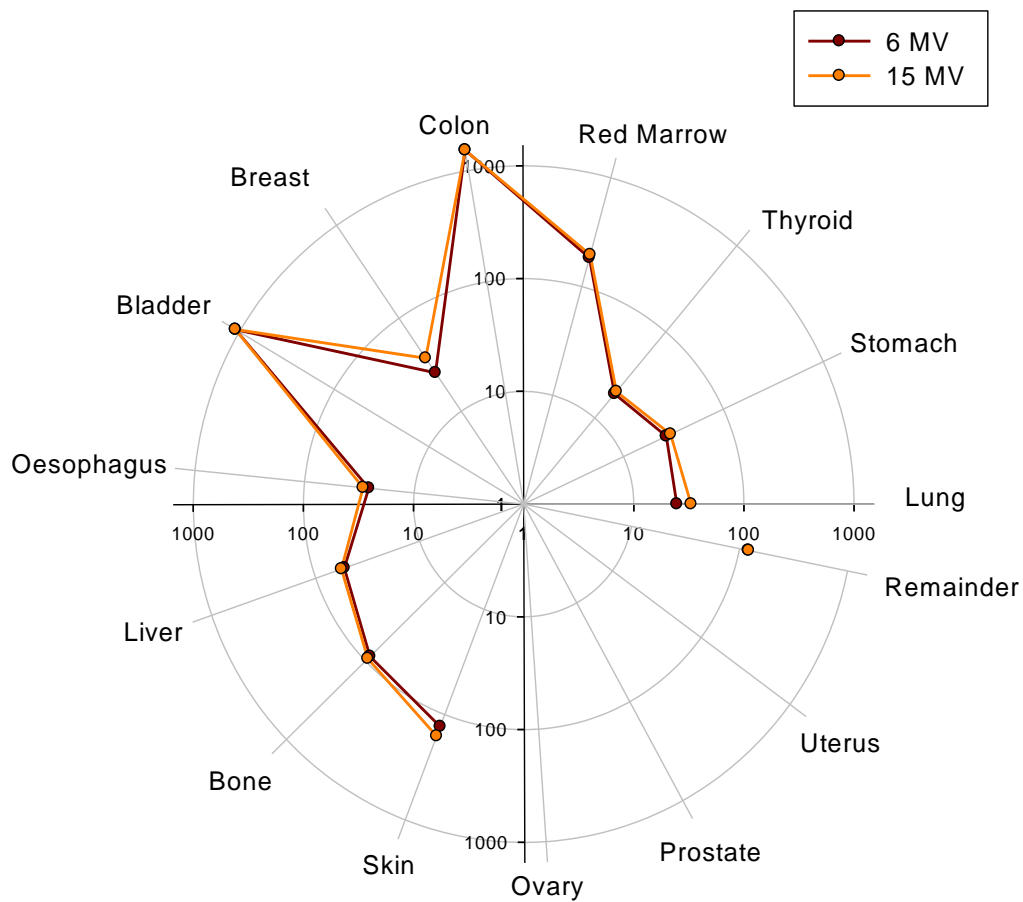


Figure 4. PDs for 11 representative out-of-field organs in all the available energies of the Siemens linac (6 and 15 MV) for the prostate SBRT plans. Polar axis is displayed in logarithmic scale, representing doses ranging between 19 mSv- 1.5×10^3 mSv.

As we have previously explained, FFF mode seems to be a better option than conventional (FF) one. Then we decided to compare PD of these two modalities in the two energies available (6 and 10 MV). As an example, [Figure 5](#) shows PD for the three-lesion hepatic case (6 MV) and PD for the adrenal (10 MV) case in Varian linac. The same data have been used to compare 6 and 10 MV in FF and FFF modalities ([Figure 6](#)).

Finally, we aimed to evaluate the performance of the combined energy modalities (6&15 MV) in terms of PD. Values were compared to those obtained when using 10 MV in both FF and FFF modalities. This comparison is shown in [Figure 7](#) for the single-lesion hepatic case in SBRT modality in Varian TrueBeam linac.

Obtained results suggest the good compromise obtained when using 10 MV and FFF mode combination with respect to other modalities. When this modality is not available/usable, 10 MV has shown as the best option in terms of PD reduction, followed by 6 MV in FFF mode and 6 MV.

In order to highlight the importance of this modern hypofractionation technique, we wanted to compare performance of one of the treatments when no SBRT is available and conventional fractionation has to be used. For that, we chose the brain case, where if this modality is not viable, usually a whole brain irradiation is performed ([Figure 8a](#)). This image shows size and location of the 8 lesions (green one is repeated) in the whole brain contour. Obtained PD results are shown in [Figure 8b](#) for both cases. As expected, lower PD are observed when irradiating lesions separately in SBRT modality than when the whole brain is treated in conformal modality. Being the first one reduced when FFF irradiation mode is used.

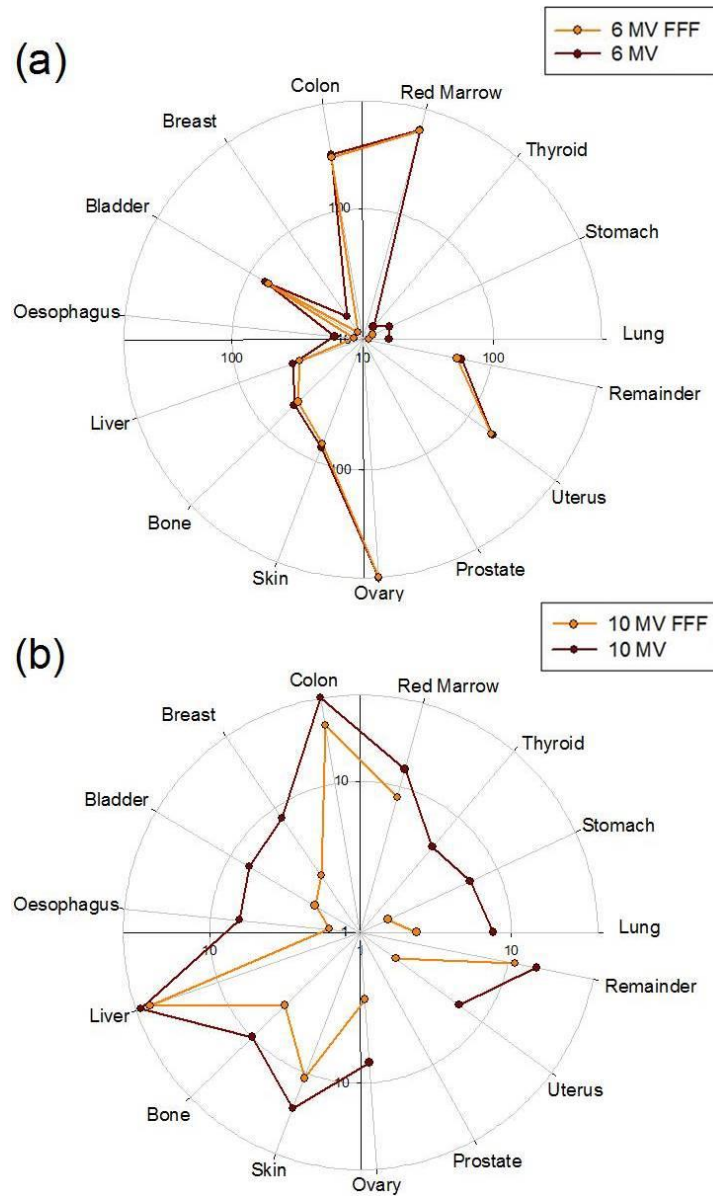


Figure 5. Comparison of (a) PPD for the three-lesion hepatic case and (b) PD for the adrenal one 14 representative out-of-field organs in all the available energies (6 and 10 MV, with and without FF) for the (a) three-lesion hepatic and (b) adrenal casse in SBRT modality in the Varian linac. Polar axis is displayed in logarithmic scale, representing doses ranging between 9 mSv- 1.7×10^3 mSv and 9 mSv-40 mSv.

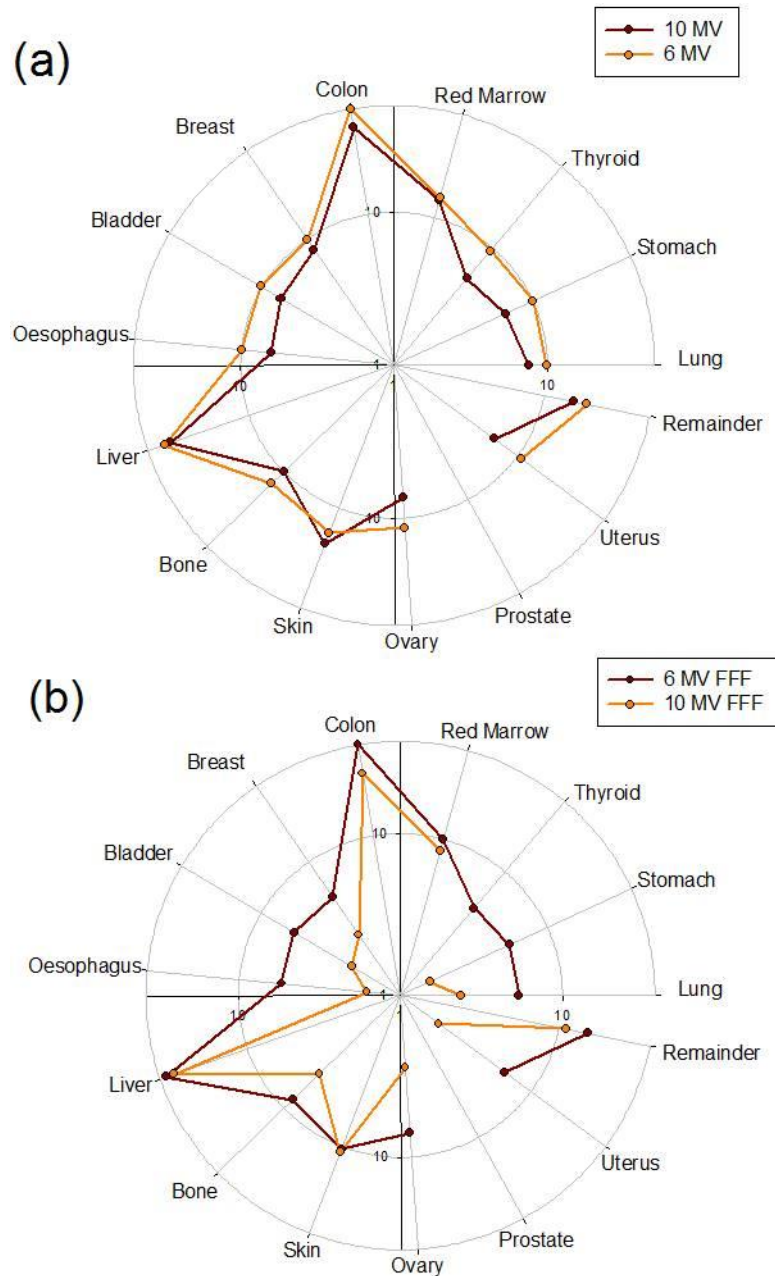


Figure 6. Comparison of PD when using: (a) 6 and 10 MV and (b) 6 FFF vs 10 FFF modalities for the adrenal case. Polar axis is displayed in logarithmic scale, representing doses ranging between 9 mSv-40 mSv and 5 mSv-50 mSv, respectively.

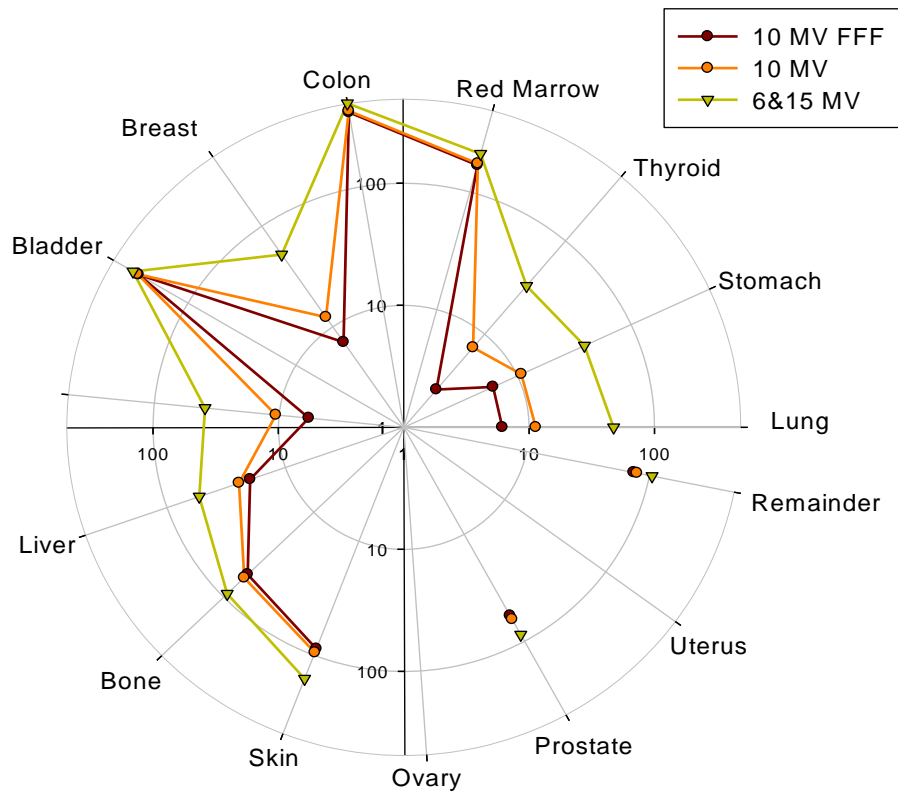


Figure 7. PD obtained for 10 MV in FF and FFF modalities compared to the use of combined low and high energies (6&15) in the single-lesion hepatic case in the Varian TrueBeam linac. Polar axis is displayed in logarithmic scale, representing doses ranging between 2.5 mSv - $1.4 \times 10^3 \text{ mSv}$.

In addition, we evaluated the treatment plans for which single tumors are treated either as combined or as separated lesions, in SBRT modality. PDs found were smaller in the first case due to an almost 3-fold increase in the number of MU when treating isolated lesions. Thus, the advantage of treating some pathologies in SBRT that wouldn't be viable with conventional ones (or would be considered as palliative) comes together with the reduction in PD. This is of special relevance in brain, breast and paravertebral cases here studied.

As a final comparison, we wanted to study differences in terms of PD between the three main linac manufacturers studied. For that, PDs were calculated for the same treatment plans (one in high energy and other in low) in the three available linacs, to separate photon and neutron components.. As an

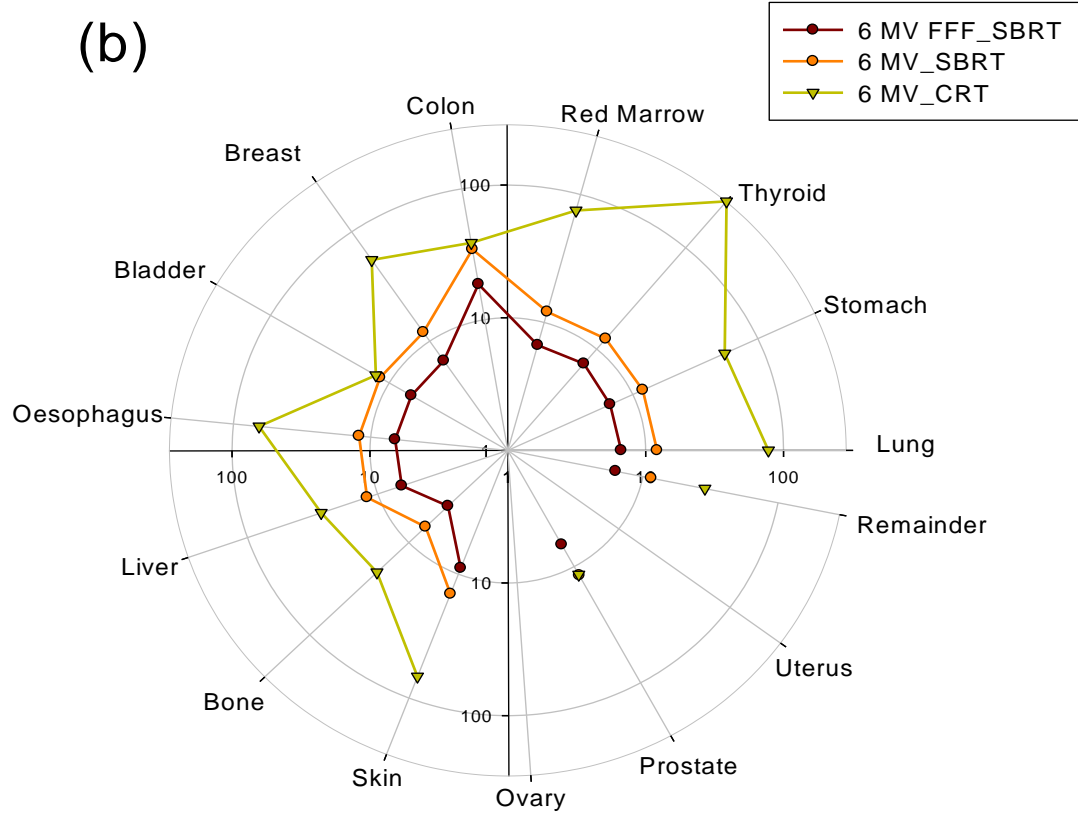
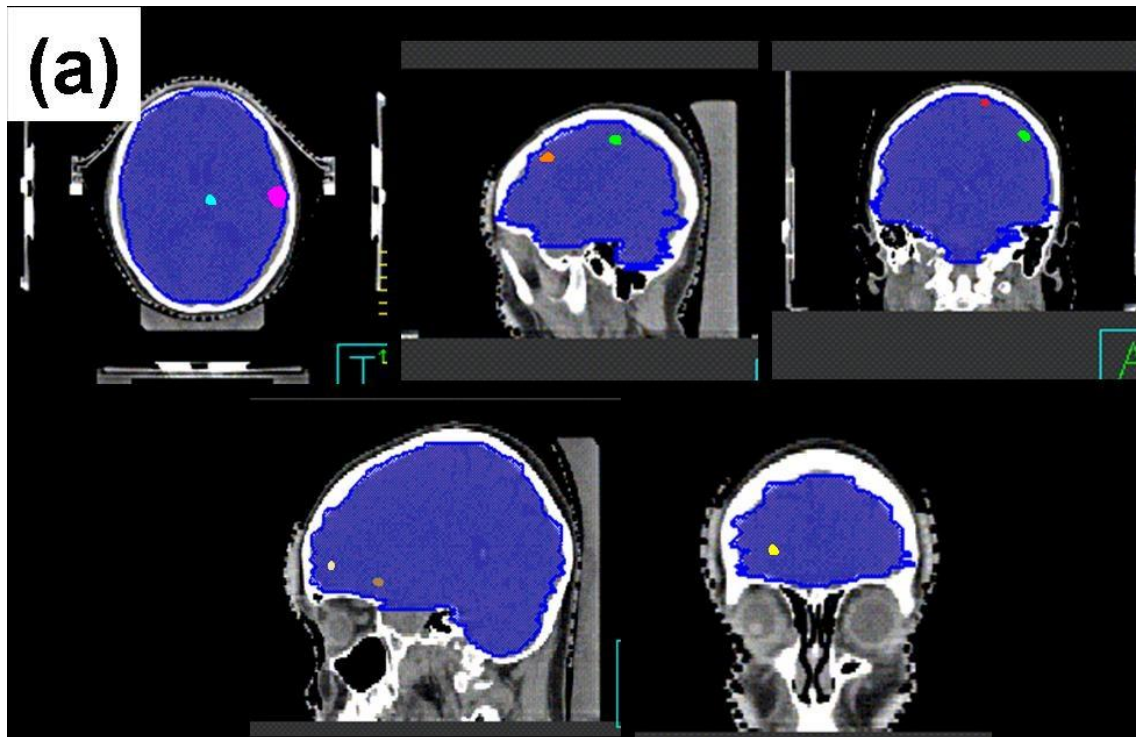


Figure 8. (a) Brain case (6 MV) contours when lesions are treated separately (ITV) and a whole brain irradiation (PTV) has to be performed and (b) corresponding PPD. Polar axis is displayed in logarithmic scale, representing doses ranging between 4 mSv-34 mSv.

example, [Figure 9](#) shows peripheral doses for two-lesion lung (6 MV) and prostate (15 MV) cases in terms of PPD, PD and PND respectively.

In agreement with previous clinical studies ([Irazola et al.,2016a](#); [Murray et al.,2015](#); [Kragl et al., 2011](#); [Huang et al.,2015](#)) lower PD for SBRT treatments, with respect to conventional fractionations, were observed. Modern techniques such as IMRT and VMAT showed slightly higher PD when compared with 3D-CRT and similar values between them. In addition, lower values were obtained for any of the studied techniques when FFF mode is used, with higher relevance in organs located at further distances.

Higher values are obtained for PD in 6 MV and 15 MV (photon+neutron contributions), while a compromise can be found when using 10 MV. These values decrease when using FFF mode, which is enhanced in the case of 10 MV FFF. Concerning linac manufacturer, lower peripheral photon dose values were obtained for the Varian linac for the low energy case, while Elekta machine is associated to lower photon and neutron doses in high energy.

As a final comparison, it was decided to test the goodness of the combined use of SBRT modality, 10 MV energy and FFF operation mode in comparison with other alternative clinically viable plan, such as 15 MV in VMAT modality for the prostate case. Obtained results in terms of PD are shown in [Figure 10](#).

As expected, the first modality has shown to highly reduce PD with respect to those obtained with the VMAT modality.

Our results seem to be in agreement with those obtained with other models as [Schneider et al.,2010](#), where second cancer risk seem to decrease when increasing the dose per fraction.

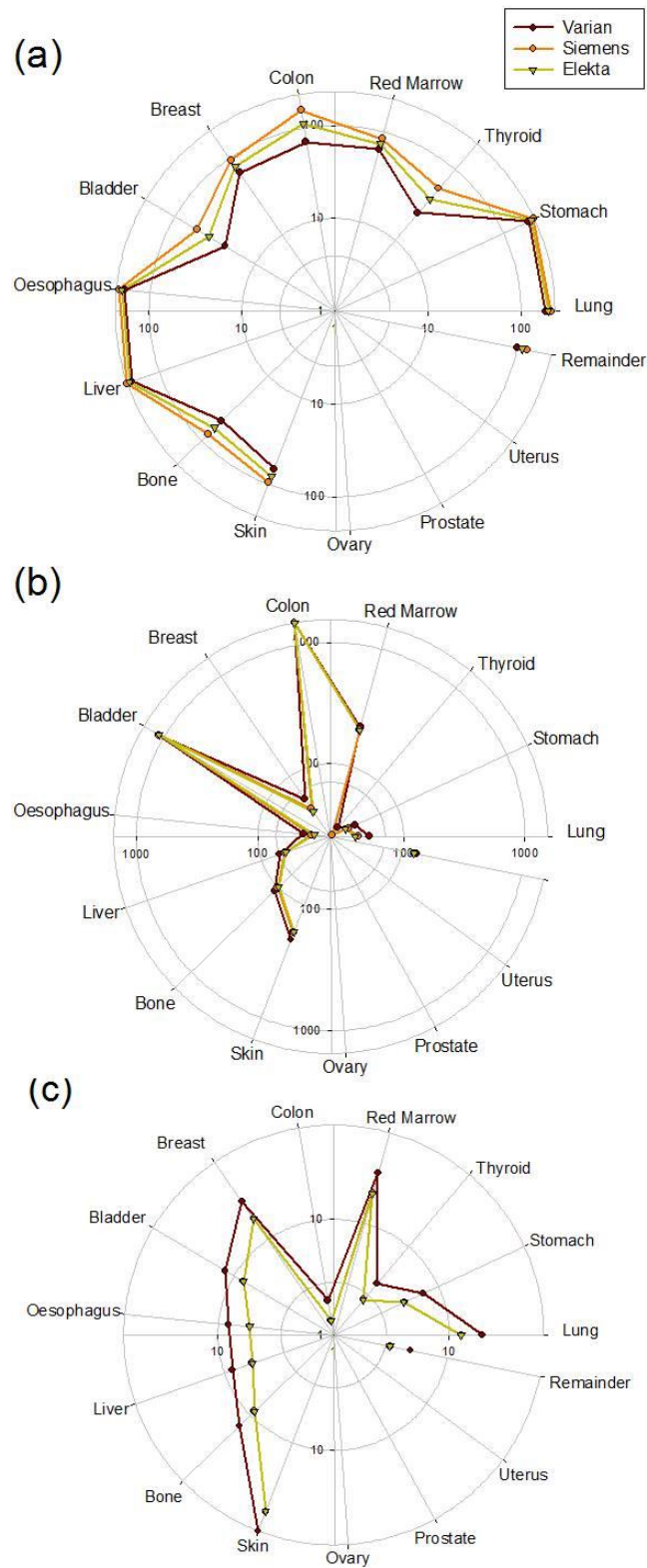


Figure 9. Comparison of the three available linacs in terms of: (a) PPD for the two-lesion lung case (6MV) and (b) PPD and (c) PND for the prostate one (15 MV). Polar axis is displayed in logarithmic scale, representing doses ranging between 23 mSv-233 mSv, 22 mSv- 1.54×10^3 mSv, 25 mSv- 1.5×10^3 mSv and 1.3 mSv-65 mSv, respectively. Curves overlapping do not permit see all the options in some graphs.

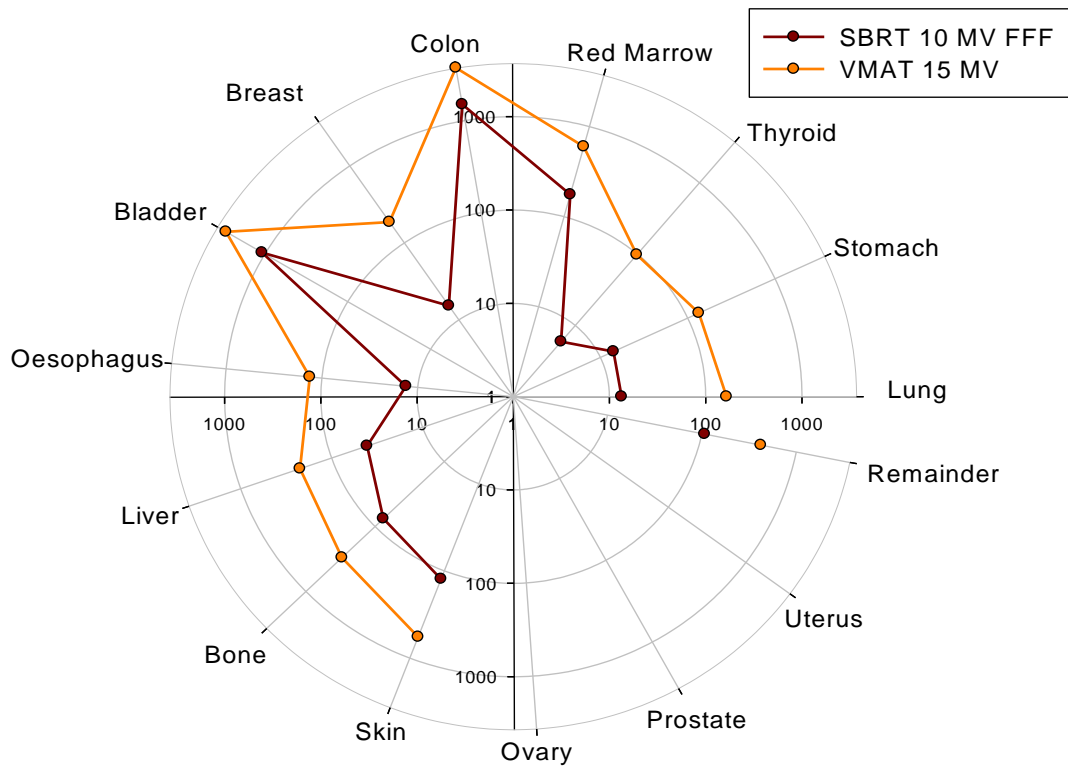


Figure 10. Comparison of PD obtained for SBRT 10 MV FFF modality and VMAT in 15 MV for the prostate case. Polar axis is displayed in logarithmic scale, representing doses ranging between 2.5 mSv–1.5x10³ mSv and 97 mSv–3.7x10³ mSv. respectively.

Although calculations of SCR have been carried out for the PDs beyond 10 cm from the field-edge, it has been estimated that around 50% of SMNs are found in this location (Diallo et al.,2009). Nevertheless, as our goal is the comparison among techniques, and no calculation of absolute values, we consider that the results of our analysis are valid.

SCP, TCP and NTCP parameters were calculated for all the prostate treatment plans (including the 4 techniques, FF and FFF and irradiation mode and energies) as an example. An average decrease in SCR of 1.5% was found for SBRT modality, especially relevant in the 10 MV FFF modality (1.8%). SCR

values vary from 0.02 cases per 1000 (thyroid in 10 MV FFF SBRT) to 39 cases per 1000 (bone in 15 MV IMRT).

Additionally, an average value of 99.7% has been obtained for TCP parameter. This value agrees with previous studies which have demonstrated the applicability of the classical LQ formula for local tumor control in fractionated SBRT for lung cancer (Guckenberger et al.,2016). Regarding normal tissue toxicity, NTCP values to OAR obtained for SBRT modality were lower than recent studies (Guckenberger et al.,2016). Particularly, for the case of 10 MV in FFF mode a decrease of 60% from the average value of all the other studied cases have been observed (Yan et al.,2015).

4. Conclusions

Ten different pathologies treated with SBRT have been calculated in all the available energies (6, 6 FFF, 10, 10 FFF and 15 MV), modalities (3D-CRT, IMRT, VMAT and SBRT) and linac manufacturers (Siemens, Varian and Elekta). A total number of 144 different treatment plans have been obtained and analysed for the first time in terms of peripheral neutron and photon doses. Two analytic models from directly available input parameters (MU, leakage, patient height, isocenter location and facility characterization in terms of neutron production) have been used for this purpose. We can conclude that lower peripheral doses are achieved for SBRT, being more evident when ITV is much lower compared to PTV. Thus, although peripheral doses may vary regarding technique used for SBRT fractionation (due to the different number of MU used for each modality), lower values are always expected. When comparing conventional fractionations, higher values are found for VMAT and IMRT techniques with respect to conformal one, as expected. In addition, a reduction in these doses has been found when using 10 MV energy, especially in FFF irradiation mode. Neutron doses have shown to contribute in small percentage to global values

(especially if combined energies are used). The low PD values obtained (< 4 Gy) makes possible to argue that linear no-threshold models for second cancer induction are valid and that they do not depend on the fractionation scheme used. The latter would ease the implementation of the model in TPS. This could be used, as an additional objective parameter for the choice of best treatment strategy. These results together with the obtained values for radiobiological TCP and NTCP parameters, suggest that hypofractionated modality in 10 MV using FFF mode, could represent the best compromise between dose delivery efficiency and peripheral doses reduction.

5. References

- Benadjaoud MA, Bezin J, Veres A, Lefkopoulos D, Chavaudra J, Bridier A, de Vathaire F and Diallo I. *A multi-plane source model for out-field head scatter dose calculations in external beam photon therapy*. *Phys Med Biol* 2012;5777:25–39.
- Benedict SH, Yenice KM, Followill D, Galvin JM, Hinson W, Kavanagh B, Keall P, Lovelock M, Meeks S, Papiez L, Purdie T, Sadagopan R, Schell MC, Salter B, Schlesinger DJ, Shiu AS, Solberg T, Song DY, Stieber V, Timmerman R, Tomé WA, Verellen D, Wang L and Yin FF. *Stereotactic body radiation therapy. The report of AAPM Task Group 101*. *Med Phys* 2010;37:4078.
- Cardenas C, Nitsch P, Kudchadker R, Howell R and Kry S. *An Evaluation of Out-Of-Field Doses for Electron Beams From Modern Varian and Elekta Linear Accelerators*. *Med Phys* 2015;42:3637.
- Cashmore J. *The characterization of unflattened photon beams from a 6 MV linear accelerator*. *Phys Med Biol* 2008;53(7):1933-46.
- Cashmore J, Ramtohul M, Ford D. *Lowering whole-body radiation doses in pediatric intensity-modulated radiotherapy through the use of unflattened photon beams*. *Int J Radiat Oncol Biol Phys* 2011;80(4):1220-27.
- Chargari C, Goodman KA, Diallo I, Guy JB, Rancoule C, Cosset JM, Deutsch E and Magne N. *Risk of second cancers in the era of modern radiation therapy: does the risk/benefit analysis overcome theoretical model?* *Cancer Metastasis Rev* 2016.
- Demaria S, Formenti S. *Radiation as an immunological adjuvant: current evidence on dose and fractionation*. *Front Oncol* 2012;2:153.
- Diallo I, Haddy N, Adjadj E, Samand A, Quiniou E, Chavaudra J, Alizar I, Perret N, Guérin S, Lefkopoulos D and Vathaire F. *Frequency distribution of second solid locatios in relation to the irradiated volume among 115 patients treated for childhood cancer*. *Int J Raiat Oncol Biol Phys* 2009;74(3):873-83.
- Expósito MR, Sánchez-Nieto B, Terrón JA, Domingo C, Gómez F and Sánchez-Doblado F. *Neutron contamination in radiotherapy: Estimation of second cancers based on measurement in 1377 patients*. *Radiother and Oncol* 2013;107:234-241.

- Fu W, Dai j, Hu Y, Han D, Song Y. *Delivery time comparison for intensity-modulated radiation therapy with/without flattening filter: a planning study*. *Phys Med Biol* 2004;48(8):1535-47.
- Guckenberger M, Klement R, Allgäuer M, Andratschke N, Blanck O, Boda-Heggeman J, Dieckmann K, Uma M, Ernst I, Ganswindt U, Hass P, et al. *Local tumor control probability modeling of primary and secondary lung tumors in stereotactic body radiotherapy*. *Radiother Oncol* 2016;118:485-491.
- Howell RM, Scarborough SB, Taddei PJ, Krishnan S, Kry SF, Newhauser WD. *Methodology for determining doses to in-field, out-of-field and partially in-field organs for late effects studies in photon radiotherapy*. *Phys Med Biol* 2010;55(23):7009–7023.
- Huang BT, Lu JY, Lin PX, Chen JZ, Kuang Y and Chen CZ. *Comparison of two RapidArc strategies in Stereotactic Body Radiotherapy of peripheal lung cancer with Flattening Filter Free beams*. *Plos One* 2015;10(7):1-13.
- ICRP International Commission on Radiological Protection. *The 2007 Recommendations of the International Commission on Radiological Protection*. ICRP Publication 103, 2007.
- Irazola L, Lorenzoli M, Bedogni R, Pola A, Terron JA, Sanchez-Nieto B, Exposito MR, Lagares JL, Sansaloni F and Sanchez-Doblado F. *A new online detector for estimation of peripheral neutron equivalent dose in organ*. *Med Phys* 2014a;41:112105.
- Irazola L, Lorenzoli M, Terrón JA, Bedogni R, Pola A, Sánchez-Nieto B, Romero-Expósito M and Sánchez-Doblado F. *Neutron model upgrade for radiotherapy patients monitoring using a new online detector*. *Med Phys* 2014b;41:280.
- Irazola L, Irazola L, Brualla L, Rosello J, Terron JA, Sanchez-Nieto B, Bedogni R and Sanchez-Doblado F. *Commissioning the neutron production of a Varian TrueBeam linac*. *Med Phys* 2015;42(6):3376.
- Irazola L, Ortiz-Seidel M, Velázquez S, García-Hernández MT, Terrón JA, Sánchez-Nieto B, Romero-Expósito M, Roselló J and Sánchez-Doblado F. *Comparison of peripheral doses associated to SBRT, VMAT, IMRT, FFF and 3D-CRT plans for lung cancer*. EP-1613 ESTRO 35th(2016a)
- Irazola L, Terrón JA, Sánchez-Nieto b, Romero-Expósito M and Sánchez-Doblado F. *Peripheral neutron dose model verification for real IMRT cases*. Poster at the 1st ECMP Congress (2016b).
- Irazola L, Terrón JA, Sánchez-Nieto B, Bedongi R and Sánchez-Doblado F. *Peripheral neutron dose model upgrade and evaluation in 510 radiotherapy patients*. Sent to *Phys Med Biol*. (2016c)
- Joosten A, Bochud F, Baechler S, Levi f, Mirimanof RO and Moeckli R. *Variability of a peripheral dose among various LINAC geometries for second cancer risk assessment*. *Phys Med Biol* 2011;56:5131–5151.
- Kirkpatrick JP, Kelsey CR, Palta M, et al. *Stereotactic body radiotherapy: a critical review for non radiation oncologists*. *Cancer* 2014;120(7):642-54.
- Kragl G, Baier f, Lutz S, Albrich D, Dalaryd M, Kroupa B, Wiezorek T, Knöös T and Georg D. *Flattening filter free beams in SBRT and IMRT: Dosimetric assessment of peripheral doses*. *Z Med Phys* 2011;21:91-101.
- Kry SF, Salehpour M, Followill DS, Stoavall M, Kuban DA, White RA and Rosen II. *The calculated risk of fatal secondary malignancies from intensity-modulated radiation therapy*. *Int J Radiation Oncology Biol Phys* 2005a;62(4):1195-1203.

- Kry SF, Salehpour M, Followill DS, Stovall M, Kuban DA, White RA and Rosen I. *Out-of-field photon and neutron dose equivalents from step-and-shoot intensity-modulated radiation therapy*. Int J Radiat Oncol Biol Phys 2005b;62(4):1204-16.
- Kry SF, Titt U, pönisch F et al. *Reduced neutron production through use of a flattening-filter-free accelerator*. Int J Radiat Oncol Biol Phys 2007;68(4):1260-64.
- Martin A and Gaya A. *Stereotactic Body Radiotherapy: A review*. J Clin Oncol 2010;22:157-172.
- Murray LJ, Thompson CM, Lilley J, Cosgrove V, Franks K, Sebag-Montefiore D and Henry AM. *Radiation-induced second primary cancer risks from modern external beam radiotherapy for early prostate cancer: impact of stereotactic ablative radiotherapy (SABR), volumetric modulated arc therapy (VMAT) and flattening filter free (FFF) radiotherapy*. Phys Med Biol 2015;60:1237-1257.
- Ong CL, Verbakel WF, Cuijpers JP, Slotman BJ, Lagerwaard FJ and Senan S. *Stereotactic radiotherapy for peripheral lung tumors: a comparison of volumetric modulated arc therapy with 3 other delivery techniques*. Radiother Oncol 2010;97:437-442.
- Prendergast BM, Fiveash JB, Pople RA, Clark GM, Thomas EM, Minnich DJ, Jacob R, Spencer SA, Bonner JA and Dobelbower MC. *Flattening filter-free linac improves treatment delivery efficiency in stereotactic body radiation therapy*. J Appl Clin Med Phys 2013;14(3):64-71.
- QUANTEC. *Quantitative Analyses of Normal Tissue Effects in the Clinic*. Radiother Oncol 2010;76(3):S1-S160. Radiation Therapy Oncology Group.
- Romero-Expósito M, Sánchez-Nieto B, Terrón JA, Lopez MC, Ferreira BC, Grishchuk D, Sandíns C, Moral-Sánchez S, Bragado-Álvarez L, Melchor M, Domingo C, Gómez F and Sánchez-Doblado F. *Commissioning the neutron production of a linac: development of a clinical planning tool for second cancer risk estimation*. Med Phys 2015;42:276-281.
- Rubio C, Morera R, Hernando O, Leroy T and Lartigau E. *Extracranial stereotactic body radiotherapy. Review of main SBRT features and indications in primary tumors*. Rep Pract Oncol Radiother 2013;18(6):387-396.
- Sánchez-Doblado F, Domingo C, Gómez F, Sánchez-Nieto B, Muñoz JL, García-Fusté MJ, Expósito MR, Barquero R, Hartmann G, Terrón et al. *Estimation of neutron equivalent dose in organs of patients undergoing radiotherapy by the use of a novel online digital detector*. Phys Med Biol 2012;57:6167-6191.
- Sánchez-Nieto, El far R, Romero-Expósito M, Lagares J, Mateo JC, Terrón JA, Irazola L and Sánchez-Doblado F. *Analytical model for Photon Peripheral Dose in Radiotherapy Treatments*. Med Phys 2014;41:231.
- Sánchez-Nieto B, El-far R, Irazola L, Expósito MR, Lagares JI, Mateo JC, Terrón JA and Sánchez-Doblado F. *Analytical model for photon peripheral dose estimation in radiotherapy treatments*. Biomed Phys Eng Express 2015a;1:045205.
- Sánchez-Nieto B, El-far R, Castrillón M, Irazola L, Terrón JA and Sánchez-Doblado F. *Validation of a photon peripheral dose model for IMRT treatments*. Radiother and Oncol 2015b;115(1):S541 (PO-1008).
- Sánchez-Nieto B, Irazola L, Romero-Expósito M, Terrón JA and Sánchez-Doblado F. *Validation of a peripheral photon dose model for clinical use: a prostate IMRT irradiation of the Alderson phantom*. Accepted at 35th ESTRO Congress 2016a; PO-808.
- Sánchez-Nieto B, Romero-Expósito M, Terrón J A, Irazola L, Paiusco M, Cagni E, Ghetti C, Filice S, Gómez F, Domingo C and Sánchez-Doblado F. *Risk assessment of*

- second cancer incidence after intensity-modulated radiation therapy and volumetric modulated arc therapy versus conventional techniques at high energy. Sent to J Appl Clin Med Phys (2016b)*
- Schneider U, Zwahlen D, Ross D, Kaser-Hotz B. *Estimation of radiation-induced cancer from three-dimensional dose distributions: concept of organ equivalent dose. Int J Radiat Oncol Biol Phys* 2005;61(5):1510-1515.
- Schneider U, Besserer J and Mack A. *Hypofractionated radiotherapy has the potential for second cancer reduction. Theor Biol Med* 2010;7:4.
- Stathakis S, Esquivel C, Gutierrez A, Buckey CR, Papanikolaou n. *Treatment planning and delivery of IMRT using 6 and 18 MV photon beams without flattening filter. Appl Radiat Isot* 2009;67:1629-1637.
- Scorsetti M. *Stereotactic Body Radiation Therapy: A useful weapon in anticancer treatment. Rep Prac Oncol Radiother Editorial* 2015;20(6).
- Timmerman RD, Kavanagh BD, Cho LC, Papiez L and Xing L. *Stereotactic body radiation therapy in multiple organ sites. J Clin Oncol* 2007;25(8):947-52.
- Xu X-G, Bednarz B, Paganetti H. *A review of dosimetry studies on external-beam radiation treatment with respect to second cancer induction. Phys Med Biol* 2008;53:R193-R241.
- Xie L, Fried D and Marks LB. *SBRT for lung cancer appears to provide superior local control to wedge resection: is this due to the therapeutic effects of low dose peripheral radiation? Int J Radiation Oncology Biol Phys* 2014;90(1):S655.
- Yan Y, Yadav P, Bsetti M, Du K, Saenz D, Harari P and Paliwal BR. *Dosimetric and Biologic Differences in Flattene and Flattening-Filter-Free Beam Treatment Plans. Submitted to Med Phys* 2015.

IV. Conclusions

The outcomes of this work lead to the following conclusions:

1. The use of the new miniaturized active online *Thermal Neutron Rate Detector*, has demonstrated to be a good alternative to both, active (*SRAMnd*) and passive (TLD, CR-39) devices, needed for the established methodology for peripheral neutron organ (and second cancer risk) estimation in high-energy radiotherapy. Consequently, this device is usable for the direct estimation of peripheral neutron doses by terms of thermal neutron fluence measurements in both 'ex-phantom' and 'in-phantom' locations.

2. An almost pure, photon-free, thermal neutron field for detector stability testing purposes has been established and characterized at the 3 MV Tandem Pelletron accelerator of CNA (Sevilla). The characterized thermal neutron beam is obtained by terms of an incident proton beam impinging into a lithium target leading to thermal neutron fluence rates up to $2 \times 10^3 \text{ cm}^{-2} \cdot \text{s}^{-1}$ with a $\pm 4\%$ reproducibility.

3. Two different methodologies to improve neutron-to-photon discrimination of *TNRD* devices under 'critical' conditions in radiotherapy environments (applicable to any thermal neutron detector) have been established. Both of them aim to estimate undesired photon contribution to detector readings in order to later correct the measurements. These approaches are based on the repetition of the high energy measurements under the same conditions:

- (a) the first one is based on the use of a borated rubber material to eliminate neutron contribution and isolate photon one.

- (b) the other one aims to represent a simpler and more universal alternative, consisting of the consideration of usual low energy (6 MV) *TNRD* reading as equal to undesired photon component in *TNRD* high energy measurements.

4. The usability of *TNRD* devices for both measurements needed in the studied methodology, based on the correlation of reference 'ex-phantom' measurements (detector located in the reference position) to equivalent organ doses (estimated from detector readings inside an anthropomorphic phantom), has allowed the improvement and generalization of the existing models. Several aspects have been enhanced:

- (a) simplification of the facility characterization to be expressed in terms of thermal neutron fluences, generalizing the methodology to any thermal neutron detector.
- (b) improvement of neutron dose estimations, allowing the enhancement of the existing Head & Neck and abdomen models.
- (c) introduction of patient size as an additional parameter to provide more specific neutron dose evaluations, especially relevant in children patients.

Results have also been validated in 510 real high-energy radiotherapy patients.

5. Neutron and photon peripheral doses have been evaluated using the two analytic models developed by our group through the duration of this work. Ten real kinds of treatments have been compared using conventional (3D-CRT) and modern (IMRT, VMAT, SBRT and FFF) techniques using low (6 MV) and high (15 MV) energies in three different linacs (Siemens, Varian and Elekta). As a general pattern, SBRT fractionation, 10 MV and FFF modality have shown as the most optimal ones in terms peripheral dose reduction. Thus, a combined

IV. Conclusions

use of these options would decrease second cancer probability. Obtained results from the comparison of these peripheral doses open the door to the introduction of an additional objective parameter in commercial TPS for the choice of the most adequate treatment plan regarding each patient.

IV. *Conclusions*

V. References*

- Atun R, Jaffray DA, Barton MB, Bray F, Bauman M, Vikram B, Hann TP, Knaul FM, Lievens Y, Lui TYM, Milosevic M, O'Sullivan B, Rodin DL, Rosenblatt E, Van Dyk J, Yap ML, Zubizarrea E and Gospodarowicz M. *Expanding global access to radiotherapy*. The Lancet Oncology 2016;16(101):1153-1186.
- Antoni D and Noel G. *Which constraints for which organs at risk in radiotherapy for adult patients?* Cancer Radiother 2015;19(6-7):479-483.
- Bedogni R, Bortot D, Pola A, Introini MV, Gentile A, Esposito A, Gómez-Ros JM, Palomba M, Grossi A. *A new active thermal neutron detector*. Radiat Prot Dosim 2014;161(1-4):241-244.
- Bedogni R, Sacco D, Gómez-Ros JM, Lorenzoli M, Gentile A, Buonomo B, Pola A, Introini MV, Bortot D and Domingo C. *ETHERNES: A new design of radionuclide source-based thermal neutron facility with large homogeneity area*. Appl Radiat and Iso 2016;107:171-176.
- Bentzen SM, Constine LS, Deasy JO, Eisbruch A, Jackson A, Marks LB, Ten Haken RK and Yorke ED. *Quantitative Analyses of Normal Tissue Effects in the Clinic (QUANTEC): An introduction to the scientific issues*. Int J Radiat Oncol Biol Phys 2010;S3-S9.
- Berdnarz B, Athar B and Xu G. *A comparative study on the risk of second primary cancers in out-of-field organs associated with radiotherapy of localized prostate carcinoma using Monte Carlo-based accelerator and patient models*. Med Phys 2010;27(5):1987-1994.
- Berrington de Gonzalez A, Curtis RE, Kry SF, Gilbert E, Lamart S, Berg CD, Stovall M and Ron E. *Proportion of second cancers attributable to radiotherapy treatments in adults: a cohort study in the US SEER cancer registries*. Lancet Oncol 2011;12(4):353-60.
- Biological Effects of Ionizing Radiation. *Health Risks from Exposure to Low Levels of Ionizing Radiation*. BEIR VII, Phase 2 (National Research Council, National Academy of Science, Washington, DC) 2006.
- Bordy JM, Bessieres I, D'Agostino E, Domingo C, D'Errico F, di Fulvio A, Knezevic Z, Miljanic S, Olkko P, Ostrowsky A, Poumarede B, Sorel S, Stolarczyk and Vermesse D. *Radiotherapy out-of-field dosimetry: Experimental and computational results for photons in a water tank*. Radiat Meas 2013;57:29-34.
- Brenner DJ, Curtis RE, Hall EJ and Ron E. *Second malignancies in prostate carcinoma patients after radiotherapy compared with surgery*. Cancer 2000;88:398-406.

*These references correspond to those cited on the Preface. Further specific ones can be found at the end of each Full Paper or Short Publication.

- Brenner DJ, Doll R, Goodhead DT, Hall EJ, Land CH, Little JB, Lubin JH, Preston DL, Preston RJ, Puskin JS, Ron E, Sachs RK, Samet JM, Setlow RB and Zaider M. *Cancer risks attributable to low doses of ionizing radiation: assessing what we really know*. Proc Natl Acad Sci USA 2003;71:13761-6.
- Brenner DJ. *Induced second cancer after prostate-cancer radiotherapy: No cause for concern?* Int J Radiat Oncol Biol Phys 2006;65:637-639.
- Cahan WG, Woodward HQ, Higonbotham NL, Stewart FW and Coley BL. *Sarcoma arising in irradiated bone; report of 11 cases*. Cancer 1948;1(1):3-29.
- Chao C, Xu L, Bell E, Cooper R and Mueller L. *Long-term Health Outcomes in Survivors of Childhood Cancer Diagnosed Between 1990 and 2000 in a Large US Integrated Health Care System*. J Pediatr Hematol Oncol 2016;38(2):123-30.
- Chargari C and Cosset JM. *The issue of low doses in radiation therapy and impact on radiation-induced secondary malignancies*. Bull Cancer 2013;100(12):1333-42.
- Chofor N, Harder D, Willborn KC and Poppe B. *Internal scatter, the unavoidable major component of the peripheral dose in photon-beam radiotherapy*. Phys Med Biol 2012;57(6):1733.
- Clarke M, Collins R, Darby S, Davies C, Elphinstone P, Evans V, Godwin J, Gray R, Hicks C, James S, MacKinnon E, McGale P, McHugh T, Peto R, Taylor C and Wang y. *Effects of radiotherapy and differences in the extent of surgery for early breast cancer on local recurrence and 15-year survival: an overview of the randomized trials*. Lancet 2005;366(9503):2087-106.
- Claude L and Laprie A. *Which dose constraints on which critical organs in paediatric radiation therapy?* Cancer Radiother 2015;19(6-7):484-488.
- Coleman MP, Forman D, Bryant H, Butler J, Rachet B, Maringe C, Nur U, Tracey E, Coory M, Hatcher J, McGahan CE, Turner D, Marrett L, Gjerstorff ML, Johannesen TB, Adolfsson J, Lambe M, Lawrence G, Meechan D, Morris EJ, Middleton R, Steward J and Richards MA. *Cancer survival in Australia, Canada, Denmark, Norway, Sweden, and the UK, 1995-2007 (the International Cancer Benchmarking Partnership): An analysis of population-based cancer registry data*. The Lancet 2011;377:127-138.
- Cristy Phantom. Description of the mathematical phantoms. <https://crpk.ornl.gov/resources/Mird.pdf> [last acces 23th May 2016].
- D'Agostino E, Bogaerts R, Defraene G, de Freitas Nascimento L, Van den Heuvel F, Verellen D, Duchateau M, Schoonjans W and Vanhavere F. *Peripheral doses in radiotherapy: a comparison between IMRT, VMAT and Tomotherapy*. Rad Meas 2013;57:62-67.

- Delaney G, Jacob S, Featherstone C and Barton M. *The role of radiotherapy in cancer treatment. Estimating optimal utilization from a review of evidence-based clinical guidelines.* Cancer 2005;104(6):1129-37.
- Diallo I, Haddy N, Adjadj E, Samand A, Quiniou E, Chavaudra J, Alizar I, Perret N, Guérin S, Lefkopoulos D and de Vathaire F. *Frequency distribution of second solid locations in relation to the irradiated volume among 115 patients treated for childhood cancer.* Int J Radiat Oncol Biol Phys 2009;74(3):873-83.
- Domingo C, García-Fusté MJ, Morales E, Amgarou K, Terrón JA, Roselló JV, Brualla L, Núñez L, Colmentares R, Gómez F, Hartmann gh, Sánchez-Doblado F and Fernández F. *Neutron spectrometry and determination of neutron ambient doses in radiotherapy treatments under different exposure conditions.* In: WC 2009, IFMBE Proceedings; O Dössel and WC Schlegel WC, editors (Springer, Berlin) 2009;25/III:523-526.
- Domingo C, Gómez F, Sánchez-Doblado F, Hartmann GH, Amgarou K, García-Fusté MJ, Romero MT, Böttger R, Nolte R, Wissmann F, Zimbal A and Schuhmacher H. *Calibration of a neutron detector based on single event upset of SRAM memories.* Radiat Meas 2010a;45:1513-1517.
- Domingo C, García-Fusté MJ, Morales E, Amgarou K, Terrón JA, Roselló JV, Brualla L, Núñez L, Colmenares R, Gómez F, Hartmann GH, Sánchez-Doblado F and Ferández F. *Neutron spectrometry and determination of neutron ambient dose equivalents in different linac treatment rooms during radiotherapy.* Radiation Measurements, 2010b;45:1391-1397.
- Domingo C, Amgarou K, García-Fusté MJ, Barquero R, Expósito MR, Terrón JA, González-Soto XL, Gómez F and Sanchez-Doblado F. *Influence of the phantom composition on peripheral neutron organ equivalent dose evaluation.* Radiother Oncol 2011;99:S411.
- Dörr W, Herrmann T. *Second primary tumors after radiotherapy for malignancies. Treatment-related parameters.* Strahlenther Onkol 2002a;178:357-362.
- Dörr W and Herrmann T. *Cancer induction by radiotherapy: dose dependence and spatial relationship to irradiated volume.* J Radiol Prot 2002b;22(3A):a117-21.
- Eaton BR, MacDonald SM, Yock TI and Tarbell NJ. *Secondary Malignancy Risk Following Proton Radiation Therapy.* Front Oncol 2015;5:261.
- Expósito MR, Sánchez-Nieto B, Terrón JA, Domingo C, Gómez F and Sánchez-Doblado F. *Neutron contamination in radiotherapy: Estimation of second cancers based on measurement in 1377 patients.* Radiother and Oncol 2013;107:234-241.
- Ferlay J, Soerjomataram I, Dikshit R et al. *Cancer incidence and mortality worldwide: sources, methods and major patterns in GLOBOCAN 2012.* Int J Cancer 2015; 136:E359-E386.

- Followill D, Geis P and Boyer A. *Estimates of whole-body dose equivalent produced by beam intensity modulated conformal radiotherapy*. Int J Radiat Oncol Biol Phys 1997;38:667-672.
- Followill DS, Stovall MS and Kry SF. *Neutron source strength measurements for Varian, Siemens, Elekta, and General Electric linear accelerators*. J Appl Clin Med Phys 2003;4(3):189-194.
- Frankish H. *15 million new cancer cases per year by 2020, says WHO*. The Lancet 2003;361:1278.
- García Hernández MT, Ortiz M, Irazola L, Terrón JA, Romero-Expósito MR, Sánchez-Nieto B and Sánchez-Doblado F. *Neutron peripheral dose estimation: treatment planning system implementation*. Radiother and Oncol 2015;115(1):S442.
- Gómez F, Sánchez-Doblado F, Iglesias A and Domingo C. *Active on-line detector for in-room radiotherapy neutron measurements*. Radiat Meas 2010a;45:1532-1535.
- Gómez F, Iglesias A and Sánchez-Doblado F. *A new active method for the measurement of slow-neutron fluence in modern radiotherapy treatment rooms*. Phys Med Biol 2010b;55:1025-1039.
- González-Soto XL, Amgarou K, Lagares JI, Muñoz J, Ménde R, Expósito MR, Gómez F, Domingo C, and Sanchez-Doblado F. *High megavoltage radiotherapy neutron spectra simulation inside an anthropomorphic phantom*. Radiother Oncol 2011;99:S409.
- González-Soto X, Amgarou K, Lagares JI, Expósito MR, Gómez F, Domingo C, Sánchez-Nieto B and Sánchez-Doblado F. *Neutron distribution in radiotherapy treatment rooms*. In: WC 2012, IFMBE Proceedings; M Long, editors (Springer, Berlin) 2012a;39:1245-1248.
- González-Soto X, Expósito MR, Sánchez-Nieto B, Amgarou K, Lagares JI, Gómez F, Domingo C and Sánchez-Doblado F. *Neutron spectra inside an adult and children anthropomorphic phantoms in high energy radiotherapy*. In: WC 2012, IFMBE Proceedings; M Long, editors (Springer, Berlin) 2012b;39:1145-1148.
- Grantzau T and Overgaard. *Risk of second non-breast cancer after radiotherapy for breast cancer: a systematic review and meta-analysis of 762,468 patients*. Radiother Oncol 2015;114:56-65.
- Gudowska I, Ardenfors O, Toma-Dasu I, Dasu A. *Radiation burden from secondary doses to patients undergoing radiation therapy with photons and light ions and radiation doses from imaging modalities*. Radiat Prot Dosim 2014;161(1-4):357-362.
- Hall EJ, Martin SG, Amols H, and Hei TK. *Photoneutrons from medical linear accelerators - radiobiological measurements and risk estimates*. Int J Radiation Oncology Biol Phys 1995;33:225-230.

- Hall EJ. *Lessons we have learned from our children: cancer risks from diagnostic radiology.* *Pediatr Radiol* 2002;32:700-706.
- Hall EJ and Wu CS. *Radiation-induced second cancers: the impact of 3D-CRT and IMRT.* *Int J Radiation Oncology Biol Phys* 2003;56(1):83-88.
- Hall EJ. *The crooked shall be made straight: dose response relationships for carcinogenesis.* *Int J Radiat Biol* 2004;80(5):327-37.
- Hall EJ and Phil D. *Intensity-modulated radiation therapy, protons, and the risk of second cancers.* *Int J Radiation Oncology Biol Phys* 2006;65(1):1-7.
- Hall EJ. *Review of essential and topical radiobiology.* *Radiobiological Modelling in Radiation Oncology* 2007;Chapter2:12-34.
- Harrison RM. *Introduction to dosimetry and risk estimation of second cancer induction following radiotherapy.* *Radiat Meas* 2013;57:1e8.
- Hauri P, Hälgl RG, Besserer J and Schneider U. *A general model for stray dose calculation of static and intensity-modulated photon radiation.* *Med Phys* 2016;43:1955-1968.
- Howell RM, Ferenci MS, Hertel NE, Fullerton GD, Fox T and Davis LW. *Measurements of secondary neutron dose from 15 MV and 18 MV IMRT.* *Radiat Prot Dosim* 2005;115(1-4):508-512.
- Howell RM and Kry SF. *Secondary neutron spectra from modern Varian, Siemens, and Elekta linacs with multileaf collimators.* *Med Phys* 2009;36(9):4027-4038.
- Howell R, Kry S and Bednarz B. *Task Group 158: Measurement and calculation of doses outside the treatment volume from external-beam radiation therapy treatment.* *Radiother Oncol* 2015;115:S272.
- Huang JY, Followill DS, Wang XA and Kry SF. *Accuracy and sources of error of out-of-field dose calculations by a commercial treatment planning system for intensity-modulated radiation therapy treatments.* *Int J Radiat Appl Clin Med Phys* 2013;14(2).
- Hung GY, Chen CC, Horng JL and Lin LY. *Cancer in adolescents: Incidences and trends during 1995-2009 in Taiwan.* *Cancer Lett* 2016;372(1):110-117.
- ICRP International Commission on Radiological Protection. *The 2007 Recommendations of the International Commission on Radiological Protection.* ICRP Publication 103, 2007.
- ICRU International Commission on Radiation Units & Measurements. *Conversion coefficients for use in radiological protection against external radiation.* ICRU Report 57, 1998.
- Irazola L, Sanchez-Doblado F, Sanchez-Nieto B, Expósito MR, Mazzotti G, Morelli M, Lorenzoli M, Bedogni R, Pola A and Terrón JA. *Evaluation of peripheral neutron*

- equivalent dose and second cancer risk in radiotherapy patients. Radiother and Oncol* 2014a;111:708-709.
- Irazola L, Lorenzoli M, Bedogni R, Pola A, Terron JA, Sanchez-Nieto B, Exposito MR, Lagares JL, Sansaloni F and Sanchez-Doblado F. *A new online detector for estimation of peripheral neutron equivalent dose in organ. Med Phys* 2014b;41:112105.
- Irazola L, Lorenzoli M, Terron JA, Bedogni R, Pola A, Sanchez-Nieto B, Romero-Exposito M and Sanchez-Doblado F. *Neutron model upgrade for radiotherapy patients monitoring using a new online detector. Med Phys* 2014c;41:280.
- Irazola L, Terrón JA, Sánchez-Nieto B, Bedogni R, Gómez F and Sánchez-Doblado F. *Effects of cable extension and photon irradiation on TNRD neutron detector in radiotherapy. IFMBE Proceedings* 2015a;51:645-648.
- Irazola L, Terrón JA, Bedogni R, Lorenzoli M, Pola A, Sánchez-Nieto B and Sánchez-Doblado F. *Signal photon component of a new thermal neutron detector TNRD in radiotherapy environments. Radiother and Oncol* 2015b;115(1):S870(EP-1589).
- Irazola L, Terrón JA, Bedogni R, Lorenzoli M, Pola A, Sánchez-Nieto B and Sánchez-Doblado F. *TNRD neutron detector signals for different gantry angles in 6 and 15 MV. Radiother and Oncol* 2015c;115(1):S761 (EP-1410).
- Irazola L, Ortiz-Seidel M, García-Hernández MT, Terrón JA, Sánchez-Nieto B and Sánchez-Doblado F. *Peripheral neutron dose estimation: comparison between experimental measurements and TPS estimation. IFMBE Proceedings* 2015d;51:397-400.
- Irazola L, Terrón JA, Sanchez-Nieto B, Ortiz-Seidel M and Sánchez-Doblado F. *Photon and Neutron Peripheral Dose Ratio for Low (6 MV) and High (15 MV) Energy for Treatment Selection. Med Phys* 2015e;42(6):3476.
- Irazola L, Praena J, Fernandez B, Macias M, Terron JA, Bedogni R, Sanchez-Nieto B and Sanchez-Doblado F. *Monitoring the stability of a thermal neutron detector using a moderated neutron beam from a Tandem Peletron. Appl Radiat Isot* 2016a;107:330-334.
- Irazola L, Terrón JA, Bedogni R, Sánchez-Nieto B, Gómez F and Sánchez-Doblado F. *Improving the neutron-to-photon discrimination capability of detectors used for neutron dosimetry in high energy photon beam radiotherapy. Appl Radiat Isot.* (2016b)
- Irazola L, Terrón JA, Bedogni R, Pola A, Lorenzoli M, Jiménez-Ortega E, Barbeiro AR, Sánchez-Nieto B and Sánchez-Doblado F. *Neutron measurements in radiotherapy: a method to correct neutron sensitive devices for parasitic photon response. Sent to Applied Radiat Isot.* (2016c)
- Irazola L, Terrón JA, Sánchez-Nieto b, Romero-Expósito M and Sánchez-Doblado F. *Peripheral neutron dose model verification for real IMRT cases. Poster at the 1st European Congress of Medical Physics (ECMP) 2016, Athens (Greece).* (2016d)

- Irazola L, Terrón JA, Sánchez-Nieto B, Bedogni R and Sánchez-Doblado F. *Neutron model upgrade for peripheral neutron dose assessment and evaluation in 500 radiotherapy patients*. Sent to Phys Med Biol. (2016e)
- Irazola L, Ortiz-Seidel M, Velázquez S, García-Hernández MT, Terrón JA, Sánchez-Nieto B, Romero-Expósito M, Roselló J and Sánchez-Doblado F. *Comparison of peripheral doses associated to SBRT, VMAT, IMRT, FFF and 3D-CRT plans for lung cancer*. ePoster at 35th ESTRO Congress 2016;EP-1613. (2016f)
- Irazola L, García-Hernández MT, Ortiz-Seidel M, Velázquez S, Linares R, Sánchez-Nieto B, Roselló J, Terrón JA, Romero-Expósito MT and Sánchez-Doblado F. *SBRT, FFF and 10 MV irradiation techniques are associated to the lowest second cancer risk*. To be sent to Radiat Oncol J. (2016g)
- Jagetic LJ and Newhauser WD. *A simple and physics based analytical method to calculate therapeutic and stray doses from external beam, megavoltage x-ray therapy*. Phys Med Biol 2015;60:4753-4775.
- Jamison DT, Summers LW, Alleyne G, Arrow J, Berkley S, Binagwaho A, Burstreo F, Wvans D, Feachem RGA, Frenk J, Ghosh G, Goldie S, Guo Y, Gupta A, Srinath R, Saxenian H, Soucat A, Ulltveit-Moe KH and Yamey G. *Global health 2035: a world converging within a generation*. The Lancet 2013;382:1898-1955.
- Jimenez-Ortega e, Exposito MR, Gonzalez-Soto X, Terrón JA, Gómez F and Sánchez-Doblado F. *Characterization of the neutron induced single event upset in SRAM around high megavoltage clinical accelerators*. 12th European Conference on Radiation and Its Effects on Components and Systems (RADECS), 2011 Proceedings-DW-25.922-925.
- Kamran SC, Berrington de González A, Ng A, Haas-Kogan D and Viswanathan AN. *Therapeutic radiation and the potential risk of second malignancies*. Cancer 2016;doi:10.1002/cncr.29841.
- Kaderka R, Schardt D, Durante M, Berger T, Ramm U, Licher J and La Tessa C. *Out-of-field dose measurements in a water phantom using different radiotherapy modalities*. Phys Med Biol 2012;57:5059-5074.
- Kohandel M, Hodgson DC, Sharpe MB and Silvaloganathan S. *The effect of radiation quality on the risks of second malignancies*. Int J Radiat Biol 2015; 2015;91(3):209-217.
- Kry SF, Salehpour M, Followill DS, Stovall M, Kuban DA, White RA, Rosen II. *The calculated risk of fatal second secondary malignancies from intensity-modulated radiation therapy*. Int J Radiation Oncology Biol Phys 2005a;62(4):1195-1203.
- Kry SF, Salehpour M, Followill DS, Stovall M, Kuban DA, White RA and Rosen II. *Out-of-field photon and neutron dose equivalents from step-and-shoot intensity-modulated radiation therapy*. Int J Radiation Oncology Biol Phys 2005b;62(4):1204-1216.

- Kry SF, Howell RM, Salehpour M and Followill DS. *Neutron spectra and dose equivalents calculated in tissue for high-energy radiation therapy*. Med Phys 2009;36(4):1244-1250.
- Kumar S. *Second malignant neoplasms following radiotherapy*. Int J Environ Res Public Health 2012;9:4744-4759.
- La Tessa C, Berger T, Kaderka R, Schardt D, Körner C, Ramm U, Licher J, Matsufuji N, Vallhagen Dahlgren C, Lomax T, Reitz G and Durante M. *Out-of-field dose studies with an antropomorphic phantom: Comparison of X-rays and particle therapy treatments*. Radiother Oncol 2012;105:133-138.
- Lee JS, DuBois SG, Coccia PF, Bleyer A, Olin RL and Goldsby RE. *Increased risk of second malignant neoplasm in adolescents and young adults with cancer*. Cancer 2016;122(1):116-123.
- Lefebvre L, Doyeux K, Linca S, Challand T and Hanzen C. *Radiotherapy of a glioma in a pregnant woman: Evaluation of the foetal dose in conformational 3D or intensity-modulated*. Cancer Radiother 2014;18(8):763-766.
- Malick S, Giridhar P and Venkatesulu BP. *In regard to "Risk of second non-breast cancer after radiotherapy for breast cancer: A systematic review and meta-analysis of 762,468 patients"*. Radiother Oncol 2015;115(3):431.
- Milecki P, Adamska A, Roszak A et Kaleta D. *Should we afraid of induced cancer in group of patients after radical radiotherapy of prostate cancer?* Review Article. Rep Pract Oncol Radiother 2009;14(5):184-190.
- Murray L, Henry A, Hoskin P, Siebert FA and Venselaar J. *Second primary cancers after radiation of prostate cancer: A systematic review of the clinical data and impact of treatment technique*. Radiother Oncol 2014;110:213-228.
- Murray L, Sethugavalan B, Robertshaw H, Bayman E, Thomas E, Gilson D and Prestwich RJD. *Involved Node, Site, Field and Residual Volume Radiotherapy for Lymphoma: A Comparison of Organ at Risk Dosimetry and Second Malignancy Risks*. Clin Oncol 2015a;27(7):401-410.
- Murray LJ, Thompson CM, Lilley J, Cosgrove V, Franks K, Sebag-Montefiore D and Henry AM. *Radiation-induced second primary cancer risks from modern external beam radiotherapy for early prostate cancer: impact of stereotactic ablative radiotherapy (SABR), volumetric modulated arc therapy (VMAT) and flattening filter free (FFF) radiotherapy*. Phys Med Biol 2015b;1237-1257.
- Nath R, Boyer a, LaRiviere PD, McCall R and Kenneth W. *AAPM Report No.19: Neutron measurements around high energy X-ray radiotherapy machines-A report of Task Group 27, Radiation Therapy Committee, AAPM, 1986*.
- NCRP National Council on Radiation Protection & Measurements. *Protection against neutron radiation*. NCRP Report No. 38, 1971.

- NCRP National Council on Radiation Protection & Measurements. *Neutron contamination from medical accelerators*. NCRP Report No. 79, 1984.
- NCRP National Council on Radiation Protection & Measurements. *Structural shielding design and evaluation for megavoltage x- and gamma-ray radiotherapy facilities*. NCRP Report No. 151, 2005.
- Nguyen J, Moteabbed M and Paganetii H. *Assessment of uncertainties in radiation-induced cancer risk predictions at clinically relevant doses*. Med Phys 2015;42(1):81-89.
- Newhauser WD and Durante M. *Assessing the risk of second malignancies after modern radiotherapy*. Review Nature 2011;11:438-448.
- Newhauser WD, Berrington de Gonzalez A, Schulte R and Choonsik Lee. *A Review of Radiotherapy-Induced Late Effects Research after Advanced Technology Treatments*. Front Oncol 2016;6:13.
- Olch A and Hua C. *Pediatric Radiation Therapy Planning, Treatment, and Late Effects*. Med Phys 2015;42(6):3556.
- Ottolenghi A, Baiocco G, Smyth V and Trott K. *The Andante Project: a multidisciplinary approach to neutron RBE*. Radiat Prot Dosimetry 2015;166(1-4):311-5.
- Pena J, Franco L, Gómez F, Iglesias A, Pardo J, and Pombar M. *Monte Carlo study of Siemens PRIMUS photoneutron production*. Phys Med Biol 2005;50:5921-5933.
- Praena J, Irazola L, Fernández B, Terrón JA, Bedogni R, Lorenzoli M, Pola A, Sánchez-Nieto and Sánchez-Doblado F. *Proposal of thermal neutron detector stability for peripheral dose estimation in clinic at a novel neutron facility*. Radiother and Oncol 2015;115(1):S735.
- Robles L, Chou S, Cole O, Hamid A, Griffiths A. *Factors influencing patients' treatment selection for localized prostate cancer: a systematic review*. Br J Med Surg Urol 2012;5(5):207-215.
- Romero-Expósito M, Sánchez-Nieto B, Terrón JA, Lopez MC, Ferreira BC, Grishchuk D, Sandíns C, Moral-Sánchez S, Bragado-Álvarez L, Melchor M, Domingo C, Gómez F and Sánchez-Doblado F. *Commissioning the neutron production of a linac: development of a clinical planning tool for second cancer risk estimation*. Med Phys 2015;42:276-281.
- Romero-Expósito M, Domingo C, Sánchez-Doblado F, Ortega-Gelabert O and Gallego S. *Experimental evaluation of neutron dose in radiotherapy patients: which dose?* Med Phys 2016;43(1):360-367.
- Ruben JD, Davis S, Evans C, Jones P, Gagliardi F, Haynes M and Hunter A. *The effect of intensity-modulated radiotherapy on radiation-induced second malignancies*. Int J Radiation Oncology Biol Phys 2008;70:1530-1536.

- Sánchez-Doblado F, Madurga F, and Arrans R. *Neutron measurements around a linac (18 MV)*. *Radioth Oncol* 1989;15:259-265.
- Sánchez-Doblado F, Domingo C, Gómez F, Sánchez-Nieto B, Muñoz JL, García-Fusté MJ, Expósito MR, Barquero R, Hartmann G, Terrón JA, Pena J, Méndez R, Gutiérrez F, Guerre FX, Roselló J, Núñez L, Brualla-González L, Manchado F, Lorente A, Gallego E, Capote R, Planes D, Lagares JI, González-Soto X, Sansaloni F, Colmenares R, Amgarou K, Morales E, Bedogni R, Cano JP and Fernández F. *Estimation of neutron equivalent dose in organs of patients undergoing radiotherapy by the use of a novel online digital detector*. *Phys Med Biol* 2012;57:6167–6191.
- Sánchez-Doblado F, Irazola L, Lorenzoli M, Pola A, Bedogni R, Gentile A, Lagares, JI Muñoz JL, Sansaloni F, Introini MV, Bortot D, Sanchez-Nieto B, Expósito MR, and JA Terrón. *Online neutron fluence measurements in phantom for second cancer risk estimation in radiotherapy*. *Radiother and Oncol* 2014;111:709-710.
- Sánchez-Nieto B, El-far R, Irazola L, Expósito MR, Lagares JI, Mateo JC, Terrón JA and Sánchez-Doblado F. *Analytical model for photon peripheral dose estimation in radiotherapy treatments*. *Biomed Phys Eng Express* 2015a;1:045205.
- Sánchez-Nieto B, El-far R, Castrillón M, Irazola L, Terrón JA and Sánchez-Doblado F. *Validation of a photon peripheral dose model for IMRT treatments*. *Radiother and Oncol* 2015b;115(1):S541.
- Sánchez-Nieto B, Romero-Expósito M, Terrón JA, Irazola L, Pausco M, Cagni E, Ghetti C, Filice S, Gómez F, Domingo C and Sánchez-Doblado F. *Risk assessment of second cancer incidence after intensity-modulated radiation therapy and volumetric modulated arc therapy versus conventional conformal techniques at high energy*. *Sent to Br J Radiol* (2016).
- Schneider U, Lomax A, Pemler P, Besserer J, Ross D, Lombriser N and Kaser-Hotz B. *The impact of IMRT and Proton Radiation Therapy on secondary cancer incidence*. *Strahlenther Onkol* 2006;11:647-652.
- Schneider U. *Modelling the risk of secondary malignancies after radiotherapy*. *Genes* 2011;2:1033-1049.
- Schneider U and Walsh L. *Age at exposure and attained age variations of cancer risk in the Japanese A-bomb and radiotherapy cohorts*. *Med Phys* 2015;42(8):4755-4761.
- Sharma SD, Upreti RR, Laskar S, Tambe CM, Deshpande DD, Shrivastava SK, Dinshaw KA. *Estimation of radiation-induced carcinogenesis in adolescents with nasopharyngeal cancer treated using sliding window IMRT*. *Radiother Oncol* 2008;177-181.
- Shuryak I, Hahnfeldt P, Hlatky L, Sachs RK, and Brenner DJ. *A new view of radiation-induced cancer: Integrating short- and long-term processes. Part II: Second cancer risk estimation*. *Radiat Environ Biophys* 2009;48, 275–286.

- Siebert BRL and Schuhmacher H. *Quality factors, ambient and personal dose equivalent for neutrons, based on the new icru stopping power data for protons and alpha particles.* Radiat Prot Dosim 1995;58:177-183.
- Siegel R, Ma J, Zou Z and Jemal A. *Cancer Statistics, 2014.* CA Cancer J Clin 2014;64:9-29.
- Slaz H, Eichner R and Wiezorek T. *Does IMRT increase the peripheral radiation dose? A comparison of treatment plans 2000 and 2010.* Z Med Phys 2012;6-12.
- Smith MA, Seibel NL, Alterkruse SF, Ries LA, Melbert DL, O'Leary M, Smith FO and Reaman GH. *Outcomes for children and adolescents with cancer: challenges for the twenty-first century.* J Clin Oncol 2010;28:2625-2634.
- Statistics SEER [ONLINE] Available at: <http://seer.cancer.gov/csr/1975/2012/> [Accessed 9 May 2016].
- Taddei JP, Jalbout W, Howell RM, Khater N, Geara F, Homann K and Newhauser WD. *Analytical model for out-of-field dose in photon craniospinal irradiations.* Phys Med Biol 2013;58:7463-79.
- Terrón JA, Irazola L, Lorenzoli M, Bedogni R, Pola A, Introini MV, Bortot D, Gentile A, Esposito A, Sánchez-Nieto B, Expósito MR and Sánchez-Doblado F. *Set-up of a new online digital detector for peripheral neutron equivalent dose estimation in radiotherapy patients.* Radiother Oncol 2014;111:564.
- Terrón JA, Irazola L, Morilla Y, Muñiz G, Bedogni R, Lorenzoli M, Pola A, Sánchez-Nieto B and Sánchez-Doblado F. *Photon energy response of TNRD neutron detector in a ⁶⁰Co irradiator and a 6 MV linac.* Radiother and Oncol 2015;115(1):S757-S758 (EP-1404).
- Thomas RH. *Personnel neutron dosimetry studies at the Lawrence Berkeley Laboratory.* 1973.
- Thomas GA, Tronko MD, Tsyb AF, and Tuttle RM. *What have we learnt from Chernobyl? What have we still to learn?* Clinl Oncol 2011;23:229-233.
- Timlin C, Warren DR, Rowland B, Madkhali A, Loken J, Partridge M, Jones B, Kruse J and Miller R. *3D calculation of radiation-induced second cancer risk including dose and tissue response heterogeneities.* Med Phys 2015;42:866.
- Travis LB et al. *Breast cancer following radiotherapy and chemotherapy among young women with Hodgkin disease.* JAMA 2003;290:465-75.
- Trott KR. *Second cancers after radiotherapy.* Basic Clin Radiobiol 2009. M Joiner and A van der Kogel, editors (Hodder Arnold, London), 2009a.
- Trott, KR. *Can we reduce the incidence of second primary malignancies occurring after radiotherapy?* Radiother and Oncol 2009b;91:1-3.

- Tubiana M, Aurengo A, Averbeck D, and Masse R. *Recent reports on the effect of low doses of ionizing radiation and its dose-effect relationship*. Radiat Environ Biophys 2006;44:245-251.
- Tubiana M. *Can we reduce the incidence of second primary malignancies occurring after radiotherapy? A critical review*. Radiother Oncol 2009;91:4-15.
- United Nations Scientific Committee on the Effects of Atomic Radiation, in Effects of Ionizing Radiation: *UNSCEAR 2006 Report, Volume I-Report to the General Assembly, with Scientific Annexes A and B* (United Nations Publications, Vienna , 2008).
- United Nations Scientific Committee on the Effects of Atomic Radiation, in Effects of Ionizing Radiation: *UNSCEAR 2013 Report, Volume II, Scientific Annex B: Effects of radiation exposure of children* (United Nations Publications, 2013).
- Uselman AJ AND Thomadsen BR. On effective dose for radiotherapy based on doses to nontarget organs and tissues. Med Phys 2015;42:977-982.
- Van der Giessen. *Peridose, a software program to calculate the dose outside the primary beam in radiation therapy*. Radiother Oncol 2001;58:209-13.
- Van Leeuwen FE. *Second Cancers in cancers*. In: De Vita Vt Jr, Hellman S, Rosenberg SA (eds) *Cancer: Principles and Practice of Oncology*. 6th edn. Philadelphia: Lippincott Williams & Wilkins 2004.
- Vaño E. *Global view on radiation protection in medicine*. Radiat Prot Dosim 2011;147:3-7.
- Vázquez-Luque A, Marin J, Terrón JA, Pombar M, Bedogni R, Sánchez-Doblado F and Gómez F. *Neutron Induced Single Event Upset Dependence on Bias Voltage for CMOS SRAM With BPSG*. IEEE TNS 2013;60(6):4692.
- Vega-Carrillo HR, de Leon-Martinez HA, Rivera-Perez E, Benites-Rengifo JL, Gallego E and Lorente A. *Induced radioisotopes in a linac treatment hall*. Appl Radiat Isot 2016 in press.
- Voyant C, Julian D, Roustit R, Biffi K and Lantieri C. *Biological effects and equivalent doses in radiotherapy: a software solution*. Rep Pract Oncol Radiot 2014;19:47-55.
- Xu GX, Bednarz B and Paganetti H. *A review of dosimetry studies on external-beam radiation treatment with respect to second cancer induction*. Phys Med Biol 2008;53:193-241.
- Zhang R, Mirkovic D and Newhauser WD. *Visualization of risk of radiogenic second cancer in the organs and tissues of the human body*. Radiat Oncol 2015;10:107.

Glossary of abbreviations

AAPM	American Association of Physicist in Medicine
BED	Biological Effective Dose
BEIR	Biological Effects of Ionizing Radiation
CRT	Conformal RadioTherapy
CT	Computed Tomography
DDREF	Dose and Dose-Rate Effectiveness Factor
EAR	Excess Absolute Risk
ERR	Excess Relative Risk
FF	Flattening Filter
FFF	Flettening Filter Free
H&N	Head & Neck
ICRP	International Commission on Radiological Protection
IGRT	Image Guided Radiation Therapy
IMRT	Intensity Modulated Radiation Therapy
LAR	Lifetime Attributable Risk
LET	Linear Energy Transfer
MC	Monte Carlo
MU	Monitor Units
NCRP	National Council on Radiation Protection & measurements
NTCP	Normal Tissue Compliation Probability
OAR	Organs At Risk
PADC	Poly-Allyl-Diglycol-Carbonate (etched track dosimeter)
PD	Peripheral Dose
PND	Peripheral Neutron Dose
PPD	Peripheral Photon Dose
PTV	Planned Target Volume
RBE	Relative Biological Efficiency
RT	RadioTherapy
SBRT	Stereotactic Body Radiation Therapy
SCP	Second Cancer Probability
SCR	Second Cancer Risk
SEER	Surveillance, Epidemiology and End Results program
SEU	Single Event Upset
SMNs	Second Malignant Neoplasms
SRAM	Static Random Access Memory
TCP	Tumor Control Probability
TLD	ThermoLuminiscent Dosimeter
TNRD	Thermal Neutron Rate Detector
TPS	Treatment Planning System
VMAT	Volumetric Modulated Radiation Therapy

Appendix A

A.1.

Set-up of a new online digital detector for peripheral neutron equivalent dose estimation in radiotherapy patients

Terrón, Irazola et al., Radiother and Oncol 2014;111:564

1. Purpose

One of the possible sources of secondary neoplastic processes is the peripheral dose received by patients undergoing radiotherapy treatments. In spite of the *International Commission on Radiological Protection (ICRP Publication 103, 2007)* recommendations, out-of-field dosimetry is a complex task which is frequently ignored. Our team has focused on neutron equivalent dose estimation.

Firstly, a methodology to estimate neutron equivalent dose in organs, based on a *Static Random Access Memory neutron detector (SRAMnd)* was set up ([Sánchez-Doblado et al.,2012](#); [Expósito et al.,2014](#)). The purpose of this work is to present a new digital diode detector sensitive to thermal neutrons ([Irazola et al., 2014](#)) which, following the established methodology, improves the performance of our previous neutron dosimetry system.

2. Material and method

The *Thermal Neutron Rate Detector (TNRD)*, based on a commercial low-cost diode device and sensitized to thermal neutrons, is able to measure neutron fluence rate in the range of 10^{-10} - 10^7 $\text{ncm}^{-2}\text{s}^{-1}$ and in the presence of an intense photon background. It provides a voltage output which is directly proportional to the thermal neutron fluence rate ([Irazola et al., 2014](#)).

Simultaneous measurements with the SRAMnd were carried out. This allowed us to establish its reference factor, linearity, reproducibility and, finally, the patient measurements.

3. Results

A reference factor of 52.9 (events by SRAMnd/V·s by TNRD) with an uncertainty of 2.0% (1SD) was obtained.

Figure 1 shows the detector's linear response as a function of *Monitor Units* (MU) in the typical dynamic range of a radiotherapy treatment, with no saturation effect observed.

A reproducibility of 1.67% (1SD) has been estimated by considering 18 measurements. This value encompasses linac's reproducibility.

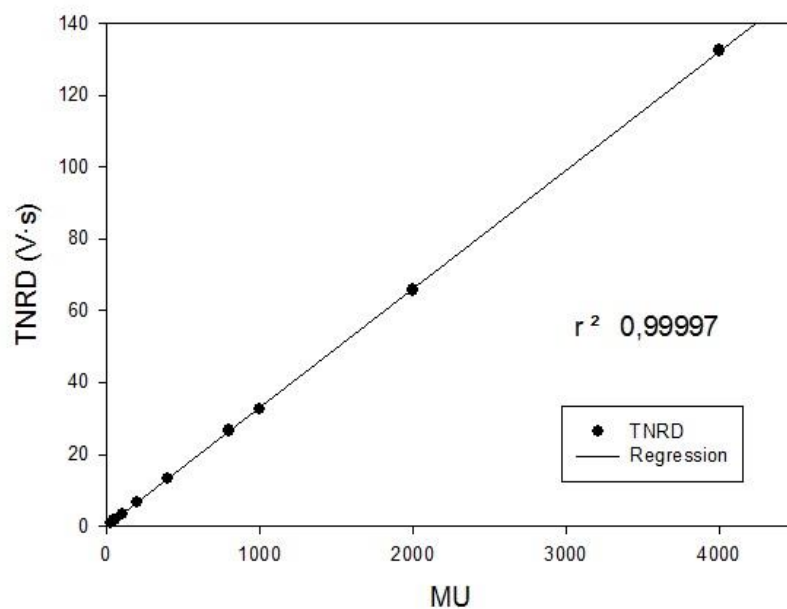


Figure 1. TNRD readings versus MU.

The variability in the response of both detectors, expressed in terms of *Total Risk of acquiring a second cancer* (TR), is shown in [Table I](#) for 50 patients, with measurements carried out in 4 facilities.

Table I. TR (%) per MU mean deviation between the values estimated by the TNRD and those of the reference SRAMnd, for the 4 studied facilities.

Facility	Mean TR deviation ($\pm 1SD$)
Siemens Primus 1 (15 MV)	0.098 \pm 0.230
Siemens Primus 2 (15 MV)	0.085 \pm 0.197
Siemens Oncor (15 MV)	-0.230 \pm 0.252
Elekta Synergy (18 MV)	-0.142 \pm 0.328

4. Conclusions

A new online neutron detector, named TNRD, has been validated and set-up for its use in the estimation of second cancer risk due to neutrons, as a consequence of radiotherapy treatments.

5. References

- ICRP Publication 103, Recommendations of the International Commission on Radiological Protection, 2007
- Expósito MR, Sánchez-Nieto B, Terrón JA, Domingo C, Gómez F and Sánchez-Doblado F. *Neutron contamination in radiotherapy: Estimation of second cancers based on measurement in 1377 patients*. *Radiother and Oncol* 2013;107:234-241
- Irazola L, Lorenzoli M, Bedogni R, Pola A, Terrón J A, Sanchez-Nieto B, Expósito M R, Lagares J I, Sansaloni F and Sanchez-Doblado F. *A new online detector for estimation of neutron equivalent dose in organ*. *Med Phys* 2014;41(11):112105:1-5
- Sánchez-Doblado, F, Domingo, C, Gómez, F, Sánchez-Nieto B, Múñiz J L, García-Fusté M J, Expósito M R, Barquero R, Hartmann G H, Terrón J A, et al. *Estimation of neutron equivalent dose in organs of patients undergoing radiotherapy by the use of a novel online digital detector*. *Phys Med Biol* 2012;57:6167–6191

A.2.

Evaluation of peripheral neutron equivalent dose and second cancer risk in radiotherapy patients

Irazola et al., Radiother and Oncol 2014;111:708-709

1. Purpose

The rapidly evolving external radiation treatment technologies have made possible a higher life expectancy of treated patients. This evolution is also associated to collateral long term effects like the risk of developing a second cancer (Xu et al.,2008). The source of this problem is the unwanted peripheral dose due to the photon leak and scattered photons, as well as to the secondary neutrons produced. Although absorbed dose due to photons is more relevant, neutrons do also have a noticeable contribution, owing to its biological weighting factor, w_R .

Neutron contribution to the doses in out-of-field organs has been previously estimated by Sánchez-Doblado et al.,2012. The introduction of a more versatile neutron detector has enabled the estimation of second cancer risk as a consequence of the neutron component of radiotherapy treatments (Expósito et al.,2013). We aimed to evaluate, using this detector, the neutron equivalent dose in peripheral organs, and the second cancer risk associated, for a group of patients.

2. Material and method

In order to evaluate, in real time, the neutron equivalent dose in peripheral organs and the second radio-induced cancer risk (Expósito et al.,2013), a

Thermal Neutron Rate Detector (TNRD) (Irazola et al.,2014) is placed inside the treatment room while performing patient measurements. Alternatively, and by means of a previous characterization of the facility (Expósito et al.,2012) with the same detector, we can estimate this risk (*Total risk of acquiring a second cancer, TR*) without the need of any measurements during the treatment.

In this work, measurements were carried out during the irradiation of 50 patients affected by different pathologies with high energies (15-18 MV). Four facilities participated in this quantification. The measurements have been compared to the estimated values, calculated with the characterization data.

3. Results

Table I shows the estimated TR per *Monitor Unit* (MU) for neck (H&N) and abdomen treatments, for the 4 characterized facilities (data are presented for men and women separately).

Figure 1 shows the differences between calculated (characterization) and measured TR values for the 50 studied patients.

Table I. *Estimated risk (TR) per MU for two types of treatments in men and women in 4 different facilities.*

Linac	Estimated risk per MU (cases per 1000) $\times 10^{-3}$			
	Man		Women	
	H&N	Abdomen	H&N	Abdomen
Elekta Synergy (18 MV)	1.69	1.82	1.74	1.93
Siemens Primus 1 (15 MV)	1.10	1.18	1.13	1.25
Siemens Primus 2 (15 MV)	0.93	1.00	0.96	1.06
Siemens Oncor (15 MV)	1.01	1.09	1.04	1.15

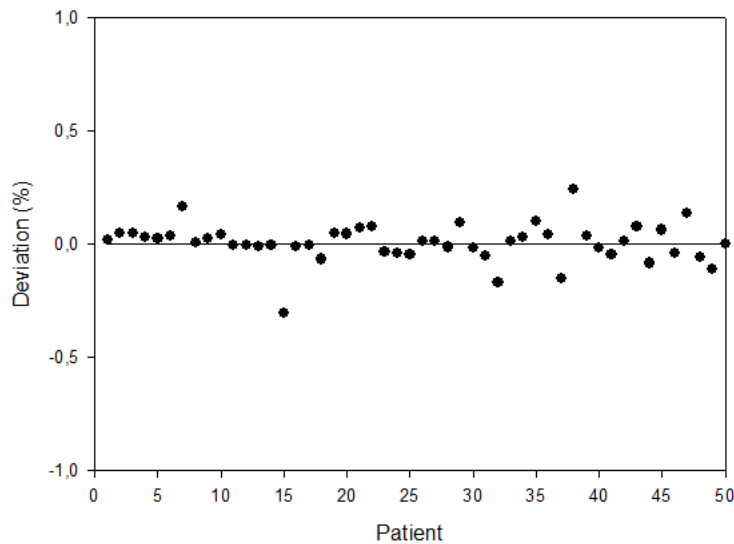


Figure 1. Percentage differences, with respect to the maximum risk (TR) of each facility, between estimated and measured value.

4. Conclusions

Peripheral neutron equivalent dose in patients undergoing radiotherapy has been measured, with a new active detector of small dimensions. Differences between the cancer risk estimations derived from direct measurements performed during patient irradiation and those estimated from a model based on a previous characterization of the linac are smaller than 0.25%. This opens the door to the implementation of models for peripheral neutron dose calculation in the context of treatment planning systems.

5. References

- Expósito MR, Sánchez-Nieto B, et al. *Experimental estimation of the second cancer risk due to neutron contamination in radiotherapy treatments*. *Radiother and Oncol* 2012;102:s516-s517.
- Expósito MR, Sánchez-Nieto B, Terrón JA, Domingo C, Gómez F and Sánchez-Doblado F. *Neutron contamination in radiotherapy: Estimation of second cancers based on measurement in 1377 patients*. *Radiother and Oncol* 2013;107:234-241.
- Irazola L, Lorenzoli M, Bedogni R, Pola A, Terrón J A, Sanchez-Nieto B, Expósito M R, Lagares J I, Sansaloni F and Sanchez-Doblado F. *A new online detector for estimation of neutron equivalent dose in organ*. *Med Phys* 2014;41(11):112105:1-5.

- Sánchez-Doblado, F, Domingo, C, Gómez, F, Sánchez-Nieto B, Múñiz J L, García-Fusté M J, Expósito M R, Barquero R, Hartmann G H, Terrón J A, et al. *Estimation of neutron equivalent dose in organs of patients undergoing radiotherapy by the use of a novel online digital detector*. Phys Med Biol 2012;57:6167–6191.
- Xu X-G, Bednarz B and Paganetti H. *A review of dosimetry studies on external-beam radiation treatment with respect to second cancer induction*. Phys Med Biol 2008;53,193-241.

A.3.

Online neutron fluence measurements in phantom for
second cancer risk estimation in radiotherapy

Sánchez-Doblado, Irazola et al., Radiother and Oncol 2014;111:709-710

1. Purpose

There is a growing concern about second cancer induction as a consequence of radiotherapy treatments (Xu et al.,2008). The main source of this problem is the unwanted peripheral dose, where neutrons represent an important contributor, owing to their relative biological effectiveness compared to photons. The equivalent dose in organ due to neutron contribution has been previously estimated by Sánchez-Doblado et al.,2012 through the use of an anthropomorphic phantom and passive detectors.

The introduction of a new miniaturized active neutron diode detector named *Thermal Neutron Rate Detector* (TNRD) (Irazola et al.,2014) allows us to estimate, online, the equivalent dose. TNRD's reduced size enables its insertion in an anthropomorphic phantom. We aimed to validate this new type of detector for the estimation of thermal neutron fluence at specific points inside a phantom.

2. Material and method

The new digital neutron detector TNRD, with an overall volume of approx. 0.9 cm³, can be placed at 16 points in an anthropomorphic phantom (NORMA), as shown in Figure 1.

This new detector was validated against *ThermoLuminiscent Dosimeter* (TLD). We have assumed a cumulative uncertainty of 15% for TLD, and 11% for



Figure 1. Anthropomorphic phantom with TNRD detectors located inside.

TNRD. Measurements were performed for 3 different treatments using 15 MV (head and neck, abdomen and prostate). The equivalent doses in organs are estimated from the thermal fluence, using neutron fluence energy spectrum for each point of the phantom, calculated with Monte Carlo (Sánchez-Doblado et al., 2012). For the risk of acquiring a second cancer we have used the procedure proposed in Expósito et al., 2013.

3. Results

Table I shows mean differences in thermal neutron fluence (and the *Standard Deviation* [SD]) between both detectors obtained for the three types of treatments, considering TLD as the reference.

Table I. Mean deviation (1SD) of thermal fluence (10^6 n.cm^{-2}) for both detectors (TLD as reference) in the different treatments.

Treatment	Deviation (%) \pm SD
H&N	-6.76 \pm 9.76
Abdomen	-10.07 \pm 14.85
Prostate	-6.06 \pm 11.86

4. Conclusions

A new active thermal neutron detector (TNRD) of small dimensions has been validated for in-phantom and online thermal neutron fluence estimation during radiotherapy treatments. This will enable direct estimation of equivalent dose in organs, and thus estimating the risk of acquiring second radio-induced cancer for any type of treatment and facility.

5. References

- Expósito MR, Sánchez-Nieto B, Terrón JA, Domingo C, Gómez F and Sánchez-Doblado F. *Neutron contamination in radiotherapy: Estimation of second cancers based on measurement in 1377 patients*. *Radiother and Oncol* 2013;107:234-241.
- Irazola L, Lorenzoli M, Bedogni R, Pola A, Terrón J A, Sanchez-Nieto B, Expósito M R, Lagares J I, Sansaloni F and Sanchez-Doblado F. *A new online detector for estimation of neutron equivalent dose in organ*. *Med Phys* 2014;41(11):112105:1-5.
- Sánchez-Doblado, F, Domingo, C, Gómez, F, Sánchez-Nieto B, Múñiz J L, García-Fusté M J, Expósito M R, Barquero R, Hartmann G H, Terrón J A, et al. *Estimation of neutron equivalent dose in organs of patients undergoing radiotherapy by the use of a novel online digital detector*. *Phys Med Biol* 2012;57:6167–6191.
- Xu X-G, Bednarz B and Paganetti H. *A review of dosimetry studies on external-beam radiation treatment with respect to second cancer induction*. *Phys Med Biol* 2008;53,193-241.

Appendix B

B.1.

Effects of cable extension and photon irradiation on TNRD neutron detector in radiotherapy

Irazola et al., IFMBE Proceedings 2015;51:645-648

Abstract

A new thermal neutron detector (*TNRD*), developed for nuclear research, has shown to be effective for clinical use in peripheral neutron dose estimation, either in patient and 'in-phantom' measurements. This work shows some *TNRD* difficulties when adapting it to radiotherapy environments, mainly due to the fact that it has shown structural limitations. Two problems have been studied: (1) the influence of cable lengthening, necessary to be operative in a radiotherapy environment and (2) cable irradiation during the measurements. As we are measuring very small signals, we have to take into account not only these two facts but also the quality of the materials and connectors used. Thus, we studied cable elongation and irradiation influences in conventional and extreme situations once the setup was improved, in order to avoid uncertainties which could be of the order of the signal. Mean deviations of -0.15% from the original *TNRD* cable extension have been noticed. For the wide variety of conditions tested, in terms of both dose delivered and setup of the radiotherapy exposure, uncertainties smaller than 1.2% have been estimated.

1. Introduction

As part of the clinical routine in radiotherapy environments, radiation dosimetry needs to be performed as complete as possible. However peripheral doses are usually not considered in routine procedures. Our group established

an easily accessible methodology for neutron component estimation (Sanchez-Doblado et al.,2012; Expósito et al.,2013). Neutron detectors used in radiotherapy for peripheral dose estimation for high-energy treatments were usually passive. Nevertheless new studies have demonstrated the viability of some active thermal neutron detectors, developed for nuclear research and aerospace applications, as suitable for both, 'in-phantom' and patient measurements (Guardiola et al., 2013; Irazola et al.,2014). Attention should be paid in the very small signals that are being measured, besides the fact that neutron presence is evaluated under an important photon background. This work studies the effects produced by the necessary modifications introduced in TNRD detector setup to adapt it from the nuclear to the radiotherapy environment, for peripheral neutron dose estimation. The effect of two parameters has been tested: (1) the cable lengthening (2) cable irradiation during the measurements. For precise estimations of weak signals, the contribution of noise currents generated during cable exposition has to be quantified (Fiorino et al.,2000; Campos et al.,1990).

In order to provide limits and recommendations for these detectors, this study was performed in the range of extreme and usual clinical conditions.

2. Material and Method

2.1 Material

a) TNRD detector

The newly miniaturized *Thermal Neutron Rate Detector*, TNRD has been developed in the INFN-LNF (*Istituto Nazionale di Fisica Nucleare*) of Frascati. Based on a low-cost commercial solid-state device sensitized to thermal neutrons through a customized physical-chemical treatment, is capable to correctly measure thermal neutrons under an intense photon background

(Bedogni et al.,2014). The signal is amplified in a low-voltage electronics module, then sent to a programmable ADC and finally controlled by a PC through a LabView© (2010 National Instruments). An improved and more compact setup was built, as shown in Figure 1a, to avoid inconvenient of the first prototype. Previous studies (Irazola et al.,2014) shown a global uncertainty in clinical environment measurements of 11% for these detectors.

Original cable length of the detectors was 0.8 m but an extension to a 2.4 m cable was found to be sufficient to reach all the anthropomorphic phantom measuring points from the electronic box (Figure 1b). For the reference detector (located close to the wall, in front of the treatment table) used for usual patient measurements, a 5.4 m total length was employed. Cables were adapted to these new lengths by using Belden Inc. RG-174/U and RG-58A/U cable type. For the box connections, BNC (Bayonet Neill Concelman) and SMA (SubMiniature version A) connectors are Amphenol® 50 Ω plugs. Amphenol® RF SMA to BNC adapters were also used here. Welding was performed at constant temperature with an electric welder and solder.

A Siemens Primus has been used at Virgen Macarena University Hospital in Seville (HUVM).

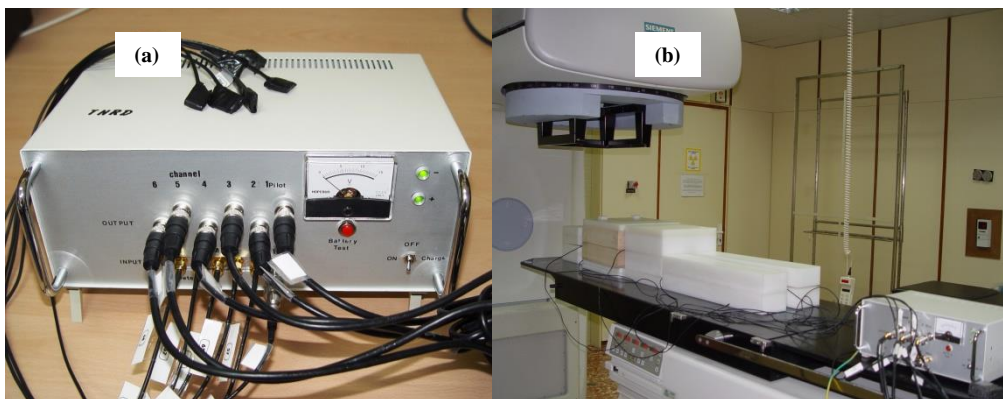


Figure 1. (a) Improved experimental setup with the new TNRD detector electronic box and (b) TNRD detectors during anthropomorphic phantom measurements in the treatment room.

2.2 Method

a) Cable length influence

In order to estimate cable influence, 0.8 m vs. 2.4 (or 5.4 m) cable, 500 MU measurements have been performed under the same irradiation conditions for the six available detectors.

Irradiation conditions were 10x10 cm² squared field in 15 MV, always with a 100 cm SSD distance. Detectors were inserted in the middle of 8 cm of polyethylene with 10 cm of the cable irradiated. Then linearity response was studied in the range of 100 to 4000 MU, corresponding to a thermal neutron fluence comprised between (4.5-230) x10⁶ neutrons per cm².

b) Cable irradiation influence

An empirical evaluation of the cable irradiation effect was made by the irradiation of 300 MU in 4 consecutive fields: (1) 40x10 cm² (2) 30x10 cm² (3) 20x10 cm² and (4) 10x10 cm² with (Figure 2a) and without (Figure 2b) cable irradiation. 40, 30, 20 and 10 cm of cable were irradiated (SSD=96.5 cm). Detector to field edge distance was always constant using asymmetric movements of the MLC (MultiLeaf Collimator). Both, cable and detectors were inserted in the middle of two layers of 0.5 cm of polystyrene and two layers of 3 cm of PMMA (polymethyl methacrylate).

First, reference measurements in 15 MV were performed without cable irradiation. Then, in order to avoid uncertainties due neutron production, 3.2 mm thick Flex-Boron sheets were used to cover the detectors (eliminating thus neutron presence in the signal as shown in Gomez et al.,2010). For that, the two polystyrene layers (were substituted by the two Flex-Boron sheets (equivalent to 5 mm of water). With this setup, with and without cable irradiation measurements were performed.

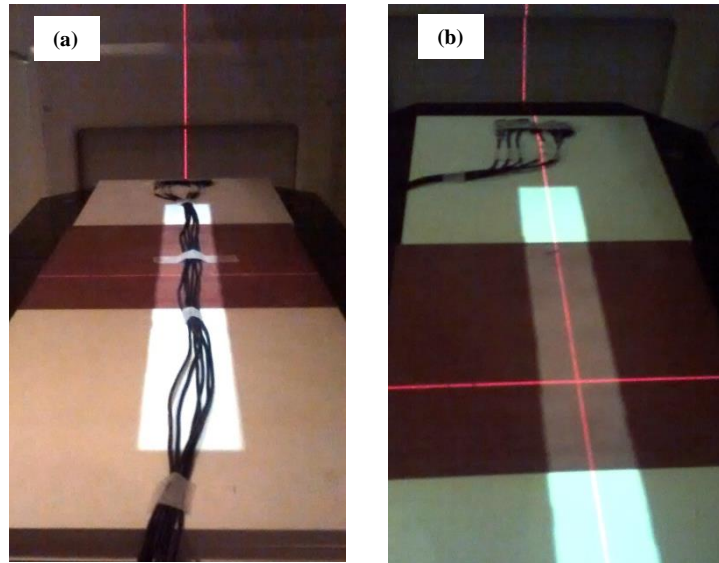


Figure 2. Setup for a field size of $40 \times 10 \text{ cm}^2$ when no irradiation (a) and irradiation (b) of the cable occurs. The upper plastic layers have been removed for a better visualization of the detectors position.

3. Results and discussion

3.1 Cable length influence

Mean loss of signal of $(-0.09 \pm 0.08) \%$ per meter of cable for the six detectors, with a maximum value of -0.24% and a minimum of -0.03% , has been obtained when measuring with extension cables with respect to the original setup. Observed differences could not only be related to cable length but also to quality of the connectors. In this sense, special care has been taken in material quality and connections when performing the setup.

A good linearity response was found ($R^2=1$) for all the detectors (with the extension cables) in the range 100-4000 MU as shown in [Figure 3](#).

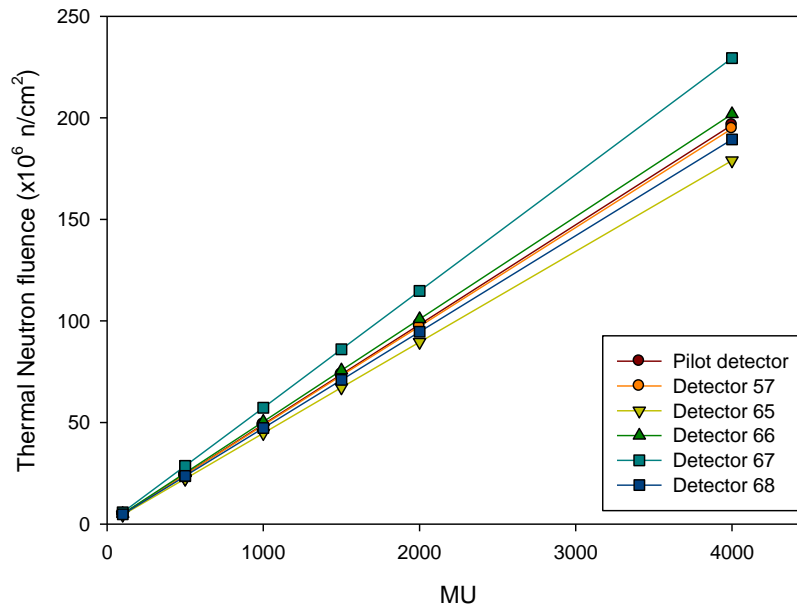


Figure 3. TNRD detectors linearity with extension cables in the range of 100 to 4000 MU, corresponding to a thermal neutron fluence comprised between $(4.5-230) \times 10^6$ neutrons per cm^2 .

When 1000 MU are delivered, a thermal fluence of around 20×10^6 neutrons per cm^2 was obtained. This implies that the studied range covers widely the usual clinical values.

3.2 Cable irradiation influence

In general, a loss of signal has been observed when cables were irradiated. The variation obtained for the different studied field shapes (between irradiated and non-irradiated measurements using Flex-Boron sheets) is shown in [Table I](#). Total signal and relative uncertainties are calculated with respect to the reference 15 MV measurement (without the neutron absorber material).

Data show the same trend in signal variation by decreasing readings when cables are being irradiated. Deviations increase when the amount of exposed cable is bigger, until the 30 cm case.

Table I. TNRD signal in 15 MV, subtraction of irradiated and no irradiated cable readings and percentage that represents the difference with respect to total values.

Field size (cm ²)	Total signal (V·s)	Irradiation -No Irradiation (V·s)	Relative Deviation (%)
10x10	74.17	-0.60	-0.63
20x10	81.49	-0.76	-0.70
30x10	87.30	-1.22	-1.19
40x10	87.68	-1.20	-1.09

Similar values were obtained for the most extreme situation (40x10 cm²) and the previous one (30x10 cm²). Thus we can assume that when cables are being irradiated, corresponding to a dose of 318.5 cGy, TNRD signal decreases at most 1.1% from the non-irradiated case. As during 'in-phantom' measurements and other experiments cables are similarly irradiated, we should consider this incertitude for now on.

4. Conclusions

Our experiences showed both, the substantial necessity of using extended cables and the impossibility of measuring in the anthropomorphic phantom points without cable irradiation. Fortunately, measurements are now possible with the proposed improved setup here detailed. The previously mentioned 11% uncertainties did not consider these studied limitations. Although cable length extension has in general negligible effect on the measurement, cable

irradiation can produce up to a 1.2% deviation in some extreme conditions studied here.

As such, it is recommended the use of longer (around 2.4 m) than the 0.8 m provided by the manufacturer. Taking special care on cable and connections quality. On the other hand, the irradiation of the cables should be considered in order to minimize its influence during the measurement. Nevertheless, this should be taken into account when considering measuring uncertainties in TNRD signal.

5. References

- Bedogni R, Bortot D, Pola A, Introini MV, Gentile A, Esposito A, Gomez-Ros JM, Palomba M, Grossi A. *A new active thermal neutron detector*. Radiat Prot Dosim 2014;161(1-4):241-244.
- Campos L and Linda VE Caldas. *Induced effects in ionization chamber cables by photon and electron irradiation*. Med Phys 1990;18(3):522-526.
- Exposito MR, Sanchez-Nieto B, Terron JA, Domingo C, Gomez F and Sanchez-Doblado F. *Neutron contamination in radiotherapy: Estimation of second cancers based on measurement in 1377 patients*. Radiother and Oncol 2013;107,234-241.
- Fiorino C, Mangili P, Cattaneo GM and Calandrino R. *Polarity effects of ionization chambers used in TBI dosimetry due to cable irradiation*. Med Dosim 25(3):121-126.
- Gomez F, Iglesias A and Sanchez-Doblado F. *A new active method for the measurement of slow-neutron fluence in modern radiotherapy treatment rooms*. Phys Med Biol 2010;55:1025-1039.
- Guardiola C, Gomez F, Fleta C, Rodriguez J, Quirion D, Pellegrini G, Lousa A, Martinez-de-Olcoz L, Pombar Mand Lozano M. *Neutron measurements with ultra-thin 3D silicon sensors in a radiotherapy treatment room using a Siemens PRIMUS linac*. Phys Med Biol 2013;58:3227-3242.
- Irazola L, Lorenzoli M, Bedogni R, Pola A, Terron JA, Sanchez-Nieto B, Exposito MR, Lagares JI and Sanchez-Doblado F. *A new online detector for estimation of peripheral neutron equivalent dose in organ*. Med Phys 2014;41:112105:1-5.
- Sanchez-Doblado F, Domingo C, Gomez F, Sánchez-Nieto B, Muñoz JL, Garcia-Fuste MJ, Exposito MR, Barquero R, Hartmann GH, Terron JA et al. *Estimation of neutron equivalent dose in organs of patients undergoing radiotherapy by the use of a novel online digital detector*. Phys Med Biol 2012;57, 6167-6191.

B.2.

Signal photon component of a new thermal neutron detector TNRD in radiotherapy environments

Irazola et al., Radiother and Oncol 2015;115(1):S870

1. Purpose

The goal of this work is to study *TNRD* (Thermal Neutron Rate Detector) response in high and low energies of clinical environments, to reject the photon component in peripheral dose measurements where mixed gamma and neutron fields are present.

2. Material and method

Four *TNRD* detectors ([Bedogni et al.,2014](#)) and a Farmer PTW ionization chamber were simultaneously used to obtain neutron and photon doses. Measurements were performed in a Siemens Primus linac with 6 and 15 MV photon beams (300MU/min) using a 40x10 cm² field. One minute irradiation times were used with both detectors placed in the middle of an 8 cm methacrylate block under out-of-field geometries ([Figure 1](#)). The study was carried out for 9 different field edge-detector distances, which meant photon dose rates ranging from 0.16 to 6 cGy/min.

3. Results

As expected, for each location, similar readings from the IC were obtained for both energies as an indication of the low dependence of photon peripheral doses with the energy ([Kry et al.,2005](#)). An average difference of 0.26 cGy



Figure 1. Setup used for the field-edge-detector study.

(photon dose) for IC readings in both energies, except for 5 cm to the field edge (not relevant for peripheral doses) was obtained. Neutron presence in 6 MV was evaluated with the *SRAMnd* (Sánchez-Doblado et al., 2012) (*Static Random Access Memory neutron detector*), with a negligible neutron presence ($\sim 1\%$). These two results allowed, from the subtraction of the 6 MV and the 15 MV readings, the neutron component discrimination for each measured situation (Table I with averaged values). Photon presence (6 MV) increases when getting closer to the field edge, which is predicted by the IC in accordance with *TNRD* readings. If we would establish a limit to trust *TNRD* neutron measurement, a noise (photon) lower than 10% of the signal (neutron) could be considered acceptable. This value is obtained 30 cm far from the field edge, corresponding to a photon dose around 0.5 cGy.

Table I. TNRD readings for 6 and 15 MV measurements and neutron component (subtraction of both readings), for the 9 studied distances.

Field-edge detector distance (cm)	TNRD 15 MV (V·s)	TNRD 6 MV (V·s)	Neutron signal (V·s)
5	152.48	83.46	69.02
10	145.22	36.56	108.67
15	143.78	34.50	109.28
20	137.09	28.36	108.72
25	129.09	25.38	103.71
30	117.96	15.95	102.01
35	106.65	9.47	97.19
55	86.38	3.31	83.07
100	63.07	1.07	62.00

4. Conclusions

A photon rejection uncertainty has been estimated for TNRD detectors under some clinical special conditions. Although patient measurements are perfectly feasible with this type of detector (Irazola et al., 2014) due to the low photon contribution when using the methodology established for model generation (Sánchez-Doblado et al., 2012), photon contribution limit should be studied for new detectors. Nevertheless, as we can assume that photon components are close for both energies, being 15 MV one at least as that of 6 MV, a good approximation to obtain more precise neutron doses, would be the subtraction of signals (corresponding to measurements at 6 and 15 MV under the same

conditions), as shown in the [Table I](#). This would allow having reliable neutron measurements much closer than 30 cm to the field-edge (e.g. 10-15 cm).

5. References

- Bedogni R, Bortot d, pola A, Introinin MV, Gentile A, Espósito A, Gómez-Ros JM, Palomba M and Grossi A. *A new active thermal neutron detector*. Radiat Prot Dosim 2014;161(1–4), 241–244.
- Irazola L, Lorenzoli M, Bedogni R, Pola A, Terrón JA, Sánchez-Nieto B, Expósito MR, Lagares JI, Sansaloni F and Sánchez-Doblado F. *A new online detector for estimation of peripheral neutron equivalent dose in organ*. Med Phys 2014 Nov; 41(11):112105.
- Kry SF, Salehpour M, Followill DS, Stovall M, Kuban DA, White RA and Rosen II. *The calculated risk of fatal secondary malignancies rom intensity-modulated radiation therapy*. In. J Radiation Oncology Biol Phy. 2005;62(4):1204-1216.
- Sánchez-Doblado F, Domingo C, Gómez F, Sánchez-Nieto B, Muñoz JL, García-Fusté, Expósito MR, Barquero R, Hartmann G, Terrón JA, et al. *Estimation of neutron-equivalent dose in organs of patients undergoing radiotherapy by the use of a novel online digital detector*. Phys Med Biol 2012;57:6167–6191.

B.3.

Photon energy response of TNRD neutron detector in a ⁶⁰Co irradiator and a 6 MV linac

Terrón, Irazola et al., Radiother and Oncol 2015;115(1):S757-S758

1. Purpose

The validation of a novel digital thermal neutron detector *TNRD* has been carried out for clinical applications. The results obtained by our group, indicated that the estimation of neutron doses, both in phantom and patients are perfectly feasible with this detector (Irazola et al.,2014). Although differences among the two diodes that compose the detectors in terms of photon sensitivity were reduced in the manufacturing process, experiments have shown them not to be completely reliable in some special clinical environment.

The goal would be to find a relation between dose-signal responses with photon dose and energy, in order to establish *TNRD* limitations in clinical environments.

2. Material and method

The ⁶⁰Co photon source used is a Gammabeam® X200 irradiator, that provides gamma photons (with energies of 1.17 and 1.33 MeV) in a wide range of dose rate (0.05-400 Gy/h), obtained with different attenuation systems. The linac used is a Primus Siemens with 6 MV and a 40x10 cm² field. Measurements were performed with a PTW Farmer ionization chamber and *Thermal Neutron Rate Detector* (TNRD), based on a pair of photodiodes and sensitized to thermal

neutrons (Bedogni et al.,2014). Pure photon response of TNRD was studied in the ⁶⁰Co facility for dose rates ranging from 0 to 4 cGy/min. As we have already confirmed that neutron presence in 6 MV is negligible, measurements ranging from 0.1 to 4.6 cGy photon doses were performed for different out-of-field detector positions.

3. Results

Although we expected to obtain a constant signal-dose relation for TNRD, different behavior was observed at both facilities. A higher reading is obtained always for the ⁶⁰Co measurements, being almost 7 times bigger for low doses (0.12 cGy) and around 3 times at higher ones (4.3 cGy). TNRD energy response, can be estimated based on the mass-energy attenuation coefficient ($\mu_{en/p}$) of ¹⁴Si (main component of TNRD detector) shown in Figure 1. The difference found in TNRD signal in ⁶⁰Co and 6 MV (Table I) is justified by the higher response observed for the ¹⁴Si at low energies, taking into account that measurements are always performed in a peripheral area where scattering is dominant and thus mean energy lower.

4. Conclusions

TNRD neutron detector has shown to be sensitive to photon dose rates even at low values (0.15-4 cGy/min). Different behaviour has been noticed for ⁶⁰Co and 6 MV photon energies. Nevertheless, similar TNRD response to 6 and 15 MV photons could be expected. In consequence, in order to reasonably avoid photon presence in peripheral neutron estimations, the subtraction of 6 MV signal to the 15 MV one (under the same irradiation conditions) could be a good approximation. Further measurements and MC simulations, should be necessary to ensure this proposal for different linac energies.

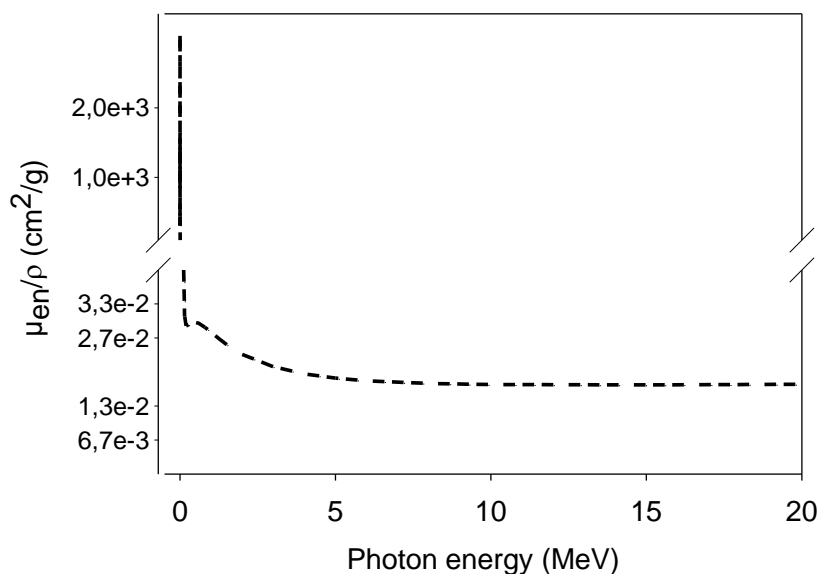


Figure 1. Logarithmic representation of the μ_{en}/ρ coefficient for ^{14}Si in the range of 0-20 MeV, data extracted from <http://physics.nist.gov/PhysRefData/XrayMassCoef/ElemTab/z14.html>.

Table I. TNRD signal in ^{60}Co and 6 MV facilities.

^{60}Co		6 MV	
D (cGy)	TNRD (V·s)	D (cGy)	TNRD (V·s)
0.14	7.61	0.11	1.07
0.15	8.37	0.23	3.31
0.16	8.73	0.42	9.47
0.33	16.82	0.67	15.95
0.43	20.17	1.11	25.38
0.67	29.82	2.14	34.50
3.30	151.16	3.29	33.92
3.88	164.54	3.65	38.74
4.03	168.88	4.60	60.67

5. References

- Bedogni R, Bortot d, pola A, Introinin MV, Gentile A, Espósito A, Gómez-Ros JM, Palomba M and Grossi A. *A new active thermal neutron detector*. Radiat Prot Dosim 2014;161(1-4), 241-244.
- Irazola L, Lorenzoli M, Bedogni R, Pola A, Terrón JA, Sánchez-Nieto B, Expósito MR, Lagares JI, Sansaloni F and Sánchez-Doblado F. *A new online detector for estimation of peripheral neutron equivalent dose in organ*. Med Phys 2014 Nov; 41(11):112105.

B.4.**TNRD neutron detector signals for different gantry angles in 6 and 15****MV**

Irazola et al., Radiother and Oncol 2015;115(1):S761

1. Purpose

The new commercial thermal neutron device (*TNRD*) has a good response with directionality in a pure neutron beam (Bedogni et al., 2014). In addition, good coincidence with TLD detectors was found for peripheral neutron dose estimation in-phantom (Irazola et al., 2014). Nevertheless, further experiments have shown that *TNRD* is not completely reliable in some special clinical conditions, due to photon contribution.

The aim of this work is the knowledge of uncertainties related to photon presence under different irradiation conditions, especially angle incidence influences at different field-edge distances. This will not only verify the goodness of *TNRD* measurements due to a possible compensation, but to find a possible correction to improve peripheral neutron doses estimation.

2. Material and method

TNRD detector is based on a pair of commercial photodiodes, and allows the measurement of thermal neutron fluences under an intense photon background (Bedogni et al., 2014). However in the case of an important photon presence, intrinsic differences among diodes make *TNRD* signal to be over or underestimated, due to their relative position with respect to the beam incidence. This could be a consequence of “shadow” effect, from one diode to

the other, as the reading is obtained by the subtraction of both signals (the one of the sensitized to neutrons and the normal one).

Six gantry angle incidences (0° , 45° , 135° , 180° , 225° and 315°) were measured in 6 and 15 MV for two different field-edge detector distances (10 and 25 cm, corresponding to an approx. dose rate 3.53 and 1.21 cGy/min). A Primus Siemens linac using a 40×10 cm² field was employed with TNRD detectors inserted in the middle of two layers of 4 cm polyethylene.

3. Results

Table I shows TNRD readings at 6 MV (photon signal) and neutron component from 15 MV (subtraction of 15 MV and 6 MV readings). Photon influence in TNRD neutron readings are up to 50% for 315° and 135° for 10 cm. However if we consider the accumulated readings among the whole arc, total photon component is compensated and reduced to 9.3% or 6.7% depending on distance to field-edge. Figure 1 shows the compensation of photon component for complementary gantry angles.

Table I. TNRD readings at 6 MV (photon signal) and neutron component from 15 MV (subtraction of 15 MV and 6 MV readings).

Distance to the field edge (cm)	10 cm		25 cm	
	Photon signal (V·s)	Neutron signal (V·s)	Photon signal (V·s)	Neutron signal (V·s)
Gantry ($^\circ$)				
0	36.13	113.234	26.03	110.51
45	51.87	93.16	22.77	96.15
135	-73.84	141.45	-34.84	105.57
180	-56.37	182.55	-39.05	138.18
225	-71.48	142.68	-37.24	107.83
315	48.34	94.11	21.48	94.20

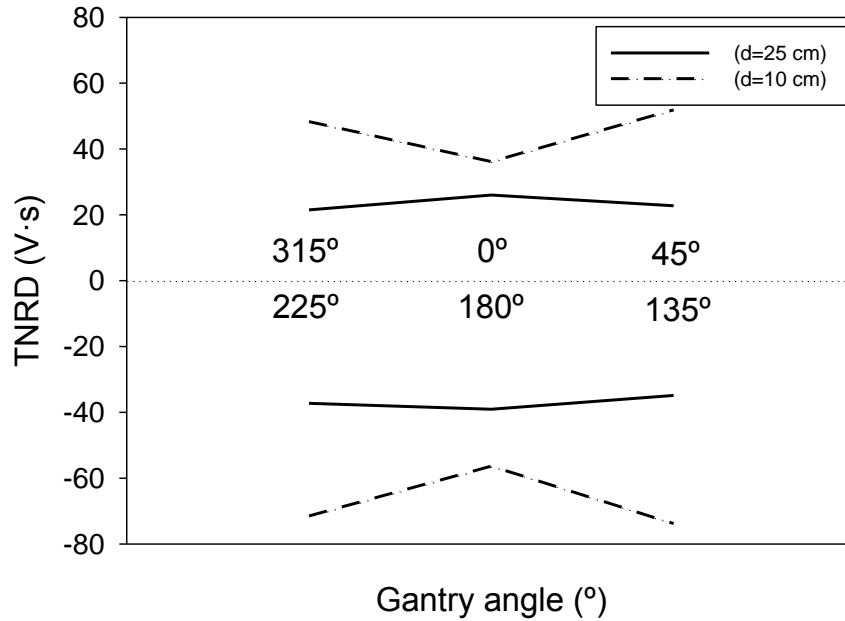


Figure 1. TNRD readings for complementary gantry angles at a field-edge detector distance of 10 (dashed line) and 25 (solid line) cm.

4. Conclusions

Results obtained here explain the problem that TNRD measurements have shown when measuring at some angle incidences at different distances to the field-edge because of photon contribution. The good relation obtained with TLD detectors in previous experiences (Irazola et al.,2014) are due to the compensation of different angle incidences shown here. Although good measurements are obtained when compensated multi-incidences are used, more accurate results would be obtained if 6 and 15 MV measurements are performed under the same conditions. This would be relevant when non-balanced gantry incidences are used.

5. References

- Bedogni R, Bortot d, pola A, Introinin MV, Gentile A, Espósito A, Gómez-Ros JM, Palomba M and Grossi A. *A new active thermal neutron detector*. Radiat Prot Dosim 2014;161(1–4), 241–244.
- Irazola L, Lorenzoli M, Bedogni R, Pola A, Terrón JA, Sánchez-Nieto B, Expósito MR, Lagares JI, Sansaloni F and Sánchez-Doblado F. *A new online detector for estimation of peripheral neutron equivalent dose in organ*. Med Phys 2014 Nov; 41(11):112105.

Appendix C

C.1.

Peripheral neutron dose estimation: comparison between experimental measurements and TPS estimation

Irazola et al., IFMBE Proceedings 2015;51:397-400

Abstract

A newly TPS algorithm, implemented in Pinnacle³, has been developed for peripheral neutron dose estimation for radiotherapy patients. The script gives doses in several organs according to gender, treatment location and delivered high energy monitor units. In order to validate these estimations, doses for a total of 119 patients were calculated with Pinnacle³ TPS script, and compared to the experimental measurements with the new Thermal Neutron Digital Detector (*TNRD*). The studied patients, cover a wide range of pathologies for three different linacs. The comparison shows that with the implemented script we obtain a good correlation between measurement and theoretical values. On the other hand, periodic neutron characterization of the facility should be considered for better estimations.

1. Introduction

Peripheral doses delivered during radiotherapy treatments are usually not considered in routine procedures. Although neutron component of these doses is difficult to estimate, our group established an easily accessible methodology for neutron component estimation ([Sanchez-Doblado et al.,2012](#); [Expósito et al.,2013](#)). A Pinnacle³ TPS (Philips Oncology Systems, Fitchburg, WI) script based on the previously validated algorithms ([Romero-Exposito et al.,2015](#)) has

been implemented. In order to verify this new tool, we compared neutron doses calculated with the TPS to the ones obtained by measurements in the treatment room. The detector used for this purpose, was a new active thermal neutron detector called *TNRD* (Irazola et al.,2014). A group of patients were evaluated from a wide range of pathologies in five linacs.

2. Material and Method

2.1 Material

a) *TNRD detector*

The *Thermal Neutron Rate Detector* (Bedogni et al.,2014) is a miniaturized thermal neutron active detector that has been validated for peripheral neutron dose estimates for radiotherapy patients (Irazola et al.,2014). For this purpose, during patient measurements, the device is located as shown in [Figure 1](#).



Figure 1. *TNRD detector (marked in red) setup during patient measurements.*

b) *Peripheral Neutron Pinnacle³ TPS script*

A screenshot of the implemented Pinnacle³ TPS script is shown in Figure 2. Values used for peripheral neutron dose calculation are directly taken from the patient plan: total number of sessions, gender, location (abdomen or H&N), total number of high energy MU and the algorithm itself. An additional coefficient, obtained by the simple characterization procedure explained in Romero-Exposito et al.,2015, has to be calculated and implemented in the TPS for each facility. This characterization value correlates thermal neutron fluence in the treatment room with the number of high energy MU delivered. This procedure only needs to be performed periodically for each facility.

From these data, the script automatically calculates equivalent neutron doses (mSv) for several organs as presented in Figure 2. These values are automatically recorded in an ASCII file, easily exportable to Excel for epidemiological studies.

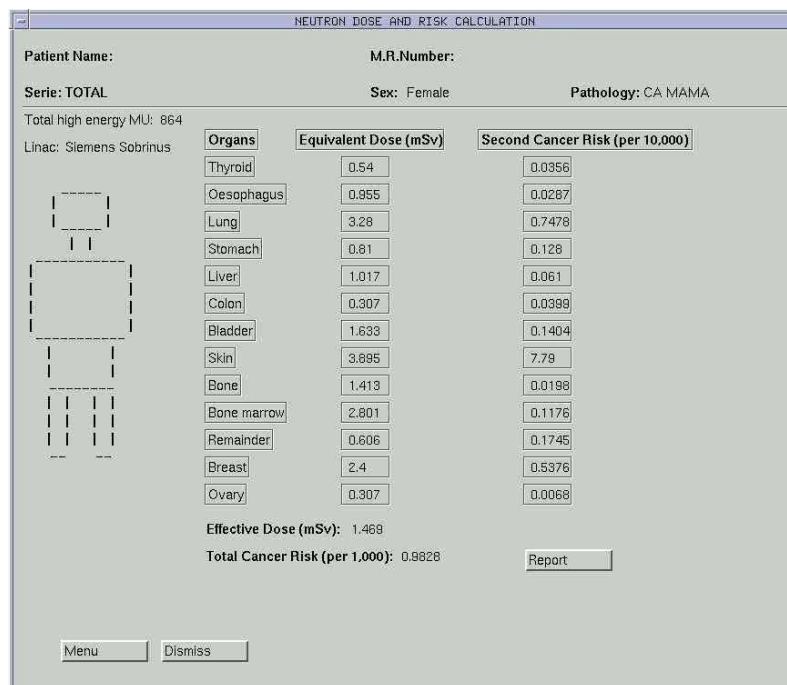


Figure 2. *Peripheral Neutron Pinnacle³ screenshot for a specific patient of breast cancer using 15 MV beams as part of the treatment.*

c) Accelerators

Five facilities from two institutions have been evaluated with three different kinds of linacs: three Siemens Primus (two of 15 MV and one of 18 MV), one Siemens Oncor (15 MV) and one Varian TrueBeam (15 MV).

2.2 Method

a) Facility characterization

In our case, the characterization factor was obtained with *TNRD* detector, following the characterization procedure explained in [Exposito et al., 2015](#). In order to establish the frequency of this characterization procedure, in parallel we studied its variation in time. For that, the parameter was calculated for three of the facilities during each series of patient measurement, in one year interval.

b) Patient Measurements

A total cohort of 119 patients was evaluated in the studied facilities, in order to compare TPS estimations against detector measurements. As example, we will represent both neutron doses for three representative organs, for the 45 patients measured in one of the Siemens Primus linac (15 MV). In addition, three selected kind of treatments in three different linacs have been chosen to show obtained differences. Here, 13 organ neutron doses have been compared for the whole treatment by extrapolating, in the case of experimental measurements values obtained for one session.

3. Results and discussion

3.1 Facility characterization

[Figure 3](#) shows the measured (symbols) characterization coefficient and the average values (lines), for three of the facilities. Error bars correspond to the SD (%) considering the three measurements performed each time. An almost constant value is shown for all the cases.

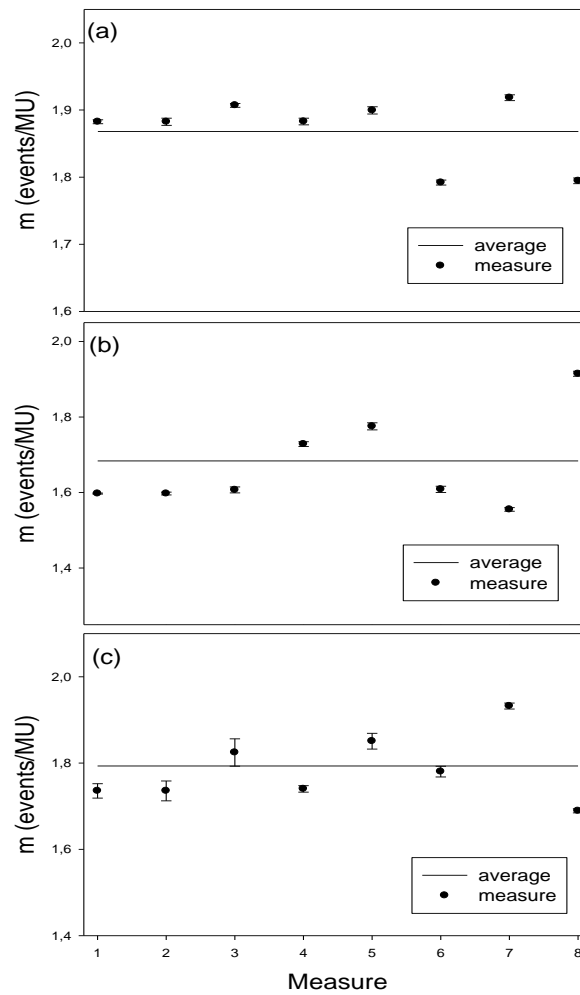


Figure 3. Characterization coefficient (m) that correlates detector readings to total number of high energy MU delivered is represented here. Measured values (symbols) and average values (lines) for three of the facilities are represented for along one year.

3.2 Patient measurements

Figure 4 shows peripheral neutron doses calculated in the TPS (bars) and measured (line), for three specific organs: (a) Thyroid, (b) Lung and (c) Colon for one of the Primus linac for a cohort of 45 patients.

Figure 5 shows peripheral neutron doses for three different treatments in three different linacs (15MV): breast in Siemens Primus, rectum in Varian TrueBeam and lung in Siemens Oncor.

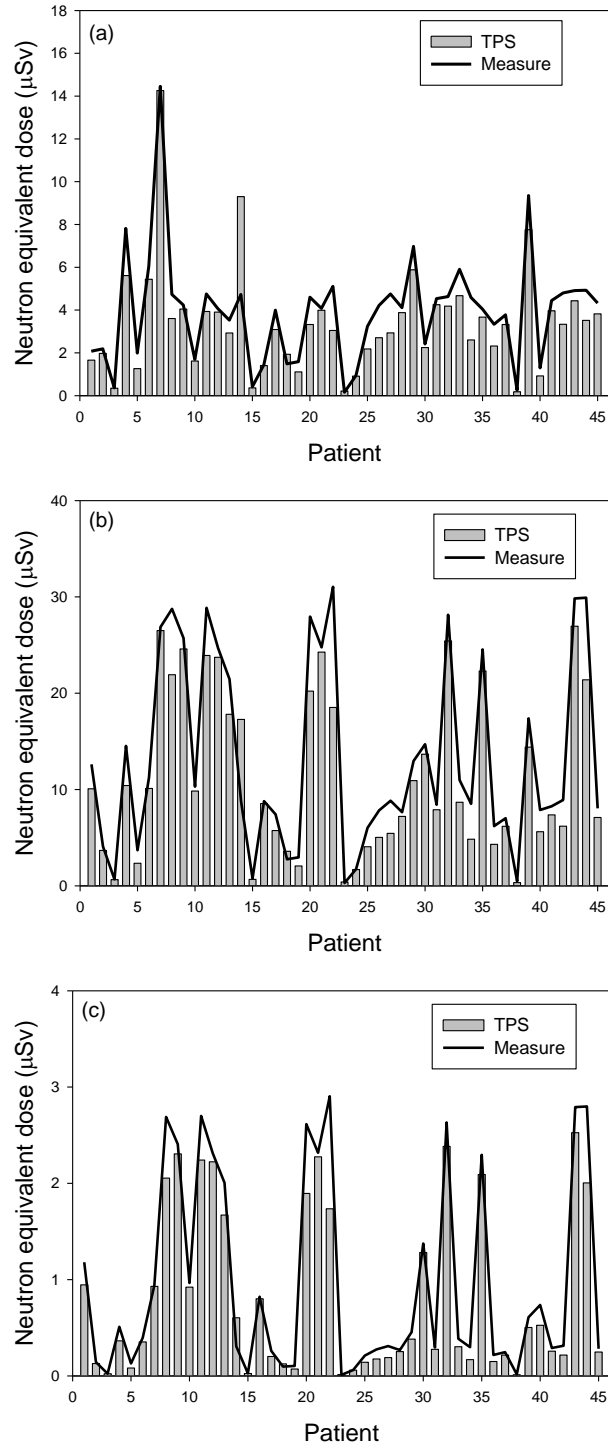


Figure 4. Peripheral neutron doses for three specific organs: (a) Thyroid, (b) Lung and (c) Colon for Siemens Primus (15 MV) linac, for a cohort of 45 patients. Bars represent TPS estimations while line shows measured values.

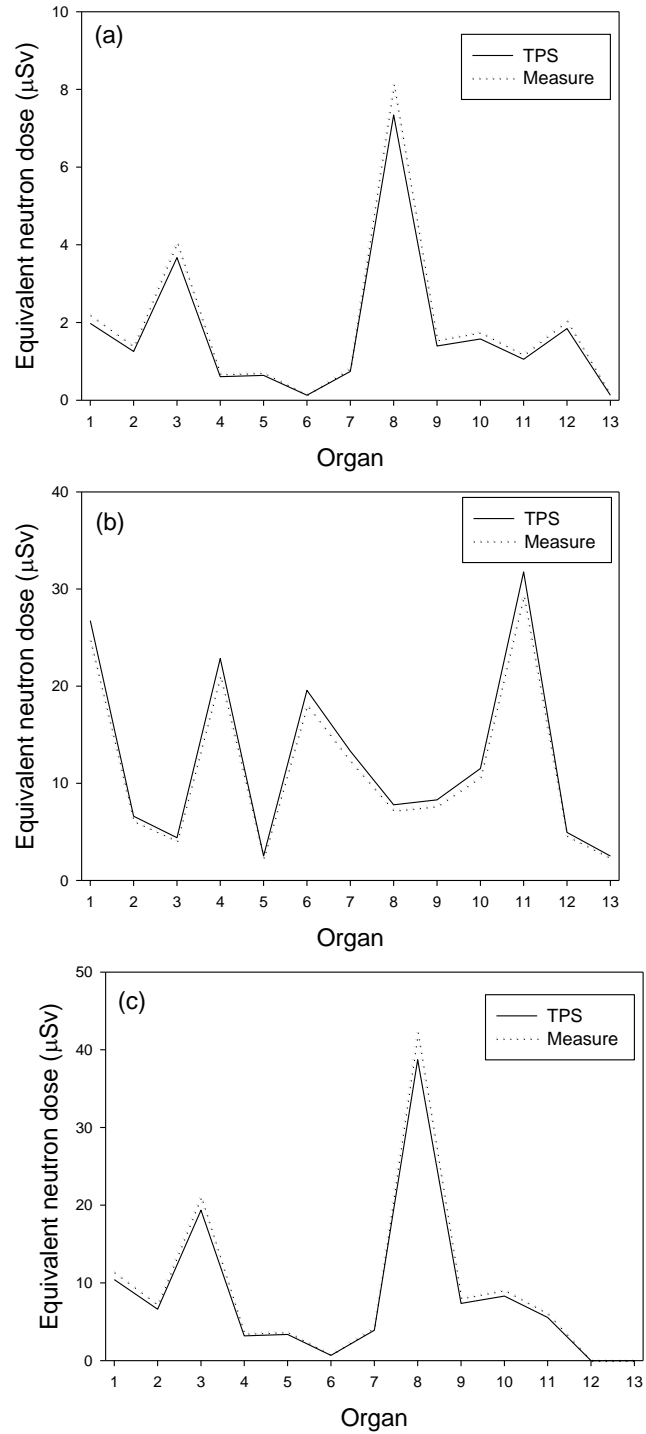


Figure 5. Peripheral neutron doses for three different treatments, using 15 MV: (a) Breast in Siemens Primus1, (b) Rectum in Varian TrueBeam and (c) Lung in Siemens Oncor, for the considered organs (1:thyroid, 2:oesophagus, 3:lung, 4:stomach, 5:liver, 6:colon, 7:bladder, 8:skin, 9:bone, 10:marrow, 11:remainder, 12:breast, 13:ovary). Solid line represents values obtained with the TPS and measurements are represented by the dashed one.

A good concordance is obtained between TPS calculation and experimental measurements for all the treatment types and facilities, as shown in the figures.

4. Conclusions

The implementation of the peripheral neutron dose calculation script in Pinnacle³ TPS has shown as an appropriate tool for peripheral neutron dose calculations. It is able to calculate peripheral neutron doses by terms of patient parameters and thus give an idea of peripheral neutron doses when choosing patient treatment strategy. Considering the obtained values, we assume that a periodicity of once a year for facility characterization, should be enough for a good TPS estimation of peripheral neutron doses in organs.

5. References

- Bedogni, R., Bortot, D., Introini, M.V., Gentile, A., Esposito, A., Gómez-Ros, J.M., Palomba, M., Gross, A., 2014. *A new active thermal neutron detector*. Radiat Prot Dosim 2014;161(1-4), 241-244.
- Expósito MR, Sánchez-Nieto B, Terrón JA, Domingo C, Gómez F and Sánchez-Doblado F. *Neutron contamination in radiotherapy: Estimation of second cancers based on measurement in 1377 patients*. Radiother and Oncol 2013;107:234-241.
- Irazola L, Lorenzoli M, Bedogni R, Pola A, Terrón J A, Sanchez-Nieto B, Expósito M R, Lagares J I, Sansaloni F and Sanchez-Doblado F. *A new online detector for estimation of neutron equivalent dose in organ*. Med Phys 2014;41(11):112105:1-5.
- Romero-Exposito M, Sanchez-Nieto B, Terron JA, Lopes MC Ferreira BC, Grishchuk D, Sandin C, Moral-Sanchez S, Melchor M, Domingo C, Gomez F and Sanchez-Doblado F. *Commissioning the neutron production of a linac: development of a simple tool for second cancer risk estimation*. Med Phys 2015;42(1):276-281
- Sánchez-Doblado, F, Domingo, C, Gómez, F, Sánchez-Nieto B, Múñiz J L, García-Fusté M J, Expósito M R, Barquero R, Hartmann G H, Terrón J A, et al. *Estimation of neutron equivalent dose in organs of patients undergoing radiotherapy by the use of a novel online digital detector*. Phys Med Biol 2012;57:6167–6191.

C.2.

Peripheral neutron dose model verification for real IMRT cases

Irazola et al., Poster accepted at the European Congress of Medical Physics (ECMP 2016), to be published in Phys Medica

1. Introduction

Peripheral doses are directly related to second cancer risk after radiotherapy. Our group developed a methodology to estimate neutron contribution to peripheral organ doses by terms of two general models, namely abdomen and head and neck ([Sánchez-Doblado et al.,2012](#)).

2. Purpose

This work aims to verify the validity of these models in real treatments, in order to evaluate the need of further improvements for specific locations beside the two generic ones.

3. Materials and Methods

Neutron doses were calculated in 12 representative organs from measured thermal neutron fluences with TNRD detectors at 16 points inside the phantom ([Irazola et al., 2014](#)), for two high energy (15MV) treatments (lung and prostate). Following the methodology described in ([Expósito et al.,2013](#)), these neutron doses were estimated by terms of number of delivered MU and facility characterization. Abdomen model was used for the prostate case while both (abdomen and head&neck) for the lung one (due to isocenter position respect to models). Then measurements have been compared to estimations obtained with the prediction models ([Sánchez-Doblado et al.,2012](#)).

4. Results

Values generally agreed within the 30% uncertainty range established for the models and the 15% for the measurement (Figure 1 a-c). Abdomen model has shown to fit better for the lung (Figure 1b-c). Further studies should be needed to improve generic models in some specific locations such as skin or organs close to the field-edge.

5. Conclusion

The generic model has shown to be good enough to cover frequent high-energy specific treatments as those studied here. It seems to be no need of more specific models, while some improvements have to be done for particular points.

6. References

- Expósito MR, Sánchez-Nieto B, Terrón JA, Domingo C, Gómez F and Sánchez-Doblado F. *Neutron contamination in radiotherapy: Estimation of second cancers based on measurement in 1377 patients*. *Radiother and Oncol* 2013;107:234-241.
- Irazola L, Lorenzoli M, Bedogni R, Pola A, Terron JA, Sanchez-Nieto B, Exposito MR, Lagares JJ, Sansaloni F and Sanchez-Doblado F. *A new online detector for estimation of peripheral neutron equivalent dose in organ*. *Med Phys* 2014;41:112105.
- Sánchez-Doblado F, Domingo C, Gómez F, Sánchez-Nieto B, Muñoz JL, García-Fusté MJ, Expósito MR, Barquero Terrón JA, et al. *Estimation of neutron equivalent dose in organs of patients undergoing radiotherapy by the use of a novel online digital detector*. *Phys Med Biol* 2012;57:6167–6191.

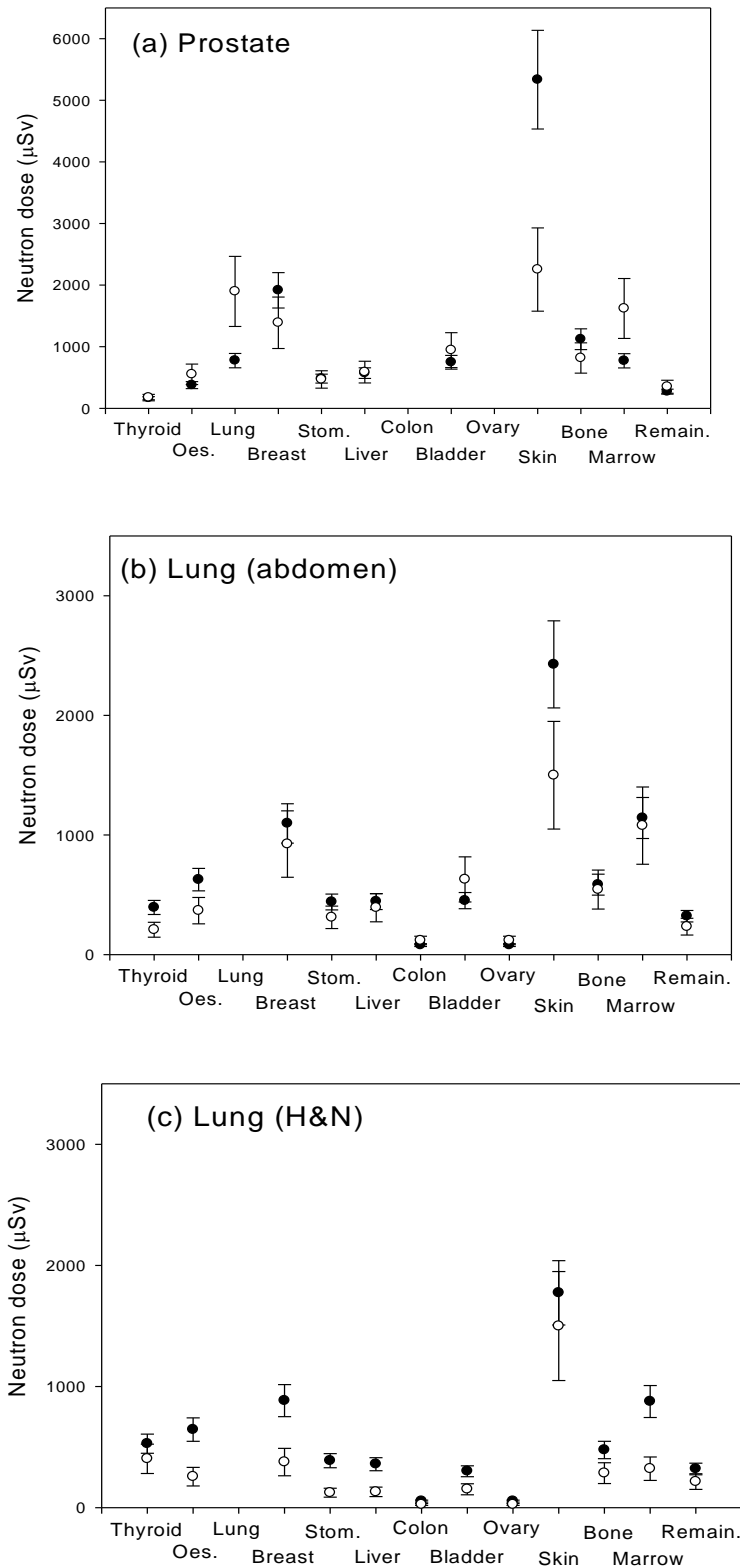


Figure 1. Neutron dose (μSv) obtained by TNRD detector compared to abdomen model for: (a) prostate and (b) lung treatments and H&N model for (c) lung treatment. (graphics were not included in the original abstract as it was not permitted but will be included in the poster).

Appendix D

Comparison of peripheral doses associated to SBRT, VMAT, IMRT, FFF and 3D-CRT plans for lung cancer

Irazola et al., 35th ESTRO Congress 2016; EP-1613, to be published in
Radiother Oncol

1. Purpose

Out-of-field doses during radiotherapy treatments (RT) are associated with an increased risk of second malignant neoplasms in cancer survivors. The purpose of this work is to evaluate the impact, in terms of peripheral dose (PD), that new techniques for lung cancer such as stereotactic body radiotherapy (SBRT), modulated beams (IMRT and VMAT) and FFF would have in comparison to more traditional plans (3DCFRT).

2. Material and method

Self-developed models ([Sánchez-Doblado et al,2012](#); [Sánchez-Nieto et al.,2015](#)) were used for neutron and photon peripheral dose (NPD and PPD, respectively) estimation to 12 organs, associated to lung treatments delivered using 3 linacs: Siemens Primus (6&15 MV), Elekta Synergy (6 MV) and Varian TrueBeam (6,10&15 MV; FFF mode available for the first two). Facilities were previously characterized in terms of neutron production ([Romero-Expósito et al.,2015](#)) and photon leakage.

17 plans were generated for a lung cancer case (60 cGy to 100%). Different PTVs were used for conventional and stereotactic treatments (factor of 20 between both volumes). Results were compared to values from the literature ([Huang et](#)

al.,2015) where PD studies were done but by terms of direct measurements of only photon component for few external points.

3. Results

Figure (a) shows estimated NPD and PPD to some selected organs for SBRT treatments in 6 and 10 MV, including FF and FFF modes. Figure (b) shows average PPD to the same representative out-of-field organs (mSv) for 4 studied techniques, considering all the linacs and plans. As an example, differences in PPD and NPD, for 3D-CRT and IMRT in low and high energies, are shown in Table I. Taking into account leakage, field size and MU, an average increase in PPD values of 8.6% and 12.6% has been obtained for Varian and Elekta linacs with respect to Siemens, when considering for the here studied 3D-CRT treatment in 6 MV. However, a decrease in 19% was noticed when using FFF mode.

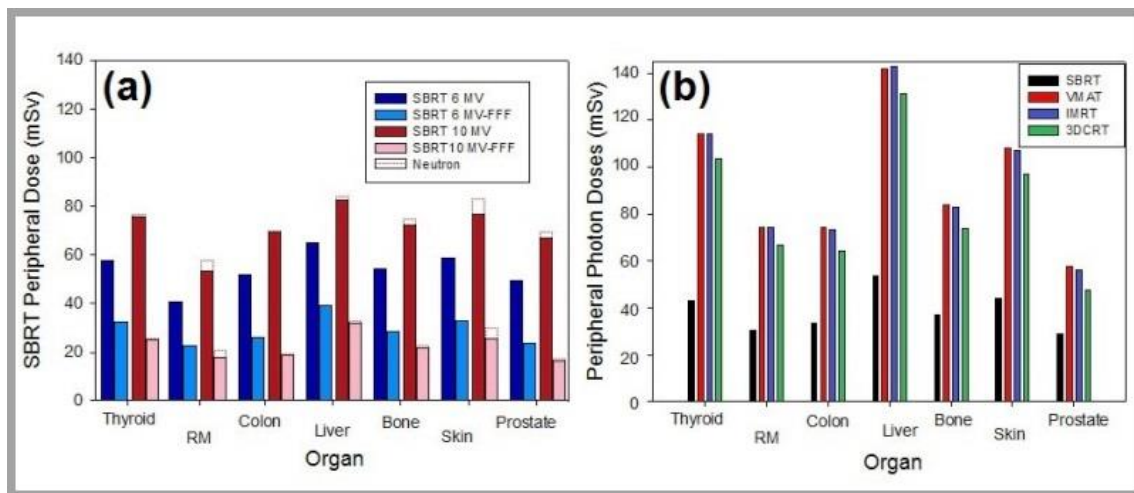


Figure 1. (a) estimated NPD and PPD to some selected organs for SBRT treatments in 6 and 10 MV, including FF and FFF modes. (b) average PPD to the same representative out-of-field organs (mSv) for 4 studied techniques, considering all the linacs and plans.

Table I. PPD and NPD for 3D-CRT and IMRT treatments in low (6 MV) and combined (6&15) energies.

Organ	3D-CRT			IMRT		
	6 MV	6&15 MV		6 MV	6&15 MV	
	Photon	Photon	Neutron	Photon	Photon	Neutron
Thyroid	96.35	108.85	3.18	114.00	113.90	5.12
Red Marr.	62.35	71.30	8.98	73.45	74.75	9.24
Colon	60.10	72.85	0.95	69.15	77.40	0.93
Bladder	48.00	60.85	5.08	54.35	65.25	5.04
Liver	122.00	134.50	3.32	145.50	140.00	3.49
Bone	68.75	81.55	5.05	79.85	85.95	5.86
Skin	90.35	103.05	16.96	106.50	107.75	23.13
Remainder	83.30	93.30	2.56	99.00	97.45	3.42

Values in mSv

4. Conclusions

Lower PD in SBRT cases could be due to the smaller size of ITV vs. conventional PTV. Our results are in agreement with previous clinical studies (Huang et al.,2015). Additionally, we have quantified the advantage of reduced PD when using FFF mode. However, this study only considers PD while ignoring the impact of radiobiological effect due to the dose per fraction.

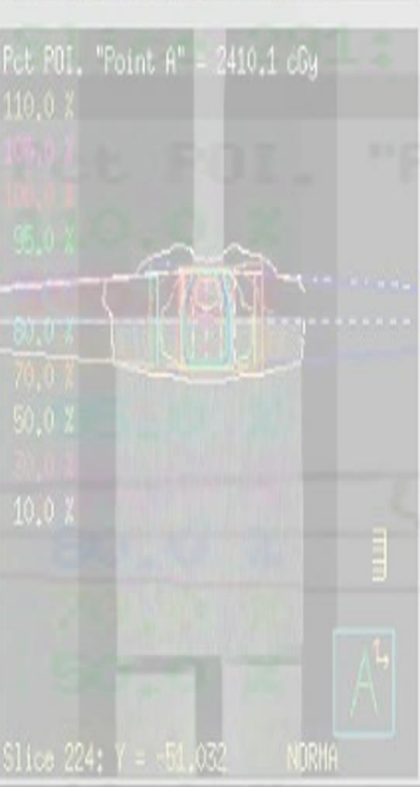
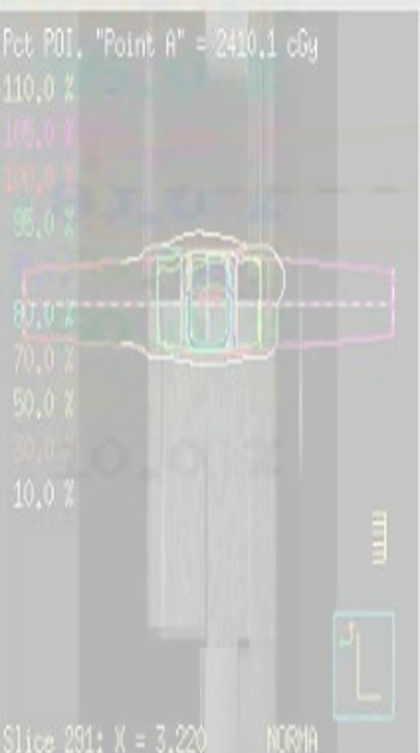
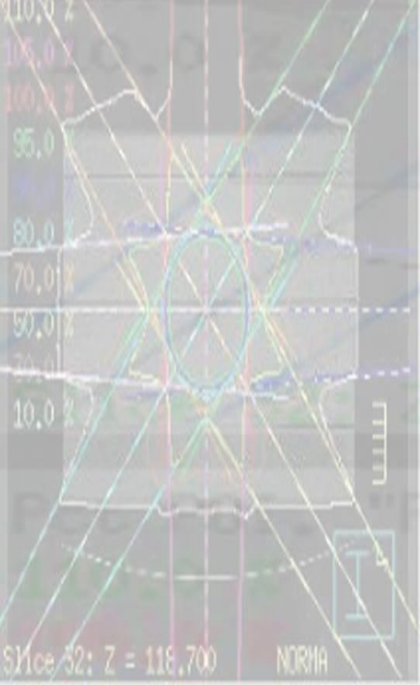
The slight differences found between techniques (3D-CRT, IMRT and VMAT) are due to the simple case chosen (in terms of target geometry). Nevertheless, the tendency shows higher values for VMAT and IMRT. Thus, further studies are desirable to extrapolate these results to complex cases.

Neutron contributes in a small percentage to global PD, this becomes especially relevant if 15 MV represents only a part of the total treatment.

5. References

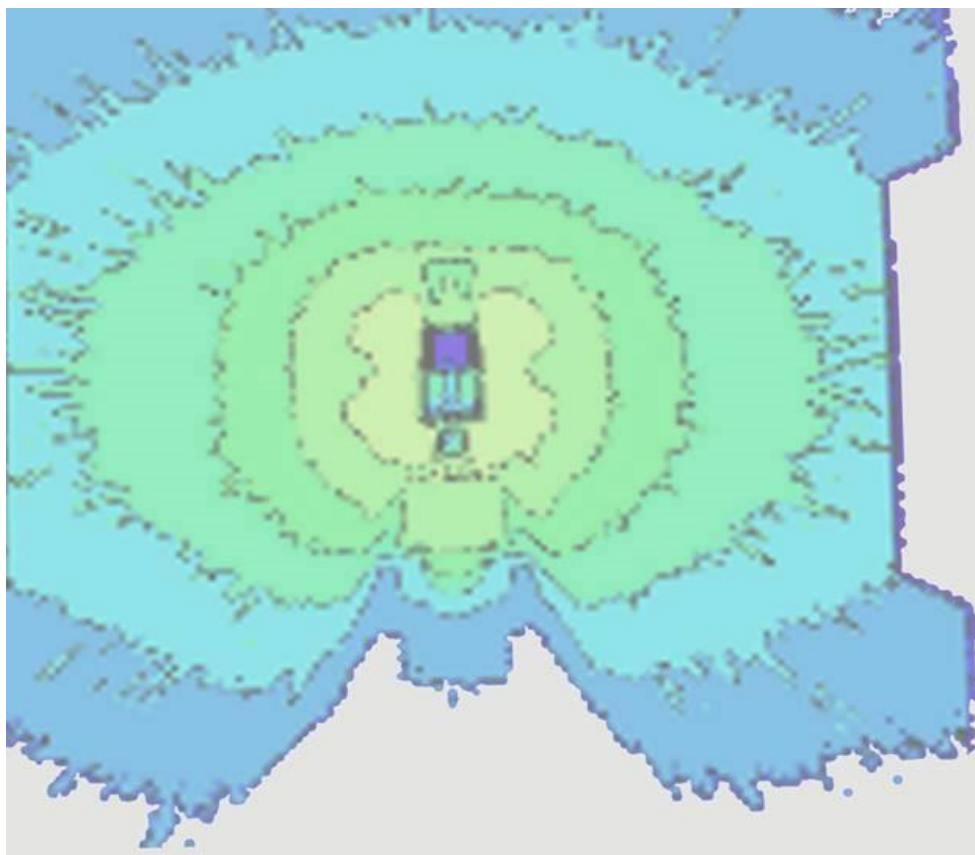
Huang BT, Lu JY, Lin PX, Chen JZ, Kuang Y et al. Comparison of two RapidArc delivery strategies in Stereotactic Body Radiotherapy of peripheral lung cancer with Flattening Filter Free beams. PLoS ONE 2015;10(7):e0127501.

- Romero-Exposito M, Sanchez-Nieto B, Terron JA, Lopes MC Fereira BC, Grishchuk D, Sandin C, Moral-Sanchez S, Melchor M, Domingo C, Gomez F and Sanchez-Doblado F. *Commissioning the neutron production of a linac: development of a simple tool for second cancer risk estimation*. Med Phys 2015;42(1):276-281.
- Sánchez-Doblado, F, Domingo, C, Gómez, F, Sánchez-Nieto B, Múñiz J L, García-Fusté M J, Expósito M R, Barquero R, Hartmann G H, Terrón J A, et al. *Estimation of neutron equivalent dose in organs of patients undergoing radiotherapy by the use of a novel online digital detector*. Phys Med Biol 2012;57:6167–6191.
- Sánchez-Nieto B, El-far R, Irazola L, Expósito MR, Lagares JI, Mateo JC, Terrón JA and Sánchez-Doblado F. *Analytical model for photon peripheral dose estimation in radiotherapy treatments*. Biomed. Phys. Eng. Express 2015;1:045205.



En Sevilla, a 9 de Junio de 2016

Día de La Rioja



**Thesis submitted in partial fulfillment of the requirements
for the degree of Doctor with International Mention Supervised by
Prof. Dr. Francisco Sánchez Doblado and Dr. José Antonio Terrón León.**

**Grupo de Física Médica, Departamento de Fisiología Médica y Biofísica.
Facultad de Medicina, Universidad de Sevilla**

